THESIS IN JOINT-SUPERVISION

With

University of Carthage
Department of Biological and Chemical Engineering, National Institute of Applied Sciences and Technology (INSAT-Tunisia)
&
Universitat Politècnica de Catalunya-Barcelona TECH
Chemical Engineering Department (UPC, Spain)

Presented by
Mehrez HERMASSI

VALORISATION OF PHOSPHATE FROM INDUSTRIAL AND DOMESTIC EFFLUENTS AS BY-PRODUCTS FOR FERTILIZERS PRODUCTION

in partial fulfillment of the requirements for the degree of

Doctor in Applied Chemistry & Chemical Process Engineering

Advisors:	Narjès Harrouch BATIS:	Professor, INSAT, Tunisia
	José Luis Cortina PALLAS:	Professor, ETSEIB, Barcelona TECH

PhD reading committee:

President:	Jameleddine BELGAIED	Professor, INSAT, Tunisia
Examinators:	Oriol GIBERT:	Ass. Prof. UPC, Barcelona TECH
	Hafedh KOCHKAR:	Professor, FST, Tunisia
Reviewers:	Jordi CAMA:	Professor IDAEA-CSIC, Barcelona
	Lotfi MONSER:	Professor, INSAT, Tunisia

Discussion: ------- February 2016

Abstract

Phosphorus P is mainly present in wastewater as inorganic phosphates, and is commonly removed through chemical co-precipitation using Al(III) and Fe(III) salts. However, precipitation is expensive and generates waste that must be disposed of specific chemical (e.g., the chemical precipitation of crystalline forms) or physico-chemical treatment processes (e.g., ion-exchange, sorption, and membrane-based methods) could be integrated to recover P as pure mineral phases or supported on low-cost inorganic sorbents.

The recovery of phosphate from diluted streams by integrating a pre-concentration step using P-selective sorbents (e.g., metal-hydrated oxide sorbents or metal-hydrated oxide-impregnated ion-exchange resins) to provide concentrated phosphate-containing effluents (e.g., from 0.1 to 2 g $P\text{-}PO_4^{3-}$/L) has been investigated; this process is typically implemented at alkaline pH because of the use of alkaline solutions in the regeneration step (e.g., 1% NaOH).

In this study, recovering P as hydroxyapatite (Hap) from alkaline phosphate concentrates (0.25 to 1 g $P\text{-}PO_4^{3-}$/L) using $CaCl_2$ solutions in batch reactors was evaluated. When alkaline pH values (from 8 to 11.5) were maintained, the Hap-precipitation efficiency was improved. At pH 11.5, a higher P-precipitation rate was observed, but the degree of

crystallinity was lower. Increasing the total initial phosphate concentration led to the formation of Hap powders with higher degrees of crystallinity and crystal diameters but lower mean particle sizes.

Subsequently, the detrimental effects of the presence of Mg (II) in synthetic brines on Hap precipitation were also evaluated. Two synthetic brines with Mg/Ca molar ratios of 2.2 and 3.3 were continuously fed to reach a Ca/P molar ratio of ~1.67 for promoting Hap formation. For both brines, the inhibition of Hap precipitation and the formation of the amorphous mineral phases of Ca, Mg, and Ca/Mg phosphates were observed at pH >9.5. Mg(II) severely inhibited phosphate precipitation, allowing the formation of amorphous Ca phosphate from meta-stable clusters via Mg(II) incorporation into Ca phosphate. In the experiments at pH 8, the formation of stable nanometre-sized pre-nucleation clusters inhibited nucleation, even in supersaturated solutions.

In contrast, phosphate P(V) recovery using low-cost reactive inorganic materials with relatively high efficiency in terms of equilibrium and kinetics has been also evaluated. The integration of powdered inorganic adsorbent fly ashes (FAs) and zeolitic materials for the selective removal of phosphate generated P-containing by-products with fertilising properties. Fly ash (FA) samples from two different coal power stations with different CaO(s) contents (Los Barrios (FA-LB)) and (Teruel (FA-TE)) were evaluated in terms of phosphate removal from aqueous solutions. Under the pH conditions (6 to 9) expected for wastewater treatment plant (WWTP) tertiary effluents, P(V) recovery

proceeds as a combination of CaO(s) dissolution and brushite ($CaHPO_4$(s)) formation on the FA particles; this process avoids the formation of relatively insoluble Ca phosphates, such as Hap, with limited fertilising properties. Removal kinetics data were well described as diffusion-based process and the CaO(s) dissolution was discarded as the rate-controlling step. A powdered zeolitic material synthesised from FA (NaP1-NA) and its Ca-modified form (CaP1-NA) were also studied as sorbent materials for the recovery of phosphate from treated wastewater effluents. The sorption capacities of both zeolites at the expected pH values for wastewater effluents (7 to 9) were slightly dependent on pH. The stabilities of the loaded phosphate zeolite samples as fertilisers were evaluated by extraction experiments, thus measuring their potential availabilities in soil applications.

Finally, the P(V)-removing performance of Ca-activated powdered zeolite (CaP1) was evaluated by integrating the sorption step and solid-phase recovery using a hybrid sorption-UF system with a hollow fibre module.

Resumen

El fósforo presente en las aguas residuales, mayoritariamente en formas inorgánicas, es eliminado a través de co-precipitación con sales de Al (III) y Fe (III) sales suponiendo un coste en reactivos y la imposibilidad de recuperarlo. Con objeto de desarrollar procesos de recuperación de P (V) para cumplir con los requisitos legislativos futuros se ha evaluado la

integración de los procesos químicos de precipitación en reactores agitados o sobre adsorbentes inorgánicos selectivos a aniones fosfato.

Una primera alternativa evaluada ha sido la recuperación de fosfato en forma de hidroxiapatita (Hap) utilizando concentrados alcalinos (0.2 -2 g $P\text{-}PO_4^{3-}$/L a pH 12) obtenidos en procesos de desorción de adsorbentes y resinas de intercambio y utilizando disoluciones de Ca(II). La eficiencia del proceso de precipitación de Hap incrementa con el incremento de pH (de 8 a 11.5). Siendo máxima a pH 11,5 pero con una pérdida de cristalinidad. El incremento de la concentración inicial de fosfato favorece la formación de Hap con un incremento del tamaño de los cristales y de la cristalinidad.

Se evaluaron los efectos de la presencia de magnesio (II) en los concentrados de cloruro de calcio en la precipitación de Hap utilizando dos salmueras sintéticas con relaciones molares Mg/Ca de 2.2 y 3.3. La presencia de Mg (II) inhibe la precipitación de Hap favoreciendo la formación de fases de fosfato de calcio, fosfato de magnesio y fosfato de calcio y magnesio en general amorfas debido a incorporación de iones Mg(II) a valores de pH > 9,5. A valores de pH 8 la precipitación supuso, la formación de clusters estables de pre-nucleación de tamaño nanométrico que promueven la inhibición de la nucleación, incluso en disoluciones sobresaturadas.

Una segunda vía de recuperación de fosfato se basó en el uso de adsorbentes inorgánicos reactivos ricos en Ca(II), como cenizas volantes y zeolitas sintetizadas a partir de cenizas volantes, para su valorización directa como fuentes de fertilización de liberación controlada. Se han evaluado dos muestras de cenizas volantes de plantas de combustión de

carbón que se caracterizan por diferentes contenidos de CaO (s). La recuperación de P(V) en las condiciones esperadas de pH, en efluentes de tratamiento secundarios de estaciones de depuración, tiene lugar a través de una disolución de CaO (s) y la formación de brushita ($CaHPO_4$(s)) sobre la partículas de las cenizas volantes evitando la formación de fosfatos de calcio más insolubles como como Hap. El proceso de extracción de P(V) se describe por un proceso con una cinética controlada por difusión de los iones fosfato en la partícula de adsorbente y donde la reacción de disolución de CaO (s) no es la etapa de control de la velocidad de recuperación de P(V). En una segunda fase se evaluaron una zeolita sódica sintetizada a partir de cenizas volantes (NaP1-NA) y su forma cálcica (CaP1-NA) comprobándose que su capacidad de adsorción está influenciada por el pH y mostrando máximas capacidades de adsorción a pH 8. El proceso va acompañado por la adsorción inicial de los iones fosfato y la formación de precipitados de brushita como en el caso de las cenizas volantes. Los ensayos de disponibilidad de P(V) en las muestras de cenizas volantes y de zeolitas utilizando ensayos de especiación y fraccionamiento indicaron que podrían ser utilizadas como fertilizantes de liberación controlada de P(V). Por último, el rendimiento del proceso de adsorción de P(V) con las muestras de zeolitas activadas con Ca (CAP1) se evaluó mediante la integración de la etapa de sorción y la recuperación de fase zeolita mediante el uso de un sistema de híbrido de adsorción y separación por membranas de ultrafiltración usando módulos de fibra hueca.

To the memory of my father and my mother

El HEDI&MABROUKA

To my sister and my brothers

To who are precious to me

Acknowledgments

What made this challenging PhD possible and indeed, what made this thesis what it is, were the numerous mentors I gained as I travelled across the globe. Mentors come in all shapes and sizes, from supervisors and colleagues, to friends and family to strangers sitting next to you on flights from Tunis to Barcelona. This web of mentors knew what tricky or reflective questions to ask, and supported my transdisciplinary approach and research when others were dismissing it as unconventional. Through my doctoral travels, there's been an unbelievable growing network of mentors, friends, colleagues and administrators who have supported my research in many ways.

I had the opportunity to be part of a joint- supervision thesis (Cotutelle thesis) with the University of Carthage (ENMA-INSAT) and Universitat Politècnica de Catalunya (EQ- ETSEIB) and to collaborate with several laboratories (Water Technology Center CETaqua, Institute of Environmental Assessment and Water Research IDAEA, Consejo Superior de Investigaciones Científicas (CSIC)). This PhD study has been supported by two projects "Valorización de sub-productos de efluentes industriales: 1) Integración de tecnologías de membranas en las etapas de separación, concentracion y purificación (Waste2Product) (CTM2014-

57302-R) and 2) Integración de procesos de membranes intercambio iónico y precipitación química en la valorización de concentrados de tratamientos de desalación de agua (ZERODISCHARGE) (CTQ2011-26799).

The work with these institutions and projects allowed me to deepen my scientific knowledge and feed my taste for research, learning from the best in each research area. It also enabled me to learn new techniques and refine my critical thinking. I had excellent scientific discussions but also made real friends. Therefore I would like to sincerely thank the people who have been part of this thesis for their support and dedication over the last years.

Firstly, I'd like to acknowledge my wonderful Supervisors. Like any long-term relationship, the student-supervisor dynamic is incredibly important. I was so fortunate to have Professor José Luis Cortina Pallas (UPC-Spain) and Professor Narjès Harrouch Batis (INSAT-Tunisia) as Supervisors. Thank you both deeply for your supervision for their continuous guidance, encouragement, availability to discuss ideas and willingness to give knowledge and correction throughout the last few years, and for letting me pursue my ideas. They have been inspiring and most supportive at difficult times. Above all, I thank them for allowing me to continue my study and stimulating my interest in research.

I thank particularly Dr. Cesar Alberto Valderrama (Professor ETSEIB-UPC) for his support, guidance, assistance and availability. For his scientific advice and knowledge with many insightful discussions, correction and his helpful suggestions.

For this dissertation I gratefully acknowledge, Professor JamelEddine BELGAIED (INSAT-Carthage University, Tunisia) for having accepted the role of president of my Ph.D reading committee.

I would like to thank: Professor Lotfi MONSER (INSAT-Carthage University, Tunisia) and Professor Jordi CAMA (Instituto de Diagnóstico Ambiental y Estudios del Agua, IDAEA-CSIC, Barcelona- Spain) for agreeing to act as Rapporteur of my reading committee members. And I would also like to thank Professor Basu Saha (School of Engineering London South Bank University-UK) for having accepted to act as extern rapporteur for the UPC international thesis agreement.

I would also like to thank the other two members as examinators of my oral defense committee, Professor Hafedh KOCHKAR (FST, Tunisia) and Professor. Oriol GIBERT (UPC, Barcelona TECH).

A huge thanks to Professor Latifa BERGAOUI (INSAT- Tunisia) for all the valuing and encouraging, advice and all the administrative help for the thesis committee and deposit.

Finally I thank to Dr. Joan Dosta (UB-Barcelone), Dr. Natalia Moreno, Professor Oriol Font and Professor Xavier Querol, (IDAEA-CSIC) for the work collaboration, also to Isaac Lopez (UPC- Barcelone) and to all the administrators at both universities.

Last but not the least; I thank all the friends with whom I spent good times in the last years. I would like to thank my old friends, but also all the friends I've met along the way.

Glossary

ACP	Amorphous calcium phosphate
BR	Batch Reactors
CEC	Cation Exchange Capacity
CEEP	Centre Européen d'Etudes sur les Polyphosphates
CFA	Coal Fly ash
C_s	saturation concentration
C_{ss}	suspended solid concentration
CSD	Size Crystal Distribution
CSTR	Continuous stirred tank reactors
DCPD	Dicalcium phosphate dehydrate (brushite)
D_e	Effective diffusion coefficient ($m^2 \cdot s^{-1}$)
EPA	Environmental Protection Agency
FAO	Food and agriculture organization
FA-LB	Fly ash Los Barrios
FA-TE	Fly ash Teruel
FWHM	Full-width at half-maximum
g	gram
Hap	Hydroxyapatite
HPDM	Homogeneous Particle Diffusion Model
IAP	Ion Activity Product
IE	Inhabitant Equivalent
IUPAC	International Union of Pure and Applied Chemistry
J	Permeation flux (J ($L.m^{-2}.h^{-1}$)
JCPDS	Joint Committee en Powder Diffraction
K_F	Mass transfer coefficient ($m\ s^{-1}$)
K_s	Reaction constant based on surface ($m\ s^{-1}$)
K_{li}	rate constant (film diffusion)
K_{so}	Solubility product
q_m	Maximum sorption capacity (mg/g)
Lp	Water permeability (Lm^2h^{-1}/bar)
MAP	Struvite
MF	Microfiltration
NF	Nanofiltration
NOM	Natural organic matter
OCP	Octacalcium phosphate
P	Phosphorous
PAZ	Powdered Calcium Activated Zeolites
P(V)	Phosphate
PZC	Point of Zero Charge
r	average particle radius, m
R_m	Hydrodynamic resistance
RO	Reverse Osmosis
R_p	Removal efficiency
R^*_t	Total resistance of the membrane (m^{-1})
S	Surface area (m^2 /g)

SEM-EDX	Scanning Electron Microscopy coupled with Energy Dispersive X-ray
SOC	Synthetic organic chemical
SI	Supersaturation index
SPM	Shell progressive model
τ	Crystallite size
Tg	1000 million kg
TMP	Transmembrane pressure (kPa)
t	Time
TCP	Tricalcium phosphate
TOC	Total organic carbon
UF	Ultrafiltration
wt-w/w	Percentage by Weight (%)
WWC	World Water Council
WWTP	Waste Water Treatment Plant
X	Fractional attainment of equilibrium
X_c	Fraction of crystalline phase
μ	Solution viscosity (Pa·s)
ρ	Theoretical density

Table of contents

List of Figures

List of Tables

List of Scientific Articles

Published Articles

1- Hermassi. M, Valderrama. C, Dosta. J, Cortina. J.L, Batis, N.H., 2015. Evaluation of Hydroxyapatite crystallization in a batch reactor for the valorisation of alkaline phosphate concentrates from wastewater treatment plants using calcium chloride. Chemical Engineering Journal.(267)142-152 (5-Year Impact factor: 4.621).

2- Hermassi. M, Valderrama. C, Dosta. J, Cortina. J.L, Batis, N.H., 2016. Detrimental effects of magnesium (II) on hydroxyapatite precipitation from synthetic industrial brines. Chemical Engineering Journal. (283) 572-581 (5-Year Impact factor: 4,621)

3- M. Hermassi, C. Valderrama, N. Moreno, O. Font, X. Querol, N.H. Batis and J.L. Cortina., 2016. Powder activated calcium zeolite for phosphate removal from treated wastewater. Journal of Chemical Technology & Biotechnology (5-Year Impact factor: 2,616).
DOI: 10.1002/jctb.4867

Articles under review

4- M.Hermassi, C. Valderrama, N. Moreno, O. Font, X. Querol, N.H. Batis and J.L. Cortina. Valorisation of phosphate by immobilization onto Ca(II) rich wastes as potential slow release fertilizer. Journal of Environmental Science and Pollution Research: A manuscript number has been assigned ESPR-[EMID:412820a8b4d50f6e] (5-Year Impact factor: 2.920).)

5- M. Hermassi, C. Valderrama, O. Gibert, N. Moreno, O. Font, X. Querol, N.H. Batis and J.L. Cortina. Integration of Powdered Calcium Activated Zeolites in a hybrid sorption-membrane ultrafiltration process (PAZ-UF) for phosphate recovery. Journal of the Taiwan Institute of Chemical Engineers (Impact factor: 3.000**)**

Introduction and objectives

Water stress and water scarcity are critical issues in many regions worldwide. More than 1.1 billion people currently live without access to potable water, and the availability of potable water has diminished by 37% in the last 30 years (AGUA, 2007). Additionally, the demand for water is expected to increase as a result of both increasing population and the uncontrolled expansion of industrial and agricultural activities (Meneses M., 2010). If no measures are taken, two thirds of the world's population will likely suffer from water stress by 2025 (WWC. World Water Council, 2000). Furthermore, the exploitation of underground aquifers in developing areas where the construction of wastewater treatment plants (WWTPs) is not possible urgently requires new solutions and sustainable water-treatment technologies.

Phosphate pollution is an increasing problem because of the growth of industrial activities involving phosphate manipulation and discharges from domestic WWTPs. P is a macronutrient constituent of most biological tissues and is a basic material used in agriculture and the fertiliser, chemical, and metal-plating industries. However, it is also a major concern in environmental chemistry. Throughout recent decades, the wastewater treatment industry has identified the discharge of nutrients, including

phosphates and nitrates, into waterways as posing a threat to natural environments because of the serious effects of eutrophication.

The removal of P has been widely studied, and currently, two effective and reliable methods have been established: chemical precipitation and biological removal (Morse, 1993). In most chemical treatment methods, P is removed from sewage by precipitation with a metal salt, i.e., Fe, Al and, especially, Ca salts (Donnert and Salecker, 1999; House, 1999). P removal through biological means has been developed during the last twenty years and is now beginning to compete with the more conventional physico-chemical precipitation approach, primarily for municipal wastewater and animal manure treatments. Both chemical and biological methods both allow P to be recycled as a sustainable product for use as raw materials in industrial or agricultural applications (Greaves et al., 1999; Bradford-Hartke et al., 2012).

As a result, the recovery of P from wastewater has become a prospective alternative solution for both water pollution and P depletion. Indeed, the valorisation of P wastes could be achieved by conversion into fertiliser by-products with agricultural applications. Advanced technologies and materials science research are offering very reliable solutions able to compete with traditional methods because of their easy application and high efficiency. Two different phosphate-valorisation approaches are evaluated in this thesis:

1) Ca(II) desalination brines from nanofiltration (NF) and reverse osmosis (RO) treatments can be used for hydroxyapatite (Hap) precipitation. The main drawback of this desalting technology is the disposal of the rejected

brine, which is generally drained back into the sea. For economic reasons, other methods, such as dilution with seawater, are not commonly applied because of their extra cost (Mickley et al. 2006). Reusing these brines can be promising in terms of reducing the resulting environmental impact; giving value to by-products, such as Ca phosphate (e.g., apatite), as raw materials for the fertiliser industry, and creating synergies between industries.

2) The removal of phosphate from wastewaters has been linked to the need for their direct reuse and valorisation as fertiliser. Both of these needs can be satisfied by using a reactive material capable of achieving high phosphate-removal ratios in solution and being used as a slow-release fertiliser in soil and agricultural applications (Desmidt et al., 2015). Two different Ca(II)-rich Ca sorbents were considered: a) coal fly ash (CFA) and b) zeolites synthesised from fly ash (FA) with microporous structures based on alumina silicate minerals with ion-exchange properties (Singer et al., 2005). This thesis evaluates FA and zeolites as potential sorbents for phosphate recovery from aqueous solution and as phosphate carriers for use in synthetic fertilisers.

1. Objectives

The main objective of this thesis is to assess the viability of using Ca(II)-rich brines, solid wastes, and by-product wastes for phosphate removal from aqueous streams (e.g., industrial and domestic) as Ca phosphates. Depending on the chemical composition and mineralogy of the Ca phosphate by-products, these recovered materials could be used as raw

materials in the fertiliser industry or, potentially, directly applied as soil enhancers to remediate degraded soils or as slow-release fertilisers for agricultural applications.

Thus, in addition to the main objective stated above, the following specific objectives were also pursued:

- Evaluating the suitability of desalination brines and domestic and industrial effluents as sources of Ca and phosphate ions, respectively for producing Ca phosphates (e.g., Hap or Ca phosphates and brushite).
- Understanding the influence of interfering ions (e.g., sulfate and Mg) on the precipitation and crystallisation of Ca phosphates (minerals phases precipitated and physico-chemical properties).
- Evaluating combustion coal FAs (CFAs) with high CaO(s) contents as reactive sorbents for phosphate removal from aqueous solutions: characterising the phosphate-removal mechanisms, identifying the phosphate mineral forms obtained, and determining the equilibrium and kinetic sorption properties (sorption isotherms and sorption kinetic rates).
- Activating and modifying synthetic zeolites (NaP1) produced from CFAs via hydrothermal processes to imbue them with phosphate ion-sorption capacities after conversion to Ca(II) forms.
- Evaluating powdered Ca-activated zeolites (Ca-P1) as reactive sorbents for phosphate removal from aqueous solutions: characterising the phosphate-removal mechanisms, identifying the phosphate mineral forms obtained, and determining the equilibrium

and kinetic sorption properties (sorption isotherms and sorption kinetic rates).

- Identifying the optimal conditions for phosphate removal by FA and Ca-activated zeolites, evaluating the influence of interfering ions present in the solution, and quantifying the phosphate availability from the phosphate-containing by-products with regard to their applications as slow-release fertilisers.
- Evaluating the integration of powdered activated zeolites as reactive sorbents for the removal of phosphate from aqueous solutions using a hybrid sorption-membrane separation in an ultrafiltration pilot plant (PAZ-UF): determining the hydraulic performance parameters and phosphate-removal performance.

2. Overview of the thesis

This thesis is organised in six chapters. In the first part, the motivation, research aims, and thesis outline are described.

Chapter 1 presents the state-of-the-art P cycle, the different P-recovery methods used in wastewater treatment, and brief descriptions of the FA and zeolite structures and their phosphate sorbent-related properties.

It also introduces the Ca-phosphate crystallisation/precipitation process and the particular case of the Hap system. Furthermore, an overview of the use of membranes in water treatment, particularly ultrafiltration (UF), is given.

The main experimental results are presented in Chapters 2 to 6.

Chapter 2 describes a study of P recovery as Hap ($Ca_5(PO_4)_3OH$(s)=Hap) from alkaline phosphate concentrates (0.25 to 1 g P-PO_4^{3-}/L) using $CaCl_2$ (6 g /L) in a batch reactor.

In Chapter 3, which builds on Chapter 2, a deep analysis of the detrimental effects of Mg(II) on P recovery as Hap from alkaline phosphate concentrates using synthetic desalinated industrial brines as the Ca source in a batch reactor is provided.

The aims of Chapters 4 and 5 is to provide an understanding of phosphate removal using Ca-rich FA and a powdered zeolitic material synthesised from FA (NaP1-NA) and its Ca-modified form (CaP1-NA) as sorbent materials for the recovery of inorganic phosphates from treated wastewater effluents. Chapter 6 covers the performance of Ca-activated powdered zeolite (CaP1) in removing P(V) from aqueous solutions in a hybrid sorption-UF system with a hollow fibre module. Finally, the last part is dedicated to summarising the main conclusions of the thesis and presenting recommendations and suggestions for future work.

Chapter 1

State of the art: Integration of separation processes for phosphate valorisation from secondary wastes

‘‘Life can multiply until all the phosphorus has gone and then there is an inexorable halt which nothing can prevent. We may be able to substitute nuclear power for coal, and plastics for wood, and yeast for meat, and friendliness for isolation - but for phosphorus there is neither substitute nor replacement.”
(Isaac Asimov, 1974)

1. P challenges: Environmental, recovery, and recycling concerns

P is an element required for life for which there is no substitute. Human adults contain approximately 0.7 kg of P in their bodies, and approximately 85% occurs as Ca phosphate salts in the bones and teeth (Lehninger, 1988). P is also present in polynucleotide structures (DNA and RNA) and membrane lipids and plays an essential role in photosynthesis because it is contained in adenosine triphosphate (ATP), a key molecule involved in energy transport during the metabolic functions of living beings. For these reasons, P is incorporated in feed (approximately 1.7 g/day, according to the FAO annual report) (FAO, 2004), and its presence in the soil is a key requirement in intensive agriculture.

Ninety-five per cent of the P used for fertilising purposes comes from phosphate rock deposits, which contain approximately 33% P_2O_5 on average (Vaccari, 2011), as shown in Figure 1.1. However, this is a non-renewable source of P that requires between 10 and 15 million years to form. Based on the annual consumption rate in 2011 (19 million tons per year), it is estimated that current phosphate rock resources will become depleted in the coming century, and this depletion could be exacerbated by the growing crop demands linked to the increasing population, which could result in an increasing demand of between 2.7 and 4.4% annually (*CEEP*, 2011).

Sustainability is an important environmental concern that is increasingly incorporated in corporate strategies, governmental policies, and international agreements, such as the Rio Summit Agenda 21 (United Nations, 1993). P is an important element that makes major contributions to agricultural and industrial development. However, its release into surface waters via agricultural runoff and wastewaters has led to legislation, such as the European Union Urban

Wastewater Directive (Commission of the European Communities. 1991), designed to remove P from domestic and industrial wastewaters.

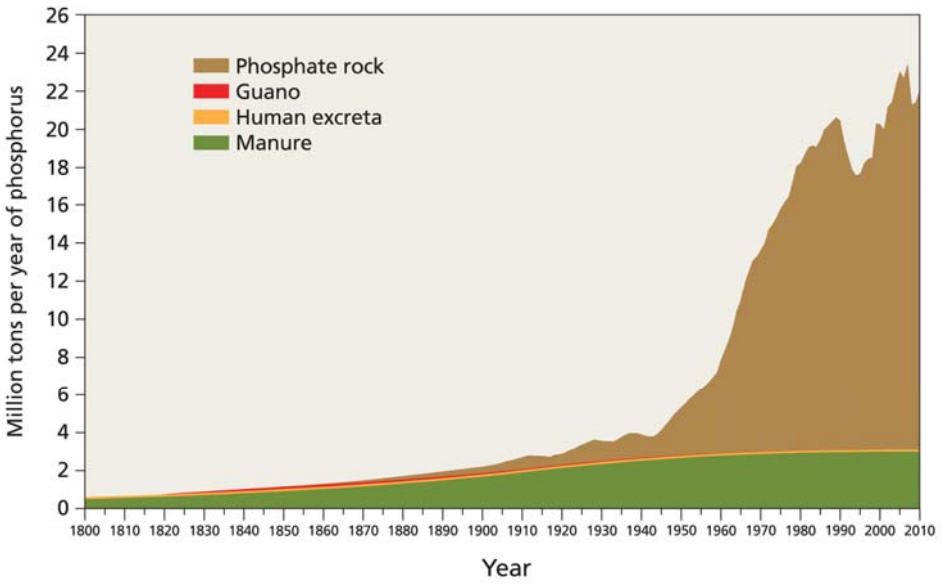

Figure 1.1. P sources used for agriculture 1800–2010 (Cordell et al., 2009).

The development of P-removal technology offers the opportunity to recycle P and increase the sustainability of the P cycle. However, a number of technologies, both established and under development, can be used to remove P from wastewater and that may potentially be included in sustainability strategies.

P-removal strategies began to be developed in the 1950s in response to issues with eutrophication and the need to reduce the levels of P entering surface waters. Removal was initially achieved by chemical precipitation, which remains the leading technology today. More recently, however, biological P removal has become firmly established, crystallisation technology has been commercialised, and technologies extending chemical precipitation to facilitate nutrient removal have progressed beyond the pilot stage. Other relevant technologies are at various stages of development or have been investigated (Morse et al., 1998).

1.1. P Cycle

P is a life-essential, non-renewable element, and the biomass potential of the Earth is P limited (Smil, 2000; Filippelli, 2008). Because P is often in short supply for optimal plant and animal growth and development, farmers use P fertilisers and P additives. P also has many industrial applications, including in household detergents. Nearly all the P used in chemical fertilisers and feeds is derived from phosphate-rich rocks, which are located in a few places on Earth. Because Europe has no significant phosphate resources, it is highly dependent on imported phosphate ore (Ridder et al., 2012). The current worldwide P reserves are estimated at 67,000 Tg P (1 Tg = 1000 million kg), and the global mining production in 2013 was 220 Tg P (Survey., 2014). Approximately 75% of the known reserves are located in Morocco (Western Sahara), which is the main exporter of phosphate ore. China and the USA also have significant reserves, but they do not sell phosphate ore on the global market, thereby further limiting the supply available to other countries (Schoumans et al., 2015). In nature, P passes through several interconnected cycles (Figure 1.2). The inorganic P cycle includes erosion, transport to the oceans, sedimentation, tectonic up lift, and phosphate alteration. The P cycle time is several million years, i.e., in terms of human lifetimes, phosphate transported into the oceans can be considered as “lost” to agricultural use. In addition to the inorganic P cycle, two organic cycles describe P as part of the food chain. One of occurs on land (soil–plants–humans/animals–organic waste–soil), and the other occurs in water. The cycle times of these processes range from a few weeks to one year (Bennett, E. & Carpenter, 2002).

These “natural” closed cycles are interrupted when the P compounds in animal and human excrements are not used in fertilisation. In this case, the

phosphate contained in wastewater is partly transported to the oceans via discharge systems and partly fixed in sewage sludge, which is deposited in landfill sites or incinerated; in the latter case, the P contained in the ash is deposited in landfill sites or subterranean storage. Similar processes are relevant for organic fertilisers (solid and liquid manure) from intensive stock-rearing (Cornel and Schaum, 2009).

As a result of modern human activities and associated industrialisation, the P cycle has been broken, and increasing quantities of P are discharged into natural water bodies from land. As illustrated in Figure 1.2, phosphate rock is mined and used in both agricultural applications (mainly as fertiliser) and industrial applications. Without P-recovery techniques, P-enriched waste is produced by sewage treatment. According to Cornel and Schaum (Cornel and Schaum, 2009), on average, 11% of the incoming P load is removed with the primary sludge during primary settlement in WWTPs. In biological treatment using activated sludge, 20-30% of the incoming P load is incorporated into the biomass and removed with the surplus sludge, even when no specific biological P-removal processes are used (Parsons and Smith, 2008). The disposal of P into natural water bodies has a major impact on the aquatic ecosystem. This phenomenon, which is known as eutrophication, leads to a sharp decline in aquatic biodiversity the loss of potable water resources and contributes to the formation of oceanic dead zones.

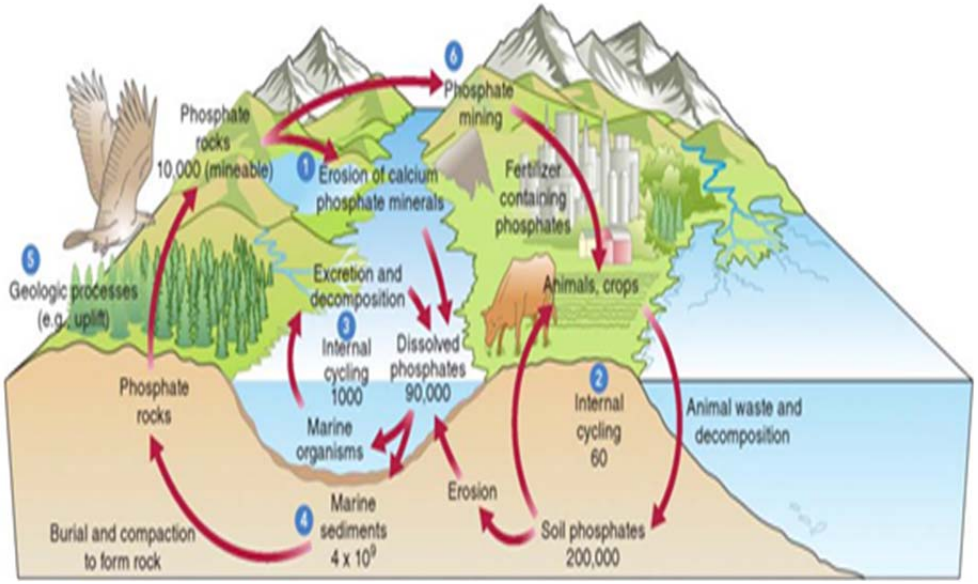

Figure 1.2. Simplified diagram of the global P cycle. The flow is presented in units of 1012 g P $year^{-1}$ (E. Solomon et al., 2010)

Therefore, phosphate discharges must be limited by increasingly stringent regulations to protect surface waters from eutrophication. Based on the permitted discharge concentrations of 1 $mg.L^{-1}$ P (10,000–100,000 inhabitant equivalent (IE)) or 2 $mg.L^{-1}$ P (> 100,000 IE) in Europe (Council Directive 91/271/EEC), approximately 50% most of the incoming P load must also be removed (Desmidt et al., 2015). Even more stringent regulations are being implemented in the USA, reducing the discharge limits to 0.1 $mg.L^{-1}$ P (U.S. Environmental Protection Agency (EPA), 2007).

1.2. Established P-removal and recovery technologies in the wastewater cycle

Phosphate-recovery technologies developed for industrial or municipal wastewater treatment can be applied at various points in the treatment process. In Figure 1.3, various applications of potential P-recovery processes

are illustrated in a model WWTP. A–C indicate the potential locations of P recovery from the liquid phase, i.e., the WWTP's effluent (A), the supernatant liquor from side-stream treatment (B), and the sludge liquor (C). As for all treatment processes, the P removed with the sewage sludge is "lost", and thus, the theoretical recovery potential from the liquid phase in common activated sludge plants is limited to 50–60% (Cornel and Schaum, 2009). The numbers 1–6 indicate the potential applications of P recovery from sewage sludge, i.e., primary (1), excess (2), and raw sludge (3); stabilised sludge before and after dewatering (4 and 5); and sewage sludge ash (6). As in WWTPs without P removal, 90–95% of the incoming P load is contained in the sewage sludge, and therefore, the theoretical recovery potential for this process is significantly higher than that of separation processes from the aqueous phase (Cornel and Schaum, 2009).

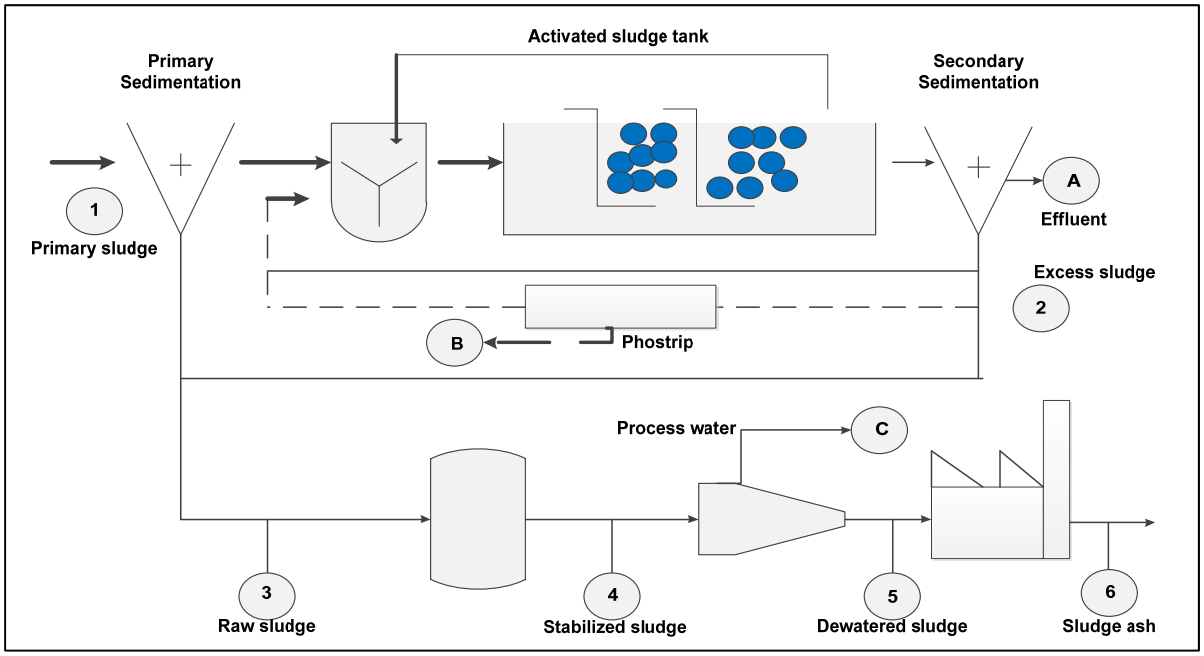

Figure 1.3. Different streams (1–6) in a WWTP suitable for the installation of P-recovery technologies (Cornel and Schaum, 2009).

Recent research has shown that P recovery is especially successful in combination with biological P removal in side streams (supernatant liquor from the anaerobic reactor) or process water during sludge treatment. P can be recovered from wastewater, sewage sludge, and sewage sludge ash, and a number of full-scale techniques are already operational. Currently, most techniques aim to recover phosphate from dewatering reject streams.

These techniques recover P from the wastewater by feeding the P-rich wastewater into a mixed precipitation/crystallisation tank or in a fluidised state. Ca or Mg salts and seed crystals (when needed) are added to recover phosphate as Ca phosphate (brushite or Hap) or Mg ammonium phosphate (struvite).

P can be also recovered from sewage sludge and sewage sludge ash by a wet chemical or a thermal method. Currently, one wet chemical method and two thermal techniques are applied in full-scale processes, and several others are under development (Lodder, and Meulenkamp, 2011).

If sludge is incinerated in a mono-incineration plant (Figure 1.3), a high-P concentrate (P ash) can be produced from waste streams (Kabbe, 2013). The P content in municipal sludge ash ranges between 4 and 13% (w/w). However, because of the low plant availability of the nutrient and the heavy metal contents of the ash, further treatment is needed before the ash can be fully utilised as a P source. Because of the lack of ash-treatment facilities and interim storage capacity, most of the P in the ash is not recovered as easily soluble mineral P. The production of fertiliser from ash via a thermochemical method, such as in the AshDec Process (Outotec) (Adam and Krüger, 2013), involves treating the ash at approximately 1000ºC to remove heavy metals and increase the bio-availability of the P in the ash. This process produces a Mg-

enriched dicalcium phosphate that can be marketed as chemical fertiliser. An alternative is wet chemical extraction, known as the EcoPhos Process, which was developed in cooperation with companies with experience in treating low-quality phosphate ore. The EcoPhos process produces phosphates suitable for use in animal feed.

The Mephrec process combines thermal valorisation and P recovery in a single step. This technology even offers the possibility of recovering precious metals in addition to P. The resulting P-rich slag is suitable for fertiliser production and is comparable to the well-known Thomas phosphate, a by-product of steel production (Schoumans et al., 2015)

2. Towards new solutions for P recovery and valorisation in the wastewater cycle

It is commonly believed that precipitation/crystallisation processes can be used to recover P from the liquid phase as either Ca phosphates, which are similar to phosphate rocks, or as Mg ammonium phosphate hexahydrate (struvite), which is a slow-release fertiliser.

2.1. Phosphate recovery by precipitating Ca phosphates

Most Ca orthophosphates are sparingly soluble in water, and the Ca-to-phosphate molar ratios (Ca/P) and solubilities are important parameters used to distinguish between the phases (Table 1.1). Generally, lower Ca/P ratios correlate with relatively acidic and soluble Ca phosphate phases. The crystallisation of many Ca phosphates involves the formation of metastable precursor phases that subsequently dissolve as the precipitation reactions proceed. Thus, complex intermediate phases may participate in the

crystallisation process (V. Dorozhkin, 2012). Studies of apatite formation are complex because of the possible formation of several Ca phosphate phases. The least soluble of these phases, Hap, is preferentially formed under neutral or basic conditions. In more acidic solutions, other phases, such as brushite (DCPD) and octacalcium phosphate (OCP), are often encountered. Even under ideal Hap-precipitation conditions, the precipitates are generally nonstoichiometric, suggesting the formation of Ca-deficient apatites. Both DCPD and OCP have been implicated as possible precursors for apatite formation, which may occur by the initial precipitation of DCPD and/or OCP, followed by transformation to a more apatitic phase (Amjad et al., 1984).

Ca phosphates have been synthesised using many methods (Lagno et al., 2012), including solid-state or glass ceramic synthesis (Pramanik et al., 2007), mechanochemical synthesis, precipitation in a heterogeneous system (microemulsion, emulsion liquid membrane system, and polyol-mediated synthesis) (Jarudilokkul et al., 2007), sol−gel synthesis, and aqueous precipitation (Rodríguez-Lorenzo and Vallet-Regí, 2000). Aqueous precipitation represents an attractive option because it is a green synthesis route (Demopoulos, 2009) that is better suited for environment-related applications. For the aqueous precipitation of Hap, a variety of procedures and starting salts have been used as sources of phosphates and Ca ions. Paschalis et al. (Paschalis et al., 1994) precipitated nanocrystalline Hap by mixing $(NH_4)_2HPO_4$ and $Ca(NO_3)_2$ solutions and using an NH_3 solution to adjust the pH to 10 for 5 h. Similarly, nanocrystalline Hap was synthesised by Mobasherpour et al. (Mobasherpour et al., 2007) using the same reagents at higher concentrations and pH 11. Recently, Hap was precipitated by Gomes et al. (Gomes et al., 2008) by the reaction of $Ca(OH)_2$ and H_3PO_4 at different

temperatures and pH values, which were controlled with NH_3. Rodriguez-Lorenzo and Vallet-Regi (2000) precipitated apatites with different stoichiometries and morphologies using $Ca(NO_3)_2$ and $(NH_4)_2HPO_4$ using different temperatures, reaction times, and pH values.

Table 1.1. Ca/P Molar Ratios, Chemical Formulas, and Solubilities of Some Ca Orthophosphate Minerals (Wang and Nancollas, 2008)

Ca/P molar ratio	Compound	formula	-log(*K*so)
1.0	Brushite (DCPD)	$CaHPO_4 \cdot 2H_2O$	6.59
1.0	Monetite (DCPA)	$CaHPO_4$	6.90
1.33	Octacalcium phosphate (OCP)	$Ca_8(HPO_4)_2(PO_4)_4\ 5H_2O$	96.6
1.2- 2.2	Amorphous calcium phosphate (ACP)	$Ca_xH_y(PO_4)_z\ nH_2O$, n =3-4.5; 15-20% H_2O	ND
1.5	α-tricalcium phosphate (α-TCP)	α-$Ca_3(PO_4)_2$	25.5
1.5	*β*-tricalcium phosphate (β-TCP)	*β*-$Ca_3(PO_4)_2$	28.9
1.67	Hydroxyapatite (Hap)	$Ca_{10}(PO_4)_6(OH)_2$	116.8
1.67	Hluorapatite (FAP)	$Ca_{10}(PO_4)_6F_2$	120.0

Ca phosphate precipitation is very complex, involving different metastable regions and depending on Ca and phosphate ion concentrations, supersaturation, ionic strength, temperature, ion type, pH, and reaction time for solid–solid transformation (Montastruc et al., 2003). Different Ca phosphate phases form in different pH regions. For example, dicalcium phosphate dihydrate (brushite) is kinetically favoured when the precipitation pH is maintained below 6.0 (Lagno and Demopoulos, 2005). In contrast, the formation of octacalcium phosphate, $Ca_8(HPO_4)_2(PO_4)_4 \cdot 5H_2O$, is favoured when precipitation occurs at solution pH values between 6.0 and 7.0, whereas when the pH exceeds 7.0, Hap is the expected final phase (Graham and

Brown, 1996). The boundaries between each phase at pH 6.0 and 7.0, which are shown in Figure 1.4, are only approximate, and they help to define the precipitation strategy selected for to synthesise dicalcium phosphate dihydrate and Hap (Lagno et al., 2012).

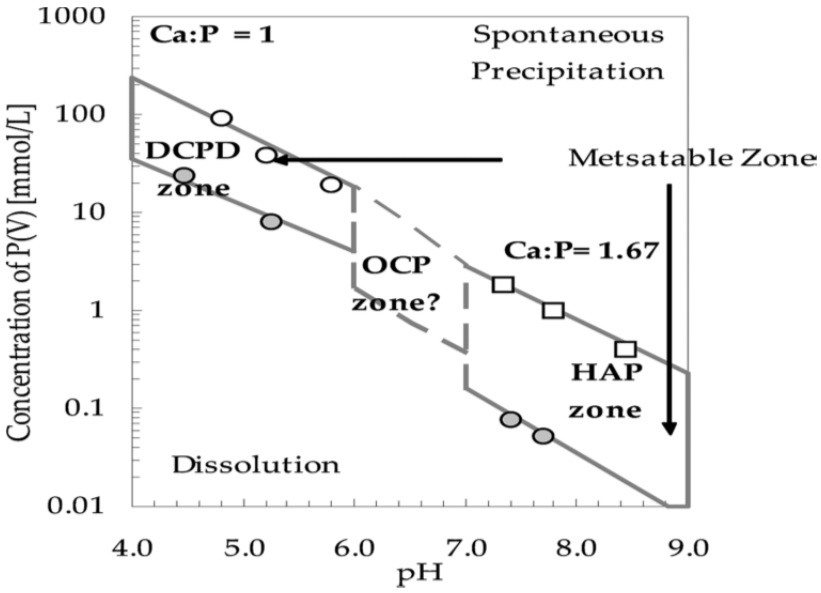

Figure 1.4. Precipitation diagram for the synthesis of Ca phosphate phases at 22ºC: $CaHPO_4.2H_2O$ (DCPD), $Ca_8(HPO_4)_2(PO_4)_4.5H_2O$ (OCP), and $Ca_{10}(PO_4)_6(OH)_2$ (Hap) (Lagno et al., 2012).

However, in practice, the kinetics of Ca phosphate precipitation play a more important role than thermodynamic equilibrium considerations (Desmidt et al., 2015). In most cases, the spontaneous precipitation of Ca phosphate does not occur at all or only under very high oversaturation, and the effects of some inhibitors account for this phenomenon. Carbonate and ammonium are the most important species in wastewater that contribute to its buffering capacity at alkaline pH values (Vanotti and Szogi, 2009).

2.2. Phosphate recovery as Hap

The latest trends in P removal are focused on recovering phosphates as marketable fertilisers, such as Hap or struvite (MAP), via controlled crystallisation in specific reactors. Hap formation has been pursued and widely developed in crystallisation reactors, such as the DHV Crystalactor® (Montastruc et al., 2003), where Ca is added as $Ca(OH)_2$. Crystallisation is a thermodynamic-dependent phenomenon, in which stable nucleus formation occurs first, followed by crystal growth. In the processes mentioned above, different chemicals are needed to modify the inlet ion concentrations and/or the pH. However, in practice, crystallisation occurs during the final stage of a series of reactions in which a number of relatively easily soluble Ca phosphates (precursors) are produced; according to Henze (1997), these species determine the phosphate solubility. Thus, the P-removal yields can decrease if other apatites are formed, as when the OH^- ion is substituted by F^- or when PO_4^{3-} is substituted by CO_3^- and Ca^{2+} is replaced by Na^+, Fe^{3+}, Al^{3+}, Mg^{2+}, or Zn^{2+}. Apatite formation is not the only process that can disrupt the production of the desired crystalline Hap; more amorphous and soluble compounds can also arise: $CaHPO_4$, $Ca_4H(PO_4)_3$, and $Ca_3(PO_4)_2$. These compounds determine the phosphate solubility if high concentration of Mg^{2+}, poly-phosphate, or HCO_3^- are present in the wastewater.

Several disadvantages are associated with the implementation of precipitation in such a system, especially in terms of the reproducibility and product quality. These systems are characterised by heterogeneous spatial and temporal distributions of process parameters, such as temperature and concentration, resulting in a variable supersaturation environment (Sultana, 2010) and thereby affecting the final product properties. Indeed, mixing problems have

been encountered in stirred batch reactors. Macromixing is achieved by intensive stirring, but micromixing is not controlled at all. Additionally, the products of batch precipitation often have wide size distributions, which result from inhomogeneous mixing, and broad residence time distributions (Jones et al., 2005).

Because of the limitations of stirred batch reactors, various systems have been used to achieve better control over reaction conditions. Among them, semi-batch configurations have been used to overcome homogeneity problems in the supersaturation distribution in the vessel. In this configuration, the precipitant is added in a controlled manner to ensure constant supersaturation (Demopoulos, 2009). Continuous stirred tank reactors (CSTRs) have also been used (J. Gomez-Morales, 2001) because they offer stable supersaturation because of their steady-state operation. Such systems usually produce fine particles with a wide size distribution. Recently, micro-devices have been applied for the continuous-flow precipitation of Hap to solve the mixing problems associated with stirred tank batch reactors. Various configurations have been used, ranging from a simple tubular reactor, in which a mixing part that is generally T-shaped is sometimes included, to more complex systems (Yang et al., 2010) (Kandori et al., 2011). Tubular micro-reactors are very interesting because of their relative easy use; however, problems with channel clogging limit their application at the industrial level (Jongen et al., 2003).

2.3. Phosphate recovery by reactive sorbents

Precipitation and biological treatment techniques are sensitive to seasonal and daily variations in temperature and changes in feed concentrations and have

limited capacities for achieving low phosphate concentrations. In contrast, sorption methods could overcome these problems (Choy et al., 2004). The efficacy of sorption technology depends on the choice of an appropriate sorbent. The screening strategies commonly used to choose sorbents are selectivity, capacity, reuse, local availability, compatibility, kinetics, and cost. Given the fact that no single sorbent can meet all the requirements, substantial attention been devoted to the development of several potential sorbents (Oguz, 2004) that may be suitable in local conditions.

The first attempt to sequentially remove ammonium and phosphate using cationic and anionic resins, respectively, was the ***RIM-NUT***® process (Liberti et al., 1986). The main drawbacks of this process were the lack of phosphate ion-selective sorbents; the resulting competition with NO_3^-, HCO_3^-, and SO_4^{2-} ions; and the long resin-regeneration times with NaCl. Recently, the use of weak-base anion exchangers impregnated with hydrated ferric oxides (HFOs), originally developed as a possible way to reduce toxic anions, such as arsenic, in drinking water applications, has been proposed for the removal of phosphate from wastewaters. However, various factors affect the phosphate removal, including the phosphate concentration, dissolved organic matter, water hardness, and presence of competitive ions and suspended solids (Sarkar et al., 2011; Awual et al., 2011). Considerable attention has been paid to developing effective and low-cost adsorbents from natural materials for phosphate adsorption with agricultural reuse potential (Jellali et al., 2010; X. Xu et al., 2010). In particular, natural and synthetic Ca compounds have been recently identified as potential materials for P removal (Yin et al., 2011).

2.3.1. Phosphate recovery by sorption-precipitation on reactive sorbents: Application of Ca-rich FA

Sorption and precipitation processes can be combined to improve total phosphate removal efficiency and recover P in a valuable mineral form. It is thus possible to take advantage of biological processes to concentrate the phosphate stream (enhance the ion supersaturation) and facilitate precipitation in a relatively soluble form (Mg or Ca phosphate instead of metallic phosphates).

FA is the most abundant by-product generated during the combustion of coal in power plants. The International Union of Pure and Applied Chemistry (IUPAC) defines FA as particles of ash blown into the combustion gases resulting from fuel combustion. Worldwide, coal ash generation exceeds 600 million tons of FA, and currently, a substantial portion of this material is deposited in landfills or dumped in the environment and is a cause for environmental concern. The utilisation rate varies between 3 and 57%, with the world average being 16% (Blissett and Rowson, 2012). The use of FA is attracting research and industrial attention regarding reducing its environmental impact and possibly generating a profit. The potential benefits and problems associated with the direct use of FA on land intended for agriculture to enhance the physical and chemical properties of the soil has also been studied in depth (Ahmaruzzaman, 2010).

The main components of coal FA (CFA) are SiO_2, Al_2O_3, Fe_2O_3, CaO, MgO, K_2O, Na_2O, and TiO_2, with varying amounts of carbon. However, the composition of CFAs varies significantly, and the chemistry of these materials is determined by the type of coal burned (Blissett and Rowson, 2012). According to the American Society for Testing Materials (ASTM) (2005), ash

containing more than 70 wt% SiO_2 + Al_2O_3 + Fe_2O_3 and being low in lime is defined as Class F, while those with SiO_2 + Al_2O_3 +Fe_2O_3 contents between 50 and 70 wt% and that are high in lime are defined as Class C. Briefly, high-Ca Class C FAs are normally produced by burning low-rank coals (lignites or sub-bituminous coals) and have cementitious properties (self-hardening after reacting with water). In contrast, low-Ca Class F FAs are commonly produced by burning higher-rank coals (bituminous coals or anthracites) that are pozzolanic in nature (hardening after reacting with $Ca(OH)_2$ and water). The main differences between Class F and Class C FAs are the Ca, silica, alumina, and Fe contents in the ash. In Class F FAs, total Ca typically ranges from 1 to 12% and mostly occurs as Ca hydroxide, Ca sulfate, and glassy components combined with silica and alumina. In contrast, Class C FAs have reported Ca oxide contents as high as 30–40%. Recently, Vassilev and Vassileva (2007) presented a new classification system based on an analysis of 41 European CFAs. This system groups the main bulk oxides together to create a four-tier classification to facilitate assessing a particular CFA for use in applications other than cement.

Kuziemska first reported the use of a water extract of brown CFA as a coagulant for phosphate precipitation. (Kuziemska, 1980). CFA has attracted substantial attention as a potential material for phosphate removal because it is easily available and cost effective (Tsitouridou and Georgiou, 1988; Gray and Schwab, 1993; Ahmaruzzaman, 2010). Ugurlu and Salman (1998) reported a Turkish FA as an efficient adsorbent for phosphate because of its high concentration of calcite (34%), and the influences of temperature, phosphate concentration, and FA dosage on phosphate removal were investigated.

The presence of Al, Fe, Ca and Mg oxides imbues FA with suitable properties for phosphate removal by complexation reactions with the metal oxides or the precipitation of Ca/Mg-phosphates (Grubb et al., 2000; Pengthamkeerati et al., 2008). Cheung and Venkitachalam (Cheung and Venkitachalam, 2000) associated the removal of phosphate by FA with high- and low-Ca contents by Ca phosphate precipitation and by Ca phosphate precipitation and ion exchange with Fe oxides, respectively. Johansson and Gustafsson (Johansson and Gustafsson, 2000) proposed the formation of amorphous Ca phosphate and/or octacalcium phosphate as the major P-removal mechanism and suggested the direct formation of Hap as the predominant phosphate-removal mechanism. Although it is generally accepted that the phosphate removal by FA involves adsorption and/or precipitation mechanisms, the interaction between phosphate and Ca incompletely described (Lu et al., 2009).

Additionally, only limited effort has been dedicated to obtaining a solution for the exhausted ash, and recently, the possibility of using these materials to improving the soil quality of areas degraded by mining or civil construction infrastructure and for forestry applications has been proposed (Yao et al., 2015). However, because of the low solubility and availability of the typically precipitated Ca phosphate mineral ($Ca_5(PO_4)_3OH(s)$, $logK_{so}$=116.8) (Parvinzadeh Gashti et al., 2013), efforts have been made to prepare relatively soluble phosphate-containing minerals, such as brushite ($CaHPO_4.2H_2O$, $logK_{so}$=6.59) (Dorozhkin, 2012)), by promoting the growth of mineral forms on the surface of Ca-containing sorbents with suitable properties for slow-release fertilisers. These sorbents include Ca silicates, such as wollasonite (Liu and Ding, 2002); Ca-Al layered double hydroxide (Watanabe et al., 2010; Zhou et

al., 2012); natural zeolites (Guaya et al., 2015); and FA (K. Xu et al., 2010). However, utilising powdered inorganic adsorbents in water treatment for selective P removal and subsequent use as slow-release fertilisers remains under development, and the equilibrium and kinetic performances remain to be characterised.

2.3.2. Phosphate recovery by sorption-precipitation on reactive sorbents: Application of zeolites

Zeolites are crystalline Al–silicates with group I or II elements as counter ions. Their structure consists of a framework of $[SiO_4]^{4-}$ and $[AlO_4]^{5-}$ tetrahedra linked to each other at their corners by shared oxygens atoms (Scott et al., 2003). These tetrahedra make up a three-dimensional network, with abundant voids and open spaces. These voids create the various unique properties of zeolites, such as the adsorption of molecules in their large internal channels. The substitution of Si(IV) by Al(III) in the tetrahedra gives the structures a negative charge, resulting in high cation-exchange capacities when the open spaces can be accessed by cations. A representative empirical formula of an oxide form is provided in Eq. 1 (Jacobs et al., 2001):

$$M_{2/n}O \cdot Al_2O_3 \cdot ySiO_2 \cdot wH_2O \quad (1)$$

where M represents the counter ions, n is the counter ion valence, and y indicates the degree of hydration and is generally equal to or greater than 2 because the AlO_4 tetrahedra are joined only to SiO_4 tetrahedra. The framework contains channels and interconnected voids, which are occupied by cations and water molecules. The cations are exchangeable and typically from group I or II.

Zeolites exhibit micro-porosity with uniform pore dimensions, ion-exchange properties, the ability to exhibit acidity, high thermal stability, and reversible hydration ability. The pores, which generally range between 3 and 10 Å in diameter, can allow certain molecules to pass through and reject others. This gives zeolites selective adsorption properties (Pfenninger, 1999). The chemical composition of a zeolite plays an important role in determining its properties. The valence of the T-atoms will affect the charge of the framework; for example, a pure silicate framework has a neutral charge, whereas an aluminosilicate framework will have a negative charge. Similarly, the composition affects the zeolite's affinity for different molecules by controlling the material's hydrophobicity and hydrophilicity. The guest species inside the channels of the zeolite are also important. In the case of a charged framework, these species are needed to balance the charge. The size of the cations that can be introduced into the zeolite structure depends on the size of the channels (Byrappa, K. & Yoshimura, 2001).

The synthesis of zeolites is attracting attention as an effective use of wastes, such as CFA, possibly because its composition is similar to that of natural precursors, such as volcanic material. Zeolite synthesis conventionally involves hydrothermal crystallisation under alkaline conditions (Querol et al., 2002). However, mullite and quartz in ash are inert and difficult to dissolve. The mechanism of zeolite synthesis consists of an alkali hydrothermal reaction involving three steps (see Figure 1.5): i) the dissolution of the alumina (Al_2O_3) and silica (SiO_2) precursors from the FA (especially from the glass phase) in a strongly alkaline solution, ii) the deposition of the initial aluminosilicate gel, and iii) zeolite crystallisation (Elliot and Zhang, 2005; Rees et al., 2007):

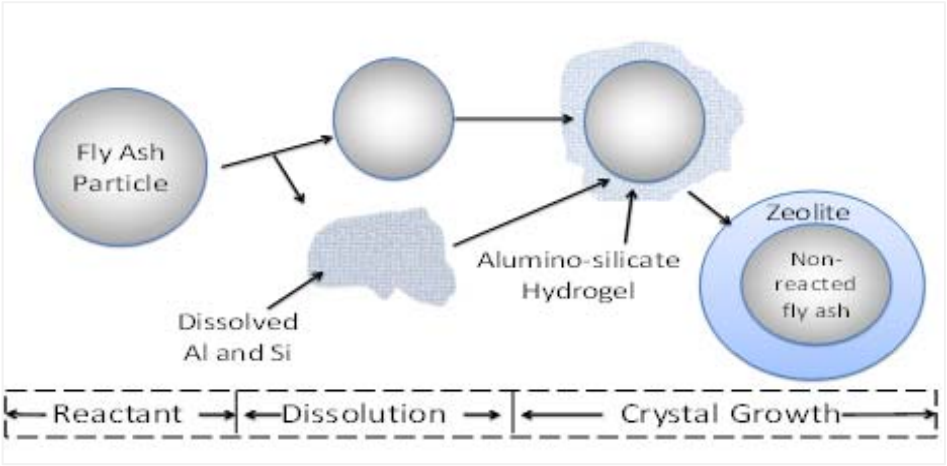

Figure 1.5. Reaction mechanism for the batch hydrothermal conversion of FA to zeolite (Elliot and Zhang, 2005).

In addition to the development of synthesis methods, intensive research has been performed to investigate the potential application of zeolites synthesised from FA. This material's high Al(III)/Si(IV) ratio provides a high CEC of up to 5 meq g^{-1} in some of zeolites, such as NaP1, 4A, X, KM, F, chabazite, herschelite, and faujasite. As a result, these zeolites have great potential for selective wastewater treatment (Ahmaruzzaman, 2010).

The removal of phosphate from wastewaters has been linked to the need for their reuse and valorisation, which can be achieved using a reactive material capable of achieving high phosphate-removal ratios in solution and that can be used as a slow-release fertiliser in soil and agricultural applications (Desmidt et al., 2015). Such a process could be developed depending on the availability of low-cost sorbents (Boyer et al., 2011). Querol et al. (2007) demonstrated the economic and technical viability of synthesising NaP1-NA under mild hydrothermal conditions without using templates. NaP1-NA was evaluated for the removal of toxic metals from acid mine drainage and brines (Moreno et al., 2001) because of its high porosity, surface area, and CEC and its unusual

framework flexibility (Cama et al., 2005). NaP1-NA also has a high capacity to adsorb ammonium and K and has been evaluated as a slow-release fertiliser; however, the sorption of oxyanions as phosphate is not facilitated by the zeolite structure (Watanabe et al., 2014). The use of mixtures of synthetic apatites and natural zeolites as solid media for growing plants and as a fertiliser has been postulated (Golden and Ming, 1999; Liu and Lal, 2014). However, because of the low solubility and availability of P from Hap in soils, efforts have been devoted to preparing relatively soluble Haps ($Ca_{10}(PO_4)_6(OH)_2$, Hap) or brushite ($CaHPO_4.2H_2O$) by growing crystals on the surface of Ca-containing minerals. These materials include Ca silicates, such as wollasonite (Liu and Ding, 2002); Ca-Al layered double hydroxide; and Hap (Watanabe et al., 2010; Zhou et al., 2012). However, little work has been done to prepare reactive materials to a) efficiently remove phosphate from wastewater effluents in the form of relatively soluble phosphates (e.g., brushite ($\log K_{so}$=6.59)) (Dorozhkin, 2012) instead of Hap ($Ca_5(PO_4)_3OH$(s), $\log K_{so}$=116.8) (Parvinzadeh Gashti et al., 2013) and b) achieve suitable properties for use as a synthetic slow-release fertiliser.

2.4. Phosphate recovery from aqueous solution by process integration: Sorption and membrane filtration

Membranes act as selective barriers, allowing some constituents (e.g., fluids) to pass through the membrane while i) blocking the passage of other constituents, as in solid separation, or ii) rejecting the dissolved species to be removed from the fluid. The movement of material across a membrane requires a driving force (i.e., a potential difference across the membrane); in the membrane processes commonly used in water treatment applications,

pressure is used as the driving force. Membrane technology has evolved significantly in the last decades, becoming increasingly applied in water treatment plants (Pressdee et al., 2006). This is particularly the case for low-pressure membrane systems (microfiltration (MF) and UF).

Membrane processes are being evaluated for phosphate recovery using NF (NF90, NF90, and HL) with synthetic and real wastewaters, and removal ratios ranging from 70 to 90% have been reported (Mohammad et al., 2007). The P-removal efficiency has been correlated with membrane properties, such as membrane charge and membrane pore radius, and membranes with smaller network pore sizes are more effective at rejecting ionic species. Membranes with larger pore sizes (such as DK5 and MPF34) resulted in lower P removal ratios at high concentrations of P than NF270 and NF200 membranes with smaller pore sizes. A highly charged membrane is better able to exclude coexisting ions from the membrane surface (e.g., phosphate ions), and decreasing the pH of the feed solutions improves the rejection ability (e.g., pH 2 for MPF34 membranes and pH 4 for DK5, DL, and NF270) (Niewersch, 2008).

Applications of pressure-driven membrane processes, such as MF and UF, have expanded in recent years as an alternative method of developing hybrid sorption/filtration systems. This expansion is attributable to the fact that UF has been shown to be an effective physical barrier to particles and colloids that are larger than the UF membrane pores and, hence, are retained by size-exclusion mechanisms, among others. Furthermore, UF provides additionally advantages over conventional treatments, including its small footprint, low energy consumption, limited chemical dosing, ability to cope with wide fluctuations in feed quality and deliver a permeate of relatively constant

quality, and relatively low scale-up risks (Lee et al., 2008). The water recovery in MF/UF systems is typically 85 to 97% and is a function of the backwash frequency and the backwash-disposal method. That is, more frequent backwashing typically results in lower recoveries. Membrane backwashing is accomplished using air, water, or a combination. Ideally, the backwash process restores the trans-membrane pressure (TMP) to the same value after each backwash.

Limited work has been performed regarding the engineering aspects of validating the integration of powdered sorbents, such as zeolites, in continuous sorption and stream-processing using membrane filtration (e.g., MF, UF, or NF). The addition of a powdered adsorbent to the membrane filtration influent is a simple and cost-effective way to remove compounds [e.g., natural organic matter (NOM) and synthetic organic chemicals (SOCs)] that cannot be removed by the membrane itself (Matsui et al, 2001). The addition of powdered activated carbon (PAC) was proposed two decades ago and is now an accepted hybrid use of adsorbent in an UF membrane system (Anselme C et al., 1997) (Chang et al., 1998). The development of hybrid process, such as PAC/UF, combines the adsorption capacity of PAC with the ability of the UF membrane to retain microorganisms and particles (including PAC particles), thereby facilitating the removal of low-molar mass compounds that cannot be removed by the UF membrane itself (large pore size). PAC/UF is a low-pressure (<1 bar) process, and thus, it has a relatively low operating cost (Campinas and Rosa, 2010). By taking advantage of the benefits afforded by this integration, this thesis will evaluate the integration of powdered Ca-activated zeolites (PAZ) with hollow fibre UF membranes for phosphate removal.

Using suspended adsorbent particles (e.g., PAZ) to recover target species (e.g., phosphate) from aqueous solution can result in rapid fouling of the membrane, decreased flux, and increased TMP. During the filtration phase, the resistance against water transport through the membrane will increase because of membrane fouling. Fouling that can be removed using backwashing alone is defined as **reversible fouling**. Fouling that is strongly adsorbed on the membrane surface or embedded within the porous structure of the membrane cannot be removed by backwashing and is defined as **irreversible fouling**. When the amount of irreversible fouling becomes too high or after a predetermined number of filtration-backwash cycles, the membrane must be chemically cleaned (as described schematically in Figure 1.6). All filtration-backwash cycles and the subsequent chemical cleaning constitute a single **chemical cleaning cycle**. Ideally, chemical cleaning removes all irreversible fouling from the membrane.

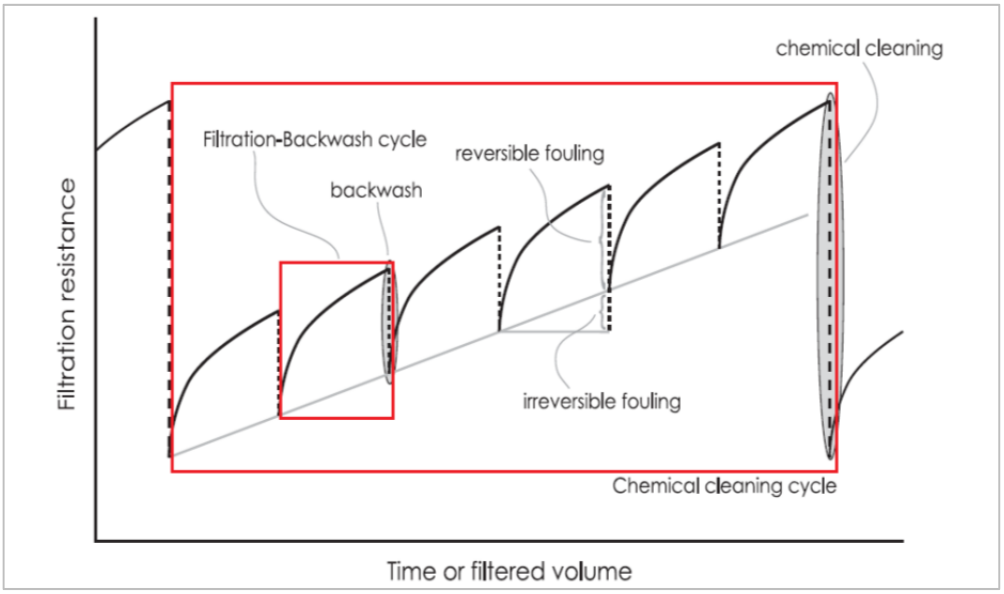

Figure 1.6. Schematic evolution of filtration cycles in a hybrid sorption-filtration system: reversible fouling and irreversible fouling are defined based on the

evolution of filtration resistance with the volume of filtered water (Wilhelmus Johannes Cornelis van de Ven, 2008) .

Yildiz (2004) investigated the removal of phosphate by FA in a crossflow MF system and demonstrated that the separation of phosphate-loaded FA by crossflow membrane filtration was better than classical batch separation in terms of efficiency. However, when the phosphate concentration in the feed solution increased, phosphate rejection decreased because of decreased reactor pH and insufficient Ca ion concentration. Recently, an adsorption-UF process for the recovery of phosphate-loaded sorbents was investigated by Zelmanov and Semiat, (2014). Both the Fe oxide/hydroxide (Fe^{3+})-based agglomerated adsorbent and the pH strongly influenced the phosphate-removal efficiency. A residual phosphate concentration of less than 0.1 mg/L as P, which is acceptable for wastewater pre-treatment, and at least 95–98% phosphate-regeneration efficiency were achieved with the proposed adsorbent. The phosphate-adsorption capacity of the hybrid system at a residual phosphate concentration of 0.1 mg/L exceeded previously reported values by more than one order of magnitude (Zelmanov and Semiat, 2011).

However, limited work has been devoted to the engineering aspects of validating the integration of powdered sorbents, such as zeolites, in continuous sorption and stream processing using membrane filtration (e.g., MF, UF, or NF). One challenge faced by this study is the investigation of phosphate removal in a hybrid system using powdered activated zeolite (PAZ) in an agitated reactor followed by an UF system. The effects of process parameters, such as the initial phosphate concentration, pH, and PAZ dose effect, were evaluated.

3. References

Adam, C., Krüger, O., 2013. Wertstoffpotential in deutschen Klärschlammaschen. Energ. aus Abfall 10, 997–1014.

AGUA “Dossier Bibliográfico de publicaciones sobre política y gestión del agua, 2007.

Ahmaruzzaman, M., 2010. A review on the utilization of fly ash. Prog. Energy Combust. Sci. 36, 327–363.

Amjad, Z., Koutsoukos, P., Nancollas, G., 1984. The crystallization of hydroxyapatite and fluorapatite in the presence of magnesium ions. J. Colloid Interface Sci. 101, 250–256.

Anselme C., Laine´ J. M., Baudin, I. and Chevalier. M.R., 1997. Drinking water production by UF and PAC adsorption. First months of operation for a large capacity plant, in: Proceedings of the American Water Works Association Membrane Conference New Orleans, LA, USA. 783–804.

ASTM standard specification for coal fly ash and raw or calcined natural pozzolan for use in concrete (C618-05). In: Annual book of ASTM standards, concrete and aggregates., 2005. , American Society for Testing Materials.

Awual, M.R., Jyo, A., El-Safty, S. A., Tamada, M., Seko, N., 2011. A weak-base fibrous anion exchanger effective for rapid phosphate removal from water. J. Hazard. Mater. 188, 164–171.

Bennett, E. & Carpenter, S., 2002. P Soup–The Global Phosphorus Cycle. Cycle. World Watch Mag. 24–32

Blissett, R.S., Rowson, N. A., 2012. A review of the multi-component utilisation of coal fly ash. Fuel 97, 1–23.

Boyer, T.H., Persaud, A., Banerjee, P., Palomino, P., 2011. Comparison of low-cost and engineered materials for phosphorus removal from organic-rich surface water. Water Res. 45, 4803–4814.

Bradford-Hartke, Z., Lant, P., Leslie, G., 2012. Phosphorus recovery from centralised municipal water recycling plants. Chem. Eng. Res. Des. 90, 78–85.

Byrappa, K. & Yoshimura, M., 2001. Handbook of Hydrothermal Technology: A Technology for Crystal Growth and Materials Processing, Publications., Park Ridge, New Jersey, U.S.A, Noyes.

Cama, J., Ayora, C., Querol, X., Ganor, J., 2005. Dissolution kinetics of synthetic zeolite NaP1 and its implication to zeolite treatment of contaminated waters. Environ. Sci. Technol. 39, 4871–7.

Campinas, M., Rosa, M.J., 2010. Assessing PAC contribution to the NOM fouling control in PAC/UF systems. Water Res. 44, 1636–1644.

CEEP: Centre d'Etudes Européen des Polyphosphates, 2011. , ScopeNewsletter.

Chang, Y., Choo, K., Benjamin, M.M., Reiber, S., 1998. Combined adsorption-OF process increases TOC removal. J. Am. Water Work. Assoc. 90, 90–102.

Cheung, K.C., Venkitachalam, T.H., 2000. Improving phosphate removal of sand infiltration system using alkaline fly ash. Chemosphere 41, 243–249.

Choy, K.K.H., Porter, J.F., McKay, G., 2004. Film-pore diffusion models-analytical and numerical solutions. Chem. Eng. Sci. 59, 501–512.

Commission of the European Communities. Directive concerning urban wastewater treatment, 1991. Off. J. 91/271/EEC.

Cordell, D., Drangert, J.O., White, S., 2009. The story of phosphorus: Global food security and food for thought. Glob. Environ. Chang. 19, 292–305.

Cornel, P., Schaum, C., 2009. Phosphorus recovery from wastewater: needs, technologies and costs. Water Sci. Technol. 59, 1069–76.

Demopoulos, G.P., 2009. Aqueous precipitation and crystallization for the production of particulate solids with desired properties. Hydrometallurgy 96, 199–214.

Desmidt, E., Ghyselbrecht, K., Zhang, Y., Pinoy, L., Van der Bruggen, B., Verstraete, W., Rabaey, K., Meesschaert, B., 2015. Global Phosphorus Scarcity and Full-Scale P-Recovery Techniques: A Review. Crit. Rev. Environ. Sci. Technol. 45, 336–384.

Donnert, D., Salecker, M., 1999. Elimination of Phosphorus from Waste Water by Crystallization. Environ. Technol. 20, 735–742.

Dorozhkin, S. V., 2012. Self-Setting Calcium Orthophosphate Formulations: Cements, Concretes, Pastes and Putties. Int. J. Mater. Chem. 1, 1–48.

Solomon, E., Berg, L., and Martin, D., 2010. Biology, in: 9th Ed. Cengage Learning.

Elliot, A.D., Zhang, D., 2005. Controlled Release Zeolite Fertilisers : A Value Added Product Produced from Fly Ash 1–32.

FAO, 2004. The State of Food Insecurity in the World, Monitoring progress towards the World Food Summit and Millennium Development Goals 4–40

Filippelli, G.M., 2008. The global phosphorus cycle: Past, present, and future. Elements 4, 89–95.

Golden, D.C., Ming, D.W., 1999. Division s-9-soil mineralogy 664, 657–664.

Gomes, J.F., Granadeiro, C.C., Silva, M. A, Hoyos, M., Silva, R., Vieira, T., 2008. An Investigation of the Synthesis Parameters of the Reaction of Hydroxyapatite Precipitation in Aqueous Media. Int. J. Chem. React. Eng. 6, 1–15.

Graham, S., Brown, P.W., 1996. Reactions of octacalcium phosphate to form hydroxyapatite. J. Cryst. Growth 165, 106–115.

Gray, C. A, Schwab, A. P., 1993. Phosphorus- fixing ability of high pH, high calcium, coal-combustion, waste materials. Water, Air, and Soil Pollution. 69, 309–320.

Greaves, J., Hobbs, P., Chadwick, D., Haygarth, P., 1999. Prospects for the Recovery of Phosphorus from Animal Manures: A Review. Environ. Technol. 20, 697–708.

Grubb, D.G., Guimaraes, M.S., Valencia, R., 2000. Phosphate immobilization using an acidic type F fly ash. J. Hazard. Mater. 76, 217–236.

Guaya, D., Valderrama, C., Farran, A., Armijos, C., Cortina, J.L., 2015. Simultaneous phosphate and ammonium removal from aqueous solution by a hydrated aluminum oxide modified natural zeolite. Chem. Eng. J. 271, 204–213.

Henze, Harremöes, La Cour, A., 1997. Waste Water Treatment. Biological and Chemical Processes.

House, W. A., 1999. The Physico-Chemical Conditions for the Precipitation of Phosphate with Calcium. Environ. Technol. 20, 727–733.

Gomez-Morales, J., Torrent-Burgues, J., Rodriguez-Clemente, R., 2001. Crystal Size Distribution of Hydroxyapatite Precipitated in a MSMPR Reactor. Cryst. Res. Technol. 36, 1065–1074.

Jacobs, P.A., Flanigen, E.M., Jansen, J.C., van Bekkum, H., 2001. Introduction to Zeolite Science and Practice, 2nd ed, Studies in Surface Science and Catalysis.

Jarudilokkul, S., Tanthapanichakoon, W., Boonamnuayvittaya, V., 2007. Synthesis of hydroxyapatite nanoparticles using an emulsion liquid membrane system. Colloids Surfaces A Physicochem. Eng. Asp. 296, 149–153.

Jellali, S., Wahab, M.A., Anane, M., Riahi, K., Bousselmi, L., 2010. Phosphate mine wastes reuse for phosphorus removal from aqueous solutions under dynamic conditions. J. Hazard. Mater. 184, 226–233.

Johansson, L., Gustafsson, J.P., 2000. Phosphate removal using blast furnace slags and opoka-mechanisms. Water Res. 34, 259–265.

Jones, A., Rigopoulos, S., Zauner, R., 2005. Crystallization and precipitation engineering. Comput. Chem. Eng. 29, 1159–1166.

Jongen, N., Donnet, M., Bowen, P., Lemaître, J., Hofmann, H., Schenk, R., Hofmann, C., Aoun-Habbache, M., Guillemet-Fritsch, S., Sarrias, J., et al., 2003. Development of a Continuous Segmented Flow Tubular Reactor and the “Scale-out” Concept – In Search of Perfect Powders. Chem. Eng. Technol. 26, 303–305.

Kabbe, C., 2013. Sustainable sewage sludge management fostering phosphorus recovery. bluefacts, wvgw, Rep. 36–41.

Kandori, K., Kuroda, T., Togashi, S., Katayama, E., 2011. Preparation of calcium hydroxyapatite nanoparticles using microreactor and their characteristics of protein adsorption. J. Phys. Chem. B. 115, 653–9.

Kuziemska, I., 1980. Application of water extract of brown coal fly ash to phosphate precipitation from polluted waters. Water Res. 14, 1289–1293.

Lagno, F., Demopoulos, G.P., 2005. Synthesis of Hydrated Aluminum Phosphate , $AlPO_4$,1.5H_2O ($AlPO_4$-H_3), by Controlled Reactive Crystallization in Sulfate Media. Ind. Eng. Chem. Res. 44, 8033–8038.

Lagno, F., Rocha, S.D.F., Katsarou, L., Demopoulos, G.P., 2012. Supersaturation-Controlled Synthesis of Dicalcium Phosphate Dihydrate and Nanocrystalline Calcium-Deficient Hydroxyapatite. Eng. Chem. Res. 51, 6605−6612

Lee, E.K., Chen, V., Fane, a. G., 2008. Natural organic matter (NOM) fouling in low pressure membrane filtration - effect of membranes and operation modes. Desalination 218, 257–270.

Lehninger, 1988. Biochemistry, in: Worth Publishers, Ed. Omega. 807.

Liberti, L., Limoni, N., Lopez, A., Passino, R., Boari, G., 1986. The 10 m^3 h^{-1} rim-nut demonstration plant at West Bari for removing and recovering N and P from wastewater. Water Res. 20(6), 735–739.

Liu, R., Lal, R., 2014. Synthetic apatite nanoparticles as a phosphorus fertilizer for soybean (Glycine max). Sci. Rep. 4, 1–6.

Liu, X., Ding, C., 2002. Morphology of apatite formed on surface of wollastonite coating soaked in simulate body fluid. Mater. Lett. 57, 652–655.

Lodder, R. and Meulenkamp, R., 2011. Fosfaatterugwinning in communale afvalwaterzuiveringsinstallaties (Recuperation of phosphate in communal

wastewater treatment plants). Rep. 2100-24, STOWA, Amersfoort, Netherlands.

Lu, S.G., Bai, S.Q., Zhu, L., Shan, H.D., 2009. Removal mechanism of phosphate from aqueous solution by fly ash. J. Hazard. Mater. 161, 95–101.

Matsui, Y., Yuasa, A., Colas, F., 2001. Effect of operational modes on the removal of a synthetic organic chemical by powdered activated carbon during ultrafiltration. Water Sci. Technol. Water Supply 5/6, 39–47.

Meneses M., Pasqualino J.C., Céspedes-Sánchez R., C.F., 2010. Alternatives for Reducing the Environmental Impact of the Main Residue from a Desalination Plant. J. Ind. Ecol. 14, 512–527.

Mickley and Associates, 2006. Membrane Concentrate Disposal : Practices and Regulation. Desalin. Water Purif. Res. Dev. Progr. Rep. No. 123 123.

Mobasherpour, I., Heshajin, M.S., Kazemzadeh, A., Zakeri, M., 2007. Synthesis of nanocrystalline hydroxyapatite by using precipitation method. J. Alloys Compd. 430, 330–333.

Mohammad, A. W., Hilal, N., Al-Zoubi, H., Darwish, N. a., 2007. Prediction of permeate fluxes and rejections of highly concentrated salts in nanofiltration membranes. J. Memb. Sci. 289, 40–50.

Montastruc, L., Azzaro-Pantel, C., Biscans, B., Cabassud, M., Domenech, S., 2003. A thermochemical approach for calcium phosphate precipitation modeling in a pellet reactor. Chem. Eng. J. 94, 41–50.

Moreno, N., Querol, X., Ayora, C., Pereira, C.F., Janssen-Jurkovicová, M., 2001. Utilization of zeolites synthesized from coal fly ash for the purification of acid mine waters. Environ. Sci. Technol. 35, 3526–34.

Morse, G.K., Brett, S.W., Guy, J. a., Lester, J.N., 1998. Review: Phosphorus removal and recovery technologies. Sci. Total Environ. 212, 69–81.

Morse GK, Lester JN, P.R., 1993. The economic and environmental impact of phosphorus removal from wastewater in the european community. 1er ed Selper Ltd, 92.

Niewersch, C., Koh, C.N., Wintgens, T., Melin, T., Schaum, C., Cornel, P., 2008. Potentials of using nanofiltration to recover phosphorus from sewage sludge. Water Sci. Technol. 57, 707–714.

Oguz, E., 2004. Removal of phosphate from aqueous solution with blast furnace slag. J. Hazard. Mater. 114, 131–137.

Parsons, S. A, Smith, J. A, 2008. Phosphorus Removal and Recovery from Municipal Wastewaters. Elements 4(2), 109–112.

Parvinzadeh Gashti, M., Stir, M., Bourquin, M., Hulliger, J., 2013. Mineralization of Calcium Phosphate Crystals in Starch Template Inducing a Brushite Kidney Stone Biomimetic Composite. Cryst. Growth Des. 13, 2166–2173.

Paschalis, E.P., Wikiel, K., Nancollas, G.H., 1994. Dual constant composition kinetics characterization of apatitic surfaces. J. Biomed. Mater. Res. 28, 1411–1418.

Pengthamkeerati, P., Satapanajaru, T., Chularuengoaksorn, P., 2008. Chemical modification of coal fly ash for the removal of phosphate from aqueous solution. Fuel 87, 2469–2476.

Pfenninger, A., 1999. Manufacture and Use of Zeolites for Adsorption Process. Mol. Sieves. Springer-verlag 2, 164–197, Berlin.

Pramanik, S., Agarwal, A.K., Rai, K.N., Garg, A., 2007. Development of high strength hydroxyapatite by solid-state-sintering process. Ceram. Int. 33, 419–426.

Pressdee, J. R., Veerapaneni, S., Shorney-Darby, H. L., Clement, J. A., Van der Hoek, J.P., 2006. Integration of Membrane Filtration Into Water Treatment Systemes. AWWA Res. Foundation, William D. Taylor, 2–281. U.S.A

Querol, X., Moreno, N., Alastuey, A., Juan, R., Ayora, C., Medinaceli, A., Valero, A., Productos, C., 2007. Synthesis of high ion exchange zeolites from coal fly ash. Geol. Acta 5, 49–57.

Querol, X., Moreno, N., Uman, J.C., Alastuey, A., Hernandez, E., Lopez-Soler, A., Plana, F., 2002. Synthesis of zeolites from coal fly ash : an overview 50, 413–423.

Ragsdale, D., 2007. Advanced wastewater treatment to achieve low concentration of phosphorus. EPA Reg. 10 EPA 910-R-.

Rees, C. A, Provis, J.L., Lukey, G.C., van Deventer, J.S.J., 2007. Attenuated total reflectance fourier transform infrared analysis of fly ash geopolymer gel aging. Langmuir 23, 8170–8179.

Ridder, M. De, de Jong, S., Polchar, J., Lingemann, S., 2012. Risks and Opportunities in the Global Phosphate Rock Market. The Hague Centre for Strategic Studies. Rep 17-12 -12.

Rodríguez-Lorenzo, L.M., Vallet-Regí, M., 2000. Controlled crystallization of calcium phosphate apatites. Chem. Mater. 12, 2460–2465.

Sarkar, S., Chatterjee, P.K., Cumbal, L.H., SenGupta, A.K., 2011. Hybrid ion exchanger supported nanocomposites: Sorption and sensing for environmental applications. Chem. Eng. J. 166, 923–931.

Schoumans, O.F., Bouraoui, F., Kabbe, C., Oenema, O., van Dijk, K.C., 2015. Phosphorus management in Europe in a changing world. Ambio 44, 180–192.

Scott M. Auerbach, Katheleen A. Carrado, Prabir. K. Dutta., 2003. Handbook of Zeolite Science and Technology, 1st ed. Taylor and Francis.

Singer, P. A., Salamanca-Buentello, F., Daar, A.S., 2005. Harnessing nanotechnology to improve global equity. Issues Sci. Technol. 21, 57–64.

Smil, V., 2000. Phosphorus in the environment: Natural Flows and Human Interferences. Annu. Rev. Energy Environ. 25, 53–88.

Sultana, M., 2010. Microfluidic Systems for Continuous Crystallization of Small Organic Molecules. PhD thesis in Chemical Engineering. Massachusetts Institute of Technology.

Survey., U.S.G., 2014. Phosphate rock. In Mineral commodity summaries, ed. S. Jewell, and S.M. Kimball 196. Reston, VA: U.S. Geological Survey.

Tsitouridou, R., Georgiou, J., 1988. A contribution to the study of phosphate sorption by three Greek fly ashes. Toxicol. Environ. Chem. 17, 129–138.

Ugurlu, A., Salman, B., 1998. Phosphorus removal by fly ash. Environ. Int. 24, 911–918.

United Nations Conference on Environment & Development Rio de Janerio, 1993. 351

V. Dorozhkin, S., 2012. Amorphous Calcium Orthophosphates: Nature, Chemistry and Biomedical Applications. Int. J. Mater. Chem. 2, 19–46.

Vaccari, D. A., 2011. Chemosphere Phosphorus Cycle Issue - Introduction. Chemosphere 84, 735–736.

Vanotti, M., Szogi, A., 2009. Technology for recovery of phosphorus from animal wastewater through calcium phosphate precipitation. International Conference on Nutrient Recovery.

Vassilev, S. V., Vassileva, C.G., 2007. A new approach for the classification of coal fly ashes based on their origin, composition, properties, and behaviour. Fuel 86, 1490–1512.

Wang, L., Nancollas, G.H., 2008. Calcium orthophosphates: crystallization and dissolution. Chem. Rev. 108, 4628–69.

Watanabe, Y., Ikoma, T., Yamada, H., Stevens, G.W., Moriyoshi, Y., Tanaka, J., Komatsu, Y., 2010. Formation of hydroxyapatite nanocrystals on the surface of Ca-Al-layered double hydroxide. J. Am. Ceram. Soc. 93, 1195–1200.

Watanabe, Y., Yamada, H., Ikoma, T., Tanaka, J., Stevens, G.W., Komatsu, Y., 2014. Preparation of a zeolite NaP1/hydroxyapatite nanocomposite and study of its behavior as inorganic fertilizer. J. Chem. Technol. Biotechnol. 89, 963–968.

Wilhelmus, Johannes., Cornelis, van de Ven., 2008. Towards Optimal Saving in Membrane Operation The development of process inspection and feedwater characterization tools. Ipskamp B.V., Enschede, Netherlands.

William, J. Cosgrove and Frank, R. Rijsberman, 2000. WWC. World Water Council, “World water vision: Making water everybody’s business. Earthscan Publications Ltd, London.

Xu, K., Deng, T., Liu, J., Peng, W., 2010. Study on the phosphate removal from aqueous solution using modified fly ash. Fuel 89, 3668–3674.

Xu, X., Gao, B.Y., Yue, Q.Y., Zhong, Q.Q., 2010. Preparation of agricultural by-product based anion exchanger and its utilization for nitrate and phosphate removal. Bioresour. Technol. 101, 8558–8564.

Yang, Q., Wang, J.-X., Shao, L., Wang, Q.-A., Guo, F., Chen, J.-F., Gu, L., An, Y.-T., 2010. High Throughput Methodology for Continuous Preparation of Hydroxyapatite Nanoparticles in a Microporous Tube-in-Tube Microchannel Reactor. Ind. Eng. Chem. Res. 49, 140–147.

Yao, Z.T., Ji, X.S., Sarker, P.K., Tang, J.H., Ge, L.Q., Xia, M.S., Xi, Y.Q., 2015. A comprehensive review on the applications of coal fly ash. Earth-Science Rev. 141, 105–121.

Yildiz, E., 2004. Phosphate removal from water by fly ash using crossflow microfiltration. Sep. Purif. Technol. 35, 241–252.

Yin, H., Yun, Y., Zhang, Y., Fan, C., 2011. Phosphate removal from wastewaters by a naturally occurring, calcium-rich sepiolite. J. Hazard. Mater. 198, 362–369.

Zelmanov, G., Semiat, R., 2014. Phosphate removal from aqueous solution by an adsorption ultrafiltration system. Sep. Purif. Technol. 132, 487–495.

Zelmanov, G., Semiat, R., 2011.Phosphate removal from water and recovery using iron (Fe^{3+}) oxide/hydroxide nanoparticles- based agglomerates suspension (AggFe) as adsorbent. Environ. Eng. Manag. J. 10, 1923–1933.

Zhou, J.Z., Feng, L., Zhao, J., Liu, J., Liu, Q., Zhang, J., Qian, G., 2012. Efficient and controllable phosphate removal on hydrocalumite by multi-step treatment based on pH-dependent precipitation. Chem. Eng. J. 185-186, 219–225.

Chapter 2

Evaluation of Hydroxyapatite crystallisation in a batch reactor for the valorisation of alkaline phosphate concentrates from wastewater treatment plants using calcium chloride

This chapter is based on the work presented in the publication:
Hermassi. M, Valderrama. C, Dosta. J, Cortina. J.L, Batis, N.H., 2015. Evaluation of Hydroxyapatite crystallization in a batch reactor for the valorisation of alkaline phosphate concentrates from wastewater treatment plants using calcium chloride. Chemical Engineering Journal.(267)142-152 (5-Year Impact factor: 4.621).

In this chapter, phosphorous recovery as hydroxyapatite ($Ca_5(PO_4)_3OH$(s)=Hap) from alkaline phosphate concentrates (0.25 to 1 g P-PO_4^{3-}/L) using calcium chloride (6 g /L) in a batch reactor was evaluated. Ca(II) solutions was continuously fed (0.1-0.3 mL/min) up to reaching a Ca/P ratio of ~1.67 (5/3) to promote Hap formation. Hap powders were characterized by structural form (using X-ray diffraction (XRD), laser light scattering (LS) and Fourier transform infrared spectroscopy (FTIR)); textural form (using Field Emission Scanning Electron Microscopy with Energy Dispersive System (FE-SEM/EDX) and Brunauer-Emmett-Teller (BET)) and thermally (using Thermogravimetric Analysis (TGA)/Differential Thermal Analysis (DTA)). When pH was kept constant in alkaline values (from 8 to 11.5), Hap precipitation efficiency was improved. At pH 11.5, higher phosphorous precipitation rate was registered compared to that obtained for pH 8 and 10, but lower degree of crystallinity was observed in the Hap powders. The increase of the total initial phosphate concentration lead to the formation of Hap powders with higher degree of crystallinity and crystal diameter, but also lower mean particle size. As Ca(II) dosing rate increased Hap precipitation rate was higher, and also the mean size and degree of crystallinity of the prepared particles increased.

1. Introduction

Phosphorus (P) management has been recently highlighted by the United Nations Environment Program as one of the main emerging problems to be faced in the next decades. The use of phosphorous needs to become more efficient and its recycling more widespread, since the demand for P is increasing and the available phosphorous resources are scarce. For

instance, the excessive P content in wastewaters should be removed for controlling eutrophication and maintaining a sustainable environment for future generations. Several physical, biological and chemical processes include adsorption/ ion exchange, chemical precipitation/coagulation, crystallisation and membrane filtration/ reverse osmosis for the removal and / or recovery of dissolved phosphates (P(V)) in water and wastewaters have been investigated (Bradford-Hartke et al., 2012; Nur et al., 2014; Dhand et al., 2014).

Different research efforts during the last decade, have probed that P recovery at low levels (e.g. 2-10 mg/L), from domestic and urban waste waters is not economically feasible, using conventional removal processes (coagulation, chemical precipitation, adsorption, ion-exchange) (Nur et al., 2014; Liu et al., 2012; Gupta et al., 2012). However, the introduction of new processes using P-selective sorbents (e.g. metal oxides sorbents or metal oxide impregnated ion exchange resins) will provide concentrated effluents of phosphate (e.g. from 0.1 to 2 g P-PO_4^{3-}/L) typically at alkaline pH values (9 to 12) due to the requirements of the regeneration step using 2 to 5% NaOH solutions (Sengupta and Pandit, 2011). The alkaline P(V)-brines are suitable candidates to recover the phosphate content as (calcium, magnesium, ammonium)–phosphate by-products using Ca(II), Mg(II), NH_4^+ brines generated in many industrial effluents, especially in processes using membrane desalination technologies or using low-cost raw materials (Katz and Dosoretz, 2008; Bradford-Hartke et al., 2012; Tran et al., 2014).

In alkaline solutions, calcium phosphates (Ca-P) are highly stable minerals (Diaz et al., 1994) however involve the crystallisation of many metastable precursor phases. Amorphous calcium phosphate (ACP, Ca/P(1.5),

$Ca_3(PO_4)_2.nH_2O$), dicalcium phosphate dihydrate (DCPD, Ca/P(1), $CaHPO_4.2H_2O$, brushite), β-whitlockite (β-TCP, Ca/P(1.5), β-$Ca_3(PO_4)_2$) and octacalcium phosphate (OCP, Ca/P(1.33) $Ca_8H_2(PO_4)_6.5H_2O$). All of them are frequently precipitated at low pH values. Hydroxyapatite (Hap) (Ca/P(1.67), $Ca_5(PO_4)_3OH$) is the less soluble phase, preferentially formed in neutral to basic solutions (Spanos and Patis, 2007; Lagno et al., 2012). Hap, is a compound with a variable composition existing over Ca/P molar ratios from 1.67 for stoichiometric up to ≈1.5 for fully calcium-deficient Hap (Wang and Nancollas, 2008), and sometimes even outside this range (Elliott, 1994). Direct precipitation of Hap has only been observed for low reactants concentrations, that is, slightly supersaturated or under saturated aqueous solutions with respect to a precursor phase (Boskey and Posner, 1974; Seckler, 1996). Thermodynamically, Hap is postulated to control the P(V) concentration in many natural and industrial aqueous streams; however, the remaining P(V) concentration appear to be controlled for lengthy periods by meta-stable phases (Diaz et al., 1994).

Hap synthesis by a precipitation route stands out because of its simplicity, low cost, and easy application in industrial production (Liu et al., 2001; Castro et al., 2012), although other methods are also used. Different procedures and starting salts have been used as source of phosphate (P(V)) and Ca(II) ions. Boskey and Posner (1974), Lagno et al. (2012), and more recently Du et al. (2013) formed Hap by adding a $CaCl_2$ solution of (pH 7.4-7.6) to a solution of Na_2HPO_4 (pH 10-11), or vice versa at 25°C for a Ca/P ratio varied between 1.0 and 1.67.

Koutsoukos et al. (1980) also studied the precipitation of Hap at 37°C. Recently, Castro et al. (2012) prepared Hap in a batch reactor by

neutralization between a saturated $Ca(OH)_2$ solution with orthophosphoric acid solution, using several mixing Ca/P molar ratios (namely, 1, 1.33 and 1.67) at 37°C and a agitation speed of 270 rpm.

Continuous Stirred-Tank Reactor (CSTR), Plug Flow Reactor (PFR) and Batch Reactors (BR) have been set up to study phosphate crystallisation. Some researchers have demonstrated that BR have the advantage of providing extreme flexibility of operation and at the same time being physically simple, since all the treatment operations (i.e. flow equalization, precipitation reactions and solids settling) take place in one single tank. Castro et al. (2013b) also studied the continuous flow precipitation of Hap performed in a meso oscillatory flow reactor at laboratory and pilot-scale at 37°C, at a molar ratio Ca/P of 1.33.

Phosphorous recovery is a topic of great concern nowadays and Hap precipitation has been reported as a suitable process to recover phosphate in a BR, thus, the integration of different technologies (sorption/ion exchange-precipitation) in a waste water treatment scheme can provide an alternative solution for phosphorous recovery. In view of that, the main objective of this work was to assess the recovery of phosphate P(V) from alkaline brines by using Ca(II) solution to precipitate Hap under different experimental conditions in a BR. The alkaline brines were obtained from a P(V) concentration process from waste water using iron-oxide impregnated ion-exchange resins. The Hap precipitation process was evaluated as a function of pH, as well as the Ca(II) dosing rate, the stirring speed and phosphate initial concentration. The Hap precipitates obtained under these operation conditions were properly characterized through the degree of crystallinity, the crystal diameter, the particle size distribution and the thermal analysis.

2. Materials and Methods

2.1. Experimental set-up and procedures

The precipitation of phosphate from aqueous solutions was performed in a two liters lab-scale batch reactor made of glass as can be seen in Figure 2.1. Agitation in the reactor was provided by a mechanical stirrer (IKA RW 20 and Heidolph RZR) and the stirring speed was ranged from 50 to 250 rpm. pH was monitored in-line by using a pH potentiometer (Crison pH 28). When pH was 0.1 units above or below the set point, strong acid (HCl 1M) or strong base (NaOH 1M) were dosed using a peristaltic pump (Master flex console drive). Experiments batch tests were carried out mixing a volume of NaH_2PO_4 solution (with an initial phosphate concentration between 0.25 to 1.0 g $P\text{-}PO_4^{3-}$ /L) with a $CaCl_2$ solution (6.0 g Ca(II)/L) added at a flow rate (Q_{Ca}) between 0.1 and 0.3 ml/min (by means of a peristaltic pump Gilson Minipuls 3). The reaction time was ranged between 6 and 24 hours depending on the initial phosphate concentration, the flow rate and in order to reach at the end of the test a molar ratio Ca/P of 1.67, suitable for Hap precipitation. Experiments were performed at room temperature. Three different types of experiments were performed: i) experiments to study the influence of pH (at 8, 10 and 11.5) at constant initial phosphate concentration (1.0 g $P\text{-}PO_4^{3-}$/L), calcium dosing rate (0.1 mL/min) and stirring speed (250 rpm); ii) experiments to study the influence of the total initial phosphate (P(V)) concentration (0.25, 0.375, 0.5 and 1.0 g/L) at constant pH (11.5), calcium dosing rate (0.1 ml/min) and the stirring speed (250 rpm), iii) experiments to study the influence of the stirring speed (50, 100, 150 and 250 rpm) and calcium dosing rate (at 0.1, 0.2 and 0.3 ml/min) at constant pH (11.5) and total initial phosphate concentration (1.0 g $P\text{-}PO_4^{3-}$/L).

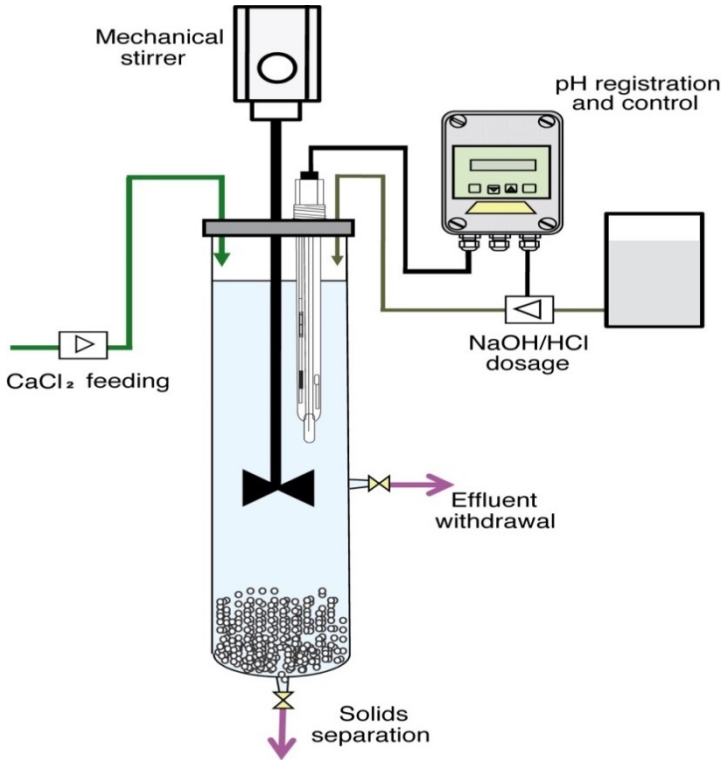

Figure 2.1. Experimental set up of the batch reactor for phosphate precipitation with calcium including a CaCl2 dosing pump, mechanical stirrer, the NaOH and HCl dosing pumps and the pH controller. Solids are removed at the bottom part of the reactor.

Batch reactor aqueous samples were taken along the experiments and filtered through 0.45 um filter. The total concentrations of the Ca(II) and P(V) were measured by Ion Chromatography using an Ionex Liquid Chromatography (ICS-1000). The accuracy of the measurements was higher than 95%.

After the conclusion of the experiments, the precipitated solids of the batch reactor were filtered, washed with water several times and dried at T=60°C during 24h. The samples were metalized with gold and then were examined using a JEOL 3400 Field Emission Scanning Electron Microscopy with Energy Dispersive System (FE-SEM-EDX). Samples were also analyzed by

Fourier transform infrared spectroscopy (FTIR), in the range 4000cm^{-1}-500cm^{-1}, (JASCO, FT/IR-4100).

2.1.1. Particle size analysis

Particle size distribution of the Ca-P powder precipitates was analyzed by laser light scattering (LS) with a Coulter diffract particle size analyzer (LS 13 320 Laser Diffraction Particle Size Analyzer Instrument, Beckman Coulter). The size crystal distribution range (CSD) detected was from 0.04 to 2000 μm. The particle size expressed as both volume and number distributions, allows to detect the presence of aggregates and also to assess the size of the majority of the particles, respectively. Particles were analyzed as obtained directly from the batch reactor without any thermal treatment and granulometric separation.

2.1.2. Thermogravimetric Analysis (TGA) and Differential Thermal Analysis (DTA)

Thermogravimetric analyses were carried out in a Mettler TGA/SDTA 851e thermo balance. Dried samples with an approximate mass of 8 mg were degraded between 30 and 800 °C at a heating rate of 10 °C/min in N_2 (100 cm^3/min measured in normal conditions) atmosphere. The precision of reported temperatures was estimated to be ±2 °C.

2.1.3. BET analysis

The specific surface area (S_{BET}) of the powders was measured using multipoint Brunauer-Emmett-Teller (BET) method at low temperature using Micrometrics Flow Sorb II 2300. The equivalent particle diameter (d_{BET}) was

calculated from the measured surface area (S_{BET}) values by using Eq. 1 (Ghosh et al., 2011).

$$d_{BET} = \frac{6}{\rho S_{BET}} \quad (1)$$

where ρ is the theoretical density of Hap (3.167 g/cm^3).

2.1.4. X-ray diffraction (XRD) analysis

The phase purity and crystallinity of the Hap powder were analyzed by X-ray diffraction with λ CuKα radiation (λ= 1.54056 Å)) at a scanning rate time of 19.2 and 57.6 s, steep angle of 0.015° and 2θ in range of 4-60°. The average crystallite size long c-direction of Hap powder was calculated from (002) reflection in XRD pattern, using Sherrer's equation (Eq. 2) (Pham et al., 2013):

$$\tau = \frac{K\lambda}{\beta \cos\theta} \quad (2)$$

where τ (nm) is crystallite size, K is the shape factor (K = 0.9), λ is the wavelength of the X-ray (λ = 0,15406 nm for CuKα radiation), β is the full width at half- maximum (FWHM) (rad) of the peak along (002) direction and θ is the Bragg's diffraction angle.

The crystallinity degree (Xc) was determined using Eq. 3:

$$Xc = (0.24/\beta)^3 . 100\% \quad (3)$$

The solids in powder form were identified by standard Joint Committee en Powder Diffraction Standards (JCPDS) file and it was matched with Powder Diffraction File (PDF) no. 00-009-0432 for Hap.

2.2. Hap precipitation: definition of the experimental conditions

Precipitation processes were designed using the HYDRA-Medusa code (Puidomènech, 2001). Measured P(V) and Ca(II) concentrations were compared when necessary with those predicted by using HYDRA-MEDUSA code. The effect of ionic strength on single salt solubility and formation of pure precipitates was taken into account in the calculations. Aqueous species and mineral phases of the $CaCl_2$-NaH_2PO_4-H_2O system considered on the calculations are detailed in Table 2.1.

Table 2.1. Formation constants K (in log value) of the main aqueous and mineral phases involved in the system $CaCl_2$-NaH_2PO_4-H_2O from the HYDRA-Medusa database (Puigdomènech, 2001).

Species/solid formation reaction	log K
$2H^+ + PO_4^{3-} + Ca^{2+} \leftrightarrow CaH_2PO_4^+$	21.0
$H^+ + PO_4^{3-} + Ca^{2+} \leftrightarrow CaH_2PO_4$	15.1
$H_2O + Ca^{2+} \leftrightarrow CaOH^+ + H^+$	-12.8
$PO_4^{3-} + Ca^{2+} \leftrightarrow CaPO_4^-$	6.5
$2H^+ + PO_4^{3-} \leftrightarrow H_2PO_4^-$	19.6
$3H^+ + PO_4^{3-} \leftrightarrow H_3PO_4$	21.7
$H^+ + PO_4^{3-} \leftrightarrow HPO_4^{2-}$	12.4
$4H^+ + 2PO_4^{3-} + Ca^{2+} \leftrightarrow Ca(H_2PO_4)_2$	39.1
$2H_2O + Ca^{2+} \leftrightarrow Ca(OH)_2 + 2H^+$	-22.8
$2PO_4^{3-} + 3Ca^{2+} \leftrightarrow Ca_3(PO_4)_2$	28.9
$H^+ + 3PO_4^{3-} + 4Ca^{2+} \leftrightarrow Ca_4H(PO_4)_3$	46.9
$3PO_4^{3-} + 4Ca^{2+} + H_2O \leftrightarrow Ca_5(PO_4)_3OH + H^+$	40.5
$H^+ + PO_4^{3-} + Ca^{2+} \leftrightarrow CaHPO_4.2H_2O$	19.0
$Ca^{2+} + H_2O \leftrightarrow CaO + 2H^+$	-32.8

Ca(II) and phosphate ions could forms different Ca-P mineral phases (e.g.$Ca(H_2PO_4)$, $Ca_3(PO_4)_2$ (s), $Ca_4H(PO_4)_3$ (s), $Ca_5(PO_4)_3OH$ (s), $CaHPO_4.2H_2O$ (s) depending of the aqueous phase composition and the concentrations of the specie involved. The species distribution diagram as a function of pH simulating the conditions of the precipitation assays in three scenarios are shown in Figure 2.2 a, b and c, respectively: a) excess of P(V)

over Ca(II) (molar ratio of 200) simulating the initial step of the precipitation assays; b) an slightly excess of P(V) over Ca(II) (molar ratio of 10) simulating the conditions approaching to the stoichiometric molar ratio, and c) an excess of Ca(II) over P(V) (molar ratio 0.5) simulating the final steps of the precipitation trials. As it can be seen the pH and the levels of concentration of both calcium and phosphate, are influencing the aqueous chemistry and then the precipitation of Ca-P minerals. For a mixture of 10 mmol/L of PO_4^{3-} with 50 µmol/L of Ca^{2+} (Figure 2.2a) the excess of PO_4^{3-} and $H_2PO_4^-$ ions promotes the formation of complexes as $CaPO_4^-$ and CaH_2PO_4 and it is expected the partial precipitation of $Ca_3(PO_4)_2(s)$ above pH 8. The increase of pH above pH 10 favors the formation of the complex $CaPO_4^-$ in solution.

The reduction of the excess of P(V) to Ca(II) for 10 mmol/L of PO_4^{3-} and 1 mmol/L of Ca(II), (Figure 2.2b) and 20 mmol/L of Ca(II) (Figure 2.2c), is traduced in the precipitation of ($Ca_5(PO_4)_3OH(s)$) from pH values above 6 for a Ca/P ratio of 1.67 and above 5 for solutions with an excess of Ca(II). This is also accompanied by a reduction the $CaH_2PO_4^+$ and $CaHPO_4$ molar fractions.

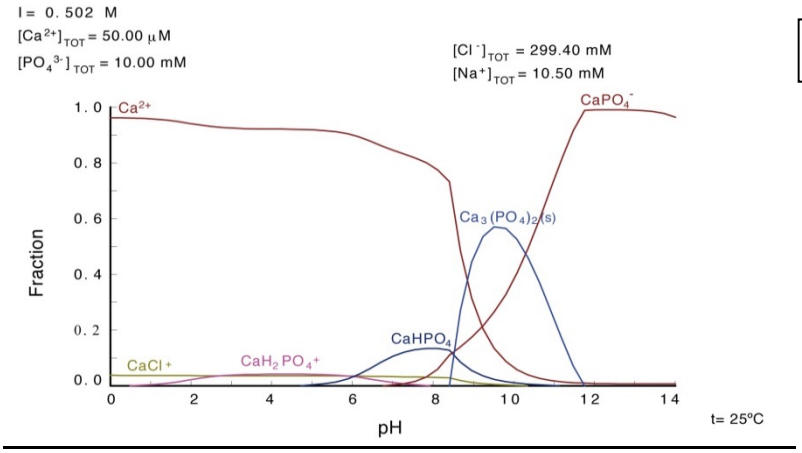

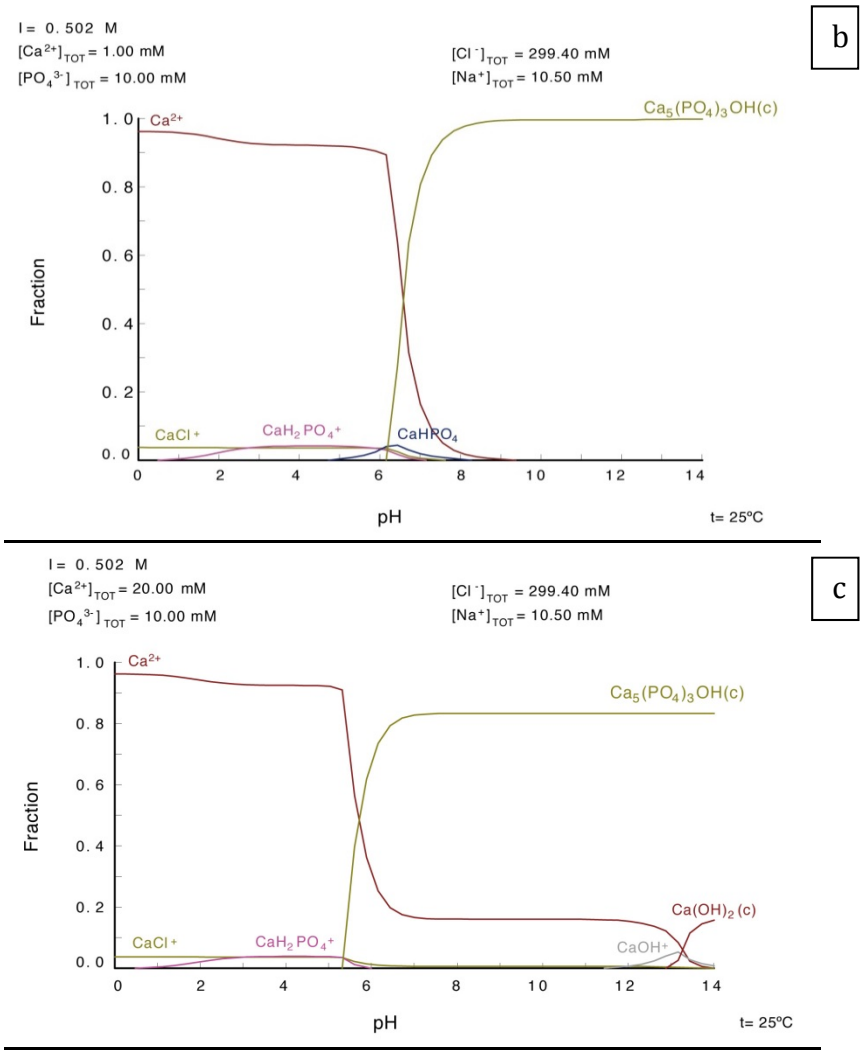

Figure 2.2. Species distribution diagram for the system $CaCl_2$-NaH_2PO_4-H_2O using the HYDRA-Medusa data base (Puigdomènech, 2001) under different P(V)/Ca(II) molar ratios: a) excess of P(V) over Ca(II) (molar ratio of 200), b) slightly excess of P(V) over Ca(II) (molar ratio of 10) and c) excess of Ca(II) over P(V) (molar ratio 0.5) for a total ionic strength of 0.5 mol/L.

3. Results and Discussion

3.1. Effect of pH in Hap precipitation

The influence of the pH in the precipitation of P(V) along the experiment for two experiments one at constant pH at 11.5 and other with an initial pH

solution at 10.5 (variable pH) as well as the evolution of calcium concentration along the experiment is shown in Figures 2.3a and b.

The evolution of pH along the experiment, shown in Figure 2.3c, follows three differentiate stages. After the initial additions of calcium (up to 0.5 mmol/L Ca(II)) the pH of solution is kept constant between 10.5 to 10.7 taking benefit of the buffer capacity of the initial solution (HPO_4^{2-}/H_2PO_4). The evolution of the total P(V) concentration shows an strong reduction (30% of the initial concentration) as a function of the addition of Ca(II) (3.6 mmol/L) and then it is stabilized around after 240 min, corresponding to the addition of 5.4 mmol/l of Ca(II).

As it is shown in Figure 2a the predominant P(V) species in solution between pH 10 and 12 is $CaPO_4^-$. Under this conditions it has been postulated a shift on the surface charge of the mineral leading to the precipitation of amorphous calcium phosphate (Han et al., 2013), $Ca_3(PO_4)_2$ or β-whitlockite (β-$Ca_3(PO_4)_2$) (Nriagu and Moore, 1984) as it is described by Eq. 4.

$$3\,CaPO_4^- + H^+ \rightarrow Ca_3(PO_4)_{2\,(s)} + HPO_4^{2-} \quad (4)$$

Although potentially such phase can be formed it was not detected at the end of the precipitation test and only Hap, was detected by XRD analysis.

The addition of Ca(II) is traduced into slightly decrease of P(V) concentration as it is observed in Figure 2.2b, and an increase of the total Ca(II) concentration in solution as can be seen in Figure 2.3a. Subsequently the pH decreased with a S-shape form due to the reduction of the HPO_4^{2-} concentration by formation of Hap (Figure 2.3c). After this abroad change the pH of the solution diminished slowly as it is reached the $H_2PO_4^-/HPO_4^{2-}$ buffer (pKa_2 = 7.2). During this second stage, pH decreased from 10 to 7.4 and

phosphate ions P(V) were present in solution mainly as $CaHPO_4$ (see Figure 2.2a) and the precipitation of Ca-P could be described by reaction Eq. 5.

$$5CaHPO_{4\,(aq)} + H_2O \leftrightarrow Ca_5(PO_4)_3(OH)_{(s)} + 2\,HPO_4^{2-} + 4H^+ \quad (5)$$

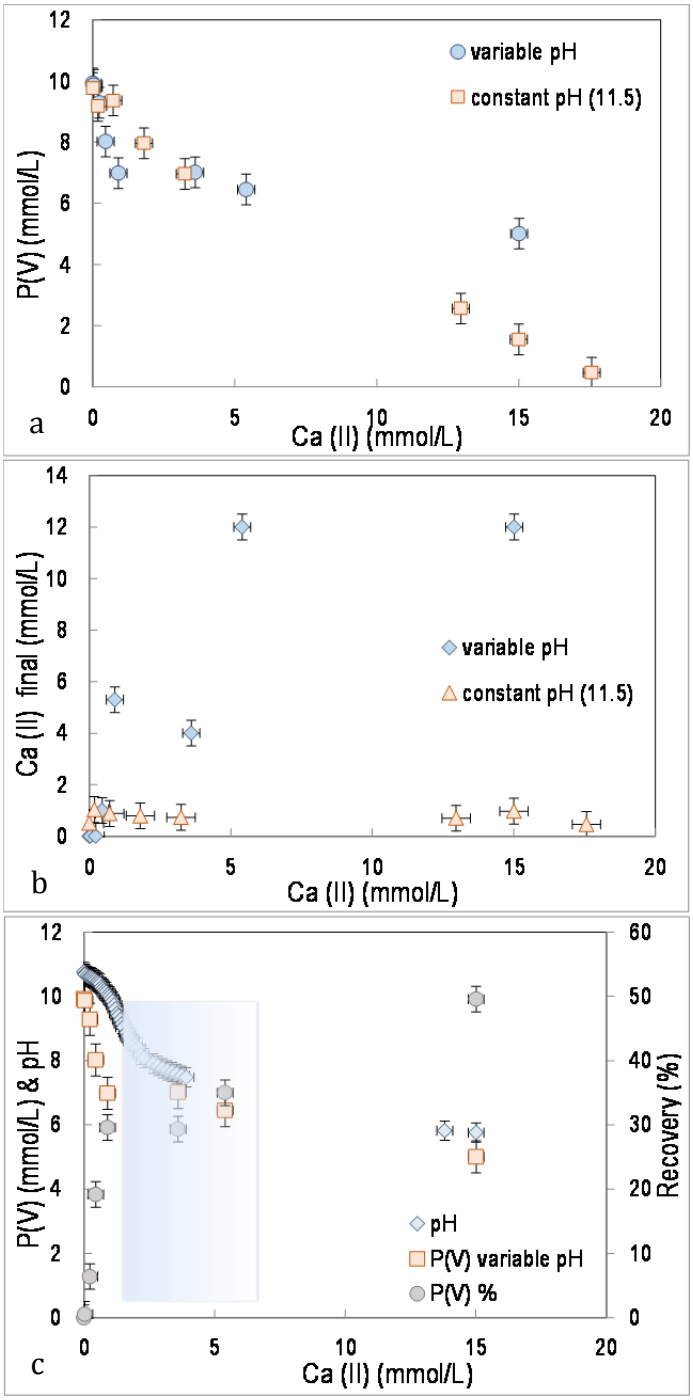

Figure 2.3. Evolution of a) phosphate and b) calcium concentration with time in Hap precipitation tests at constant pH (11.5) and variable pH; c) phosphate recovery and pH evolution in variable pH experiment in the batch reactor.

The addition of Ca(II) is traduced in a small decrease of pH during the last stage indicating the growing of formed Hap. Although an excess of Ca(II) was added the removal of phosphate from solution only reached a 50%.

On the other hand, in the experiment with constant pH (11.5 ± 0.1) the phosphate profile shows a continuous decrease with the addition of Ca(II) reaching a removal of phosphate higher than 96% (± 2%) (Figure 2.3a). At the end of the experiment the precipitated solid was identified as Hap as described latter. The levels of total Ca(II) concentration in solution were below of 20 mmol/L. These values were two orders of magnitude higher than those predicted assuming that the system was equilibrated with Hap, which indicates that the system did not reach equilibrium.

The evolution of phosphate P(V) concentration and recovery as a function of calcium concentration at constant pH values (8, 10 and 11.5) are shown in Figure 2.4.

It can be seen (Figure 2.4b) that precipitation/crystallisation of Hap can be divided in three well-defined stages for experiments at constant pH of 10 and 11.5 and just two stages for pH 8. In the stage 1 (stage 1), induction period, early nucleation took place and a reduced amount of phosphate was removed during the first 30 min (0.36 mmol Ca(II)/L).

The maximum P(V) removal ratios were observed for pH 10 and 11.5 (11 and 6 %, respectively). This initial step in alkaline pH conditions has been described by reaction Eq. 6 (Skoog, 1976; Castro et al., 2012; Han et al., 2013):

$$3Ca^{2+} + 2HPO_4^{2-} \leftrightarrow Ca_3(PO_4)_{2\,(s)} + 2H^+ \quad (6)$$

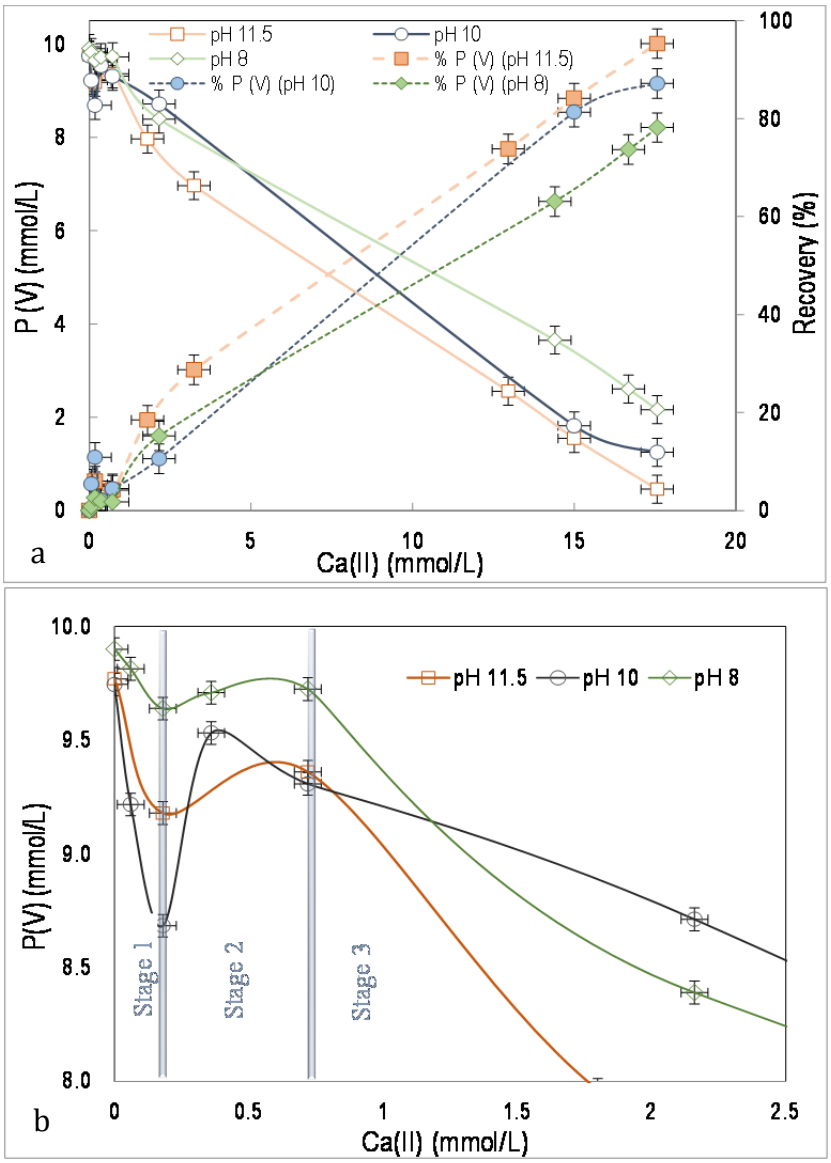

Figure 2.4. a) The recovery and phosphate evolution profile and as a function of calcium concentration at constant pH values of 8, 10 and 11.5 and b) detail of three crystallisation stages in the batch reactor.

Han et al. (2013) identified at pH 10, the precipitation of an amorphous calcium phosphate (ACP) phase at the initial reaction time and then it crystallized into Hap after 2h of reaction. In the second stage (stage 2), the homogenous nucleation of Hap occurred (from 30 to 180 min equivalent to 1.8 mmol Ca(II)/L). During the nucleation stage, the total concentration of Ca(II) remained constant to 0.80 ± 0.2 mmol Ca (II)/L and the P(V) removal

increased from 2 to 10% for pH 10 and from 5 to 20% for pH 11.5 (Figure 2.4). In the final stage (stage 3), further homogeneous nucleation bulk precipitation of Hap was observed, until reaching a final P(V) removal efficiency of 81% and 95%, for pH 10 and 11.5, respectively. Analysis at the end of the experiment of solid samples by XRD analysis determined the presence of Hap. Values of Ca(II) concentration measured along the experiments were higher than those predicting equilibrium with the formation of Hap, indicating a kinetic control, however at the end of the experiment under excess of Ca(II) the measured and calculated values were in agreement.

At pH 8, the two stages observed were the precipitation of Hap, with a phosphate removal ratio up to 20%, followed by a homogeneous nucleation stage of Hap with a phosphate removal ratio up to 78%. This is in agreement with results reported in literature at pH 7.5 in which Hap phase was directly observed immediately the reaction was started (Skoog, 1976).

3.2. Influence of initial P(V) concentration

The evolution of total P(V) concentration phosphate profiles for experiments carried out at constant pH (11.5±0.2) for initial phosphate concentrations of 0.25, 0.375, 0.5 and 1.0 g $P\text{-}PO_4^{3-}$ /L are shown in Figure 2.5. The total P(V) concentration decreased with the addition of Ca(II) reaching a final concentration below 0.2 mg $P\text{-}PO_4^{3-}$ /L (limit of quantification for (P(V)) in this study), which stands for more than 65 % of P(V) removal as Hap as it was determined by XRD analysis. Total Ca(II) concentrations in solutions were below the limit of quantification, for the lower P(V) concentrations and below 1 mmol/L for the concentrated experiment (1.0 g/L), indicating a total

phosphate removal (>99%) as a Hap with a Ca/P ratio of 1.67, approximately.

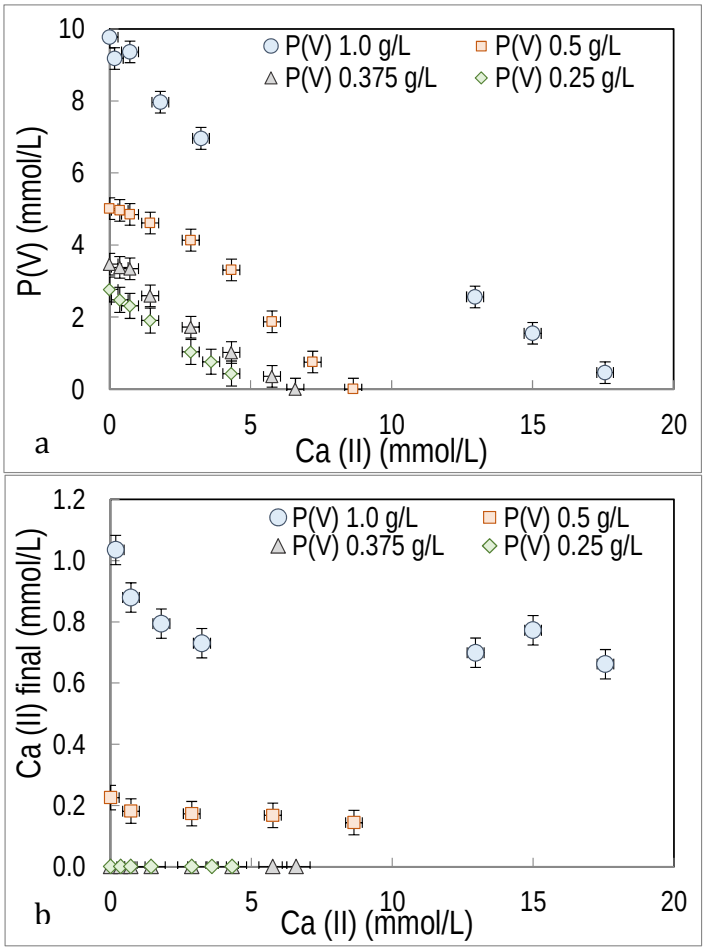

Figure 2.5. Influence of the initial phosphate concentration onto the Hap precipitation at pH 11.5 as a function of total calcium concentration in the batch reactor for a) Phosphate concentration and b) calcium concentration.

The kinetics of precipitation of Hap is important in explaining the oversaturation of aqueous phase with respect to initial phosphate and calcium concentration. Consequently, several empirical equations have been used to describe the kinetics of Hap based on driving forces calculated from disequilibrium (Koutsoukos and .Amjad, 1980; Moreno and Varughese, 1981). Inskeep and Silvetooh (1988) determined the rate reaction order with

respect to solution or surface area and determined that the rate of Hap at pH 7.4 to 8.4 could be expressed by Eq. 7 as follow:

$$R = K_f \,.\gamma\,(\mathrm{Ca^{2+}}).\gamma\,(\mathrm{PO_4^{3-}})\mathrm{S}\,[\mathrm{Ca^{2+}}][\mathrm{PO_4^{3-}}] \quad (7)$$

where R is the rate of Hap precipitation (mol Hap/ L·s), k_f is the rate constant (L^2 /mol·m^2·s), γ (Ca^{2+}) and, γ (PO_4^{3-}) are the divalent and trivalent ion activity coefficients, respectively, S is the surface area (m^2 /g), and [Ca^{+2}] and [PO_4^{3-}] are the molar concentrations of Ca(II) and P(V) (mol/L).

As it could be seen in Figure 2.5, for each experiment at a given concentration, the Ca(II) concentration was below 0.05 mmol/L (the detection limit in this study) for 0.25 and 0.375 g P- PO_4^{-3}/L; 0.15 mmol/L for 0.5 g P-PO_4^{3-}/L and 0.7 mmol/L for 1.0 g P-PO_4^{3-}/L. Additionally the surface area of the precipitated Hap, in each experiment, ranged from 67 g/m^2 up to 90 g/m^2 as the initial concentration increases. Then, assuming that for each experiment at a given concentration the values of k_F, γ(Ca^{2+}), γ(PO_4^{3-}), S and [Ca^{2+}] are constant, the precipitation rate equation could be simplified to Eq. 8:

$$R = -\frac{1}{3}\left(\frac{d[PO_4^{3-}]}{dt}\right) = k_f.\gamma\,(\mathrm{Ca^{2+}}).\gamma\,(\mathrm{PO_4^{3-}})\mathrm{S}\,[\mathrm{Ca^{2+}}][\mathrm{PO_4^{3-}}] = \mathrm{k'_f}[\mathrm{PO_4^{3-}}] \quad (8)$$

and integrating Eq. 8 between a given t, with [P(V)] and time t=0 for $[P(V)]_0$ it could be obtained:

$$ln\,\frac{[PO_4^{3-}]}{[PO_4^{3-}]_0} = -k'_f t \quad (9)$$

where t is time (s), and $\mathrm{k'_f} = k_f.\gamma\,(\mathrm{Ca^{2+}}).\gamma\,(\mathrm{PO_4^{3-}})\mathrm{S}\,[\mathrm{Ca^{2+}}]$

The evolution of the $ln\,\frac{[PO_4^{3-}]}{[PO_4^{3-}]_0}$ as a function of time (Figure 2.6) follows a linear dependence for each [P(V)] concentration. The slopes of these functions were used to calculate the precipitation rate constants $\mathrm{k'_f}$ at pH 11.5 (Table 2.2). The decrease of P(V) concentration from 1.0 to 0.25 P-

PO_4^{3-} g/L is traduced in an increase of the k'_f constant up to 2.5 times. It indicates that the rate of Hap precipitation follows the proposed first order rate with respect to Ca^{2+}, PO_4^{3-}, and surface area (Inskeep and Silvertooth, 1988; Liu et al., 2001).

Table 2.2. Initial experimental condition and linear regression parameters of $\ln[P(V)/P(V)_0]$ as a function of time.

$P(V)_i$ (g/L; mol/L)	$[Ca^{2+}]$ (Hydra-Medusa) (mol /L)	Slope rate $\ln P(V)-\ln P(V)_0 = f(t)$	R^2
1.0; 0.0105	0.839	$k'_f = 0.0014$	0.98
0.5; 0.0052	0.894	$k'_f = 0.0016$	0.84
0.375; 0.0039	0.908	$k'_f = 0.0031$	0.96
0.250; 0.0026	0.922	$k'_f = 0.0041$	0.98

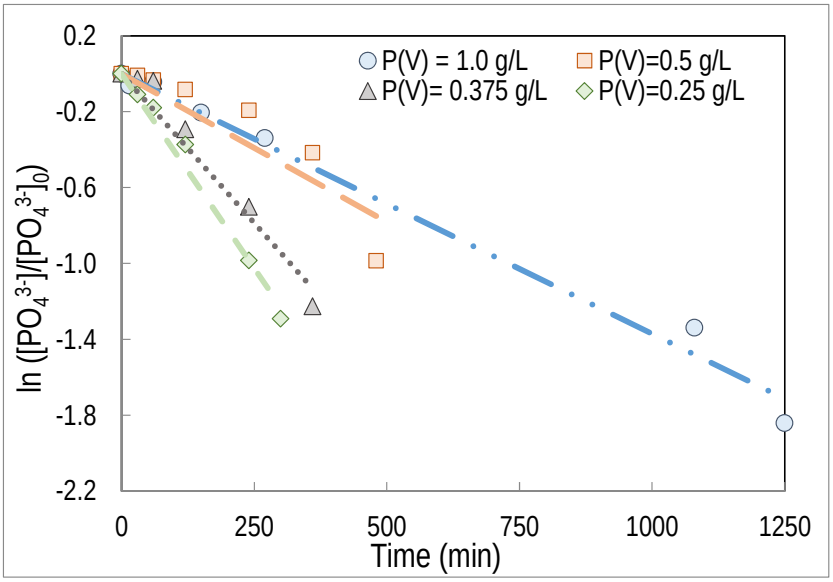

Figure 2.6. Evolution of the $\ln[P(V)/(P(V)_0]$ as a function of time for the precipitation experiments at constant pH (11.5) for phosphate initial concentrations between 0.25 up to 1 g/L using a batch reactor.

3.3. Influence of stirring and Ca(II) addition rate

Phosphate precipitation experiments under different stirring speeds in the range 50 rpm up to 250 rpm were carried out. The phosphate concentration

evolution did not show any significant influence on the P(V) recovery ratio as it can be seen in Figure 2.7a, and indicating the absence of mass transfer phenomena limitations. The percentage of P(V) recovery was always above 95± 3 %.

On the other hand, the increase of Ca(II) dosing addition up to 0.3 mL/min, was traduced in the increase of the phosphate removal ratio above 99% (Figure 2.7b) and the phosphate precipitation rate was slightly higher than for lower dossing ratios as was described previously by Xie et al. (2014).

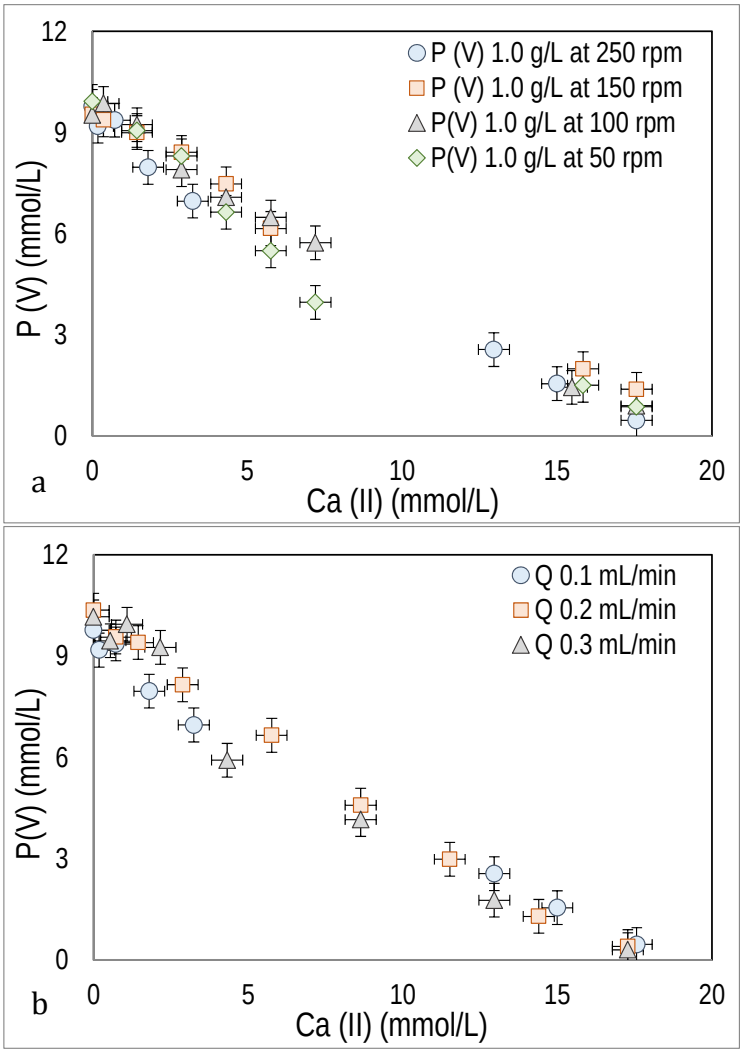

Figure 2.7. Influence of a) stirring speed and b) Ca(II) addition rate on phosphate concentration evolution as function of time during phosphate precipitation in a batch reactor.

3.4. Precipitate Characterization

The nature of the solids and crystals formed were characterized by XRD (diffraction patterns are shown in Figure 2.8 and summarized in Tables 2.3 and 4). A single phase Hap powder is shown in Figure 2.8, according to the reference Hap (see Table 2.3), was obtained in the different experiments (e.g. constant and variable pH and also at different initial phosphate concentration).

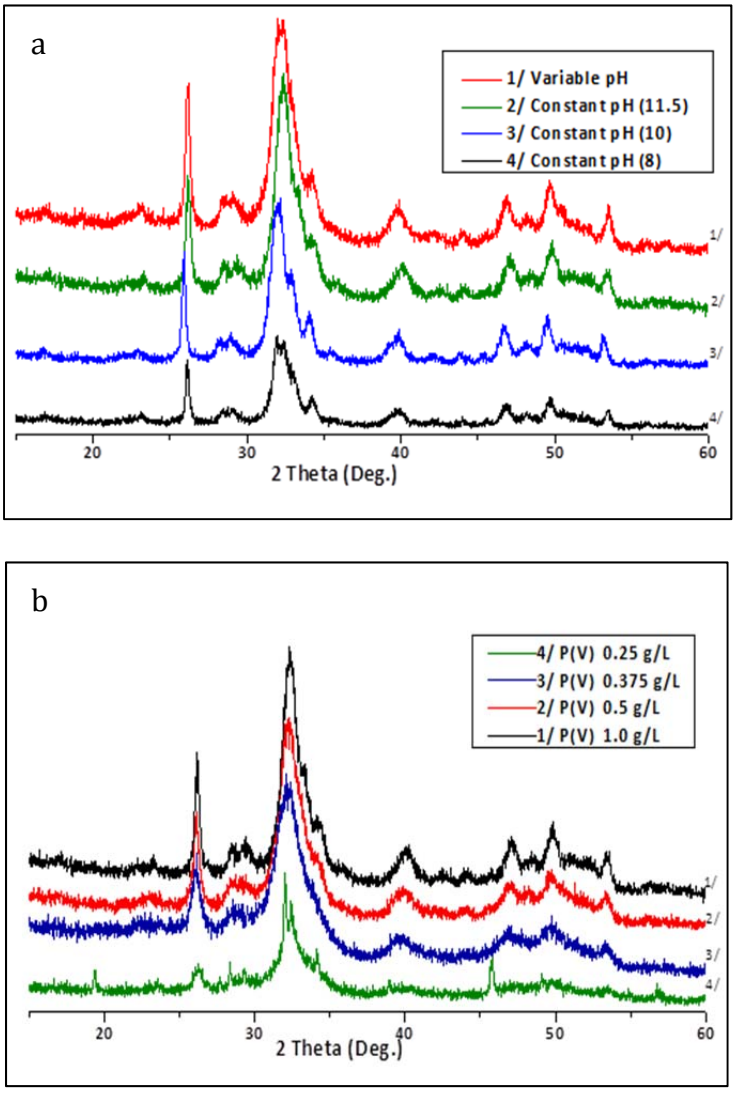

Figure 2.8. XRD analysis of the samples obtained in phosphate precipitation experiments for a) precipitation tests at constant and variable pH and b) precipitation tests under different initial phosphate concentration.

The strongest peak intensity of the Hap samples at *2θ = 31.87°* was of the (211) crystal plan and the other peak at *2θ =25.87°* corresponds to the (002) crystal plane. Besides, the other characteristic peaks with less intensity were of the (112) and (300) crystal plane.

It is important to point out that 211 and 002 reflection intensities showed an increased trend by increasing solution phosphate concentration as is shown in Figure 2.8, which indicates that maturation in Hap crystallinity took place with time.

In fact, the degree of crystallinity or the fraction of the crystalline phase Xc for the hydroxyapatites obtained through different initial phosphate concentration can be evaluated by using equation 3.

Table 2.3. The full-width at half-maximum (FWHM) and Miller Index (hkl) determined from XRD analysis for HAPs samples.

Test number	$FWHM_{002}$	hkl (002) *2θ (°)*	hkl (211) *2θ (°)*	hkl (112) *2θ (°)*	hkl (202) *2θ (°)*	hkl (310) *2θ (°)*	hkl (222) *2θ (°)*
1	0.329	26.14	31.86	32.38	34.21	40.06	46.9
2	0.370	26.18	31.87	32.39	34.21	40.06	46.87
3	0 .268	26.13	31.87	32.19	34.16	39.80	47.11
4	0.272	25.89	31.87	32.06	33.94	39.71	46.73
5	0.383	26.13	31.86	32.25	33.84	39.89	46.98
6	0.586	26.10	31.87	32.20	-	39.66	46.95
7	0.667	26.25	31.87	32.43	34.15	38.95	45.77
8	0.255	25.87	31.85	32.20	34.31	39.93	46.90
9	0.401	26.14	30.66	-	34.15	39.61	47.00
10	0.340	25.98	31.92	32.10	33.87	39.70	46.81
11	0.302	25.80	31.86	32.17	-	39.72	46.87
Hap*	Relative intensities 2θ (°)	40 (25.87)	100 (31.87)	60 (32.19)	25 (34.04)	20 (39.81)	30 (46.71)

*(Hap reference); Powder diffraction File 00-009-0432

Table 2.4. Physicochemical characterizations of Hap precipitation under different experimentations conditions: XRD patterns, particle size (LS), S ($_{BET}$)

Experimental conditions							XRD			LS		BET	
Test number	pH control	pH	P (V)	Ca^{2+} (Q_{Ca}) addition	Stirring speed	P(V) removal efficiency	*$FWHM_{002}$	Crystal diameter(ε_{hkl})	Degree of crystallinity (Xc)	Particle size, d_{50} (in volume)	Particle size, d_{50} (in number)	S_{BET}	d_{BET}
-	-	-	g/L	mL/min	rpm	%	-	nm	%	µm	µm	m^2/g	nm
1	No	11→5.5	1	0.1	250	50	0.329	24.8	38.6	56.5	0.11	59.9	31.6
2	Yes	11.5	1	0.1	250	95	0.370	22.0	27.2	8.7	0.09	88.3	21.5
3	Yes	8	1	0.1	250	96	0.268	30.4	71.3	69.5	0.08	34.5	31.6
4	Yes	10	1	0.1	250	93	0.272	29.9	69.2	6.1	0.11	67.7	28.0
5	Yes	11.5	0.5	0.1	250	>99	0.383	21.3	24.5	429.3	0.09	90.3	21.0
6	Yes	11.5	0.375	0.1	250	99	0.586	12.2	6.9	21.3	0.33	73.2	25.9
7	Yes	11.5	0.25	0.1	250	84	0.667	13.9	4.7	86.5	0.49	66.7	28.4
8	Yes	11.5	1	0.1	150	85.2	0.255	31.9	83.1	729.9	0.35	93.2	20.3
9	Yes	11.5	1	0.1	50-75	91.3	0.401	20.3	21.3	23.9	0.09	91.8	20.6
10	Yes	11.5	1	0.2	250	99	0.340	23.9	35.0	8.3	0.09	53.6	35.3
11	Yes	11.5	1	0.3	250	>99	0.302	27.0	50.2	587.0	0.43	92.9	20.4

*The full-width at half-maximum (FWHM)

Main functional groups of the different powder Hap samples were confirmed by FTIR analysis (Figure 2.9). It was detected the presence of characteristic bands around 600 cm^{-1} corresponding to v4 (OPO, PO_4^{3-}) bending mode. Also the 960 cm^{-1} band was assigned to v1 (PO) symmetric stretching and a band in the range 1100-1000 cm^{-1} was assigned to v3 (PO, PO_4^{3-}) antisymmetric stretching mode. The small band around 875 cm^{-1} can be attributed to the vibrational frequencies of carbonate ions or HPO_4^{2-} group (Koutsopoulos, 2002).

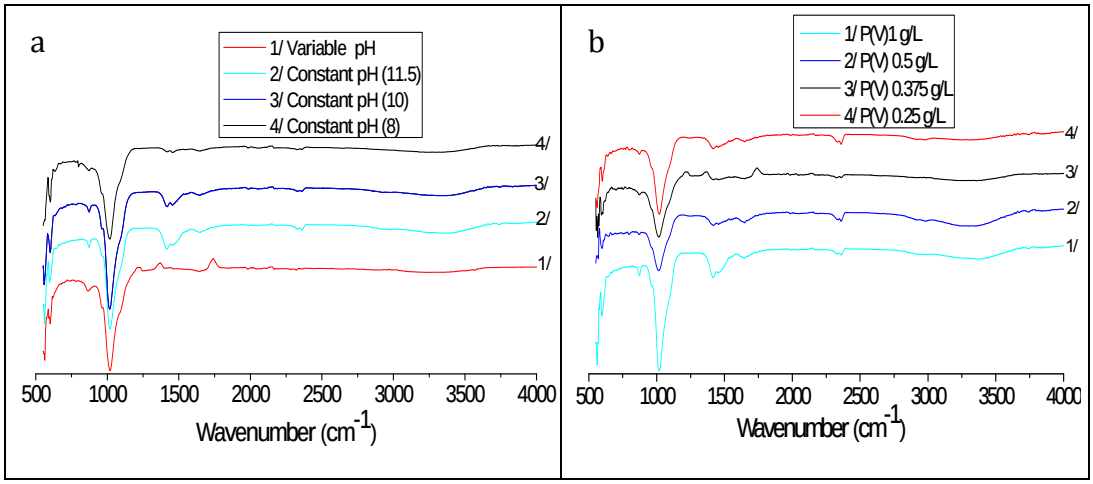

Figure 2.9. FTIR analyses of the samples obtained in phosphate precipitation for a) precipitation tests at constant and variable pH and b) precipitation tests under different initial phosphate concentration.

Furthermore, the carbonate peaks in the range 1400-1500 and 868 cm^{-1}, corresponding to the asymmetric stretching (v3 mode) and out of plane bending (v2 mode) vibrations, respectively (Sporysh et al., 2010; Paz et al., 2012; Castro et al., 2013a) were identified. Presence of these bands is characteristic of a carbonate Hap of B-type, where the carbonate ions occupy the phosphate ions sites. The formation of carbonate could be due to the adsorption of atmospheric CO_2 during the ripening time, due to the highly

alkaline conditions in the solution (Müller et al., 2007; Paz, et al., 2012; Castro et al., 2013a).

3.5. Characterization of the degree of crystallinity, crystal diameter and particle size distribution

The Hap crystal diameters (calculated by Eq. 2) showed that the powders prepared are mostly constituted by nanoparticles as it is summarized in Table 2.4 and Figures 2.10. The crystal diameter increased with decreasing the pH of the crystallisation process, namely from 22 nm (pH 11.5) to around 30 nm (pH 8). Moreover, the crystal diameter and the degree of crystallinity were similar for pH values of 10 and 8 and presented the lower values. The experiment at variable pH reported similar nanometric powder sizes and crystallinity than those obtained for constant pH at 11.5.

Also, the stirring speed affected the degree of crystallinity, with, 83% at 150 rpm, and ranged between and around 20 to 27 % for 75 and 250 rpm. The increase of the Ca(II) dosing flow-rate (from 0.1 to 0.3 ml/min) revealed an slight increase of both crystal size and crystallinity degree (from 22 to 27 nm, and from 27% to 50 %, respectively).

For experiments under different phosphate concentrations, the highest degree of crystallinity (27%) and crystal diameter (22 nm) were obtained when the maximum initial P(V) concentration was used (1.0 g P- PO_4^{3-}/L). These findings can be explained by the process of particle formation, inducing, nucleation, growth and aggregation.

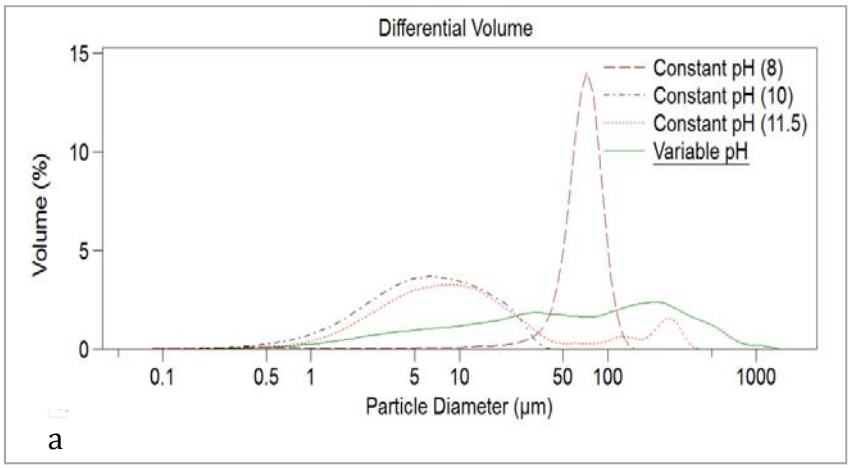
Differential Volume
Constant pH (8)
Constant pH (10)
Constant pH (11.5)
Variable pH
Volume (%)
Particle Diameter (µm)
0
5
10
15
0.1
0.5
1
5
10
50
100
1000

a

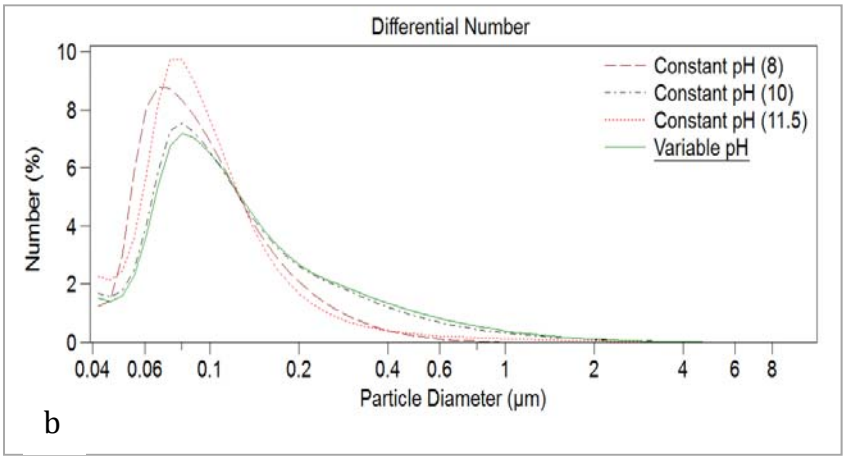
Differential Number
Constant pH (8)
Constant pH (10)
Constant pH (11.5)
Variable pH
Number (%)
Particle Diameter (µm)
0
2
4
6
8
10
0.04
0.06
0.1
0.2
0.4
0.6
1
2
4
6
8

b

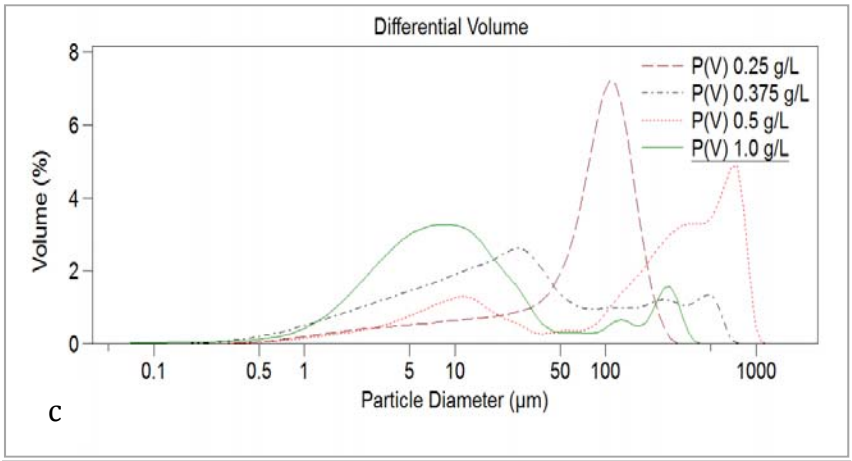
Differential Volume
P(V) 0.25 g/L
P(V) 0.375 g/L
P(V) 0.5 g/L
P(V) 1.0 g/L
Volume (%)
Particle Diameter (µm)
0
2
4
6
8
0.1
0.5
1
5
10
50
100
1000

c

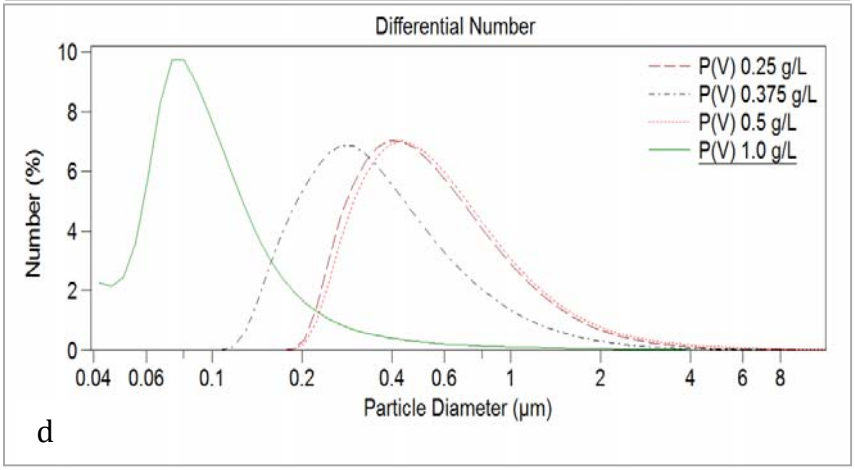
Differential Number
P(V) 0.25 g/L
P(V) 0.375 g/L
P(V) 0.5 g/L
P(V) 1.0 g/L
Number (%)
Particle Diameter (µm)
0
2
4
6
8
10
0.04
0.06
0.1
0.2
0.4
0.6
1
2
4
6
8

d

Figure 2.10. Particle size distribution in a) volume and b) number of Hap obtained from phosphate precipitation test at constant and variable pH and c) volume and d) number of Hap obtained from phosphate precipitation test at different initial phosphate concentration.

Additionally, and according to Figure 2.10, the granulometric analysis of precipitated particles in volume of particles (Figure 2.10a) revealed the formation of aggregates with an average equivalent diameter around 57 µm for variable pH and from 8.8 to 70 µm for constant pH (11.5 to 8). From the particle size laser analysis in number (Figure 2.10b), the crystals obtained with Hap precipitation with not constant pH ranged in size from 0.063 to 0.405 µm and have a mean equivalent diameter of 0.112 µm, presenting a narrow size distribution curve, similar to those obtained with constant pH (0.107 µm). From the particle size distribution in number of particles, it is observed that powders prepared were mostly constituted by nanoparticles.

This enormous decrease variation of the average diameter in the aggregates and the constant crystal mean size (d_{50}) with an increase at constant pH, it is attributed to some degree of heterogeneous nucleation as well as to an aggregation process in the nanometric scale. This aggregation process reduces the number of small crystals (Gomez-Morales et al., 2001).

Results also show that the mean size and the aggregation degree of the precipitated particles increased with increasing of the calcium flowrate dosing. As stated in Table 4, Hap particles with a mean size (d_{50}) of 89 nm were obtained at calcium flowrates of 0.1 and 0.2 ml/min. For 0.3 ml/min, d_{50} was 431 nm and in large aggregates of about 587 µm.

Therefore, it was observed that as the Ca(II) dosing flow-rate was higher, the aggregation phenomenon was more pronounced. Xie et al. (2014) described this behaviour and observed that when Ca(II) is added rapidly, the high local super-saturation will affect the dehydratation process and it will influence ions association and the nucleation behavior. On the other hand, the increased d_{50} number through the increase of the flowrate contributes to a distribution of supersaturation in the reaction environment, thereby leading to uniform distribution of the driving force for the nucleation and growth processes and give rise to a narrow size distribution (Yang et al., 2010).

The influence of the initial phosphate concentration on the mean particle size of Hap nanoparticles is shown in Figure 2.10(c-d). The results indicate that the mean particle size (d_{50}) decreased with the increase of the initial P(V) concentration. The decrease of particle size was 494, 332, 92 and 89 nm for 0.25, 0.375, 0.5 and 1.0 g P- PO_4^{3-}/L, respectively. Therefore, for initial P(V) concentrations above 0.5 g P- PO_4^{3-}/L, Hap particles with size around 90 nm were obtained. This it is attributed to the fact that the increase of initial P(V) concentration led to a high supersaturation level, which made nucleation and growth very fast, thereby resulting in the generation of small particles as described previously (Kucher et al., 2006; Yang et al., 2010). However, a large amount of Hap primary nuclei were spontaneously formed when the concentration reached a rather high value. In this case, the aggregation of Hap primary nuclei was greatly intensified during the reaction, causing the poly-dispersity of Hap nanoparticles as described by Yang et al. (2010).

From large scale application point of view, the settling velocity was accounted by using the Stokes law. This law describes the dependency of

unhindered terminal particle settling velocities on the basis of their diameters and densities under laminar flow condition.

If Hap is stimulated to precipitate, the crystal formed must reach a certain minimum size to enable them to acquire enough downward velocity to naturally settle to the base of a typical clarifier tank for collection. Thus, according to the Stokes law for particle settling, the average settling was determined to be 0.005 m/s, this value was constant for experiments at different stirring speed and also for those at initial phosphate concentration above 500 mg P-PO_4^{3-}/L.

In addition, Table 2.4 reports the specific surface area (S_{BET}) estimated from the specific area (d_{BET}) methodology. An increase in specific surface area of Hap was observed as pH was increased from 8 to 11.5. Moreover, at constant pH of 11.5, S_{BET} increased with increasing initial P(V) concentration. Thus, the increase of surface area represents an increase of the powder reactivity for crystal growth.

The specific surface area obtained for experiment at variable pH (initial pH of 11.5) was in the range of 60 m^2/g, but with at constant pH (initial pH =11.5) was incremented to 90 m^2/g. The stirring speed and calcium dosing rate (at pH 11.5) did not significantly affect the specific surface area.

The EDX analysis indicated that the samples were predominantly composed of Ca, P and O, the major elements of Hap powders. The SEM/EDX micrographs of the powders obtained from various initial phosphate concentrations, at variable or constant pH are shown in Figure 2.11. The powders consisted of rod like shape and plate-shaped nanometric sized particles. As it can be seen from the particles morphology, there is a

distribution of small particles and large agglomerates (consisting of fine cold welded particles).

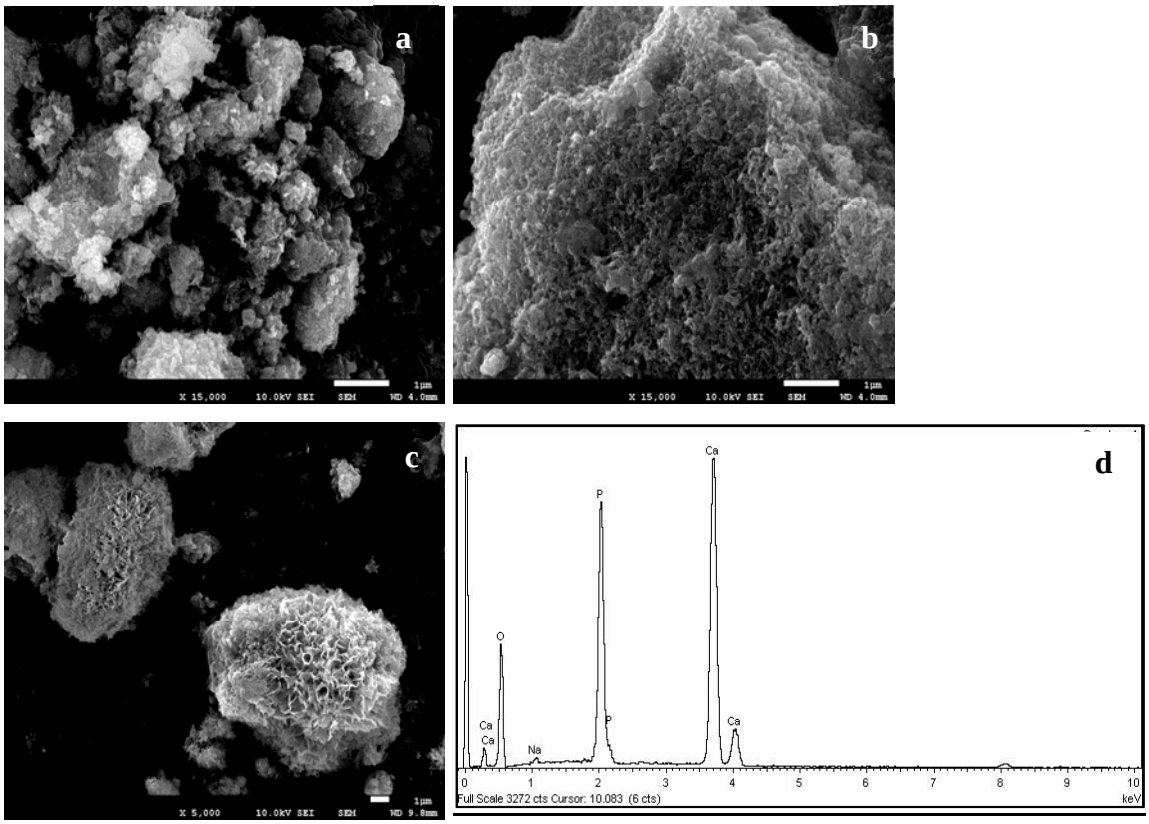

Figure 2.11. FE-SEM of Hap samples obtained from phosphate precipitation at constant pH and different initial phosphate concentration a) 0.5 g P-PO_4^{3-}/L, b) 1.0 g P-PO_4^{3-}/L and c) at 1.0 g P-PO_4^{3-}/L and variable pH and d) EDX analysis of samples at 1.0 g P-PO_4^{3-}/L and constant pH.

A higher tendency to form aggregates was observed with higher initial phosphate concentration and at constant pH (Figure 2.11b). More nearly monodisperse plate shaped with a length of about 1µm-100 nm was found for initial phosphate concentration above 0.5 g P- PO_4^{3-}/L. This is in accordance with the results reported by Dirksen and Ring (1991) who described the appearance of different growth morphologies with the existence of concentration gradients at the crystal surface, which lead to growth instabilities and the formation of dendrites (Figure 2.11a and b).

Besides, the powders obtained in batch tests with variable and constant pH (at initial phosphate concentration of 1.0 g P- PO_4^{3-}/L) showed a morphology of plate-shaped or rod-shaped (Figure 2.11b-c) with a size around 100 nm. Powders presented a certain degree of aggregation, which can be justified by the amorphous nature of the particles (degree of crystallinity around 27 and 39 % for constant and variable pH, respectively (Table 2.4)).

3.6. Thermal characterization

In the thermogram analysis, Hap crystals were characterized by a continuous mass loss throughout the increase of temperature. Hap crystals with low degree of crystallinity (Test number 2) reported three thermal transitions of mass loss in the temperature region (Figure 2.12). The first one is of 8% at 560° C ≥ T ≥T_{room} corresponding from physic-sorbed and surface absorbed water molecule. The second mass loss of 2.5% (between 560 and 830 °C) can be attributed firstly to the loss of water present in the lattice structure (the so-called strongly related intra-crystalline water) and secondly to the decomposition of phosphate ions (300-500 °C) (Dhand et al., 2014) and corresponding to the early stages of crystallisation. The third mass loss occurs at temperatures higher than 830 °C, in which Hap will dehydrate partially to form the oxy-hydroxyapatite according to Eq. 10 (Bernache-assollant et al., 2003):

$$Ca_{10}(PO_4)_6OH_{2\,(s)} \rightarrow Ca_{10}(PO_4)_6OH_{2-2x}O_{x\,(s)} + xH_2O_{(g)} \quad (10)$$

The thermogram obtained for Hap samples with high degree Hap crystallinity (Test number 8) presented just two thermal transitions in the temperature region. The first one, from room temperature to 830 °C, corresponds to a weight loss of about 12%. This weight loss could be associated to the

formation of Hap in advanced crystallisation stages and it can be attributed to the phase transitions within hydroxyapatite crystals as was previously reported by Piccirillo et al. (2013). A further thermal process for temperature up to 830 °C, corresponding to a negligible weight loss is assumed to be the result of gradual dehydroxylation of Hap powder by reaction 10.

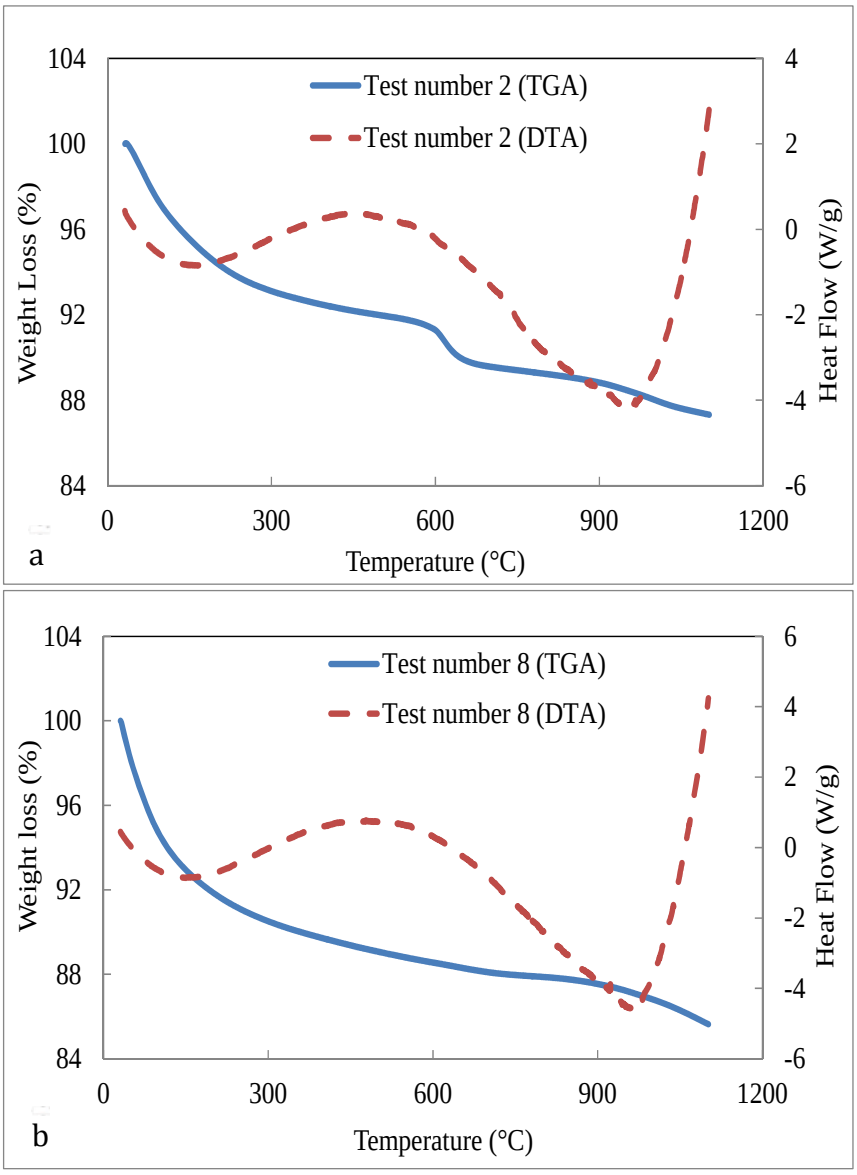

Figure 2.12. Thermogravimetric Analysis (TGA) and Differential Thermal Analysis (DTA) of Hap synthesized at different agitation speed reactor for a) experiment 2 (low degree of crystallinity) and b) experiment 8 (high degree of crystallinity).

4. Conclusions

In this study Hap powders, mostly constituted by nanoparticles, were obtained in a batch reactor from the treatment of concentrated alkaline P(V) effluents obtained in the regeneration of ion-exchange resins using a Ca(II) solution.

Three stages were identified in the precipitation of phosphate as Hap for pH values ranging from 8 to 11.5: a) induction period, with a small decrease in phosphate concentration, b) homogeneous nucleation, with maintaining or even a little increase of phosphate concentration and c) further homogeneous nucleation, with a constant decrease of phosphate.

A constant pH of 11.5 favored a higher precipitation rate of phosphate to form Hap when compared with rate obtained for pH 8, 10 and also at variable pH. However, the degree of crystallinity was higher for lower pH values assessed in this study (namely, 8 and 10).

Higher initial P(V) concentration lead to the formation of Hap precipitate powders with higher degree of crystallinity and crystal diameter, but also lower mean particle size.

As Ca(II) dosing rate increased, phosphate precipitation rate was higher, also the mean size and degree of crystallinity of the prepared particles were increased. Furthermore, the stirring speed (between 50 and 250 rpm) not reported any significate effect on the phosphate precipitation rate.

5. References

Bernache-assollant, D., Ababou, A., Champion, E., Heughebaert, M., 2003. Sintering of calcium phosphate hydroxyapatite $Ca_{10}(PO_4)_6(OH)_2$ I. Calcination and particle growth 23, 229–241.

Boskey, L., Posner, S., 1974. Formation of Hydroxyapatite at Low Supersaturation I. The Journal of Physical Chemistry 80 (1) 40–45.

Bradford-Hartke, Z., Lant, P., Leslie, G., 2012. Phosphorus recovery from centralised municipal water recycling plants. Chem. Eng. Res. Des. 90, 78–85.

Castro, F., Ferreira, A., Rocha, F., Vicente, A., António Teixeira, J., 2012. Characterization of intermediate stages in the precipitation of hydroxyapatite at 37°C. Chem. Eng. Sci. 77, 150–156.

Castro, F., Kuhn, S., Jensen, K., Ferreira, A., Rocha, F., Vicente, A., Teixeira, J.A., 2013a. Process intensification and optimization for hydroxyapatite nanoparticles production. Chem. Eng. Sci. 100, 352–359.

Castro, F., Rocha, F., Anto, J., 2013b. Continuous-Flow Precipitation of Hydroxyapatite at 37 ° C in a Meso Oscillatory Flow Reactor. Ind. Eng. Chem. Res. 52, 9816–9821.

Dhand, V., Rhee, K.Y., Park, S.-J., 2014. The facile and low temperature synthesis of nanophase hydroxyapatite crystals using wet chemistry. Mater. Sci. Eng. C. Mater. Biol. Appl. 36, 152–159.

Diaz, O.A., Reodyit, K.R., More, Jr. P.A., 1994. Solubility of inorganic phosphorous in stream water as influenced by pH and calcium concentration 28, 1755–1763.

Dirksen, J. A., Ring, T. A., 1991. Fundamentals of crystallization: Kinetic effects on particle size distributions and morphology. Chem. Eng. Sci. 46, 2389–2427.

Du, L.-W., Bian, S., Gou, B.-D., Jiang, Y., Huang, J., Gao, Y.-X., Zhao, Y.-D., Wen, W., Zhang, T.-L., Wang, K., 2013. Structure of Clusters and Formation of Amorphous Calcium Phosphate and Hydroxyapatite: From the Perspective of Coordination Chemistry. Cryst. Growth Des. 13, 3103–3109.

Elliott, J.C., 1994. Structure and Chemistry of the Apatites and Other Calcium Orthophosphates. Studies in Inorganic Chemistry 18.

Ghosh, S.K., Roy, S.K., Kundu, B., Datta, S., Basu, D., 2011. Synthesis of nano-sized hydroxyapatite powders through solution combustion route under different reaction conditions. Mater. Sci. Eng. B 176, 14–21.

Gupta, M. Das, Loganathan, P., Vigneswaran, S., 2012. Adsorptive Removal of Nitrate and Phosphate from Water by a Purolite Ion Exchange Resin and Hydrous Ferric Oxide Columns in Series. Sep. Sci. Technol. 47, 1785–1792.

Han, G.S., Lee, S., Kim, D.W., Kim, D.H., Noh, J.H., Park, J.H., Roy, S., Ahn, T.K., Jung, H.S., 2013. A Simple Method To Control Morphology of Hydroxyapatite Nano- and Microcrystals by Altering Phase Transition Route. Cryst. Growth Des. 13, 3414–3418.

Inskeep, W.P., Silvertooth, J.C., 1988. Kinetjcs of hydroxyapatite precipitation at pH 7 . 4 to 8. Cosmochim. Acta. 4, 1883–1893.

Katz, I., Dosoretz, C.G., 2008. Desalination of domestic wastewater effluents: phosphate removal as pretreatment. Desalination 222, 230–242.

Koutsopoulos, S., 2002. Synthesis and characterization of hydroxyapatite crystals: a review study on the analytical methods. J. Biomed. Mater. Res. 62, 600–612.

Kucher, M., Babic, D., Kind, M., 2006. Precipitation of barium sulfate: Experimental investigation about the influence of supersaturation and free lattice ion ratio on particle formation. Chem. Eng. Process. Process Intensif. 45, 900–907.

Lagno, F., Rocha, S.D.F., Katsarou, L., Demopoulos, G.P., 2012. Supersaturation-Controlled Synthesis of Dicalcium Phosphate Dihydrate and Nanocrystalline Calcium-Deficient Hydroxyapatite. Ind. Eng. Chem. Res. 51, 6605−6612.

Liu, C., Huang, Y., Shen, W., Cui, J., 2001. Kinetics of hydroxyapatite precipitation at pH 10 to 11. Biomaterials 22, 301–6.

Liu, Y., Sheng, X., Dong, Y., Ma, Y., 2012. Removal of high-concentration phosphate by calcite: Effect of sulfate and pH. Desalination 289, 66–71.

Bruisma, O.S.L., Vanrosmalen, G.M., Seckler, M.M., 1996. Phosphate removal in a fluidized bed -I. Identification of physical processes. Wat.Res 5, 1585–1588.

Moreno, E.C., Varughese, K., 1981. Crystal growth of calcium apatite from dilute solutions. J. Cryst. Growth. 53, 20–30

Müller, F.A., Müller, L., Caillard, D., Conforto, E., 2007. Preferred growth orientation of biomimetic apatite crystals. J. Cryst. Growth 304, 464–471.

Nriagu, J.O. and, Moore, P.B., 1984. Phosphate Minerals. Springer-Veriag.

Nur, T., Johir, M.A.H., Loganathan, P., Nguyen, T., Vigneswaran, S., Kandasamy, J., 2014. Phosphate removal from water using an iron oxide impregnated strong base anion exchange resin. J. Ind. Eng. Chem. 20, 1301–1307.

Paz, A., Dainelys G., Monica L., Jesus E. G., Brizuela.N., and Aragón, J., 2012. A comparative study of hydroxyapatite nanoparticles synthesized by different routes,. Quim. Nov. 35, 1724–1727.

Pham, T.T.T., Nguyen, T.P., Pham, T.N., Vu, T.P., Tran, D.L., Thai, H., Dinh, T.M.T., 2013. Impact of physical and chemical parameters on the hydroxyapatite nanopowder synthesized by chemical precipitation method. Adv. Nat. Sci. Nanosci. Nanotechnol. 4. 1–9.

Piccirillo, C., Silva, M.F., Pullar, R.C., Braga da Cruz, I., Jorge, R., Pintado, M.M.E., Castro, P.M.L., 2013. Extraction and characterisation of apatite- and tricalcium phosphate-based materials from cod fish bones. Mater. Sci. Eng. C 33, 103–110.

Puigdomènech, I., 2001. Chemical Equilibrium Software Hydra and Medusa. Inorg. Chem. Dep.

Rodriguez-Clemente, R., Gomez-Morales, J.,Torrent-Burgues, J., 2001. Crystal Size Distribution of Hydroxyapatite Precipitated in a MSMPR Reactor. Ind. Eng. Chem. Res. 36, 1065–107.

Sengupta, S., Pandit, A., 2011. Selective removal of phosphorus from wastewater combined with its recovery as a solid-phase fertilizer. Water Res. 45, 3318–30.

Skoog, D.A. and Donald.M.W., 1976. Fundamental of Analytical Chemistry, 3th Edition. Saunders Philadelphia, 804.

Sporysh, I., Shynkaruk, E., Lysko, O., Shynkaruk, A., Dubok, V., Buzaneva, E., Ritter, U., Scharff, P., 2010. Biomimetic hydroxyapatite nanocrystals in composites with C60 and Au-DNA nanoparticles: IR-spectral study. Mater. Sci. Eng. B 169, 128–133.

Tran, A.T.K., Zhang, Y., De Corte, D., Hannes, J.-B., Ye, W., Mondal, P., Jullok, N., Meesschaert, B., Pinoy, L., Van der Bruggen, B., 2014. P-recovery as calcium phosphate from wastewater using an integrated selectrodialysis/crystallization process. J. Clean. Prod. 77, 140–151.

Tomson, M.B., Koutsoukos, P., Amjad, Z., 1980. Calcium Phosphates. A Constant Composition Study. J. Am. Chem. Soc. 1553–1557.

Wang, L., Nancollas, G.H., 2008. Calcium orthophosphates: crystallization and dissolution. Chem. Rev. 108, 4628–69.

Xie, B., Halter, T.J., Borah, B.M., Nancollas, G.H., 2014. Tracking Amorphous Precursor Formation and Transformation during Induction Stages of Nucleation. Cryst. Growth Des. 14, 1659–1665.

Yang, Q., Wang, J.-X., Shao, L., Wang, Q.-A., Guo, F., Chen, J.-F., Gu, L., An, Y.-T., 2010. High Throughput Methodology for Continuous Preparation of Hydroxyapatite Nanoparticles in a Microporous Tube-in-Tube Microchannel Reactor. Ind. Eng. Chem. Res. 49, 140–147.

Chapter 3

Detrimental effects of Magnesium (II) on hydroxyapatite precipitation from synthetic industrial brines

This chapter is based on the work presented in the publication:
Hermassi. M, Valderrama. C, Dosta. J, Cortina. J.L, Batis, N.H., 2016. Detrimental effects of magnesium (II) on hydroxyapatite precipitation from synthetic industrial brines. Chemical Engineering Journal. (283) 572-581 (5-Year Impact factor: 4,621).

The influence of Mg(II) on phosphorous recovery as hydroxyapatite (Hap) from alkaline phosphate concentrates using desalinated industrial brines as the calcium source in a batch reactor was evaluated. Two synthetic brines with Mg/Ca molar ratios of 2.2 and 3.3 were continuously fed to reach a Ca/P molar ratio of ~1.67 to promote Hap formation under different constant pH values (8, 9.5, 10.5, 11.5 and 12). For both brines, inhibition of Hap precipitation and formation of the amorphous mineral phases of Ca-, Mg- and Ca/Mg-phosphates were observed at pH >9.5. Mg(II) severely inhibited phosphate precipitation, allowing the formation of amorphous calcium phosphate from meta-stable clusters due to Mg(II) incorporation into Ca-phosphate. For the Mg/Ca (3.3) brine, a more soluble Mg-phosphate mineral (cattiite) was formed at pH 11.5. Thermal treatment of the amorphous solids to increase crystallinity confirmed the presence of Hap and chlorapatite as Ca-phosphate, stanfieldite as Ca-Mg-phosphate and farringtonite as Mg-phosphate. In the experiments at pH 8, the formation of stable nanometre-sized pre-nucleation clusters promoted nucleation inhibition, even in supersaturated solutions, and no solids were recovered after filtration. Although sulfate was involved in some of the precipitation reactions, its role in the inhibition of Hap formation is not clearly elucidated.

1. Introduction

Phosphorus (P) is a non-renewable resource, non-substitutable for agriculture and food production and directly linked to global food security, as well as being important in other industrial and technical uses. At the same time, P losses are the principal contributor to eutrophication of surface waters, globally the P footprint of human diets continues to increase and the

world mineral phosphate reserves decrease and there is a debate about their extent and extractability and about their geographical concentration. Improving the efficiency of P processing and use, in industry, agriculture, livestock production, food processing, and developing P reuse or recovery-recycling can reduce costs, contribute to reducing nutrient pollution, and create jobs in the frame of circular economy (Circular Economy Strategy, 2014).

Phosphate is typically present at low concentrations in urban wastewaters (from 10 to 30 mg P-PO_4^{3-}/L) and in industrial wastewaters, such as detergent manufacturing, food processing or metal-coating processes (50 to 150 mg P-PO_4^{3-}/L) (Barca et al., 2012; Li and Brett, 2012; Mezenner and Bensmaili, 2009). The removal of phosphate from water bodies is important because it causes eutrophication, which has a harmful effect on aquatic life, resulting in a reduction in biodiversity. On the other hand, the recovery of phosphate from P-containing wastewater is essential for developing an alternative P source to overcome the global challenge of its scarcity (Nur et al., 2014). However, one of the disadvantages that complicate phosphate recovery is the low concentration of phosphate in the target effluents.

Many different processes have been proposed for pre-concentration of phosphate, such as adsorption, ion exchange and biological treatment (Kodera et al., 2013; Liu et al., 2012; Sengupta and Pandit, 2011). The introduction of new P-selective sorbents (e.g., hydrated metal oxide based sorbents) would generate alkaline phosphate concentrates due to the requirements of the sorbent regeneration with NaOH solutions (Sengupta and Pandit, 2011).

Chemical P recovery using Ca(II) and Mg/NH_4 salts to precipitate or crystallize phosphate as NH_4-Mg or Ca salts are the primary solutions postulated (Tran et al., 2014). To address this objective, the use of industrial wastes as alternative Ca(II) sources for Ca-phosphate precipitation has been suggested. Ca-phosphates can be recovered by crystallisation of Hap in appropriate reactors via pH and chemical dosing control, as reported previously (Elisabeth V. Munch and Keith Barr, 2001; Castro et al., 2013a; Hermassi et al., 2015). Recently, the use of seawater reverse osmosis and nanofiltration brines for the recovery of economically valuable constituents (Kim, 2011) or specifically as an inexpensive Mg(II) and Ca(II) source, and for struvite recovery from anaerobic digesters in municipal wastewater treatment plants was suggested (Telzhensky et al., 2011; Lahav et al., 2013). The significant Ca(II) concentration present in seawater brines (up to 0.4 g Ca/L) may enhance the precipitation of Ca-phosphate minerals (e.g., $Ca_3(PO_4)_2$ and $Ca_5(PO_4)_3(OH)$, among others). However, the influence of high concentrations of Mg(II) up to 1 g Mg(II)/L is unknown. Salami et al. (Salimi et al., 1985) reported no detectable effect of Mg(II) ions on the growth of dicalcium phosphate dihydrate, but they did report that the Mg(II) ions appreciably decelerated the rate of octacalcium phosphate growth, most likely by adsorption at active growth. More recently, Cao and Harris (Cao and Harris, 2008) studied the interactive effects of CO_3^{2-} and Mg(II) ions on Ca-phosphate precipitation under conditions simulating dairy manure-amended soil leachate and phosphate recovery from manure wastewater. The inhibition effects of Mg(II) and the synergistic effect of both of the ions on Hap crystallinity and the precipitation rate promoted the formation of amorphous Ca-phosphate (ACP), presumably due to Mg(II) incorporation into the crystal

structure. However, the presence of Mg(II) or SO_4^{2-} ions in the case of using industrial desalinated brines at concentrations higher than the calcium ions has not been studied. Moreover, few studies in literature are devoted to study the potential precipitation of Ca-Mg-phosphate minerals and the mechanism involved.

It should be mentioned the work done by Golubev et al. (Golubev et al., 1999, 2001) who postulated the formation of ($(Ca, Mg)_4H(PO_4)_3.xH_2O$) in the precipitation of phosphate with sea water and more recently Muster et al. (Muster et al., 2013) who postulated theoretically the formation of potential Ca-Mg phases.

Therefore, the goal of this study is to evaluate the potential inhibition of Mg(II) on hydroxyapatite (Hap) precipitation during the valorisation of concentrated phosphate effluents when using synthetic industrial desalinated brines as the calcium source. Two brines with different Mg/Ca molar ratios of (2.2) and (3.3) were used. The precipitation/crystallisation of Ca- and/or Mg-phosphate processes at different constant pH values were evaluated in a batch reactor and the precipitate properties were also studied. The variation of the Ca- and Mg-phosphate nucleation profiles was used to elucidate the formation mechanism of Hap or Mg-phosphates with high Mg(II) concentration brine.

2. Materials and Methods

2.1. Experimental set-up and procedures

The precipitation of phosphate (P(V)) was performed in a 2 L glass batch reactor at constant pH values (8, 9.5, 10.5, 11.5 and 12), following the conditions defined in a previously study (chapter 2). These alkaline pH values were selected based on the thermodynamic prediction for the precipitation of

Ca and Mg phosphates. Stirring at 250 rpm was achieved using a mechanical stirrer (IKA RW 20). The pH was monitored on-line using a pH potentiometer (Crison pH 28), when the pH was 0.1 units above or below the set point, 1 M HCl or 1 M NaOH was dosed using a peristaltic pump.

Batch experiments were performed by mixing a 1.0 g $P\text{-}PO_4^{3-}$/L solution with Mg/Ca brine. NaH_2PO_4 was used to prepare the phosphate solutions. Composition was fixed according to the expected conditions of the elution of ion exchange resins on the recovery of phosphate from treated waste water effluents.

Two synthetic solutions with different Mg/Ca molar ratios (2.2 and 3.3) were prepared by mixing given amounts of NaCl, $CaCl_2.2H_2O$, Na_2SO_4 and $MgCl_2.6H_2O$. The compositions of both of the brines are summarized in Table 3.1. The presence of antiscalants typically present on desalination brines (e.g. 1-2 mg/L) and the temperature were not included in the experimental design.

Brine solution was added at a flow rate of 0.3 mL/min (using a Gilson Minipuls 3 peristaltic pump) to reach a Ca/Pa molar ratio of 1.67 suitable for Hap precipitation. Experiments were performed at room temperature (22±2 °C) in duplicate.

Table 3.1. Composition of industrial desalinated brines used in this study.

	Ca (g Ca(II)/L)	Na g Na(I)/L	Cl g Cl^-/L	SO_4^{2-} g SO_4^{2-}/L	Mg[a] g Mg(II)/L	pH_0
Mg/Ca (2.2) brine	0.23	23.5	34.2	3.4	0.30	8.8
Mg/Ca (3.3) brine	0.41	18.9	16.4	20.1	0.85	8.9

[a] The Mg content is low because Mg(II) was recovered as $Mg(OH)_2$

Batch reactor aqueous samples were obtained during the experiments and then filtered through a 0.22-μm filter. The total concentrations of ions were determined by ion chromatography using an Ionex Liquid Chromatograph (ICS-1000). The accuracy of the measurements was higher than 95%. At the end of the experiments, the solid phase was removed from the reactor by filtration, washed with deionised water several times and dried at 60°C for 24 h.

2.2. Particle analysis

The solid phase particle size distribution was analysed by LS with a Coulter diffraction particle size analyser (LS 13 320 Laser Diffraction Particle Size Analyser Instrument, Beckman Coulter). The crystal size distribution range (CSD) varied from 0.04 to 2000 μm. Particles were analysed as obtained directly from the batch reactor without any thermal treatment or particle size separation.

The phase purity and crystallinity of powder were analysed by X-ray diffraction with λ CuKα radiation (λ= 1.54056 Å) at a scanning rate of 19.2 and 57.6 s, a steep angle of 0.015° and 2θ over range of 4 to 60°. The solids in powder form were identified by the Joint Committee Powder Diffraction Standards (JCPDS) file and were compared with the Powder Diffraction File (PDF) no. 00-009-0432 for Hap ($Ca_{10}(PO_4)_6(OH)_2$), 00-011-0231 for stanfieldite ($Ca_4Mg_5(PO4)_6$), 00-025-1373 for farringtonite ($Mg_3(PO4)_2$) and 00-001-1011 for chlorapatite ($Ca_{10}Cl_2(PO4)_6$) (International center of diffraction data, 2003).

To elucidate the potential inhibition mechanism, a portion of the amorphous phases was heated at 1050°C for 4 h and cooled at room temperature to

enhance the crystallinity of the precipitated phases. It cannot been discarded that the thermal treatment promotes additionally to an increase of crystallinity a change on the crystal structure or the chemical composition. However, the information provided after this treatment is valued as it is improving the mechanisms discussion (Suchanek et al., 2004).

2.3. Prediction of phosphate precipitation processes

Phosphate precipitation processes using Mg/Ca brines were studied using the HYDRA-Medusa (Puidomènech, 2001) and the Visual Minteq codes (Gray-Munro and Strong, 2013). The measured P(V), Mg(II), Ca(II), SO_4^{2-}, and Cl^- concentrations were compared when required to those estimated using both of the codes. Although conditions in the precipitation tests could be far away from the equilibrium, measured and predicted values were used to identify the potential reactions and mechanism involved, especially when the solids formed were not appropriately characterized.

The expected total phosphate concentration in solution at a given time ($[P(V)]_t$ (mol/L)) was calculated using the mass balance given in Equation 1 and considering the initial phosphate concentration $[P(V)]_0$ (mol/L), the total metal concentration added at time t ($[M_{ad}]_t$ (mol/L)) and the total measured metal concentration at time t ($[M]_t$(mol/L), as follows:

$$[P(V)]_t = [P(V)]_0 - [P(V)]_{consumed\ (t)} = \frac{V_t}{(V_0+V_t)} \times ([P(V)]_0 - ([M_{ad}]_t - [M]_t) \times \frac{q}{r}) \quad (1)$$

where M represents Ca(II) or Mg(II), q and r are the stoichiometric coefficients of the mineral phosphate phase ($M_r(PO_4)_q(s)$), V_0 (L) is the initial volume of P(V) in the reactor, and V_t (L) is the volume of solution in the reactor at time t.

The supersaturation index (SI) was calculated by Visual Minteq and using Equation 2, as follows:

$$SI = \log(\frac{IAP}{K_{so}}) \quad (2)$$

where IAP is the ion activity product, and K_{so} is the solubility constant. Equilibrium solubility data for Ca-Mg-phosphates were critically reviewed from the HYDRA and PHREEQ C databases, and the selected values are shown in Table 3.2.

Table 3.2. Crystalline phase identified in Mg-Ca-PO_4 mixtures

Compound	Formula	log K_{so}
Hydroxyapatite (Hap)	$Ca_5(PO4)_3OH$	-57,8
Brushite	$CaHPO_4.2H_2O$	-19.0
Octacalcium phosphate (OCP)	$Ca_4H(PO_4)_3.3H_2O$	-48.0
Tricalcium phosphate (TCP)	$Ca_3(PO_4)_2$	-28.9
Monotite	$CaHPO_4$	-19.3
Chloroapatite	$Ca_5(PO_4)_3Cl$	-46.9
Newberyite	$MgHPO_4.3H_2O$	-5.8
Cattiite	$Mg_3(PO_4)_2\ 22H_2O$	-23.1
Bobierrite	$Mg_3(PO_4)_2.8H_2O$	-25.2
Farringtonite	$Mg_3(PO_4)_2$	-23.3
Stanfieldite	$Ca_4Mg_5(PO_4)_6$	n.a.
Brucite	$Mg(OH)_2$	-11.2
Collinsite	$Ca_2Mg(PO_4).2H_2O$	n.a.

n.a.: Not available

2.4. Fundamental precipitation inhibition effects on nucleation growth kinetics

Lamer and Dinegar (LaMer.V. K. and Dinegar.R. H., 1950) described the formation of colloidal nanocrystals in a solution phase through a crystal nucleation process involving the following three steps: i) ions start to aggregate into nuclei via self-nucleation as the monomer concentration increases in the solution to supersaturation levels, ii) monomers continuously

aggregate on the pre-existing nuclei or seed, which leads to a gradual decrease in the monomer concentration, and iii) nuclei grow into nanocrystals of increasingly larger sizes until reaching an equilibrium state.

The nucleation and growth steps are two relatively separated processes, and the formation of nuclei occurs only at a reactant concentration substantially higher than the saturation concentration (C_s); otherwise, growth of the existing nuclei dominates. The subsequent growth steps will strongly govern the final morphology of the nanocrystals (Destrée et al., 2006; Viswanatha and Sarma, 2007) and (Sarode et al., 2014).

The free energy change required for the formation of nuclei (ΔG) is determined by the free energy change for the phase transformation (ΔG_v) and the free energy change for the formation of a solid surface (ΔG_s) (Sun, 2013). Then, the driving force (Δμ) required for Hap ($Ca_5(PO_4)_3OH(s)$) crystallisation is defined by Eq. 3, as follows (Zettlemoyer, 1969):

$$\Delta\mu = KTln\,(1+\sigma) = KTln\frac{[a(Ca^{2+})]^5[a(PO_4^{3-})]^3[a(OH^-)]}{K_{so}(Hap)} \quad (3)$$

where K is the Boltzmann constant, T (K) is the absolute temperature, K_{so} is the solubility product, a is the activity of species i, and σ is the relative solution supersaturation index.

At a given Δμ, natural nucleation is a kinetically controlled process in which the Hap nuclei overcome a homogeneous nucleation barrier (ΔG_{homo}^*) (Zettlemoyer, 1969) that could be estimated by Eq. 4, as follows:

$$\Delta G_{homo}^* = \frac{16\pi\gamma_{cf}^3\Omega^2}{3[KT\ln(1+\sigma)]} \quad (4)$$

where γ_{cf} is the specific interfacial free energy between the crystals and the mother phase, and Ω is the volume of the growth units.

The nucleation induction time (t_s and (Jiang et al., 2005) at different supersaturation levels could be used to characterize the kinetics of nucleation and could be calculated by Equation 5, as follows:

$$lnt_s = \frac{k_n f(m)}{[\ln(1+\sigma)]^2} - ln\left(VR_S^2 N_0\, f^{"}(m)[f(m)]^{1/2} B\right) \quad (5)$$

where R_s is the crystal radius, N_0 is the mineral density, B is the kinetic constant, V is the solution volume, and m is a factor that depends on the interaction and interfacial structural match between the crystalline phase and substrate; it is expressed as a function of the interfacial free energy difference among the different phases, as shown in Eq. 6 as follows (Jiang and Liu, 2004):

$$m = \frac{\gamma_{sf} - \gamma_{sc}}{\gamma_{cf}} \quad (-1 < m < 1) \quad (6)$$

where γ_{sf}, γ_{sc}, and γ_{cf} correspond to the interfacial tension between substrate and fluid, crystal and substrate, and crystal and fluid, respectively.

Furthermore, *f(m)* is the interfacial correlation factor describing the reduction of the nucleation barrier ΔG^*_{homo} due to the occurrence of the substrate and is defined by Eq. 7; *f"(m)* is the pre-exponential term describing the ratio between the average effective collision in the presence and absence of substrate and is defined by Equation 8. Finally, k_n is the nucleation constant, which remains constant under a given condition m, and is defined by Eq. 9.

$$f(m) = \frac{1}{4}(2 - 3m + m^3) \quad (7)$$

$$f''(m) = \frac{1}{2}(1 - m) \quad (8)$$

$$\mathrm{k_n} = \frac{16\pi\gamma_{cf}^3\Omega^2}{3(\mathrm{KT})^3} \quad (9)$$

For a crystalline phase m, f(m) takes only those values corresponding to some crystallographically preferred orientations; then, it is possible according

to Eq. 5, to obtain a set of intercepting straight lines by plotting ln t_s versus $1/[\ln (1+\sigma)]^2$. These lines with different slopes $k_n f(m)$ in the different regimes indicate that nucleation is governed by a sequence of progressive heterogeneous processes, as described by Lamer and Dinegar (1950) (LaMer.V. K. and Dinegar.R. H., 1950).

3. Results and Discussion

3.1. Influence of pH on the phosphate recovery with Ca/Mg brines

Precipitation of Hap with Mg/Ca (2.2) and Mg/Ca (3.3) brines was studied as a function of pH (8, 9.5, 10.5, 11.5 and 12). The change of total phosphate concentration and recovery (%) as a function of reaction time is shown in Figure 3.1 in which the dotted lines represent the expected total phosphate concentration if any precipitation reaction was involved. Phosphate recovery efficiency in the richest Mg brine (Mg/Ca 3.3) (Figure 3.1c and d) is larger at pH up to 10.5. Higher recoveries were measured in only 18 hours, while for the Mg/Ca (2.2) brine were observed after 34 hours (Figure 3.1a and b). A similar trend was reported by Su et al. (Su et al., 2014) when precipitating phosphate with magnesium chloride solutions (Mg/P (2.1)) in alkaline media (pH 10-12) in a fluidized bed reactor.

The lowest phosphate recoveries (20%) were reported at pH 8 for Mg/Ca (2.2) brine and at pH 8 and 9.5 for Mg/Ca (3.3) brine. For both of the brines (at lower pH) at the end of the experiment after filtration, the solutions presented turbidity, and no precipitate was recovered on the 0.22-μm filter. This result was associated with the inhibition of the nucleation process and the formation of clusters of the nanometre size, as discussed in Section 3.3.

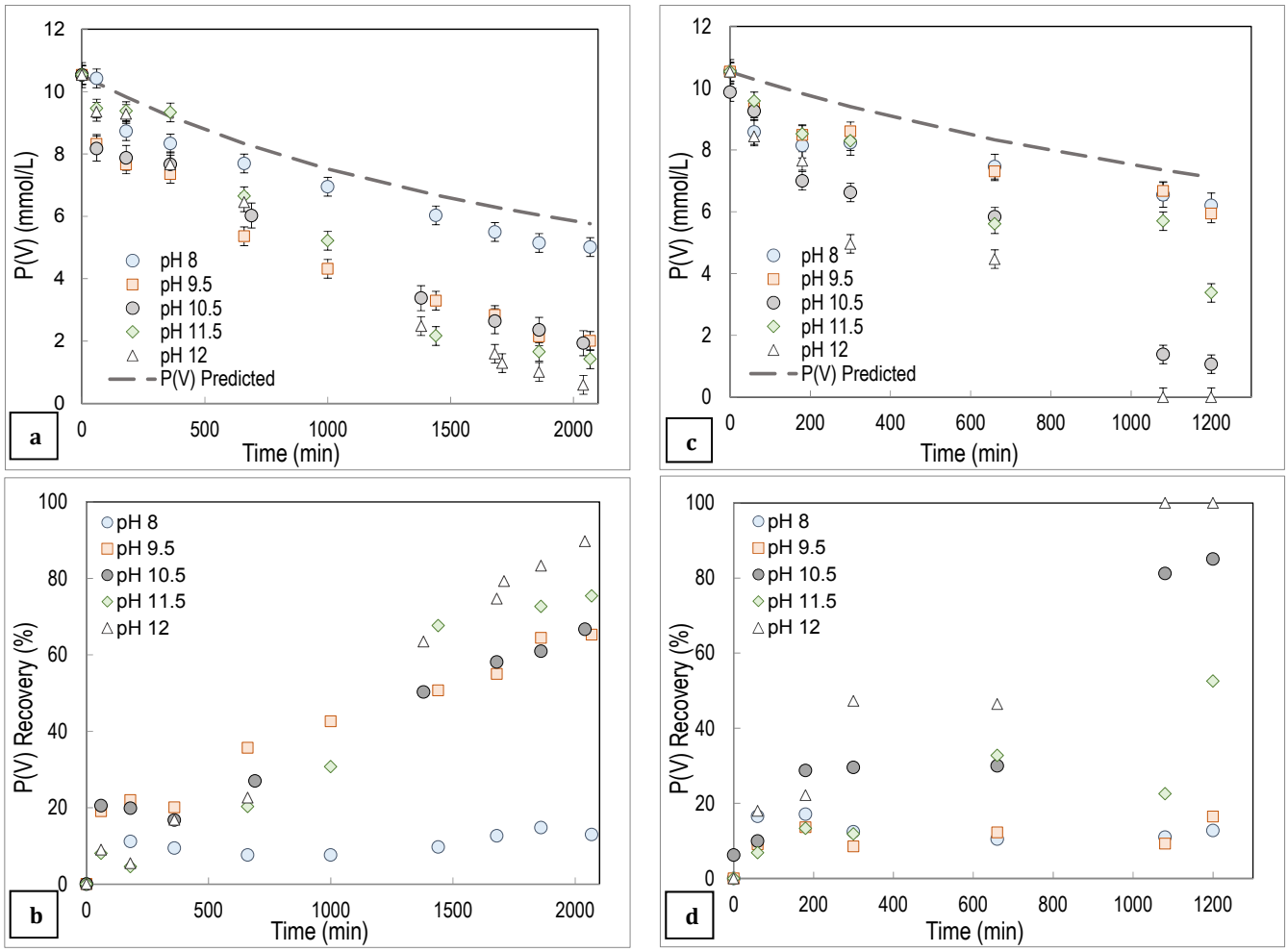

Figure 3.1. Effect of pH on a) the P(V) concentration variation and b) the P(V) recovery by precipitation using the Mg/Ca (2.2) brine, c) the P(V) concentration variation and d) the P(V) recovery by precipitation using the Mg/Ca (3.3) brine (dotted line represents the expected P(V) concentration if any precipitation).

The increase of phosphate recovery efficiency with increasing pH is explained by the change of P(V) speciation. At pH 8, 45% of P(V) is present in solution as HPO_4^{2-}, and less than 4% is present as PO_4^{3-} for the initial additions of brine with 12-8 mmol/L P(V) concentrations. However, at pH 11.5, 41% of P(V) is present as PO_4^{3-} and 20% as HPO_4^{2-}, and a higher SI is achieved.

As demonstrated by Gunawan et al. (Gunawan.E.K, Warmadewanthi, 2010), the degree of supersaturation and the type of precipitates formed depend on the pH. A higher pH leads to higher SI and accelerates the precipitation reaction as well as increasing its efficiency.

3.2. Influence of brine composition on Hap formation and precipitation inhibition

3.2.1. Recovery of phosphate by Mg/Ca (2.2) brines

The change of the Mg(II), Ca(II), SO_4^{2-} and Cl^- contents as a function of precipitation reaction time is plotted in Figure 3.2 in which the solid lines represent the total ion concentration added to the reactor throughout the experiment, which is the concentration expected to be measured for a species not involved in any precipitation or solid formation reaction.

As can be seen in Figure 3.2, Mg(II) concentration is reduced to less than 0.2 mmol/L, independent of the pH value, while the Ca(II) concentrations are maintained below 1 mmol/L, with the exception of pH 8, where values are equal to the total added Ca(II) concentration. In the case of SO_4^{2-}, the measured concentrations agree with the total added concentration, except for the experiment at pH 8 with values below 10%. For Cl^-, the measured concentrations showed a reduction from 700 to 400 mmol/L. This behaviour confirms that these ions (Mg(II), Ca(II) and Cl^-) are involved in the precipitation reactions.

The variation of the SI of the expected mineral phases along the reaction time, such as Hap, tricalcium phosphate (TCP), octacalcium phosphate (OCP), monotite and brushite for Ca(II) as well as $Mg(OH)_2$ and $Mg_3(PO4)_2(s)$ for Mg(II) is shown in Figure 3.3 for pH 11.5 and 8. At higher

pH values (9.5 and 11.5), the precipitation of Ca-phosphates is favoured (up to 90% of P(V) recovery at pH 11.5, as shown in Figure 3.1).

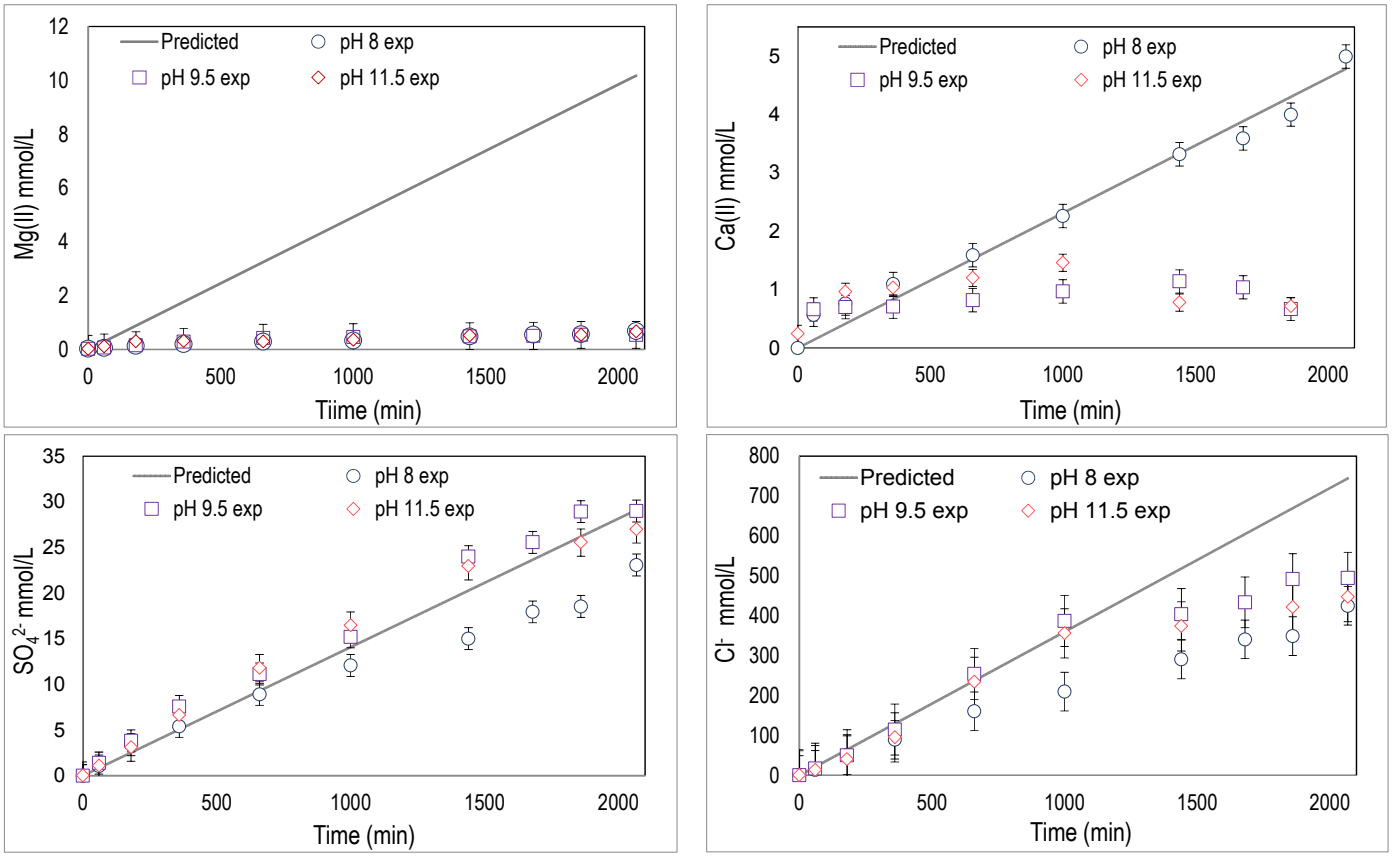

Figure 3.2. Variation concentration of major components (Mg(II), Ca(II), SO_4^{2-} and Cl^-) in experiments under different pH conditions using the Mg/Ca (2.2) brine (solid lines are the total ion concentration added throughout the precipitation experiment).

The SI of the Ca-phosphate mineral phases were close to zero for brushite and monotite, close to 4 for TCP and OCP, and close to 18 for Hap (Figure 3.3a). Therefore, nucleation of Hap, the most stable phase among the Ca-phosphates, is expected to occur instantaneously (Edzwald.J, 2010). Typically, supersaturation of Hap is achieved by a simple increase in pH (Jones, 2001), and then it follows a three-stage process in which the initially formed amorphous ACP may be redissolved and form Hap nuclei followed by

formation of hydroxyapatite (Boskey A.L. and Posner A.S., 1973; Meyer, 1983; Sugiura et al., 2011).

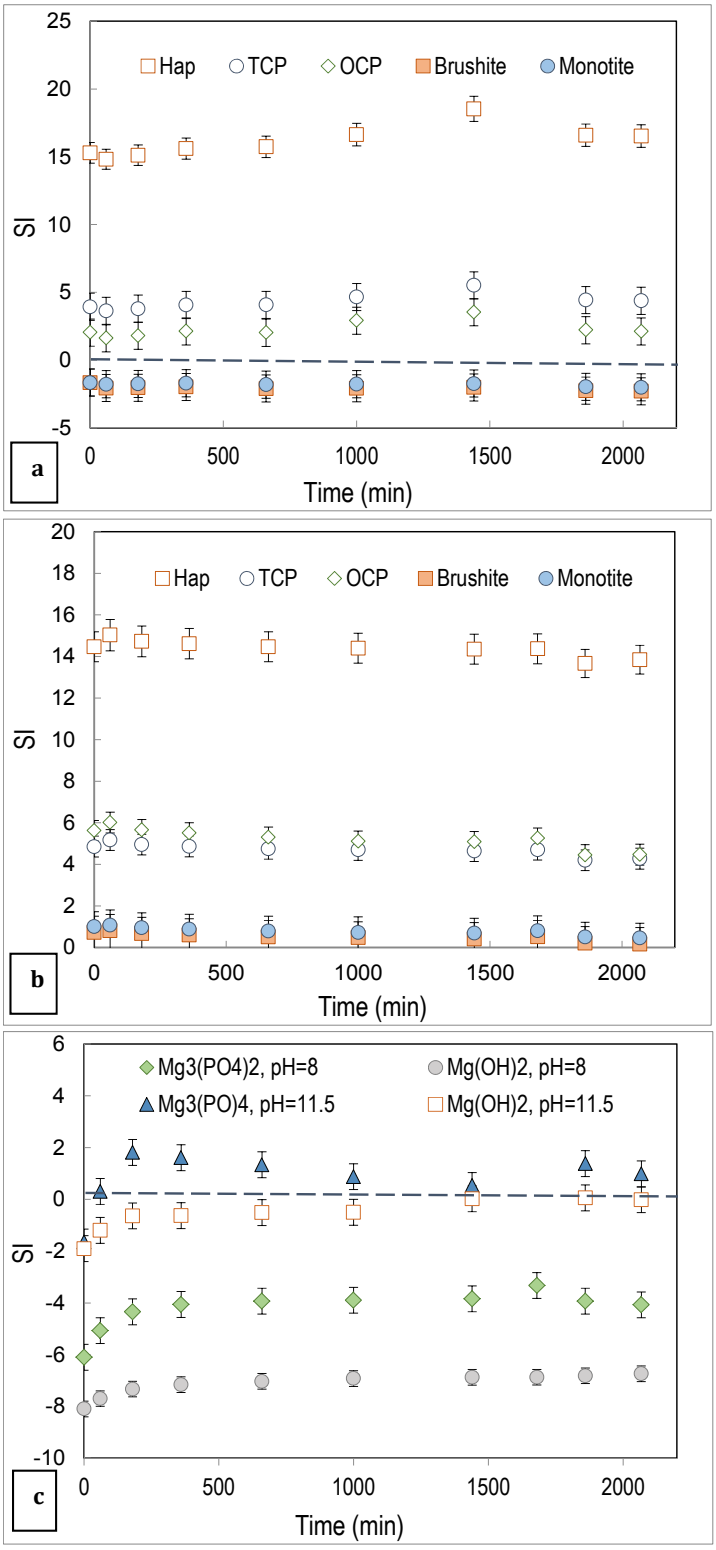

Figure 3.3. Saturation index (SI) for several minerals in the reactor for brine (Mg/Ca=2.2) at a) pH 11.5 for Ca-phosphate minerals, b) pH 8 for Ca-phosphate minerals and c) pH 8 and 11.5 for Mg-phosphate minerals.

XRD analysis of the precipitates collected in both of the experiments at pH 9.5 and 11.5 reveals that the formed Ca-phosphates were amorphous, as shown by a broad peak between 23° and 35° (2θ) (Figure 3.4a). These patterns are typical of ACP (Alvarez et al., 2004), indicating that Mg(II) promoted the formation of the relatively unstable ACP, in the form of ACP-adsorbed Mg(II), and then hindered the expected Hap formation according to the saturation indexes (Cao et al., 2007; Ding et al., 2014).

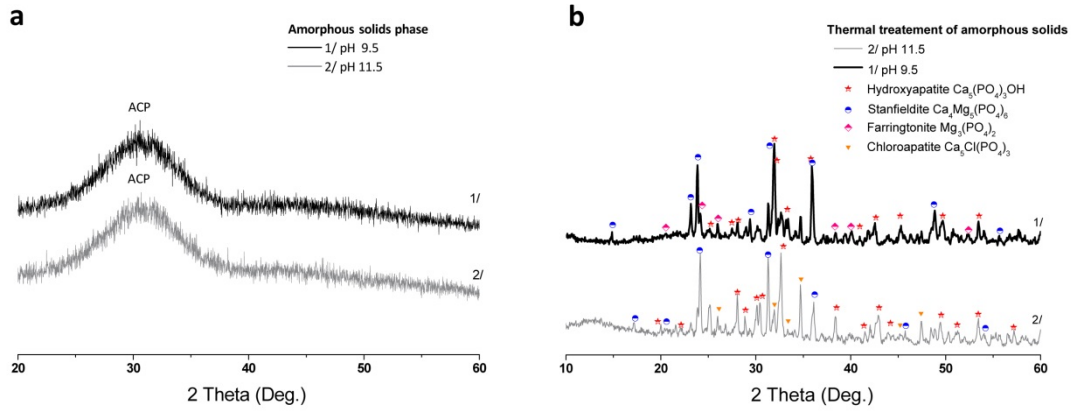

Figure 3.4. XRD spectra of the particles obtained in the stirred batch reactor with Mg/Ca (2.2) brine a) ACP at pH 9.5 and 11.5 and b) Crystal solid at different pH values after thermal treatment.

Yang et al. (Yang et al., 2011a) reported that Mg(II) ions reduce the nucleation rate of Hap in Ca-phosphate supersaturated solutions by stabilizing the gel-like ACP phase and increasing the induction and transformation time. Ding et al. (Ding et al., 2014) described that Mg(II) ion adsorption onto ACP is more effective than the phase incorporation at inhibiting phase transformation from ACP to Hap. Additionally, at these pH values, sulfate was not involved in the formation of solid phases (measured values agree with the total added concentration), and it is present in solution primarily as complexed species (e.g., $MgSO_{4(aq)}$ and $CaSO_{4(aq)}$), avoiding the

precipitation or re-dissolution of potential Ca-phosphate precipitates (Liu et al., 2012).

The SEM–EDX analysis of the amorphous solids confirmed the major presence of precipitates containing Ca–P–O and to a minor extent, Mg(II) and Cl^-. Considering that the Mg(II) and Ca(II) removal ratios for both of the pH values were higher than 90%, the solubility data of different Ca/Mg-phosphate mineral phases ($Mg_3(PO_4)_2(s)$, $Ca_5OH(PO_4)_3(s)$) were used to predict the expected P(V) concentration throughout the experiment at each given pH. For both of the pH values Figures 3.5b and c), the measured P(V) concentrations were better predicted when assuming the formation of Mg-phosphate minerals than when assuming the formation of Ca-phosphate minerals.

The XRD analysis of the amorphous precipitate at pH 9.5, after treatment at 1050°C to increase its crystallinity, identified the presence of a Ca-phosphate mineral (Hap ($Ca_5OH(PO_4)_3(s)$), a Ca-Mg-phosphate mineral (stanfieldite ($Ca_4Mg_5(PO_4)_6$)) and a Mg-phosphate mineral (farringtonite $Mg_3(PO_4)_2$) (Figure 3.4b). In the case of the amorphous precipitate at pH 11.5, in addition to the presence of Hap and stanfieldite, a Ca-phosphate-chloride mineral (chlorapatite ($Ca_5Cl(PO_4)_3(s)$) was detected (Figure 3.4b). Therefore, the consumption of chloride in the precipitation reactions was confirmed (Figure 3.2), and it was also identified by EDX analysis, as described in Table 3.3.

In the experiment at pH 8 because Ca(II) was not consumed, and Mg(II) was completely consumed, the P(V) recovery (up to 20%) should be associated with the formation of Mg-phosphate or magnesium hydroxide. The SI indicates that the solution is not supersaturated in $Mg(OH)_2(s)$ (Figure 3.3c); thus, the recovery of P(V) should be associated with the formation of Mg-

phosphate and, potentially, with the formation of minerals containing sulfate because the measured values are lower than the total added concentration. A comparison of the measured and expected P(V) concentration provides a good prediction of the measured P(V) concentration profile considering the formation of Mg-phosphate, as shown in Figure 3.5a.

Table 3.3. SEM-EDX analysis of precipitates recovered from batch reactors using Mg/Ca (2.2) and Mg/Ca (3.3) brines at pH values of 9.5 and 11.5.

Elements / Experiments	O	Mg	P	S	Cl	Ca
Mg/Ca 2.2 at pH 9.5	56.0	4.9	16.1	0.4	2.2	20.4
Mg/Ca 3.3 at pH 9.5	52.8	7.9	13.8	0.7	13.3	11.5
Mg/Ca 2.2 at pH 11.5	55.1	11.1	15.6	0.7	6.9	10.6
Mg/Ca 3.3 at pH 11.5	64.8	15.1	15.1	0.5	0.5	4.0

All of the results in weight %, processing option; All of the elements analysed (normalised)

Although solutions were supersaturated in Hap, OCP, TCP, brushite and monotite (Figure 3.3b), the observed Ca-phosphate mineral inhibition could be due to the formation of $CaSO_4$ as a precursor because sulfate is present at a substantially higher concentration than phosphate or due to the inhibition of Mg(II) ions. At the end of the experiment, no solid was recovered after solution filtration because the size of the precipitate is expected to be of nanometre size (ca. below 1 nm); thus, it was not possible to confirm its chemical or mineral composition or the potential inhibition effect of sulfate ions.

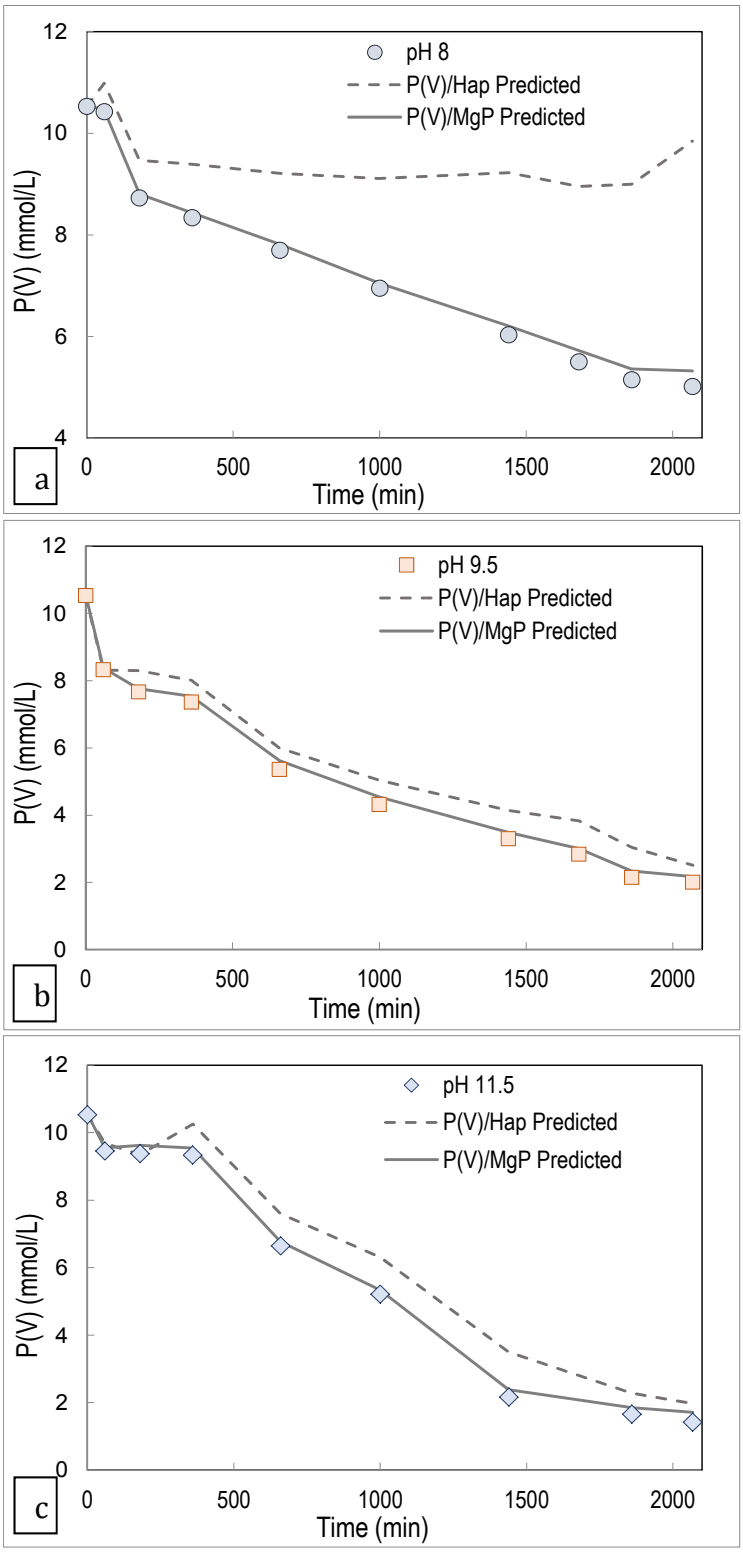

Figure 3.5. Variation of experimental and predicted P (V) concentrations assuming the formation of the Ca- and/or Mg-phosphate mineral phase at different pH values using Mg/Ca (2.2) brine at: a) pH 8, b) pH 9.5 and c) pH 11.5.

3.2.2. Recovery of phosphate by Mg/Ca (3.3) brines

The change of the major ion concentration as a function of reaction time at different pH values is plotted in Figure 3.6. Mg(II) concentration was reduced from 15 mmol/L to less than 5 mmol/L at the end of the experiments at pH 9.5 and 11.5. The Ca(II) concentration was reduced to values of 1 mmol/L for the experiment at pH 9.5, while for the test at pH 8 and 11.5, the measured values approached the total added Ca(II) concentration (4 mmol/L), indicating that Ca(II) did not participate in any precipitation reaction. Sulfate concentration was reduced from 80 mmol/L to 60 mmol/L at the end of the experiments, indicating that sulfate was involved in the precipitation reactions. The measured chloride concentrations approached the total added concentration, indicating that it was not involved in any precipitation reaction, contrary to the observed behaviour for Mg/Ca (2.2) brine.

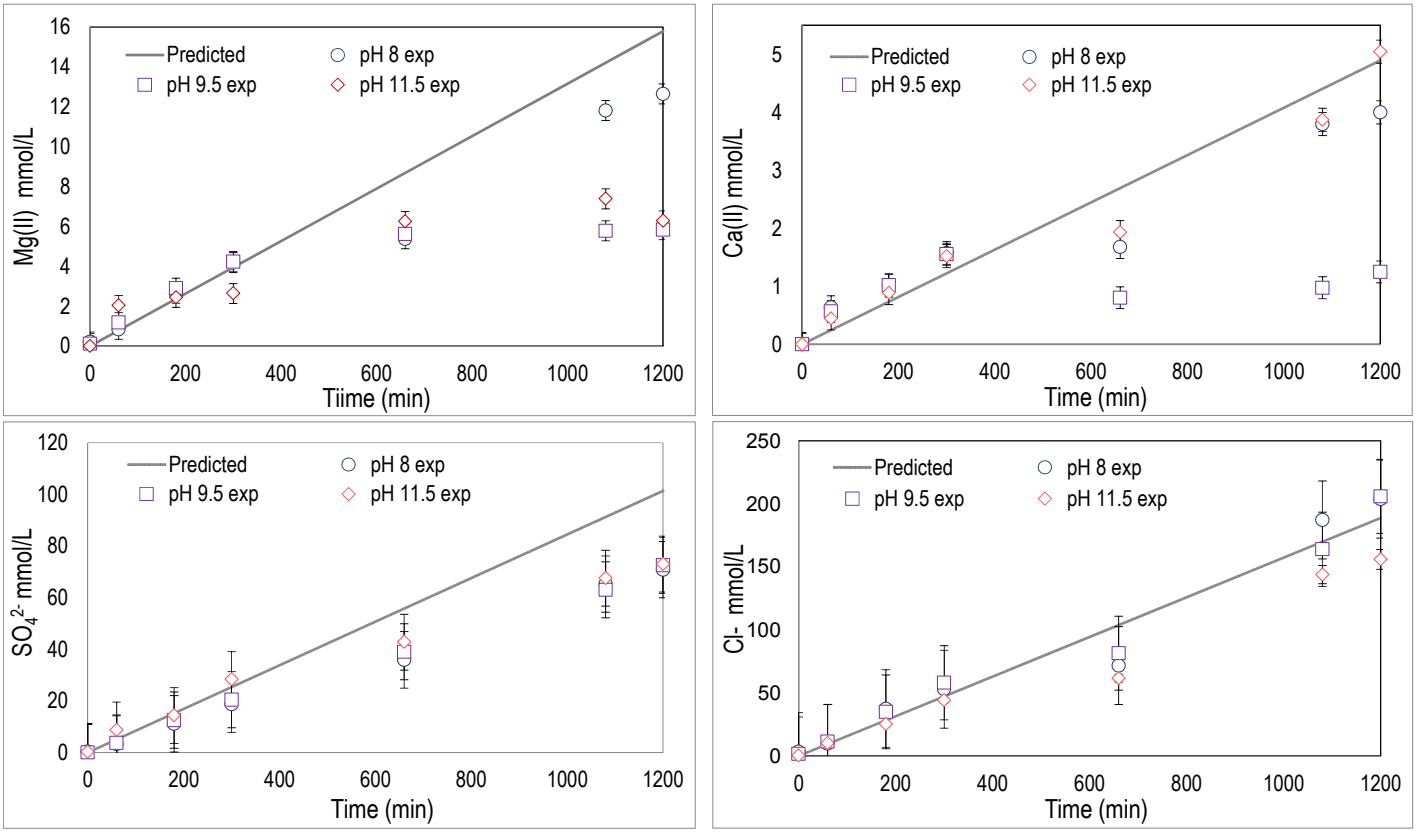

Figure 3.6. Variation of major components (Mg(II), Ca(II), SO_4^{2-} and Cl^-) in the batch experiments under different pH conditions using the Mg/Ca (3.3) brine (solid lines are the total ion concentration added along the precipitation experiment).

XRD analysis revealed that the solid product collected at pH 9.5 was amorphous, while at pH 11.5, cattiite ($Mg_3(PO_4)_2.22H_2O$) was detected (Figure 3.7). These results confirm the profiles of Ca(II) and Mg(II) shown in Figure 3.6 in which the Ca(II) concentration was not reduced as the experiment progressed, as revealed when it was identified by EDX analysis, as summarized in Table 3.3.

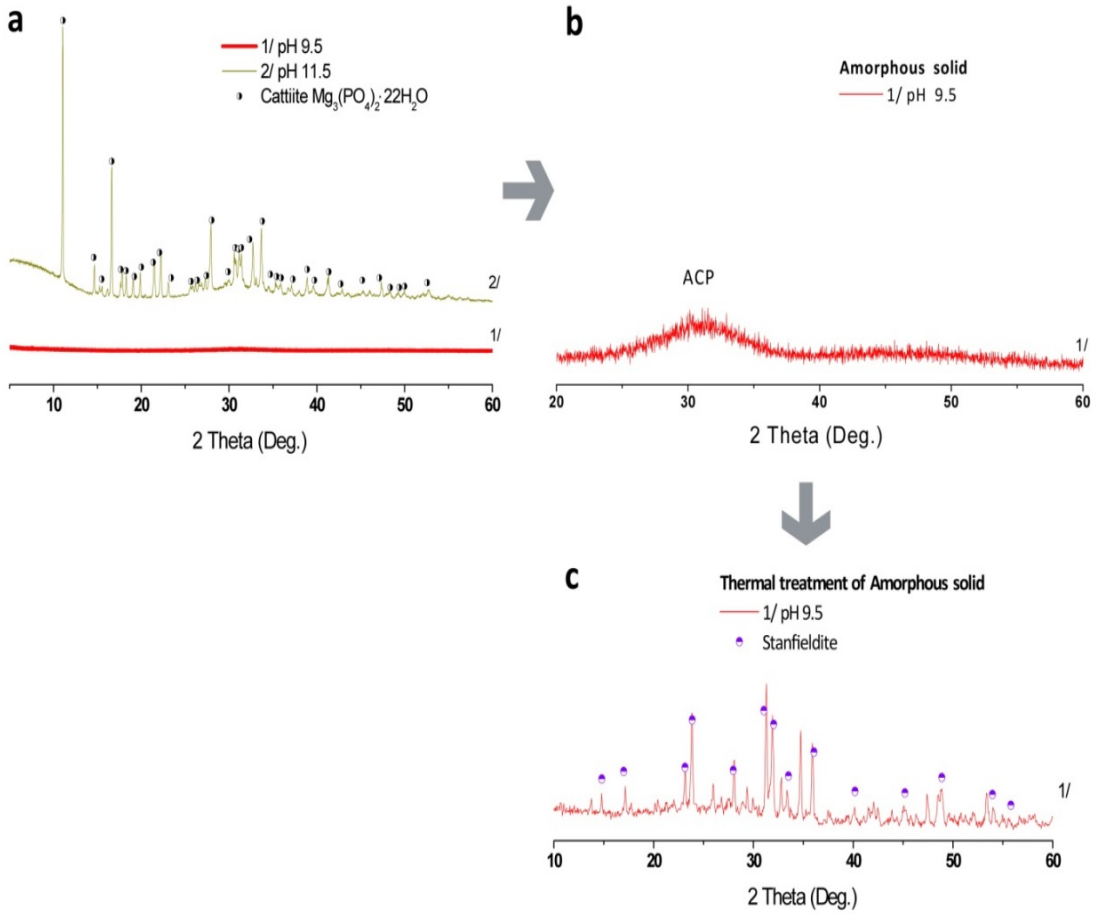

Figure 3.7. XRD spectra of the particles produced in the stirred batch reactor with Mg/Ca (3.3) brine at a) pH 11.5 and 9.5 and b) pH 9.5 amorphous solid and c) pH 9.5 after thermal treatment of amorphous precipitates.

At pH 11.5, the solution is supersaturated in Hap; however, the higher initial magnesium concentration inhibited its precipitation, and cattiite was found ($logK_{so}$= 23.1) (Taylor et al., 1963) as shown in Figure 3.7a. Note that cattiite was formed in the presence of a high Mg(II) concentration instead of the less-soluble solid Hap ($logK_{so}$= 57.8) due to the effect of Mg(II) ions on the field stability of the solids, promoting the precipitation of more soluble solids (Jenkins and Ferguson, 1971; Cusick et al., 2014). The measured P(V) concentrations were well predicted assuming the formation of cattiite, as shown in Figure 3.8.

The amorphous precipitate at pH 9.5 shows a broad peak between 23° and 35° (2θ) (Figure 3.7b) of ACP. The SEM–EDX examination of the amorphous sample detected the presence of Ca-Mg–P–O solids and the minor presence of S. The XRD analysis of the treated sample at 1050°C identified the presence of stanfieldite ($Ca_4Mg_5(PO_4)_6$)) (Figure 3.7c), thus confirming the consumption of Mg(II) and Ca(II), as described in Figure 3.6. The higher Mg(II) concentration inhibits the Hap precipitation, favouring the formation of mixed Ca-Mg-phosphates, such as stanfieldite (Ca_4Mg_5 $(PO_4)_6$), as detected by XRD. Mg(II) stabilizes ACP, which is the precursor phase during Hap formation from highly supersaturated solutions (Yang et al., 2011). It was also described that Mg(II) could be included in the precipitated solid and could modify the solids by its smaller size and greater tendency to bond covalently (John and Mccarty, 1969). Lahav et al. (Lahav et al., 2013) postulated that the complexation of Ca(II) ions in the precipitation of P(V) using seawater desalination brines reduces their free concentrations, thus reducing their precipitation potential and reducing the purity of the Ca-phosphates.

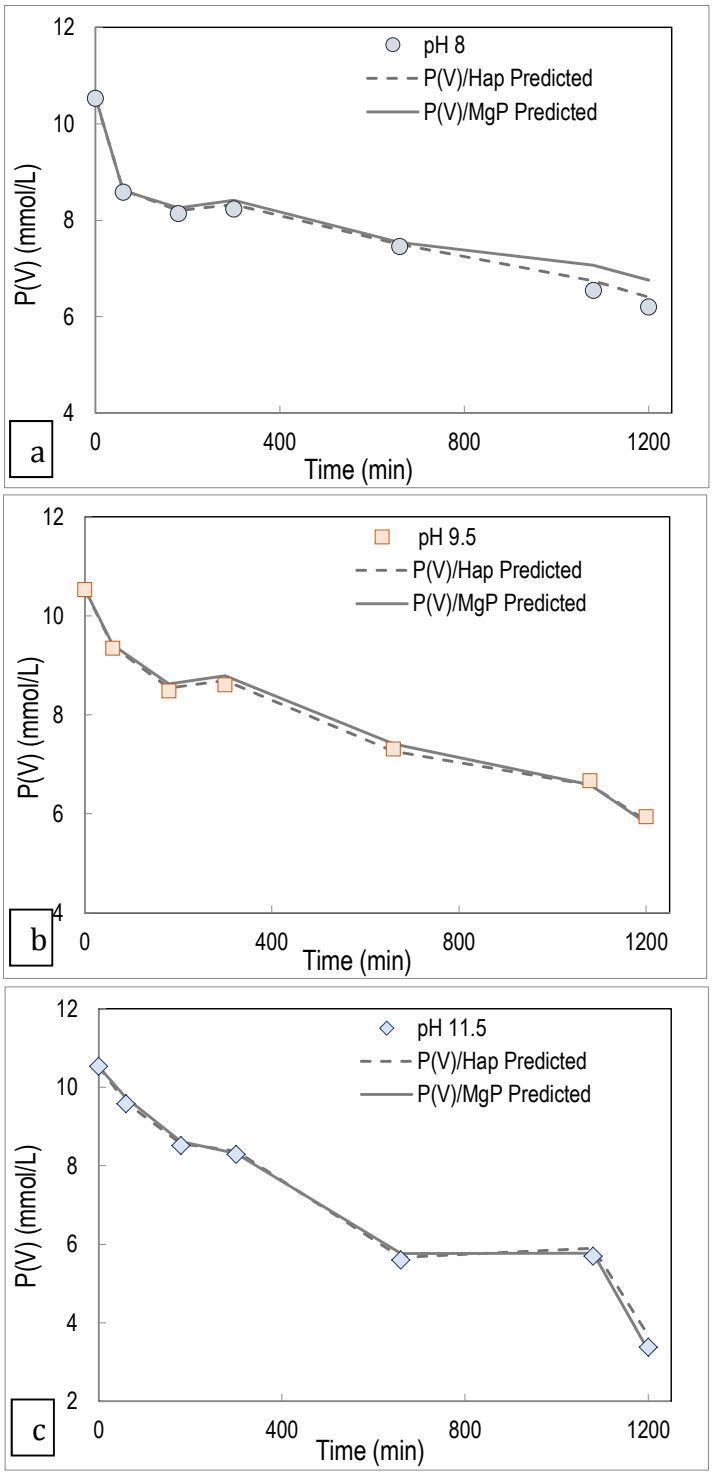

Figure 3.8. Variation of experimental and predicted P (V) concentrations assuming the formation of the Ca- and/or Mg-phosphate mineral phase at different pH values using Mg/Ca (3.3) brine at: a) pH 8, b) pH 9.5 and c) pH 11.5.

The analysis of solids by SEM-EDX detected the presence of S and Cl, indicating their presence in the precipitates obtained at basic pH; however, XRD analysis did not detect any crystalline form.

For the experiment at pH 8, Ca(II) and Mg(II) were partially removed (approximately 10%) with a phosphate recovery of up to 20%.

The SI analysis indicated that the solution is not supersaturated in $Mg(OH)_2(s)$, and the removal of P(V) should be associated with the formation of Ca-Mg-phosphates and, potentially, with minerals containing sulfate, because the measured values were lower than the total added concentration. A good prediction of the measured concentrations was obtained when considering the formation of Mg- and Ca-phosphates, as shown in Figure 3.8a. Although solutions were also supersaturated in OCP, TCP, brushite and monotite, the observed inhibition could be either due to Mg(II) ions or the formation of $CaSO_{4aq}$ of $MgSO_{4aq}$ species because sulfate is present at a substantially higher concentration than phosphate. As previously described for the Mg/Ca (2.2) brine, after solution filtration, no solids were recovered due to the nanometre size of the formed clusters, and it was not possible to confirm its chemical or mineral composition or the potential inhibition effect of sulfate ions.

3.3. Evaluation of precipitation inhibition: Effects on nucleation growth kinetics

According to the XRD results, it was observed that nucleation of Hap begins with the formation of the ACP precursor during the early induction steps, and after a relatively long induction period, it proceeds to the appearance of nuclei. However, in the presence of Mg(II), the formation of Mg-phosphate

ion-pairs reduces the P(V) species activity, thereby reducing the relative supersaturation and prolonging the induction period (Yang et al., 2011). Figure 3.1 shows that the change of the P(V) concentration and recovery rate for pH values between 9.5 and 12 for Mg/Ca (2.2) brine and between 10.5 and 12 for Mg/Ca (3.3) brine is different than for the experiments at pH 8 for Mg/Ca (2.2) brine and at pH 8 and 9.5 for Mg/Ca (3.3) brine.

The presence of meta-stable pre-nucleation clusters (PNCs) decreases the energetic barrier, thereby facilitating nucleation (pH 9.5 and 11.5), while at pH = 8, stable clusters are considered to increase the barrier, thus inhibiting nucleation (Gebauer et al., 2011 and 2014).

Phosphate precipitation can be evaluated considering the variation of the SI at pH 8, 9.5 and 11.5 (Figure 3.9) and by using the LaMer model (Eqs 3 to 9, section 2.4) describing the crystallisation processes as three well-defined stages. At pH 11.5, there was an initial stage in which no precipitation occurred; in the second stage in which the SI reached values from 17 to 18.5, homogenous nucleation occurred; and the third stage is completed with the aggregation of small particles of the homogeneously nucleated material and their heterogeneous deposition (Lagno and Demopoulos, 2005). For the experiment at pH 9.5 from the initial additions, a supersaturation condition was observed (SI>18.5), and then the homogenous nucleation and final aggregation stages followed the trend defined at pH 11.5. The observed behaviour for the experiment at pH 8 (no solid was recovered) is associated with the formation of stable clusters, increasing the energetic barrier, hindering nucleation and achieving heterogeneous nucleation. The longer induction time for nucleation as the Mg(II) ions extend the induction and transformation time (Yang et al., 2011a; Ding et al., 2014;) promotes the

formation of nanometre-sized nuclei (Posner's clusters of 0.7 to 1.0 nm (Onuma and Ito, 1998)). These nanometre-sized crystals could not be recovered by the 0.22-µm filter.

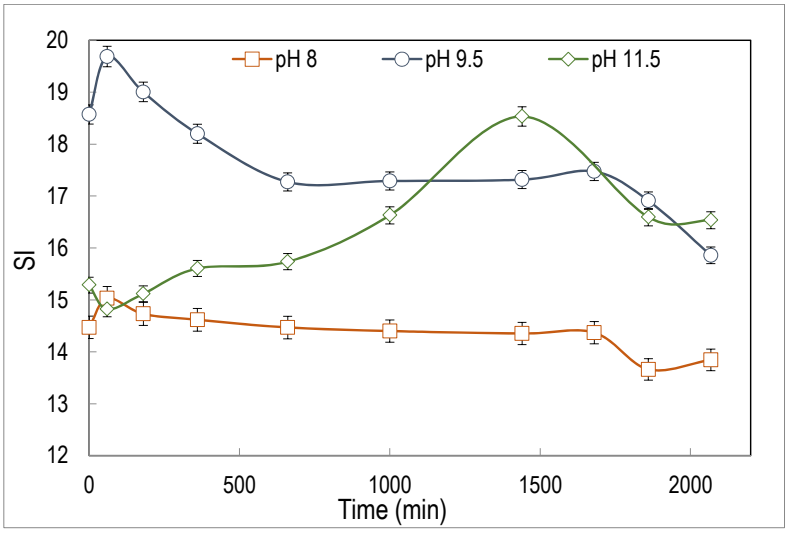

Figure 3.9. Supersaturation index (SI) for Ca/Mg (2.2) brine with respect to Hap at different pH values (8, 9.5 and 11.5) as a function of precipitation time in the batch reactor.

To evaluate the influence of the pH and the supersaturation on the Hap nucleation kinetics, the plot of $\ln(t_s)$ versus $1/[\ln(1+\sigma)]^2$ was constructed for experiments with Mg/Ca (2.2) brine at pH 8 and 9.5, as shown in Figure 3.10.

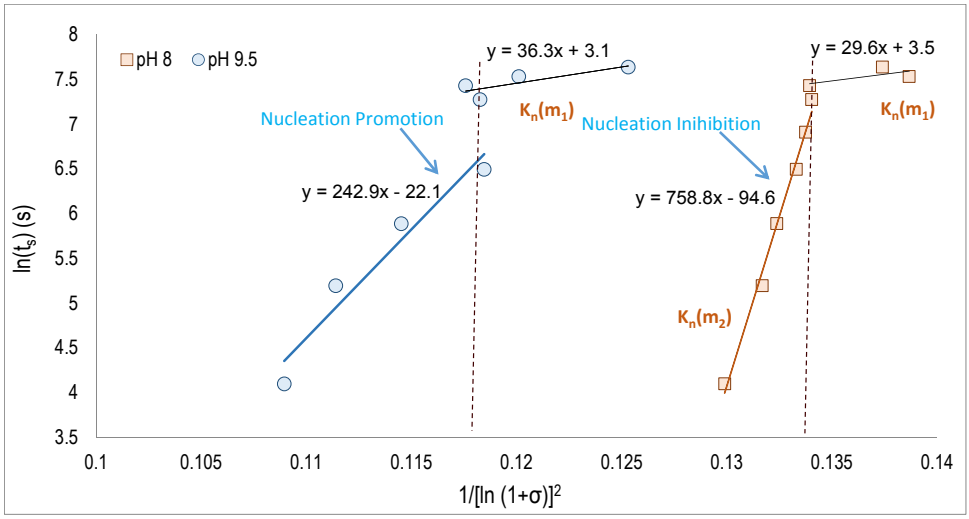

Figure 3.10. Evaluation of the nucleation kinetics using the dependence of $\ln(t_s)$ versus $1/[\ln (1+\sigma)]^2$ (Jiang et al., 2005) for Hap nucleation with Mg/Ca (2.2) brine at different pH values (8 and 9.5).

According to Eq. 5 the charge in the crystalline phase structures can be analysed for a given system (k_n and B are constant) in terms of the variation of the slope ($k_n f(m)$). As shown in Figure 3.10, the depicted functions can in a first approach, be fitted by two intersecting straight lines with two slopes, which divide the supersaturation space into two regimes.

For both of the pH values (8 and 9.5), the function has a positive slope (regime 2) reaching a transition point (indicated by a vertical dotted line) followed by a plateau (regime 1) with a decrease of the slope. When comparing both of the experiments, a case of nucleation inhibition was identified at pH 8, as was postulated by Jian et al. (Jiang et al., 2005) who determined the inhibition effect by the increase in the slope and the decrease of the intercept. On the other hand, for the experiment at pH 9.5, a case of nucleation promotion was identified, with a factor of ($k_n f(m2)$= 243), referring to regime 2, which was much lower than that reported at pH =8 ($k_n f(m2)$=760). This result indicates that at pH 8, it is possible to reduce the nucleation barrier by improving the interfacial structure correlation (Gebauer et al., 2014; Jiang et al., 2005; Lagno and Demopoulos, 2005; Onuma and Ito, 1998). Similar results were obtained for the Mg/Ca (3.3) brines.

The particle size distribution in terms of volume and the number of particles for both of the Mg/Ca brines at pH 11.5 is shown in Figure 3.11. The number of particles with a mean size (d_{50}) increases with the Mg(II) concentration from 310 nm to 1400 nm for the Mg/Ca (2.2) and Mg/Ca (3.3) brines,

respectively. The precipitate particle size analysis in terms of volume revealed the formation of aggregates with an average equivalent diameter of approximately 113 µm and 62 µm for the Mg/Ca (2.2) and Mg/Ca (3.3) brines, respectively. The initially formed particles are smaller, thus having a higher tendency to aggregate due to their amorphous state and small size (Castro et al., 2013b).

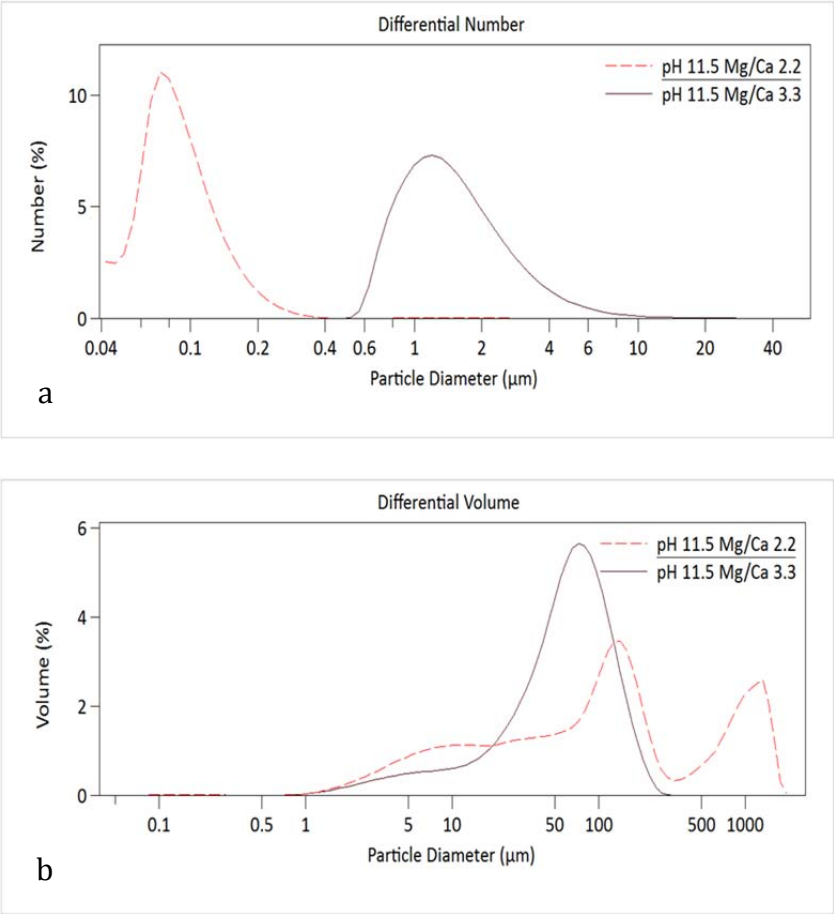

Figure 3.11. Particle size distribution in a) number and b) volume of particles obtained from the phosphate precipitation test at a constant pH of 11.5 for Ca/Mg (2.2) and Ca/Mg (3.3) brines.

Excess Mg(II) negatively affects the final powder crystal sizes because it causes a higher supersaturation, consequently increasing the nuclei population density, which suggests a higher nucleation rate. Therefore,

crystals reach larger sizes, as described by (Hutnik et al., 2013) for Hap crystallisation in the presence of excess of Mg(II) ions. The obtained precipitates consist of a population of nanometre-sized primary particles and a population of micrometre-sized aggregates. The aggregates most likely result from the aggregation of primary nanoparticles because small particles have a high surface area-to-volume ratio, resulting in a high surface tension, which tends to diminish by adhering to other particles. (Luque de Castro and Priego-Capote, 2007).

4. Conclusions

In this study, the influence of Mg(II) ions on phosphate recovery by Hap precipitation from basic solutions with desalinated industrial brines containing mixtures of Ca and Mg was confirmed.

For both of the Mg/Ca (2.2 and 3.3) brines at higher pH values (9.5 and 11.5), the precipitation inhibition of Hap was observed, and although solutions were supersaturated, the process proceeded with the formation of typically amorphous mineral phases (e.g. Ca, Mg, and Ca-Mg-phosphates). The presence of meta-stable clusters decreases the energetic barrier, thereby facilitating nucleation (pH 9.5 and 11.5). In the case of experiments at pH = 8, formation of stable clusters increased the barrier, thus promoting nucleation inhibition, and in this case, nanocrystals were formed, and solids were not recovered after filtration with a 0.22 μm filter.

The presence of pre-nucleation clusters in under-and super-saturated solutions and their participation in the phase separation process were proposed. Mg(II) severely inhibited precipitate crystallinity and the precipitation rate, allowing formation of ACP. This result is presumably due to

Mg(II) incorporation into the Ca(II)-phosphate structure to form a Mg(II)-substituted structure that crystallized to stanfieldite $Ca_4Mg_5(PO4)_6$ upon thermal treatment to increase crystallinity. According to literature, this mineral has not been postulated previously in the precipitation of phosphate solutions with Mg/Ca brines. The surface adsorption of Mg(II) (rather than the incorporated Mg(II)) played a critical role in regulating the transformation rate of ACP to Hap. Mg(II) altered the stability of the mineral phases, and the more soluble solids were precipitated (e.g., $Mg_3 (PO_4)_2.22H_2O$) at pH 11.5. Sulfate ions have a high capacity to form complexes with Ca(II) and Mg(II), and participated in the precipitation reactions. However, although sulfur was detected by EDX, no mineral containing sulfate was identified by XRD.

The use of industrial desalinated brines containing mixtures of Cd and Mg could be a suitable source for the recovery of phosphate in the form of mixed Ca-Mg phosphates suitable for the chemical industries producing fertilizers.

5. References

Alvarez, R., Evans, L. A., Milham, P.J., Wilson, M. A., 2004. Effects of humic material on the precipitation of calcium phosphate. Geoderma 118, 245–260.

Barca, C., Gérente, C., Meyer, D., Chazarenc, F., Andrès, Y., 2012. Phosphate removal from synthetic and real wastewater using steel slags produced in Europe. Water Res. 46, 2376–84.

Boskey A.L. and Posner A.S., 1973. Conversion of amorphous calcium phosphate to microcrystalline hydroxyapatite. A pH dependent, solution-mediated, solid-solid conversion. J. Phys. Chem. 77, 2313–2317.

Cao, X., Harris, W., 2008. Carbonate and magnesium interactive effect on calcium phosphate precipitation. Environ. Sci. Technol. 42, 436–42.

Cao, X., Harris, W.G., Josan, M.S., Nair, V.D., 2007. Inhibition of calcium phosphate precipitation under environmentally-relevant conditions. Sci. Total Environ. 383, 205–215.

Castro, F., Kuhn, S., Jensen, K., Ferreira, A., Rocha, F., Vicente, A., Teixeira, J.A., 2013a. Continuous-flow precipitation of hydroxyapatite in ultrasonic microsystems. Chem. Eng. J. 215-216, 979–987.

Castro, F., Kuhn, S., Jensen, K., Ferreira, A., Rocha, F., Vicente, A., Teixeira, J.A., 2013b. Process intensification and optimization for hydroxyapatite nanoparticles production. Chem. Eng. Sci. 100, 352–359.

Communication from the commission to the European parliament, the european economic and social committee and the committee of the regions, Towards a circular economy: a zero waste programme for Europe, Circular Economy Strategy, 2014. COM 398, 1–8.

Cusick, R.D., Ullery, M.L., Dempsey, B. A, Logan, B.E., 2014. Electrochemical struvite precipitation from digestate with a fluidized bed cathode microbial electrolysis cell. Water Res. 54, 297–306.

Destrée, C., Debuigne, F., Jeunieau, L., Nagy, J.B., 2006. Mechanism of formation of inorganic and organic nanoparticles from microemulsions. Adv. Colloid Interface Sci. 123-126, 353–67.

Ding, H., Pan, H., Xu, X., Tang, R., 2014. Toward a Detailed Understanding of Magnesium Ions on Hydroxyapatite Crystallization Inhibition. Cryst. Growth Des. 14, 763–769.

Edzwald.J, 2010. Water quality and treatment: A Handbook on drinking water.

Elisabeth V. Munch and Keith Barr, 2001. Controlled struvite crystalisation for removing phosphorus from anaerobic digester sidestreams. Water Res. 35, 151–159.

Gebauer, D., Cölfen, H., 2011Prenucleation clusters and non-classical nucleation, Nano Today. 6, 564–584.

Gebauer, D., Kellermeier, M., Gale, J.D., Bergström, L., Cölfen, H., 2014. Pre-nucleation clusters as solute precursors in crystallisation. Chem. Soc. Rev. 43, 2348–2371.

Golubev, S. V, Pokrovsky, O.S., Savenko, V.S., 1999. Unseeded precipitation of calcium and magnesium phosphates from modified seawater solutions. Journal of Crystal Growth. 205, 354–360.

Golubev, S. V., Pokrovsky, O.S., Savenko, V.S., 2001. Homogeneous precipitation of magnesium phosphates from seawater solutions. J.Cryst. Growth 223, 550–556.

Gray-Munro, J.E., Strong, M., 2013. A study on the interfacial chemistry of magnesium hydroxide surfaces in aqueous phosphate solutions: influence of Ca^{2+}, Cl^{-} and protein. J. Colloid Interface Sci. 393, 421–428.

Gunawan.E.K, Warmadewanthi, L.J., 2010. Removal of phosphate and fluoride from optoelectronic wastewater by calcite. Int.J.Technol.Manage. 12, 308–321.

Hermassi, M., Valderrama, C., Dosta, J., Cortina, J.L., Batis, N.H., 2015. Evaluation of hydroxyapatite crystallization in a batch reactor for the valorization of alkaline phosphate concentrates from wastewater treatment plants using calcium chloride. Chem. Eng. J. 267, 142–152.

Hutnik, N., Kozik, A., Mazienczuk, A., Piotrowski, K., Wierzbowska, B., Matynia, A., 2013. Phosphates (V) recovery from phosphorus mineral fertilizers industry wastewater by continuous struvite reaction crystallization process. Water Res. 47, 3635–43.

International center of diffraction data, 2003. PCPDF Win (JCPDS-ICDD) data base software.

Jenkins, D., Ferguson, J.F., 1971. Chemical processes for phosphate removal. Water Res. 5, 369–389.

Jiang, H., Liu, X.-Y., 2004. Principles of mimicking and engineering the self-organized structure of hard tissues. J. Biol. Chem. 279, 41286–93.

Jiang, H., Liu, X.-Y., Zhang, G., Li, Y., 2005. Kinetics and template nucleation of self-assembled hydroxyapatite nanocrystallites by chondroitin sulfate. J. Biol. Chem. 280, 42061–42066.

John, F., Mccarty, L., 1969. Effects of Carbonate and Magnesium on Calcium Phosphate Precipitation. Environ. Sc. Technol. 6, 534-540.

Jones, E.V., 2001. Mineralogical controls on phosphorus recovery from wastewaters. Nat. Museum, Hist. Road, Cromwell 65, 611–620.

Kim, D.H., 2011. A review of desalting process techniques and economic analysis of the recovery of salts from retentates. Desalination. 270, 1–8.

Kodera, H., Hatamoto, M., Abe, K., Kindaichi, T., Ozaki, N., Ohashi, A., 2013. Phosphate recovery as concentrated solution from treated wastewater by a PAO-enriched biofilm reactor. Water Res. 47, 2025–32.

Lagno, F., Demopoulos, G.P., 2005. Synthesis of Hydrated Aluminum Phosphate , $AlPO_4$,$1.5H_2O$ ($AlPO_4$-H_3), by Controlled Reactive Crystallization in Sulfate Media. Ind. Eng. Chem. Res. 44, 8033–8038.

Lahav, O., Telzhensky, M., Zewuhn, A., Gendel, Y., Gerth, J., Calmano, W., Birnhack, L., 2013. Struvite recovery from municipal-wastewater sludge centrifuge supernatant using seawater NF concentrate as a cheap Mg(II) source. Sep. Purif. Technol. 108, 103–110.

LaMer.V. K. and Dinegar.R. H., 1950. Theory, ptoduction and mechanism of formation of monodispersed Hydrosols. J. Am. Chem. Soc. 72, 4847–4854.

Li, B., Brett, M.T., 2012. The impact of alum based advanced nutrient removal processes on phosphorus bioavailability. Water Res. 46, 837–44.

Liu, Y., Sheng, X., Dong, Y., Ma, Y., 2012. Removal of high-concentration phosphate by calcite: Effect of sulfate and pH. Desalination 289, 66–71.

Luque de Castro, M.D., Priego-Capote, F., 2007. Ultrasound-assisted crystallization (sonocrystallization). Ultrason. Sonochem. 14, 717–24.

Meyer, J., 1983. Phase-transformations in the spontaneous precipitation of calcium phosphate. Croat. Chem. Acta 56, 753–767.

Mezenner, N.Y., Bensmaili, A., 2009. Kinetics and thermodynamic study of phosphate adsorption on iron hydroxide-eggshell waste. Chem. Eng. J. 147, 87–96.

Muster, T.H., Douglas, G.B., Sherman, N., Seeber, A, Wright, N., Güzükara, Y., 2013. Towards effective phosphorus recycling from wastewater: quantity and quality. Chemosphere 91, 676–84.

Nur, T., Johir, M.A.H., Loganathan, P., Nguyen, T., Vigneswaran, S., Kandasamy, J., 2014. Phosphate removal from water using an iron oxide impregnated strong base anion exchange resin. J. Ind. Eng. Chem. 20, 1301–1307.

Onuma, K., Ito, A., 1998. Cluster Growth Model for Hydroxyapatite. Chem. Mater. 10, 3346–3351.

Puidomènech, I.S.S., 2001. Chemical Equilibrium Software Hydra and Medusa. Stock. Sweden.

Salimi, M.H., Heughebaert, J.C., Nancollas, G.H., 1985. Crystal growth of calcium phosphates in the presence of magnesium ions. Langmuir 1, 119–122.

Sarode, A.L., Wang, P., Obara, S., Worthen, D.R., 2014. Supersaturation, nucleation, and crystal growth during single- and biphasic dissolution of amorphous solid dispersions: polymer effects and implications for oral bioavailability enhancement of poorly water soluble drugs. Eur. J. Pharm. Biopharm. 86, 351–60.

Sengupta, S., Pandit, A., 2011. Selective removal of phosphorus from wastewater combined with its recovery as a solid-phase fertilizer. Water Res. 45, 3318–30.

Su, C.-C., Dulfo, L.D., Dalida, M.L.P., Lu, M.-C., 2014. Magnesium phosphate crystallization in a fluidized-bed reactor: Effects of pH, Mg:P molar ratio and seed. Sep. Purif. Technol. 125, 90–96.

Suchanek, W.L., Byrappa, K., Shuk, P., Riman, R.E., Janas, V.F., TenHuisen, K.S., 2004. Mechanochemical-hydrothermal synthesis of

calcium phosphate powders with coupled magnesium and carbonate substitution. J. Solid State Chem. 177, 793–799.

Sugiura, Y., Onuma, K., Kimura, Y., Miura, H., Tsukamoto, K., 2011. Morphological evolution of precipitates during transformation of amorphous calcium phosphate into octacalcium phosphate in relation to role of intermediate phase. J. Cryst. Growth 332, 58–67.

Sun, Y., 2013. Controlled synthesis of colloidal silver nanoparticles in organic solutions: empirical rules for nucleation engineering. Chem. Soc. Rev. 42, 2497–511.

Taylor, A. W., Frazier, A. W., Gurney, E.L., 1963. Solubility products of magnesium ammonium and magnesium potassium phosphates. Trans. Faraday Soc. 59, 1580.

Telzhensky, M., Birnhack, L., Lehmann, O., Windler, E., Lahav, O., 2011. Selective separation of seawater Mg^{2+} ions for use in downstream water treatment processes. Chem. Eng. J. 175, 136–143.

Tran, A.T.K., Zhang, Y., De Corte, D., Hannes, J.-B., Ye, W., Mondal, P., Jullok, N., Meesschaert, B., Pinoy, L., Van der Bruggen, B., 2014. P-recovery as calcium phosphate from wastewater using an integrated selectrodialysis/crystallization process. J. Clean. Prod. 77, 140–151.

Viswanatha, R., Sarma, D.D., 2007. Growth of Nanocrystals in Solution. Nanomater. Chem. Chapter 4, 139-170.

Yang, X., Xie, B., Wang, L., Qin, Y., Henneman, Z.J., Nancollas, G.H., 2011b. Influence of magnesium ions and amino acids on the nucleation and growth of hydroxyapatite. CrystEngComm 13, 1153–1158.

Zettlemoyer, A.C.,Ed. 1969. Nucleation. New York, NY: Dekker.

Chapter 4

Fly Ash as a reactive sorbent for phosphate removal from treated wastewater as a potential slow-release fertiliser

This chapter is based on the work presented in a publication submitted to the Journal of Environmental Science and Pollution Research
Manuscript ESPR-[EMID:412820a8b4d50f6e] (M. Hermassi, C. Valderrama, N. Moreno, O. Font, X. Querol, N.H. Batis and J.L. Cortina) (5-Year Impact factor: 2.920).

There is increasing interest in recovering phosphate (P(V)) from secondary sources, such as streams in WWTPs, for potential use as fertilisers, reducing the environmental impacts of excess P(V) on receiving waters and providing alternative P(V) sources. The goal of this work was to provide an understanding of phosphate removal by FA from coal power plants. Phosphate removal using Ca-rich FA was evaluated in terms of (a) sorption equilibrium, (b) sorption kinetics under the expected pH values and P(V) concentrations in wastewater effluents, and (c) P(V) availability of the FAs in agricultural applications. Batch experiments were conducted using synthetic P(V) solutions with various compositions to determine the processes of its removal from aqueous solutions and its removal rates. At the pH values (6 to 9) expected for wastewater effluents, P(V) removal proceeds as a combination of CaO(s) dissolution and brushite ($CaHPO_4$(s)) formation on the FA particles; this process avoids the formation of relatively insoluble Ca phosphates, such as, Hap with limited fertilising properties. High P-loadings were achieved (up to 50 mgP-PO_4/g FA (5% P(V) by weight)) at a pH of 8. The removal kinetics data were well described as a diffusion-based process of phosphate ions ($H_2PO_4^-$ and HPO_4^{2-}) on FA particles, and the CaO(s) dissolution process was discarded as the rate-controlling step. The P(V) availability from loaded samples was determined via an agronomical test with $NaHCO_3$ solutions with P(V) release ratios of 10 to 30 mgP-PO_4/g in FA, confirming the appropriateness of this material as a fertiliser, even in calcareous soils.

1. Introduction

Increasing energy demands worldwide have led to increased utilisation of coal and, thus, the production of large quantities of FA as a waste product (Hui and Chao, 2006; Yan et al., 2007; Pengthamkeerati et al., 2008). In 2011, coal-fired generation accounted for 29.9% of the world's electricity supply, and its share is anticipated to reach 46% by 2030. Sustained prices for oil and natural gas make coal-fired generation relatively economically attractive, particularly in nations with rich coal resources, such as China, the USA, and India (Lior, 2010; Yao et al., 2015). Recycling CFA can be a good alternative disposal method and could provide significant economic and environmental benefits. The global average FA utilisation ratio is estimated to be nearly 25% (Bhattacharjee and Kandpal, 2002; Wang et al., 2008). Most FA is alkaline, and its surface is negatively charged at high pH values; thus, it could be used to remove metal ions from solutions by precipitation (Penilla et al., 2006) or adsorption in water and wastewater treatment (Pengthamkeerati et al., 2008; Penilla et al., 2006; Wu et al., 2006). Furthermore, it contains a certain amount of unburnt carbon, which has a high adsorption capacity for organic compounds (Yao et al., 2015).

P is an important element in industry and agriculture and is frequently present in domestic, industrial, and farming wastewaters. In the last decades, phosphate has been considered an environmental concern because of its role in the eutrophication of water bodies (de-Bashan and Bashan, 2004; Ma and Zhu, 2006). Currently, it is becoming increasingly economically concerning because its natural deposits are diminishing because of the continuous growth of the world population. Domestic, industrial, and farming wastewaters and sludge containing P (less than 1% by weight) are

considered secondary P sources that should be mined (Lu et al., 2009). In the European Union, P has been included in the list of priority elements, and new technological methods to recover P from secondary sources are being promoted. Most such methods have focused on the recovery of P from solid wastes (e.g., incineration ashes), whereas for the recovery of P from liquid wastes, most methods have focused on the recovery of MAP (struvite) from concentrated streams.

Few efforts have been devoted to P recovery from diluted streams, although various techniques for phosphate removal are available (Zelmanov and Semiat, 2014). Because chemical precipitation and coagulation processes are not cost effective and because polymeric ion exchangers are not applicable because of the presence of dissolved and particulate organic matter, phosphate-removal/recovery solutions have focused on the use of low-cost inorganic materials with high pollutant-removal efficiencies in terms of equilibrium and kinetics. CFA has attracted substantial attention as a potential material for phosphate removal because it is easily available and cost effective (Tsitouridou and Georgiou, 1988; Gray and Schwab, 1993; Ahmaruzzaman, 2010). The presence of Al, Fe, Ca, and Mg oxides imbues FA with suitable properties for phosphate removal by complexation reactions with the metal oxides or the precipitation of Ca/Mg phosphates (Grubb et al., 2000; Pengthamkeerati et al., 2008). Cheung and Venkitachalam (Cheung and Venkitachalam, 2000) associated the removal of phosphate by FA containing high- and low-Ca contents with Ca phosphate precipitation. Johansson and Gustafsson (Johansson and Gustafsson, 2000) proposed the formation of amorphous Ca phosphate and/or octacalcium phosphate as the major P-removal mechanism and suggested the direct formation of Hap as

the predominant phosphate-removal mechanism. Although it is generally accepted that phosphate removal by FA involves adsorption and/or precipitation mechanisms, the interaction between phosphate and Ca remains incompletely described (Lu et al., 2009).

Additionally, little work has been done to obtain a solution for the exhausted ash, and recently, the possibility of using these materials to improve the soil quality of areas degraded by mining or civil construction infrastructure or for forestry applications has been proposed (Yao et al., 2015). However, because of the low solubility and availability of the Ca phosphate mineral that is typically precipitated ($Ca_5(PO_4)_3OH(s)$, $logK_{so}$=116.8) (Parvinzadeh Gashti et al., 2013), efforts have been made to prepare relatively soluble phosphate-containing minerals, such as brushite ($CaHPO_4.2H_2O$, $logK_{so}$=6.59) (Dorozhkin, 2012)), by promoting the growth of mineral forms on the surface of Ca-containing sorbents with properties suitable for slow-release fertilisers. These materials include Ca silicates, such as wollasonite (Liu and Ding, 2002); Ca-Al layered double hydroxide (Watanabe et al., 2010; Zhou et al., 2012); natural zeolites (Guaya et al., 2015); and FA (Xu et al., 2010). However, the utilisation of powdered inorganic adsorbents in water treatment processes for selective P removal and, subsequently, as slow-release fertilisers remains under development, and the equilibrium and kinetic performances remain to be characterised.

In this study, two different types of FA from two different coal power stations with different CaO(s) contents (Los Barrios (FA-LB (2.8% w)) and Teruel (FA-TE (4.8% w))) were evaluated as adsorbents for phosphate recovery from aqueous solution. The equilibrium and kinetic performances for phosphate sorption were studied and characterised by varying the experimental

conditions, such as the solution pH and initial phosphate concentration. The phosphate-sorption mechanisms were evaluated using a speciation method. Although the phosphate-removal mechanism is complex, the results are presented in terms of equilibrium isotherms and kinetic diffusion parameters.

2. Materials and methods

2.1. Batch equilibrium experiments of FA dissolution

FA samples (0.2 g) from Teruel (FA-TE) (Andorra Coal Power Plant, Power company ENDESA, Spain)and Los Barrios (FA-LB) (Los Barrios Coal Power Plant, Power company SE, Spain) were mechanically mixed in special polyethylene stoppered tubes with demineralised water (10 mL) at different initial pH values (6–9) and room temperature (21±1°C) until equilibrium was achieved (24 h). The influence of the initial pH on FA dissolution was evaluated by varying the initial pH with 0.1-mol/L HCl or NaOH solution. After phase separation with a 0.2-μm syringe filter, the equilibrium pH was measured using a pH electrode (Crison GLP22); the total Ca, Na, Mg, and K concentrations were measured by ion chromatography; and the total Si, Al, Fe, P, and Ti concentrations were determined by inductively coupled plasma mass spectrometry (ICP-MS) or atomic emission spectrophotometry (ICP-AES) (X-Series II, Thermo Fisher SCIENTIFIC).

2.2. Batch equilibrium experiments of phosphate removal

Phosphate solutions were prepared by dissolving a weighed amount of $Na_2HPO_4.2H_2O$ in water obtained from a Milli-Q-Academic-A10 apparatus (Millipore Co. France). FAs from Teruel (FA-TE) and Los Barrios (FA-LB) (0.2 g) were mechanically mixed in special polyethylene stoppered tubes with an

aqueous phosphate solution (10 mL) at different initial P(V) concentrations (100–16000 mgP-PO_4/L) at room temperature (21±1 ºC) until equilibrium was achieved (24 h). The influence of pH on the phosphate sorption was evaluated by varying the initial pH with 0.1-mol/L HCl or NaOH solution. After phase separation with a 0.2-µm syringe filter, the equilibrium pH was measured using a pH electrode (Crison GLP22), and the total phosphate concentration was measured by ion chromatography (Thermo Scientific Dionex ICS-1100) or visible absorption spectrophotometry (UVmini-1240). The P(V) equilibrium sorption capacity was determined using Eq. 1.

$$q_e = \frac{(C_0 - C_e)\, v}{m_s} \quad (1)$$

where C_0 (mg/L) and C_e (mgP-PO_4/L) represent the initial and equilibrium total P(V) concentrations, respectively; v (L) is the aqueous solution volume; and m_s (g) is the mass of the FA sample.

2.3. Batch kinetic experiments of phosphate removal

Batch kinetic experiments were performed by adding 0.2 g of FA to solutions containing 100 and 500 mgP-PO_4/L. The tubes were mechanically shaken at 200 rpm and room temperature (21±1°C), and samples were withdrawn sequentially at specified times. All tests were performed in triplicate, and the average values are reported.

The samples were centrifuged for 10 min and filtered with cellulose nitrate membrane filters (45 µm). The total phosphate concentration and pH of the initial and remaining aqueous solutions were measured using spectrophotometric colourimetry (Kitson, R.E; Mellon, 1944).

2.4. Speciation of phosphate-loaded FA samples.

The speciation of the adsorbed P in both FA samples (FA-TE and FA-LB) was achieved using a modified four-step sequential extraction methodology (Ann et al., 2000; Hedley and Stewart, 1982; Moharami and Jalali, 2014). First, 30-mL aliquots of 1000 mg P-PO_4^{3-}/L at pH 7 were equilibrated with pre-weighed tubes containing 3 g of FA. After shaking for 24 h at room temperature, the suspensions were centrifuged, and the FA powders were dried at 50–60°C. The adsorbed phosphate was sequentially extracted using 1-g samples and 50 mL of the extraction solutions described in Table 4.1. The samples were mechanically shaken at 21±1°C. After equilibrium was achieved (24 h), the samples were centrifuged, and the phosphate content of the liquid phase was analysed.

Table 4.1. Chemical extraction scheme for P speciation of loaded FA samples.

Extraction solutions	Speciation name	P Speciation	Step
40-mL 2 M KCl for 2h	KCl-P	Soluble and exchangeable P	1
40-mL 0.1 M NaOH for 17h	NaOH-P	Fe- and Al-bound P	2
40-mL 0.5 M HCl for 24h	HCl-P	Ca-bound P	3
40-ml 10 M HNO_3/10M $HClO_4$ (5/2)	Res-P	Residual P	4

2.5. Phosphate availability from loaded FA samples using bicarbonate solutions

Samples (0.5 g) of loaded FAs (contents ranging from 11 to 108 mmol/L) were mixed with 20 mL of 0.5-M $NaHCO_3$ (pH=8.3) in 50-mL plastic bottles. The bottles were mechanically shaken at 21±1°C for 24 h at a constant agitation speed of 200 rpm. After phase separation with a 0.45-µm syringe filter, the equilibrium pH was measured using a pH electrode (Crison GLP22),

and total phosphate concentration was measured using spectrophotometric colourimetry.

2.6. Physicochemical characterisation of FA samples

The major, minor, and trace element concentrations of the FA powders were determined. The samples were acid-digested via a special two-step digestion method to analyse the trace elements in coal and combustion wastes by Inductively Coupled Plasma Mass Spectrometry (ICP-MS) and Inductively Coupled Plasma Atomic Emission Spectrometry (ICP-AES) (Querol et al., 1997).

After the sorption and desorption experiments, the FA samples were washed with water to remove the interstitial water and then oven-dried at 60°C for structural and textural analysis. The mineralogical composition was analysed by a Bruker D8 A25 Advance X-Ray Diffractometer θ-θ with $CuK_{\alpha 1}$ radiation, Bragg-Brentano geometry, and a linear LynxEyeXE detector. The diffractograms were obtained from 4º to 60º of 2θ with a step size of 0.015º and a counting time of 0.1 s as the sample was rotated. The solids in powder form were identified according to standard Joint Committee on Powder Diffraction Standards (JCPDS) file and were matched with Powder Diffraction Files (PDFs) no. 009-0077 for brushite, 046-1045 for quartz, 015-0776 for mullite, 033-0664 for hematite, and 039-1346 for maghemite. The morphology of the samples was examined using field emission scanning electron microscopy with an energy dispersive system (FE-SEM-EDS, JEOL 3400) after prior metallisation with gold.

The FA point of zero charge (PZC) was determined by acid-based potentiometric titrations using the common intersection point method

(Skartsila and Spanos, 2007; Liu et al., 2013; Zebardast et al., 2014). First, 0.1 g of FA was equilibrated with 25 mL of KNO_3 solution at various ionic strengths (0.01, 0.05, 0.1, and 0.5 M) for 24 h at 200 rpm and 21±1°C. After equilibrium was achieved, a given volume of 0.1-M KOH solution was added to the suspension to increase the pH value over 10. The suspension was then titrated with 0.05-M HNO_3 to pH≈3 using an automatic titrator (Mettler Toledo). The net surface charge was correlated with the PZC by considering the adsorbed amounts of H^+ and OH^- ions along the titration assay: the titration curves obtained at different ionic strengths intersect at pH=pH_{PZC}. The surface charge was calculated according to Eq. 2 (Martinez et al., 2008).

$$b = C_b - C_a + [H^+] - [OH^-] \quad (2)$$

where b (mol/g) is the net amount of hydroxide ions consumed; C_b and C_a (mol/L) are the base and acid concentrations, respectively; and $[H^+]$ and $[OH^-]$ denote the proton and hydroxide concentrations, respectively, calculated from the measured pH for a given mass of FA (g) and a given volume of solution (L). All measurements were performed in triplicate, and the average values are reported.

2.7. **Sorption models**

Equilibrium models: The Langmuir (Eq. 3) and Freundlich (Eq. 4) isotherms were used to describe the equilibrium data:

$$\frac{C_e}{q_e} = \frac{1}{K_l q_m} + \frac{C_e}{q_m} \quad (3)$$

$$\log q_e = \log K_f + \frac{1}{n} \log C_e \quad (4)$$

where C_e (mg P-PO_4/L) and q_e (mg/g) are the equilibrium total P(V) concentrations in the aqueous and FA phases, respectively; q_m (mg P-PO_4/g) is the maximum sorption capacity; K_L (L/mg) is the Langmuir sorption

equilibrium constant; n is a constant indicating the Freundlich isotherm curvature; and K_f ((mg/g)/(mg/L)^n) is the Freundlich equilibrium constant. The adjustable parameters—q_m and K_L or K_F and 1/n—were obtained by fitting the experimental data (q_e and C_e) to Eqs. 3 and 4 using nonlinear least squares regression (Excel version 2010).

Kinetic equilibrium models: The homogeneous particle diffusion (HPDM) and shell progressive (SPM) models were used to describe the kinetic data (L. Liberti, R. Passino, in : J.A. Marinsky, 1977). Both models assume that the extraction mechanism involves the diffusion of phosphate ions ($H_2PO_4^-$ and HPO_4^{2-}) from solution into the FA phase through a number of possible pathways: diffusion across the liquid film surrounding the FA particle, transfer across the solution/particle interface, diffusion into the bulk of the FA particle, and possible interactions with reactive groups on the FA surface.

Homogeneous Particle Diffusion Model (HPDM): This model describes the adsorption of the phosphate ions via diffusion in a quasi-homogeneous medium according to Fick's law equation with two rate-control scenarios:

- If the particle diffusion rate controls the P(V) sorption on spherical FA particles:

$$-\ln(1-X^2(t)) = 2Bt \qquad \text{where } B = \frac{\pi^2 D_e}{r^2}. \tag{5}$$

- If liquid film diffusion controls the rate of P(V) sorption:

$$-\ln\big(1-X(t)\big) = K_{li}\,t \qquad \text{where } K_{li} = \frac{3D_eC}{rC_r} \tag{6}$$

The X(t) values can be calculated using Eq. 7:

$$X(t) = \frac{q_t}{q_e} \tag{7}$$

where X(t) is the phosphate fractional attainment of equilibrium at time t; q_t and q_e are the phosphate loadings on the FA phase at time t and when

equilibrium is attained (mg g^{-1}), respectively; C is the total concentration of sorbing species; C_r is the total concentration of sorbing in the sorbent phase; K_{li} is the rate constant for film diffusion (infinite solution volume condition); D_e is the effective diffusion coefficient of phosphate ions in the FA phase (m^2s^{-1}); and r the radius of the FA particle, which is assumed to be spherical (m).

Shell progressive model (SPM): This model describes the sorption process in terms of a concentration profile of the solution containing phosphate ions advancing into a partially sorbed saturated spherical FA particle ("Shell Progressive") and is applicable when the sorbent porosity is low (e.g., FA) (G. Schmuckler, S. Golstein, in: J.A. Marinsky, 1977). The relationships between the degree of sorption and time are given by Eqs. 7–9:

- If sorption is controlled by the fluid film:

$$X(t) = \frac{3C_{Ao}K_F}{a_sC_{so}}\ t \tag{8}$$

- If sorption is controlled by diffusion though the sorption layer:

$$\left[3 - 3(1 - X(t))^{\frac{2}{3}} - 2X(t)\right] = \frac{6D_eC_{Ao}}{a_s^2C_{so}}\ t \tag{9}$$

- If sorption is controlled by the chemical reaction:

$$\left[1 - (1 - X(t))^{1/3}\right] = \frac{K_sC_{Ao}}{r}\ t \tag{10}$$

where a_s is the stoichiometric coefficient, C_{Ao} is the concentration of sorbing species A in the bulk solution, C_{so} is the concentration of sorbing species at the bead's uncreated core, K_F is the mass-transfer coefficient of species A through the liquid film (m s^{-1}), and K_s is the reaction constant based on the surface (m s^{-1}).

All experimental data were treated graphically and compared to all fractional attainment of equilibrium functions (F(X) = f (t)) defined previously for both HPDM (Eqs. 5–6) and SPM (Eqs. 8–10).

2.8. Prediction of phosphate-precipitation processes

Phosphate precipitation processes were studied using the HYDRA-Medusa (Puidomènech, 2001) and Visual Minteq codes (Gray-Munro and Strong, 2013). When necessary, the measured P(V), Ca(II) concentration, and pH were compared to those estimated using both codes. The supersaturation index (SI) was calculated using Visual Minteq and Eq. 11, as follows:

$$SI = \log(\frac{IAP}{K_{so}}) \quad (11)$$

where IAP is the ion activity product, and K_{so} is the solubility constant. Equilibrium solubility data for Ca phosphates from the HYDRA and PHREEQ C databases were critically reviewed.

3. Results and discussion

3.1. Characterisation of the Teruel and Los Barrios FAs

SEM analysis revealed spherical particles containing smaller encapsulated particles. Five different types of particles in terms of size and porous texture were identified: (i) spherical filled particles—Plerospheres—in the particle size range below 10 μm; (ii) large, irregular silicate masses exhibiting spherical pitting; (iii) hollow spherical particles—Cenospheres—containing small encapsulated particles; (iv) elongated blades and hollow spherical particles with interior voids; and (v) agglomerates of small spherical particles forming large non-spherical particles (Figure 4.1b). The chemical compositions of both FA samples (Table 4.2) primarily consist of Al_2O_3 and SiO_2, which account for 73% and 83% of the FA-TE and FA-LB samples, respectively. FA-TE had higher contents of Fe_2O_3 (18.9%) and CaO (4.2%) than FA-LB (with 7.4% and 2.3%, respectively). The X-ray diffraction (XRD) patterns of FA-TE and FA-LB are shown in Figure 4.1a. Hematite and

maghemite (Fe_2O_3), mullite ($Al_2Si_2O_{13}$), and quartz (SiO_2) were the main phases identified in both FA samples.

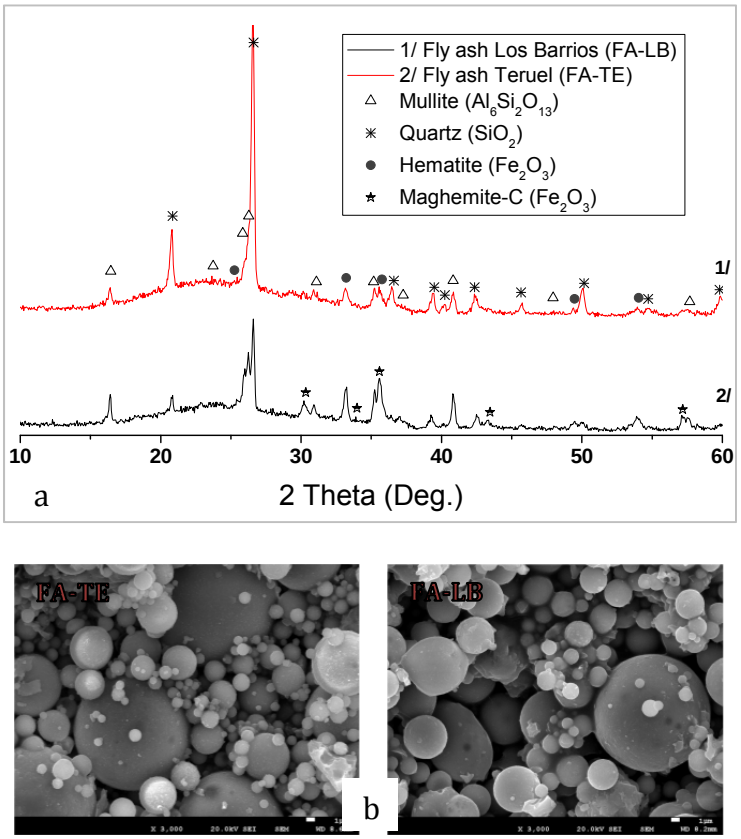

Figure 4.1. a) XRD patterns of both FA samples (FA-TE and FA-LB) and b) SEM micrographs of FA-TE and FA-LB.

Table 4.2. The average chemical compositions of FA-TE and FA-LB.

	SiO_2	Al_2O_3	Fe_2O_3	CaO	MgO	Na_2O	K_2O	P_2O_5	SO_3
FA- TE (% wt)	45.10	28.10	18.90	4.20	1.14	0.18	1.45	0.21	0.83
FA- LB (% wt)	61.20	21.10	7.40	2.25	2.26	1.15	2.42	1.60	0.68

The acid-base characterisation revealed pH_{PZC} values of 4.9±0.5 for FA-TE and 5.1±0.5 for FA-LB (Figure 4.2) The electrophoretic mobility (pH_{ZPC} value of approximately 4.9–5.1) is close to the theoretically predicted value and is reported in Table 4.3 (Schwarz et al., 1984) based on the percentages of silica and alumina in the FA.

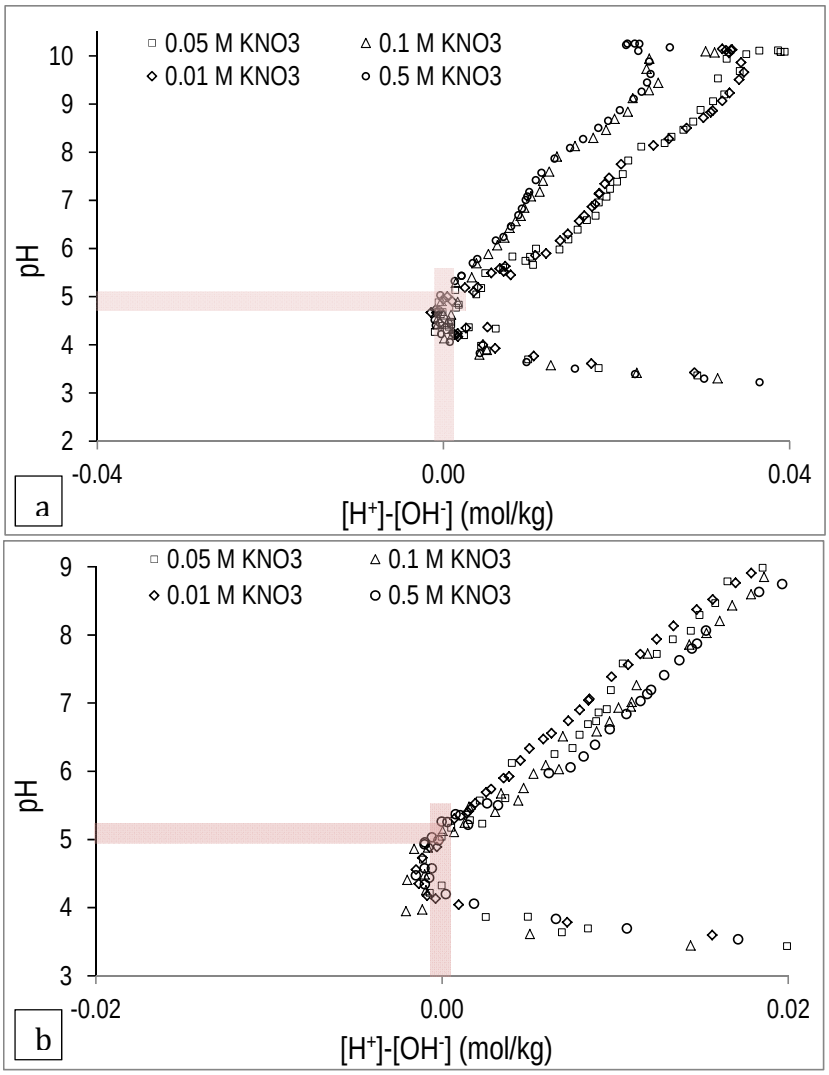

Figure 4.2. FA potentiometric titration curves at 0.01-, 0.05-, 0.1-, and 0.5-M KNO_3 for a) FA-TE and b) FA-LB.

The deviation between the theoretical and experimental data is ascribed to the presence of other oxides in the FA samples (e.g., MgO and CaO). The determined pH_{PZC} values are in good agreement with those reported for α-$Al(OH)_3$(s) (pH_{PZC} 5.0) and $Fe(OH)_3$ (pH_{PZC} from 5 to 7) (Malarvizhi et al., 2013). Indeed, Chen et al. and Zhang et al. (Reed et al., 2000; Chen et al., 2006; Zhang et al., 2007) reported that Fe and Al surface groups at pH values below the pH_{PCZ} have anion-sorption capacities.

Table 4.3. Comparison of the pH_{zpc} values of selected FA-based materials.

Material	Mineral composition(wt%)					pH_{ZPC}	References
	SiO_2	Al_2O_3	Fe_2O_3	CaO	MgO		
FA-TE	45.1	28.1	18.9	4.2	1.2	4.9	This study
FA-LB	61.2	21.1	7.4	2.2	2.2	5.1	This study
FA	43.7	15.7	6.4	9.8	0.9	7.7	(Banerjee et al., 2014)
FA	45.3	26.2	7.6	10.1	6.5	9	(Wawrzkiewicz et al., 2015)
High CaFA	31.3	17.8	7.1	31.9	6.3	10.3	(Vordonis et al., 1988)
Silica/alumina (%)	100	-	-	-	-	4.1	(Schwarz et al., 1984)
	90	10				4.4	
	75	25				4.9	
	34	66				5.9	
	10	90				6.7	

FA-dissolution experiments at initial pH values between 6 to 9 revealed a Ca(II) concentration in solution of 2 to 3.5 mmol Ca/L, while the values of K, Mg and Na were an order of magnitude lower, ranging from 0.01 mmol/L to 0.4 mmol/L, as shown in Figure 4.3.

The substantial concentration of Ca(II) in solution can be explained by the dissolution of CaO(s) particles present on the FA, as described by Eq. 12:

$$\mathrm{CaO(s)} + H_2\mathrm{O} \quad \leftrightarrow \quad \mathrm{Ca(OH)_2(s)} \leftrightarrow \quad \mathrm{Ca^{2+}} + 2\mathrm{OH^-} \qquad (12)$$

The measured Ca(II) value decreases as pH increases, as expected based on the CaO(s) dissolution reaction, and the values are slightly higher for FA-TE, which has a higher Ca content (4.2% CaO). Although mineral phases containing Ca were detected in both FAs, Ca is expected to be present as Ca oxide minerals (e.g., portlandite) (Hooton et al., 1999). The measured concentrations of other major components of FA, such as Al, Fe, Si, and Ti, were below 0.01 mmol/L. These values are in accordance with the solubility data of the main mineral phase identified by XRD in both FA samples: quartz (SiO_2), Mullite ($Al_6Si_2O_{12}$) and hematite (Fe_2O_3) (Figure 4.1a).

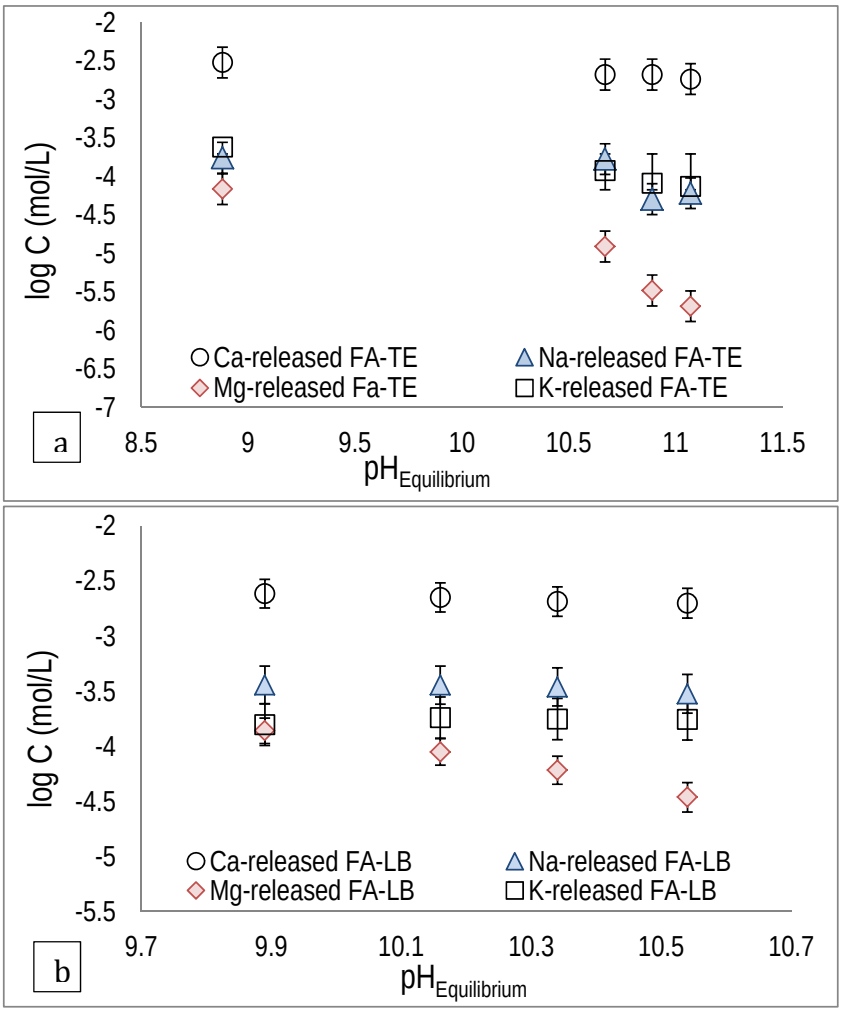

Figure 4.3. Molar Ca, Mg, Na, and K concentrations (in logarithm form) as functions of the equilibrium pH in the FA-dissolution experiments (0.2 g of FA and 10 mL of demineralised water) for both FA samples: a) FA-TE and b) FA-LB.

3.2. Phosphate sorption capacities of FA-TE and FA-LB: Effects of pH and P(V) concentration

P(V) sorption isotherms for both FA samples revealed a dependence on the pH (Figure 4.4), and the equilibrium data was well described by the Langmuir isotherm (Table 4.4).

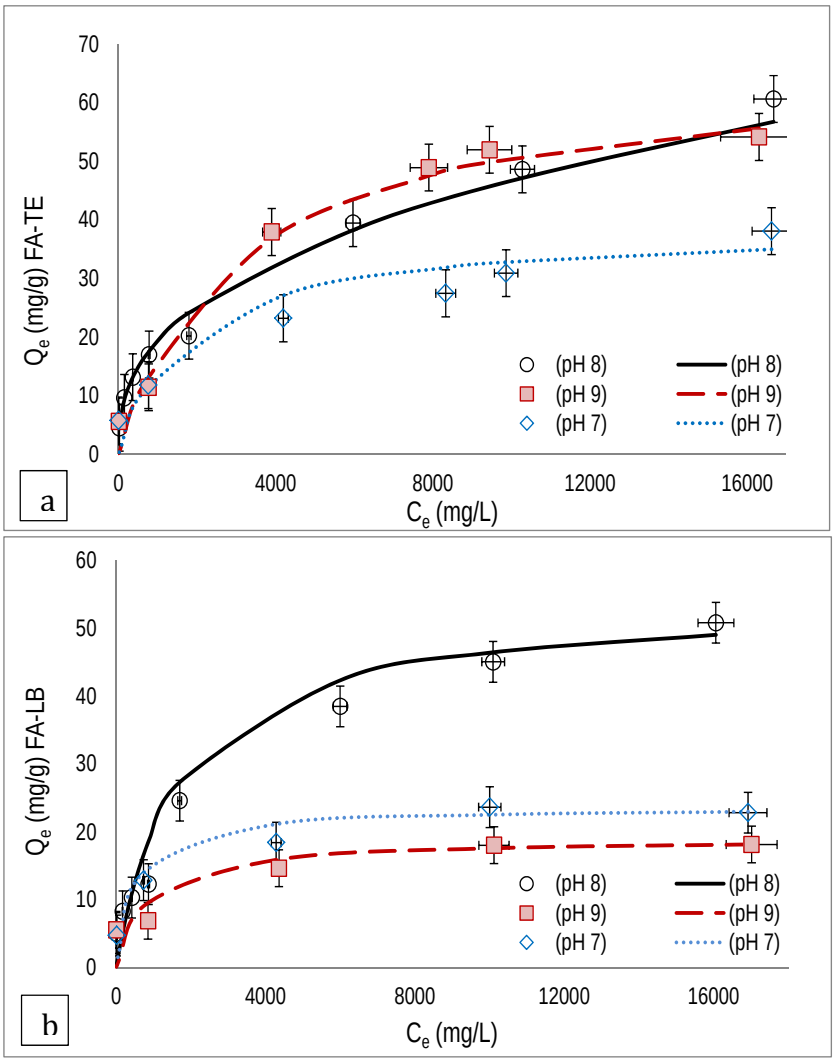

Figure 4.4. Phosphate sorption isotherms at different pH values and predicted by the Langmuir model for a) FA-TE and b) FA-LB (dots: experimental data; line: predicted values).

Table 4.4. Langmuir and Freundlich isotherm parameters for FA-TE and FA-LB at different pH values.

Adsorbent / Models		FA-TE			FA-LB		
		pH 7	pH 8	pH 9	pH 7	pH 8	pH 9
Langmuir isotherm	q_m	38.8±3.4	59.5±4.3	56.2±3.8	23.7±2.3	54.1± 3.7	19.1±1.7
	K_L	0.0005	0.0005	0.0003	0.0019	0.0006	0.0015
	R^2	0.98	0.99	0.99	0.99	0.97	0.99
Freundlich isotherm	K_f	4.87	1.35	2.85	2.35	1.80	3.78
	n	5.24	2.6	3.32	4.09	2.98	6.52
	R^2	0.91	0.95	0.89	0.85	0.92	0.81

The maximum P(V)-sorption capacities (q_m) were 38.8±3.4 and 19.1±1.7 mgP/g for FA-TE and FA-LB, respectively, when the pH value exceeded 7. At pH 8, the maximum uptakes were 59.5±4.3 and 54.1±3.7 mgP/g for FA-TE and FA-LB, respectively. The P(V)-sorption capacities measured here are higher than those reported by Chen et al., (2006) (5.5 to 42.6 mg P-PO_4/g) with CaO contents from 2.08 to 20.37% in FA samples.

3.3. **P(V)-sorption mechanism on FA**

Given that $H_2PO_4^-$ and HPO_4^{2-} are the predominant species of P(V) at pH values between 7 and 9, two main sorption mechanisms can be postulated:

a) Surface complexation with ≅AlOH and ≅FeOH functional groups of Al and Fe oxides through the following reactions:

Labile complexes with $\cong MOH_2^+$:

$$\cong MOH_2^+ + H_2PO_4^-/HPO_4^{2-} \leftrightarrow \cong MOH_2^+ H_2PO_4^-/HPO_4^{2-} \quad (13)$$

Inner-sphere complexes with ≅MOH:

$$\cong MOH + H_2PO_4^-/HPO_4^{2-} \leftrightarrow \cong MH_2PO_4^-/HPO_4^{2-} + OH \quad (14)$$

where M represents Al or Fe.

b) Formation of Ca phosphate minerals with Ca(II) ions present on the FA samples as CaO(s):

$$HPO_4^-/HPO_4^{2-} + CaO(s) = \text{Ca phosphates } (CaHPO_4(s) \text{ or } Ca_5(OH)(PO_4)_3\ (s)) \quad (15)$$

XRD analysis of FA samples after the sorption experiments revealed the presence of brushite ($CaHPO_4(s)$) at pH 7 and 8; the presence of Ca phosphate minerals was only not detected at pH 9, as can be seen in Figure 4.5. This could be because of the formation of undetectable nanocrystals or amorphous structures because the removal rate at pH 9 is faster than those

at pH 7 and 8, as indicates by the kinetic analysis (see section 4). Generally, precipitation processes with fast kinetics produce less-crystalline solids. In addition to hematite and/or maghemite, mullite and quartz were detected in all samples.

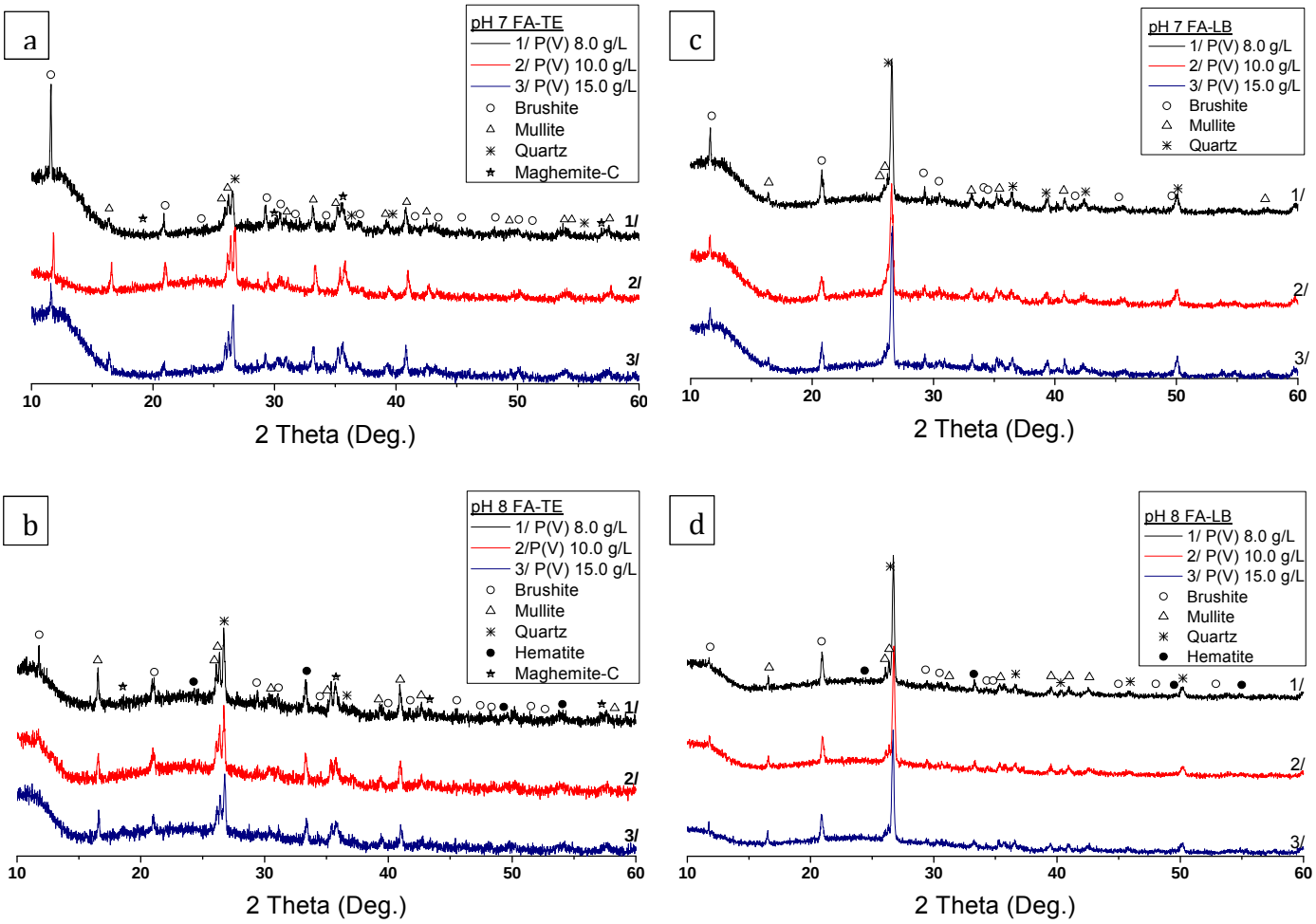

Figure 4.5. XRD analysis of FA samples after phosphate sorption at different pH values and phosphate concentrations: FA-TE (a,b) and FA-LB (c,d).

The P-speciation analysis of loaded samples shown in Figure 4.6 indicates that the loosely bound P fraction (KCl speciation fraction) associated with the labile complexes (Eq. 13) accounted for 18% in FA-TE and 4% in FA-LB. The Ca+Mg-speciation (HCl-P speciation fraction) associated with Ca phosphate forms (Eq. 15) accounted for 81% in FA-TE and 95% in FA-LB. The NaOH–P fraction associated with P(V) bound to the hydrated metal oxides (Eq. 14)

exhibited a residual contribution of less than 1%, while the residual P speciation represents less than 0.9%.

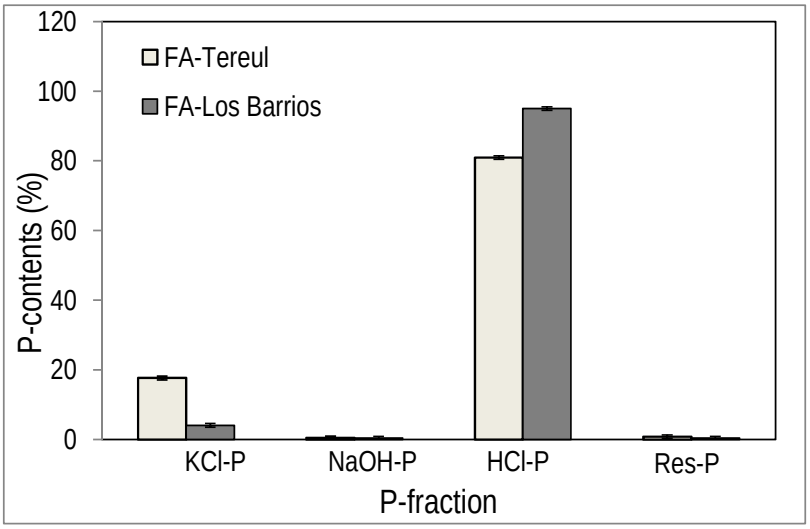

Figure 4.6. Phosphate speciation of FA-TE and FA-LB with initial amounts of phosphate in equilibrium (q_e=7.5±0.5 mg/g).

The formation of Ca phosphates (e.g., brushite and Hap) is thermodynamically favoured under the studied conditions, as shown in Figure 4.7; Hap is a more stable phase than brushite, which is considered its precursor phase. However, as the reaction proceeds on the microporous FA structure under the controlled Ca(II) ion release provided by CaO(s) dissolution, which avoids oversaturation, and brushite is formed and then stabilised, stopping the conversion to Hap. Thus, the main P(V) sorption process can be postulated according to Eqs. 16–17:

$$Ca(OH)_2(s) + HPO_4^{2-} \rightleftarrows CaHPO_4(s) + 2OH^- \quad \log K = 32.2 (25^{\circ}C) \quad (16)$$

$$Ca(OH)_2(s) + H_2PO_4^- \rightleftarrows CaHPO_4(s) + H_2O + OH^- \quad \log K = 22.2 (25^{\circ}C) \quad (17)$$

The removal of P(V) by brushite is accompanied by a release of 1 to 2 mole of OH^- ions per mole of P(V), which increases the pH, as observed in the sorption tests. For both FA samples, the sorption capacity is maximised at pH 8 and decreases as the pH increases to 9 or decreases to 7. This sorption

behaviour is in agreement with the formation of brushite. The logarithmic solubility of brushite and the P(V) sorption capacity as a function of pH are plotted in Figure 4.8. The minimum solubility, which corresponds to the highest brushite stability, is found at pH 8, where the maximum sorption capacities were also observed. Increasing or decreasing the pH increased the brushite solubility and accordingly decreased the P(V)-sorption capacity.

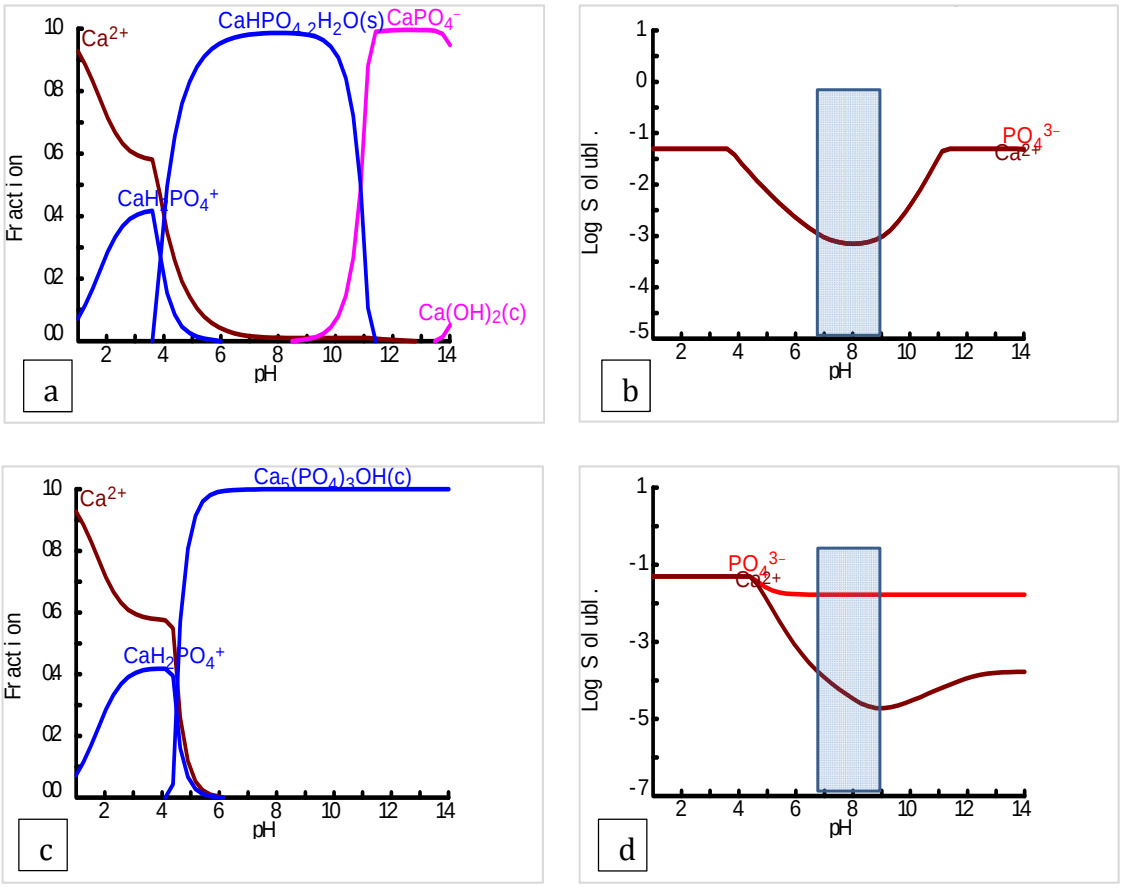

Figure 4.7. Species distribution diagram and solubility as a function of pH for the Ca and phosphate system using the HYDRA-Medusa database (Puigdomènech, 2001) for both phases: (a-b) $CaHPO_4.2H_2O$ (brushite) and (c-d) $Ca_5(PO_4)_3OH$ (Hap). The box indicates the pH range evaluated (maximum and minimum values).

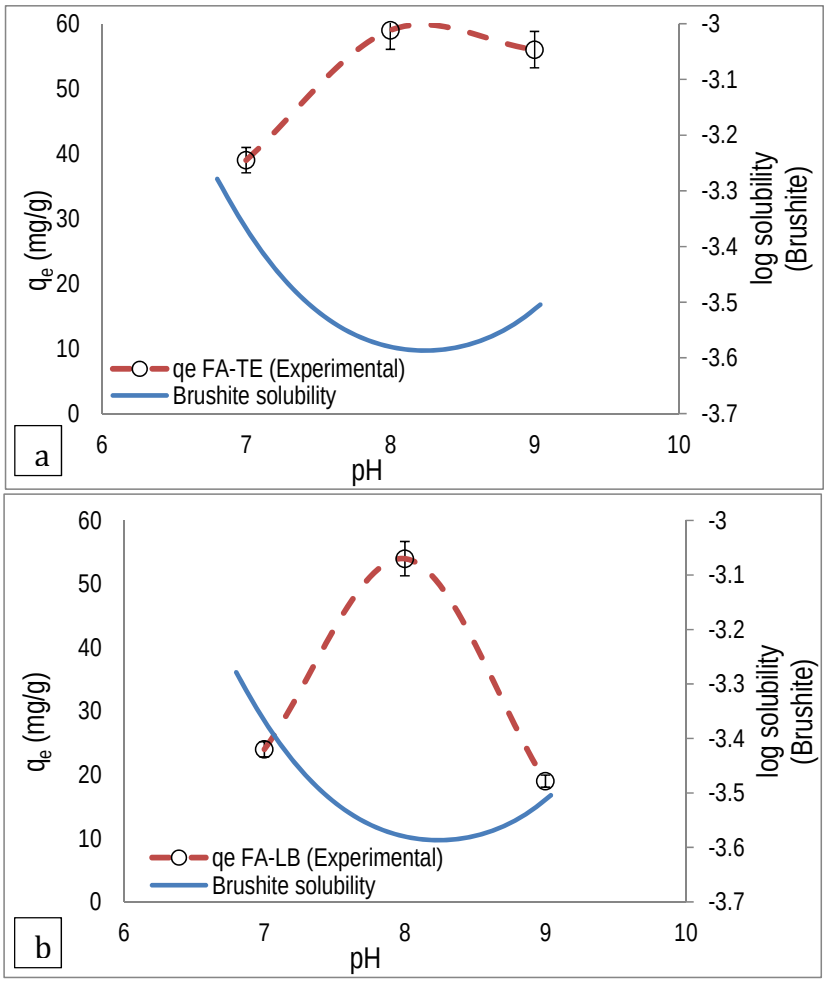

Figure 4.8. The experimental P(V)-sorption capacities at different pH values and the estimated brushite solubility curves for a) FA-TE and b) FA-LB.

4. Phosphate sorption kinetics

The results of the kinetic experiments involving P(V) solutions containing 100 and 500 mgP-PO_4/L at an initial pH value of 8 are shown in Figure 4.9a-b, and the evolution of the total Ca(II) concentration is presented in Figure 4.9c. The sorption profiles with time exhibit decreased phosphate and Ca(II) concentrations and increased pH values. For the kinetic test at 500 mg P-PO_4/L, the sorption rates of both FA samples (Figure 4.9a-b) are quite similar because this rate controlled by the excess phosphate relative to the Ca(II) provided by the FA.

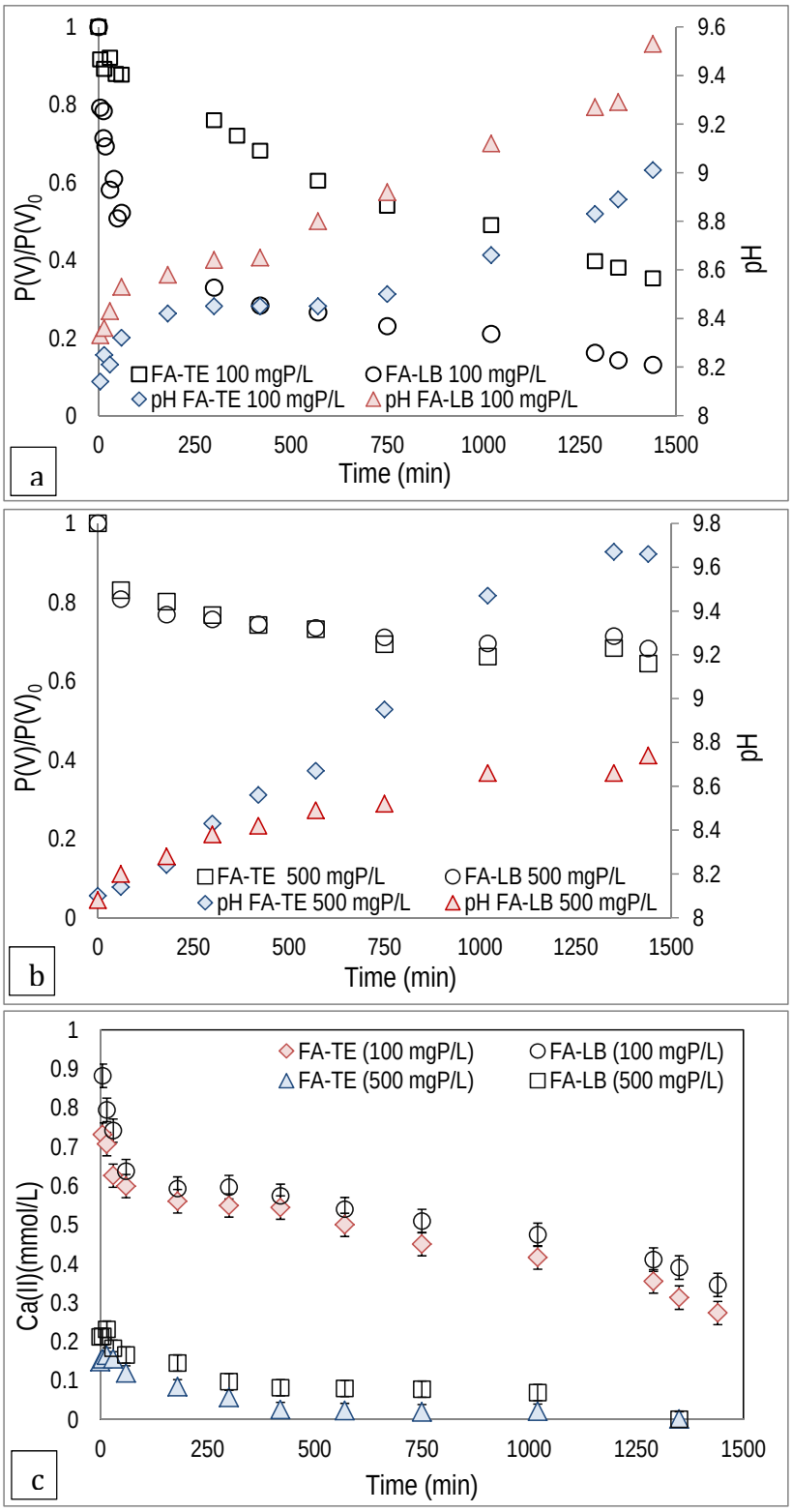

Figure 4.9. Variations of the $P(V)/P(V)_0$ ratio and pH as a function of time for initial concentrations of 100 mg/L (7a) and 500 mg/L (7b) at an initial pH of 8 and c) variation of the Ca(II) concentration as a function of contact time for initial P(V) concentrations of 100 and 500 mg/L at an initial pH of 8 (sorbent dose: 0.2 g/10 mL).

The sorption process can be divided into two steps: a first, faster step and a second, slower one. Initially, phosphate rapidly reached the boundary layer to interact with dissolved Ca(II) ions from the CaO(s) grains, and then, it slowly diffused from the boundary layer film onto the FA particle. At that time, P(V) removal was coupled with CaO(s) dissolution, which supplied the reactant needed to facilitate brushite formation.

The evolution of Ca(II) for both FA samples in the kinetic experiments with 100 and 500 mgP-PO_4/L (Figure 4.9c) revealed that the total Ca(II) concentration follows a profile very similar to that of the total P(V) concentration (Figure 4.9a). The total Ca(II) and P(V) concentration and the measured pH were used to determine the saturation indexes for brushite and Hap. The saturation index values (Figure 4.10) indicated that the system was oversaturated by Hap; however, as discussed previously, its precursor, brushite, was the only mineral phase identified by XRD analysis in this study.

The influence of the initial pH on the kinetics of both FA samples with 100-mgP/L phosphate solutions is shown in Figure 4.11.

The $P(V)/P(V)_0$ ratio profiles with time for both FA samples (Figure 4.11a-b) are strongly affected by pH, especially that of FA-LB. As the extraction reaction proceeds, the pH increases, as described by Eqs. 16–17 and shown in Figure 4.11b-d. Experiments at pH values of 7–8 exhibited greater increases (ΔpH>0.5 units) than that at pH 9 because of their lower buffer capacities (ΔpH<0.5 units). For FA-LB, most of the phosphate removal was achieved in the first 120 min: 40% at pH 7 to 80% at pH 9. In contrast, FA-TE exhibited a lower sorption rate, and longer contact times (more than 1000 minutes) were therefore required to reach equilibrium values. These differences are related the compositions of the FA samples, including the

SiO_2 and Al_2O_3 contents and especially that of mullite, which can be adjusted to improve the material's hydrophilic properties.

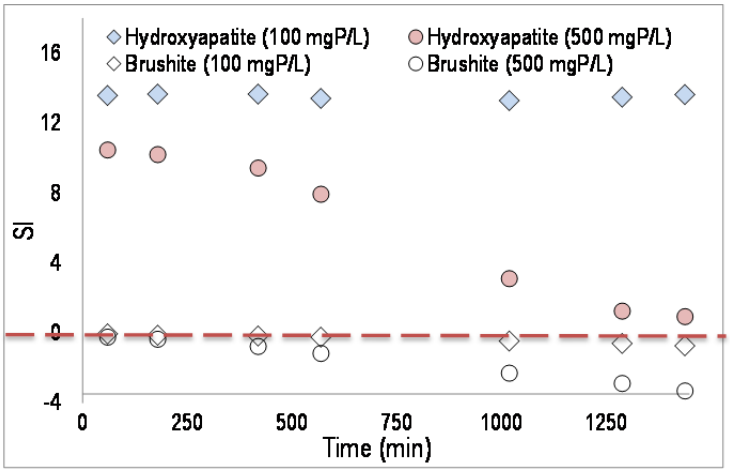

Figure 4.10 Supersaturation index (SI) of Ca –P(V) with respect to Hap and brushite as a function of the time (FA-TE example with P(V) solutions containing 100 and 500 mgP-PO_4/L at an initial pH value of 8)

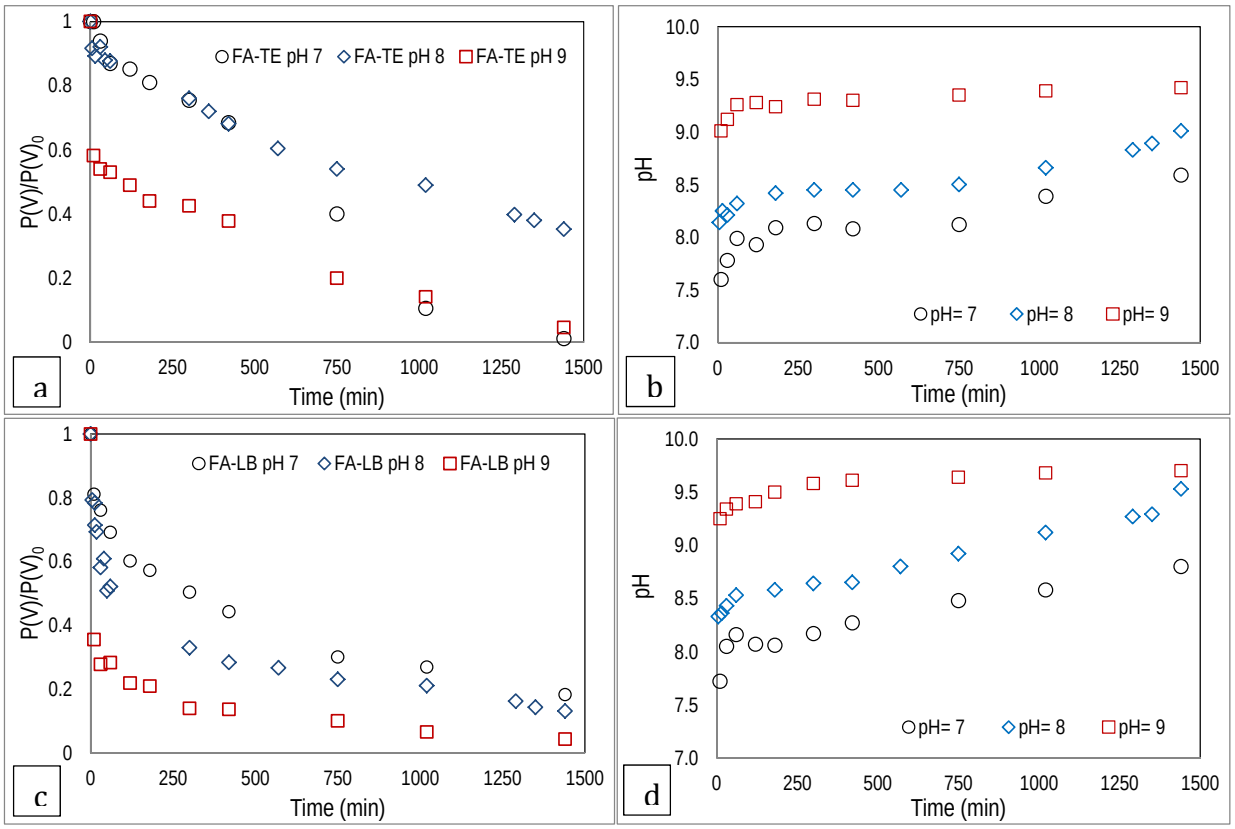

Figure 4.11. Variation in the $P(V)/P(V)_0$ ratios of FA-TE (a) and FA-LB (c) and pH as a function of contact time for an initial concentration of 100 mg P-PO_4^{3-}/L (sorbent dose: 0.2 g/10 mL) of FA-TE (b) and FA-LB (d).

4.1. Sorption kinetic modelling results

The results of the kinetic modelling of phosphate sorption onto FA are shown in Figure 4.12 Kinetic data fitting results in Eqs. 5–6 using the HPDM and Eqs. 8–10 using the SPM, as summarised in Table 4.5. The linear correlation coefficients indicate that film diffusion can be discarded as the sorption-controlling step because the fit did not exhibit the expected linear dependence. Both models fit the data satisfactorily for the entire time range of FA-phase diffusion. The predicted curves obtained using both models for FA-LB and FA-TE at different initial pH values are shown in Figure 4.12a-b. FA-TE and FA-LB showed better agreement between the predicted and experimental data at pH 7 and 8 than at pH 9. Taking into account the fact that the pH changes as a consequence of the sorption process in the kinetic experiments (Figure 4.11b and d), the $H_2PO_4^-/HPO_4^{2-}$ ratio (%) is 12/88 at pH 8.2 and 1/99 at pH 9.5; therefore, the effective diffusion coefficient can be considered to account for HPO_4^{2-}.

Table 4.5. Linear regressions of phosphate sorption onto FA samples modelled using HPDM and SPM with an initial concentration of 100 mgP-PO_4^{3-}/L at different initial pH conditions.

	HPDM					SPM					
	-ln (1-X^2)			-ln (1-X)		X		[3-3(1-X)$^{2/3}$-2X]		[1-(1-X)$^{1/3}$]	
	$pH_{t,m}$	R^2	D_e	R^2	D	R^2	K_F	R^2	D_e	R^2	k_s
FA-TE	(8.0)*	0.99	$3.3\ 10^{-15}$	0.94	$1.1\ 10^{-9}$	0.78	$2.9\ 10^{-10}$	0.99	$3.6\ 10^{-15}$	0.93	$7.1\ 10^{-12}$
	(8.3)*	0.98	$6.7\ 10^{-16}$	0.91	$2.2\ 10^{-10}$	0.90	$7.6\ 10^{-11}$	0.98	$7.6\ 10^{-16}$	0.93	$1.3\ 10^{-12}$
	(9.2)*	0.98	$8.1\ 10^{-16}$	0.96	$2.3\ 10^{-10}$	0.89	$5.5\ 10^{-11}$	0.98	$1.2\ 10^{-15}$	0.95	2.310^{-12}
FA-LB	(8.2)*	0.99	$8.6\ 10^{-16}$	0.95	$2.7\ 10^{-10}$	0.88	$1.5\ 10^{-10}$	0.99	$1.3\ 10^{-15}$	0.97	$2.3\ 10^{-12}$
	(8.5)*	0.97	$5.0\ 10^{-15}$	0.87	$4.8\ 10^{-10}$	0.74	$5.9\ 10^{-11}$	0.97	$6.4\ 10^{-15}$	0.89	$2.1\ 10^{-12}$
	(9.3)*	0.99	$3.7\ 10^{-15}$	0.92	$4.1\ 10^{-10}$	0.85	$7.3\ 10^{-11}$	0.97	$5.1\ 10^{-15}$	0.91	$1.9\ 10^{-12}$

* Values in brackets are the pH along the kinetic test with time t and specific point m.

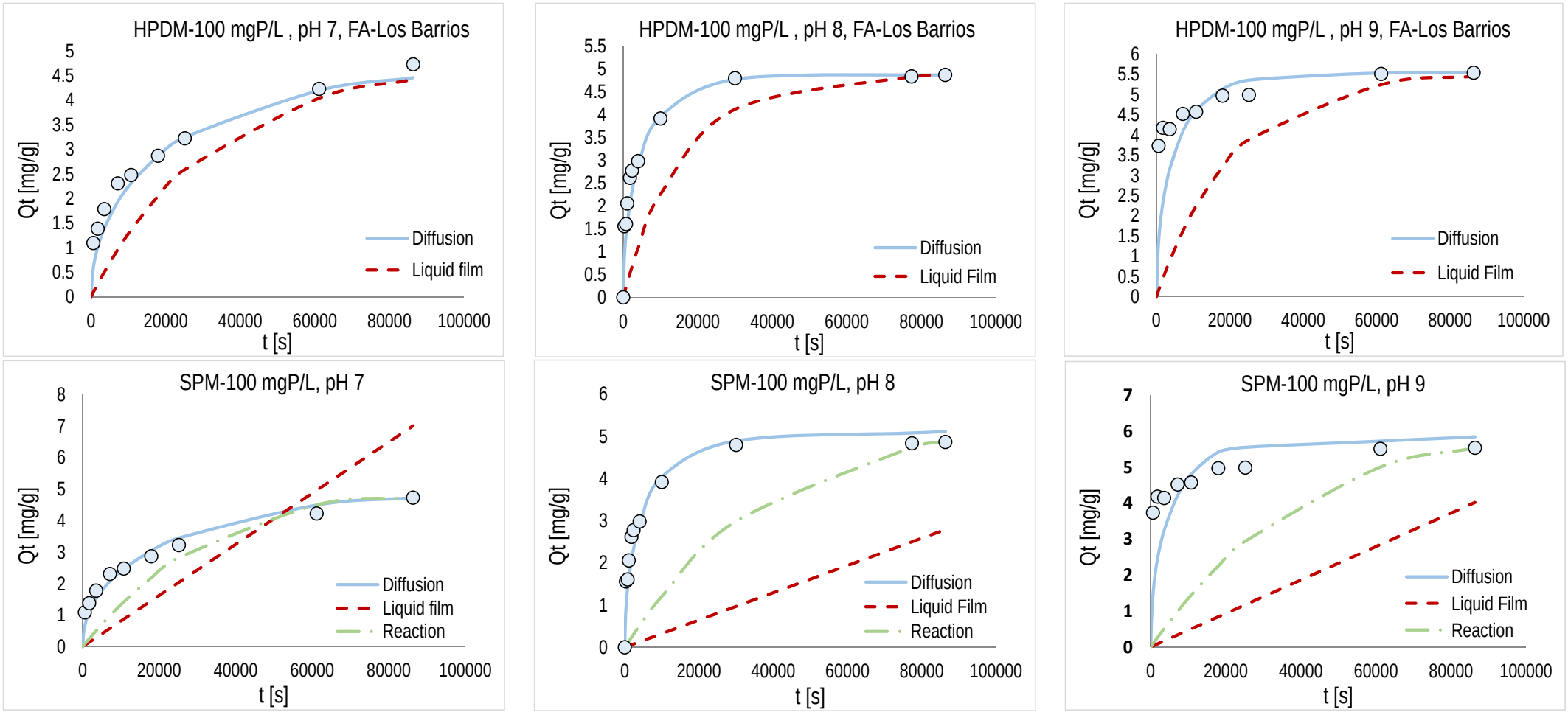

Figure 4.12. (a)The predicted curves obtained by linear regression analysis of HPDM and SPM for FA-LB with an initial phosphate concentration of 100 mg/L and different pH values (7, 8, and 9).

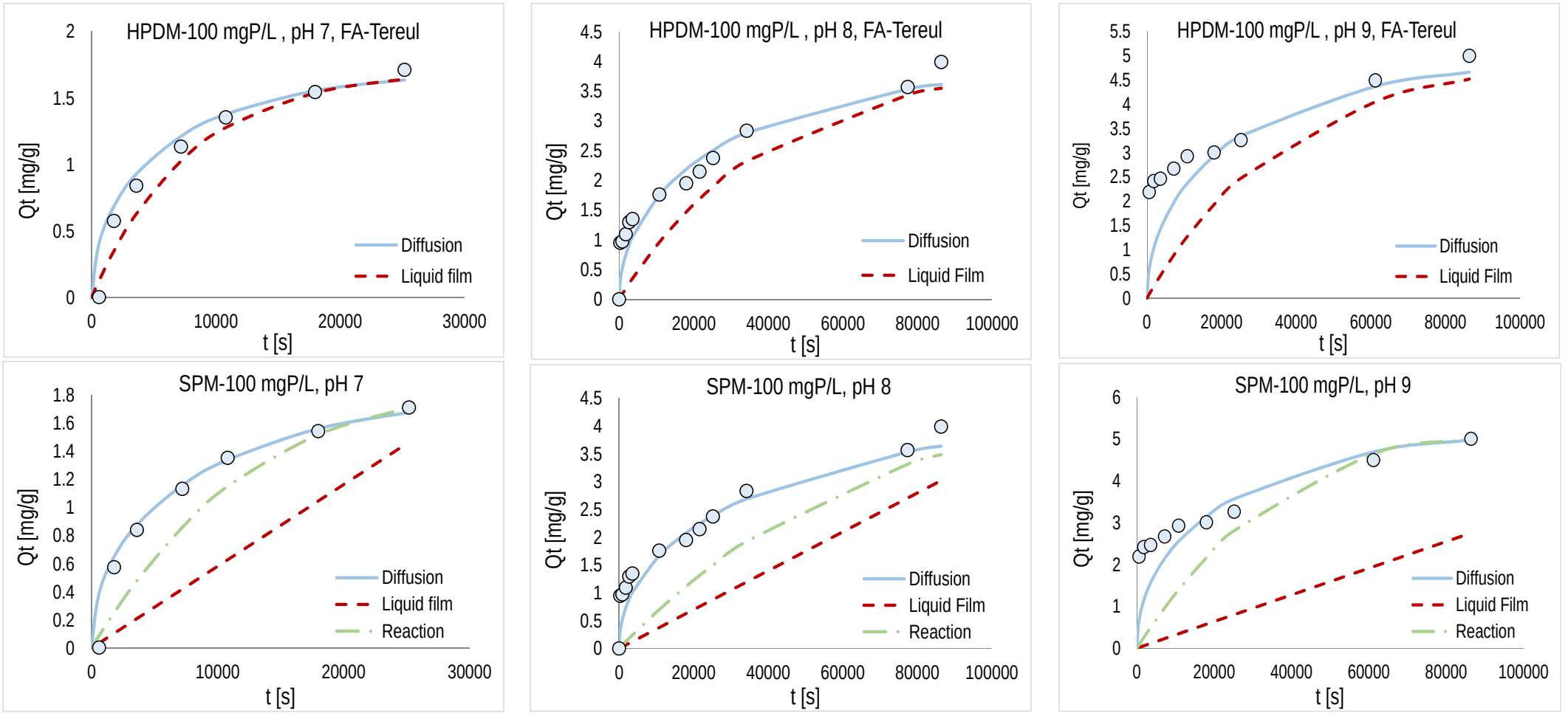

Figure 4.12. (b) The predicted curves obtained by linear regression analysis of HPDM and SPM for FA-Teruel with an initial phosphate concentration of 100 mg/L and different pH values (7, 8, and 9).

5. Evaluation of phosphate availability from loaded FA

Olsen et al. (Olsen, S.R. ; Cole, C.V; Watanabe, F.S; Dean, 1954) suggested bicarbonate extraction as a suitable method for predicting the plant availability of phosphate in calcareous soils where the main role of $NaHCO_3$ in phosphate extraction is decreasing the Ca^{2+} activity by forming $CaCO_3$. The phosphate-availability data in 0.5-M $NaHCO_3$ are plotted in Figure 4.13 as the extracted amount of phosphate per mass of FA (mgP-PO_4/g FA). For both FA samples, ratios from 8 to 30 mgP-PO_4/g FA were obtained. Partial extraction of 20 to 70% was reported in a single-extraction trial for both FA samples.

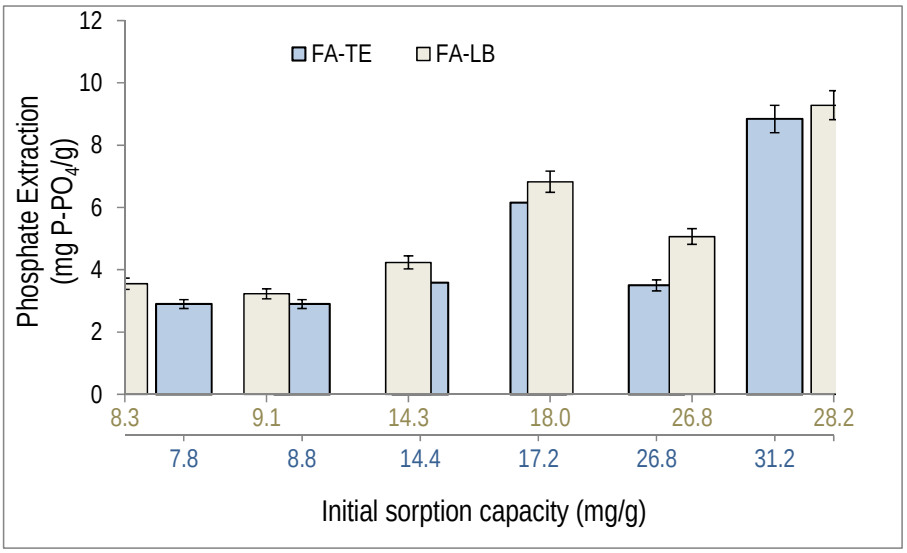

Figure 4.13. Phosphate extraction using $NaHCO_3$ (0.2 mol/L) from loaded FA samples: (a) FA-TE and (b) FA-LB.

These results are in good agreement with the speciation results reported in Figure 4.6. In the presence of excess bicarbonate ions, the labile phosphate fraction (P-KCl) will be displaced by bicarbonate ions, and partial brushite dissolution will be achieved according to Eq. 18:

$$CaHPO_4(s) + HCO_3^- \rightleftharpoons CaCO_3(s) + H_2PO_4^- \qquad \log K=-1.3\ (25ºC) \quad (18)$$

The sorbed P(V) on FA samples has been demonstrated to dissolve in solutions containing moderate to high bicarbonate concentrations similar to those expected in basic soils characterised by a high content of calcareous rocks (e.g., limestone) and where other Ca phosphate minerals, such as Hap, are very insoluble with limited plant availability.

6. Conclusions

The P(V)-removal results in the expected pH range (6 to 9) of wastewater effluents indicated that sorption proceeds via a diffusion-controlled process involving phosphate ions within the FA particles coupled with CaO(s) dissolution from FA, which provides the Ca(II) ions required for brushite ($CaHPO_4$(s)) formation at the FA surface. This process is important because it avoids the formation of relatively insoluble Ca phosphates, such as Hap, which have more limited fertilising properties. P(V) availability from loaded FAs was determined using $NaHCO_3$ solutions and revealed P(V)-release ratios of 10 to 30 gP-PO_4/g FA. In addition, phosphate removal is highly efficient, as indicated by the rapid removal and high P loadings obtained (up to 50 mgP-PO_4/g FA (5% P(V) by weight) at pH 8.

The use of phosphate-containing mineral-based sorbents as soil amendments may be advantageous when other agronomic benefits are expected, such as the provision of other plant nutrients or the enhancement of the soil moisture-holding capacity.

Future research should be performed to scale this process up from the laboratory scale to pilot- and full-scale systems integrating sorption and UF membrane filtration and to evaluate other types of powdered Ca-rich inorganic sorbents for phosphate removal and direct use as fertiliser.

7. References

Ahmaruzzaman, M., 2010. A review on the utilization of fly ash. Prog. Energy Combust. Sci. 36, 327–363.

Ann, Y., Reddy, K.R., Delfino, J.J., 2000. Influence of chemical amendments on phosphorus immobilization in soils from a constructed wetland Ecological Engineering. 14, 157–167.

ASTM standard specification for coal fly ash and raw or calcined natural pozzolan for use in concrete (C618-05). In: Annual book of ASTM standards, concrete and aggregates. 2005, American Society for Testing Materials.

Banerjee, S., Sharma, G.C., Chattopadhyaya, M.C., Sharma, Y.C., 2014. Kinetic and equilibrium modeling for the adsorptive removal of methylene blue from aqueous solutions on of activated fly ash (AFSH). J. Environ. Chem. Eng. 2, 1870–1880.

Bhattacharjee, U., Kandpal, T.C., 2002. Potential of fly ash utilisation in India. Energy. 27, 151–166.

Blissett, R.S., Rowson, N. A., 2012. A review of the multi-component utilisation of coal fly ash. Fuel. 97, 1–23.

Chen, J., Kong, H., Wu, D., Hu, Z., Wang, Z., Wang, Y., 2006. Removal of phosphate from aqueous solution by zeolite synthesized from fly ash. J. Colloid Interface Sci. 300, 491–497.

Cheung, K.C., Venkitachalam, T.H., 2000. Improving phosphate removal of sand infiltration system using alkaline fly ash. Chemosphere 41, 243–249.

de-Bashan, L.E., Bashan, Y., 2004. Recent advances in removing phosphorus from wastewater and its future use as fertilizer (1997-2003). Water Res. 38, 4222–46.

Dorozhkin, S. V., 2012. Self-Setting Calcium Orthophosphate Formulations: Cements, Concretes, Pastes and Putties. Int. J. Mater. Chem. 1, 1–48.

G. Schmuckler, S. Golstein, in: J.A. Marinsky, Y.M. (Eds., 1977. Ion Exchange and Solvent Extraction Marcel Dekker Inc., New York, in: Marcel Dekker Inc., New York. Chapter 1.

Gray, C. A, Schwab, A. P., 1993. Phosphorus- fixing ability of high pH, high calcium, coal-combustion, waste materials. Water, Air, and Soil Pollution. 69, 309–320.

Gray-Munro, J.E., Strong, M., 2013. A study on the interfacial chemistry of magnesium hydroxide surfaces in aqueous phosphate solutions: influence of Ca^{2+}, Cl^{-} and protein. J. Colloid Interface Sci. 393, 421–428.

Grubb, D.G., Guimaraes, M.S., Valencia, R., 2000. Phosphate immobilization using an acidic type F fly ash. J. Hazard. Mater. 76, 217–236.

Guaya, D., Valderrama, C., Farran, A., Armijos, C., Cortina, J.L., 2015. Simultaneous phosphate and ammonium removal from aqueous solution by a hydrated aluminum oxide modified natural zeolite. Chem. Eng. J. 271, 204–213.

Hedley, M.J., Stewart, J.W. B., Chauhan, B. S.,1982. Changes in Inorganic and Organic Soil Phosphorus Fractions Induced by Cultivation Practices and by Laboratory Incubations. Soil.Sci.AM.J 46, 970–976

Hooton, R., Tishmack, J., Olek, J., Diamond, S., 1999. Characterization of High-Calcium Fly Ashes and Their Potential Influence on Ettringite Formation in Cementitious Systems. Cem. Concr. Aggregates. 21, 82.

Hui, K.S., Chao, C.Y.H., 2006. Effects of step-change of synthesis temperature on synthesis of zeolite 4A from coal fly ash. Microporous Mesoporous Mater. 88, 145–151.

Johansson, L., Gustafsson, J.P., 2000. Phosphate removal using blast furnace slags and opoka-mechanisms. Water Res. 34, 259–265.

Kitson, R.E; Mellon, M. G., 1944. Colorimetric determination of phosphorus as molybdovanadophosphoric acid. Ind. Eng. Chem. Anal. Ed. 16, 379–383.

Liberti, L., Passino, R., in : J.A. Marinsky, Y.M. (Eds), 1977. Ion Exchange and Solvent Extraction, Marcel Dekker, Inc, New York.

Lior, N., 2010. Sustainable energy development: The present (2009) situation and possible paths to the future. Energy. 35, 3976–3994.

Liu, X., Ding, C., 2002. Morphology of apatite formed on surface of wollastonite coating soaked in simulate body fluid. Mater. Lett. 57, 652–655.

Liu, Y., Naidu, R., Ming, H., 2013. Surface electrochemical properties of red mud (bauxite residue): zeta potential and surface charge density. J Colloid Interface Sci 394, 451–457.

Lu, S.G., Bai, S.Q., Zhu, L., Shan, H.D., 2009. Removal mechanism of phosphate from aqueous solution by fly ash. J. Hazard. Mater. 161, 95–101.

Ma, J., Zhu, L., 2006. Simultaneous sorption of phosphate and phenanthrene to inorgano-organo-bentonite from water. J. Hazard. Mater. 136, 982–988.

Malarvizhi, T.S., Santhi, T., Manonmani, S., 2013. A Comparative Study of Modified Lignite Fly Ash for the Adsorption of Nickel from Aqueous Solution by Column and Batch Mode Study. 3, 44–53.

Martinez, R.E., Pokrovsky, O.S., Schott, J., Oelkers, E.H., 2008. Surface charge and zeta-potential of metabolically active and dead cyanobacteria. J. Colloid Interface Sci. 323, 317–325.

Moharami, S., Jalali, M., 2014. Phosphorus leaching from a sandy soil in the presence of modified and un-modified adsorbents. Environ. Monit. Assess. 186, 6565–6576.

Olsen, S.R., Cole, C.V., Watanabe, F.S., Dean, L., 1954. Estimation Of Available Phosphorus In Soils By Extraction With Sodium Bicarbonate, United Sta. ed. United States Department Of Agriculture ; Washington.

Parvinzadeh Gashti, M., Stir, M., Bourquin, M., Hulliger, J., 2013. Mineralization of Calcium Phosphate Crystals in Starch Template Inducing a Brushite Kidney Stone Biomimetic Composite. Cryst. Growth Des. 13, 2166–2173.

Pengthamkeerati, P., Satapanajaru, T., Chularuengoaksorn, P., 2008. Chemical modification of coal fly ash for the removal of phosphate from aqueous solution. Fuel. 87, 2469–2476.

Penilla, R.P., Guerrero Bustos, a., Goñi Elizalde, S., 2006. Immobilization of Cs, Cd, Pb and Cr by synthetic zeolites from Spanish low-calcium coal fly ash. Fuel. 85, 823–832.

Puigdomènech, I., 2001. Chemical Equilibrium Software Hydra and Medusa. Inorg. Chem. Dep.

Querol, X., Whateley, M.K.G., Fernández-Turiel, J.L., Tuncali, E., 1997. Geological controls on the mineralogy and geochemistry of the Beypazari lignite, central Anatolia, Turkey. Int. J. Coal Geol. 33, 255–271.

Reed, B.E., Vaughan, R., Jiang, L., 2000. As (III), As (V), Hg and removal by Fe-Oxide impregnated activated carbon. J. Environ .Eng. 126, 869–873.

Schwarz, J., Driscoll, C., Bhanot, A., 1984. The zero point of charge of silica-alumina oxide suspensions. J. Colloid Interface Sci. 97, 55–61.

Skartsila, K., Spanos, N., 2007. Surface characterization of hydroxyapatite: Potentiometric titrations coupled with solubility measurements. J. Colloid Interface Sci. 308, 405–412.

Tsitouridou, R., Georgiou, J., 1988. A contribution to the study of phosphate sorption by three Greek fly ashes. Toxicol. Environ. Chem. 17, 129–138.

Vassilev, S. V., Vassileva, C.G., 2007. A new approach for the classification of coal fly ashes based on their origin, composition, properties, and behaviour. Fuel. 86, 1490–1512.

Vordonis, L., Koutsoukos, P.G., Tzannini, A., Lycourghiotis, A., 1988. Uptake of inorganic orthophosphate by greek fly ashes characterized using various techniques. Colloids and Surfaces. 34, 55–68.

Wang, C.F., Li, J.S., Wang, L.J., Sun, X.Y., 2008. Influence of NaOH concentrations on synthesis of pure-form zeolite A from fly ash using two-stage method. J. Hazard. Mater. 155, 58–64.

Wang, S., 2008. Application of solid ash based catalysts in heterogeneous catalysis. Environ. Sci. Technol. 42, 7055–7063.

Watanabe, Y., Ikoma, T., Yamada, H., Stevens, G.W., Moriyoshi, Y., Tanaka, J., Komatsu, Y., 2010. Formation of hydroxyapatite nanocrystals on the surface of Ca-Al-layered double hydroxide. J. Am. Ceram. Soc. 93, 1195–1200.

Wawrzkiewicz, M., Wiśniewska, M., Gun'ko, V.M., Zarko, V.I., 2015. Adsorptive removal of acid, reactive and direct dyes from aqueous solutions and wastewater using mixed silica–alumina oxide. Powder Technol. 278, 306–315.

Wu, D., Zhang, B., Li, C., Zhang, Z., Kong, H., 2006. Simultaneous removal of ammonium and phosphate by zeolite synthesized from fly ash as influenced by salt treatment. J. Colloid Interface Sci. 304, 300–306.

Xu, K., Deng, T., Liu, J., Peng, W., 2010. Study on the phosphate removal from aqueous solution using modified fly ash. Fuel 89, 3668–3674.

Yan, J., Kirk, D.W., Jia, C.Q., Liu, X., 2007. Sorption of aqueous phosphorus onto bituminous and lignitous coal ashes. J. Hazard. Mater. 148, 395–401.

Yao, Z.T., Ji, X.S., Sarker, P.K., Tang, J.H., Ge, L.Q., Xia, M.S., Xi, Y.Q., 2015. A comprehensive review on the applications of coal fly ash. Earth-Science Rev. 141, 105–121.

Zebardast, H.R., Pawlik, M., Rogak, S., Asselin, E., 2014. Potentiometric titration of hematite and magnetite at elevated temperatures using a ZrO_2-based pH probe. Colloids Surfaces A Physicochem. Eng. Asp. 444, 144–152.

Zelmanov, G., Semiat, R., 2014. The influence of competitive inorganic ions on phosphate removal from water by adsorption on iron (Fe^{3+}) oxide/hydroxide nanoparticles-based agglomerates. J. Water Process Eng. 5, 143–152.

Zhang, B.-H., Wu, D.-Y., Wang, C., He, S.-B., Zhang, Z.-J., Kong, H.-N., 2007. Simultaneous removal of ammonium and phosphate by zeolite synthesized from coal fly ash as influenced by acid treatment. J. Environ. Sci. (China) 19, 540–545.

Zhou, J.Z., Feng, L., Zhao, J., Liu, J., Liu, Q., Zhang, J., Qian, G., 2012. Efficient and controllable phosphate removal on hydrocalumite by multi-step treatment based on pH-dependent precipitation. Chem. Eng. J. 185-186, 219–225.

Chapter 5

Powdered Ca-activated zeolites for phosphate removal from treated wastewater as slow-release fertilisers

This chapter is based on the work presented in the publication:
M. Hermassi, C. Valderrama, N. Moreno, O. Font, X. Querol, N.H. Batis and J.L. Cortina. 2016. Powdered Ca-activated zeolite for phosphate removal from treated waste-water. Journal of Chemical Technology and Biotechnology (DOI: 10.1002/jctb.4867.) (5-Year Impact factor: 2,616)**.**

A powdered zeolitic material synthesised from FA (NaP1-NA) and its Ca-modified form (CaP1-NA) were studied as sorbent materials for the recovery of phosphate from treated wastewater effluents. Phosphate-sorption equilibrium experiments were performed by varying the experimental conditions, including the solution pH, phosphate concentration, and the presence of competing ions. The maximum phosphate-sorption capacities were 57±5 and 203±11 mgP-PO_4/g for NaP1-NA and CaP1-NA, respectively. The sorption capacities of both zeolites in the pH range expected for wastewater effluents (pH from 7 to 9) were slightly dependent on pH, exhibiting maxima at pH 8. Phosphate removal proceeds through two main mechanisms: a) surface complexation with ≅AlOH and ≅FeOH groups of the zeolitic structure or unreacted minerals from the FA, and b) the formation of Ca phosphate phases, mainly brushite, with Ca(II) ions from the CaO present on the FA or occupying the charged sites of the zeolite. The removal mechanisms were confirmed by XRD analyses and P speciation. Finally, the stabilities of the phosphate-loaded zeolite samples as fertilisers were evaluated by extraction experiments to determine their potential availabilities in soil applications.

1. Introduction

Increasing energy demands worldwide have led to increased utilisation of coal and the production of large quantities of FA as a waste product. The global production of FA in 2010 exceeded 750 million tons/year, with 38 million tons produced in Europe alone (Blissett and Rowson, 2012; Yao et al., 2015). FA is enriched with SiO_2 and Al_2O_3, and thus, it can be transformed by

chemical treatment into zeolite-like crystalline materials. The synthesis of zeolites is attracting attention as an effective use for CFA, possibly because of its similar composition to the volcanic material that serves as the precursor of natural zeolites.

Zeolites are microporous aluminosilicate minerals that could be used as ion exchangers in domestic and industrial water purification and softening applications (Singer et al., 2005). The substitution of Si by Al atoms in the crystal framework leads to extra negative charges that must be balanced by surrounding counter ions (such as Na^+, K^+, Ca^{2+}, and Mg^{2+}); these counter ions can be easily exchanged for other surrounding cations in contact with aqueous solutions. Therefore, several studies on the use of zeolites for the removal of hazardous cations (Xie et al., 2013; Yang et al., 2014) and anions and organic compounds with modified zeolites (Zhou et al., 2014) have been reported. By applying several synthesis methods, different families of zeolites have been synthesised from FA (Querol et al., 2002; Ansari et al., 2014; Zhou et al., 2014); however, few have been successfully converted into pure-phase zeolites (Hollman et al., 1999; N Moreno et al., 2001).

The removal of phosphate from wastewaters has been linked to the need for their reuse and valorisation, both of which could be achieved using a reactive material capable of achieving high phosphate-removal ratios in solution and suitable for use as a slow-release fertiliser in soil and agricultural applications (Desmidt et al., 2013). This process could be developed if low-cost sorbents are available (Boyer et al., 2011). Querol et al. (2007) demonstrated the economic and technical viability of synthesising NaP1-NA under mild hydrothermal conditions without using templates. NaP1-NA was evaluated for the removal of toxic metals from acid mine drainage and brines (N Moreno et

al., 2001) because of its unique ion-exchange and water-sorption properties, which are attributable to its high porosity, surface area, and CEC and its unusual framework flexibility (Cama et al., 2005). NaP1-NA also has a high capacity to adsorb ammonium and K, and it has been evaluated as a slow-release fertiliser; however, the sorption of oxyanions as phosphate is not favoured by the zeolite structure (Watanabe et al., 2014). The use of mixtures of synthetic apatites and natural zeolites as solid media for growing plants and as a fertiliser has been postulated (Golden and Ming, 1999; Liu and Lal, 2014). However, because of the low solubility and availability of P from Hap in soils, efforts have been directed towards the preparation of relatively soluble Hap ($Ca_{10}(PO_4)_6(OH)_2$) and brushite ($CaHPO_4.2H_2O$) by growing crystals on the surface of Ca-containing minerals. These materials include Ca silicates, such as wollasonite (Liu and Ding, 2002); Ca-Al layered double hydroxide; and Hap (Watanabe et al., 2010; Zhou et al., 2012). However, little work has been done to prepare a reactive material to a) efficiently remove phosphate from wastewater effluents in the form of relatively soluble phosphates (e.g., brushite ($\log K_{so}$=6.59)) (Dorozhkin, 2012) compared to Hap ($Ca_5(PO_4)_3OH$(s), $\log K_{so}$=116.8) (Parvinzadeh Gashti et al., 2013) and b) to achieve suitable properties for use as a synthetic slow-release fertiliser.

In this study, both the Na^+-zeolite (NaP1-NA), synthesised from CFA, and its Ca-modified form (CaP1-NA) were evaluated as sorbents for phosphate recovery from aqueous solution. The phosphate-sorption performance was studied by varying the experimental conditions, such as the solution pH, coexisting ions, and initial phosphate concentration. The results are presented in terms of equilibrium isotherms in non-competitive and

competitive experiments with other common anions present in wastewater effluents. Furthermore, the phosphate-sorption removal mechanisms were evaluated using a speciation methodology. Finally, the stability of the phosphate-loaded zeolite samples was evaluated by extraction experiments using bicarbonate solutions to determine their potential availability in soil applications.

2. Materials and methods

2.1. Synthesis of NaP1-NA and CaP1-NA

Na^+-zeolite (NaP1-NA) was synthesised from Narcea CFA with 3-mol/L NaOH at 125°C for 8 h using a hydrothermal method, as described elsewhere (Querol et al., 2007). Ca-zeolite (Ca^{2+}-zeolite CaP1-NA) was prepared by a cation-exchange process. First, 250 g of NaP1-NA was immersed in 1000 mL of a 0.5-mol/L $CaCl_2$ solution for 1 h at room temperature, which was then filtered through a 0.2-μm membrane filter and rinsed with distilled water to remove the $CaCl_2$ solution (Watanabe et al., 2014). The cation-exchange and washing cycle was repeated five times. The sample obtained was dried for 72 h at 50–60°C.

2.2. Phosphate-removal equilibrium experiments

Phosphate test solutions were prepared by dissolving a weighed amount of $Na_2HPO_4.2H_2O$ in water obtained from a Milli-Q-Academic-A10 apparatus (Millipore Co. France). Batch experiments were performed at room temperature (21±1ºC). Samples of zeolites (0.2 g) were mechanically mixed in special polyethylene stoppered tubes with an aqueous phosphate solution (12 mL) at different initial concentrations of P(V) (100–16,000 mg L-1) until

equilibrium was achieved (24 h). The influence of pH on the phosphate sorption was evaluated by using 0.1-mol/L HCl or NaOH solution to adjust the initial pH. After phase separation with a 0.2-μm syringe filter, the equilibrium pH was measured using a pH electrode (Crison GLP22), and the total phosphate concentration was measured using spectrophotometric colourimetry (Kitson, R.E; Mellon, 1944). The P(V) equilibrium sorption capacity determined using Eq. 1.

$$q_e = (C_0 - C_e)\frac{v}{m_s} \quad (1)$$

where C_0 (mg/L) and C_e (mg/L) represent the initial and equilibrium total P(V) concentrations, respectively; v (L) is the aqueous solution volume; and m_s (g) is the mass of zeolite.

2.3. Phosphate-removal equilibrium experiments in the presence of competing ions

The effect of common coexisting ions in wastewater, such as chloride, sulfate, nitrate, and bicarbonate, on the sorption of phosphate was investigated by adding 300 mg HCO_3^-/L, 300 mg Cl^-/L, 250 SO_4^{2-}/L, and 50 mg NO_3^-/L to 100-15,000 mg P-PO_4^{3-}/L. A given mass of CaP1-NA (0.2 g) was added, and the solution was agitated at 400 rpm for 24 h at 21±2°C. After filtration with a 0.2-μm membrane filter, the residual phosphate concentration was analysed using spectrophotometric colourimetry. The typical values of the effluent streams from secondary and tertiary treatments at the El Prat wastewater treatment plant WWTP (Barcelona, Spain) were used to determine the feed composition.

2.4. Speciation of phosphate-loaded zeolite samples using a sequential extraction protocol

The speciation of P adsorbed in loaded zeolites (NaP1-NA and CaP1-NA) was achieved using a modified four-step sequential extraction (M.J.Hedley and J.W. B Stewart, 1982; Ann et al., 2000; Moharami and Jalali, 2014). First, 30-mL aliquots of 1000 mg P-PO_4^{3-}/L at pH 7 were equilibrated with pre-weighed tubes containing 3 g of each type of zeolite: NaP1-NA and CaP1-NA. After shaking for 24 h at room temperature, the suspensions were centrifuged, and the powders were collected and dried in an oven at 50–60°C. The adsorbed phosphate was sequentially extracted. One gram of each sample was weighed into a 50-mL centrifuge tube and then treated as described in Table 5.1.

Table 5.1. Chemical extraction scheme for the phosphate speciation of loaded zeolites.

Reagent conditions	Speciation name	Speciation (associated P(V) forms)	Step
40-mL 2 M KCl for 2h	KCl-P	Soluble and exchangeable P	1
40-mL 0.1 M NaOH for 17h	NaOH-P	Fe- and Al-bound P	2
40-mL 0.5 M HCl for 24h	HCl-P	Ca-bound P	3
40 ml 8 M HNO_3/5 M $HClO_4$	Res-P	Residual P	4

2.5. Desorption of phosphate from loaded zeolites samples using bicarbonate solutions

First, 0.5-g samples of phosphate-loaded zeolites (NaP1-NA and CaP1-NA) with phosphate contents ranging from 11 to 173 mmol/L were mixed with 20-mL solutions containing a mixture of $NaHCO_3$ (0.1 M) and Na_2CO_3 (0.1 M) in 50-mL plastic bottles. The bottles were mechanically shaken (Heidolph) at 21±1°C for 24 h at a constant agitation speed of 200 rpm. At the end of the

experiment, the samples were withdrawn from the test bottles and filtered through a 0.45-μm membrane filter; the residual phosphate concentration was analysed using spectrophotometric colourimetry.

2.6. Physicochemical characterisation of zeolites

At the end of the sorption and desorption experiments, the zeolite samples were washed with water to remove the interstitial water and then oven-dried at 60°C for structural and textural analysis. The mineralogical composition was analysed by a Bruker D8 A25 Advance X-Ray Diffractometer θ-θ with $CuK_{\alpha 1}$ radiation, Bragg-Brentano geometry, and a linear LynxEyeXE detector. The diffractograms were obtained from 4º to 60º of 2θ with a step size of 0.015º and a counting time of 0.1 s as the sample rotated. The solids in powder form were identified by standard JCPDS files and were matched with PDFs no. 009-0077 (brushite), no. 039-1374 (garronite), 039-0219 (NaP1), 046-1045 (quartz), and 015-0776 (Mullite).

The samples' morphologies were examined by FE-SEM-EDS with prior gold metallisation.

The PZC values of NaP1-NA and CaP1-NA were determined, and the common intersection point (CIP) method was applied to the potentiometric titration curves obtained at four ionic strengths (Skartsila and Spanos, 2007; Liu et al., 2013; Zebardast et al., 2014). First, 0.1 g of zeolite was equilibrated with 25 mL of solutions with different ionic strengths (0.01-, 0.05-, 0.1-, and 0.5-M KNO_3) for 24 h at 200 rpm and 21±1°C. Following equilibration, a small quantity of 0.1-M KOH was added to the suspension to increase the pH beyond 10 (pHin). The suspension was then titrated with 0.0454-M HNO_3 to pH≈3 using an automatic titrator (Mettler Toledo). The net surface charge

was correlated with the PZC determined from the titration data for the adsorbed amounts of [H^+] and [OH^-] ions.

Therefore, the titration curves of different ionic strength intersect at pH=pH_{PZC}. The surface charge was calculated according to Eq. 2 (Martinez et al., 2008).

$$b = C_b - C_a + [H^+] - [OH^-] \quad (2)$$

where b (mol/g) is the net amount of hydroxide ions consumed; C_b and C_a (mol/L) are the base and acid concentrations, respectively; and [H^+] and [OH^-] denote the proton and hydroxide concentrations, respectively, calculated from the measured pH for a given mass of zeolite (g) and a given volume of solution (L). All measurements were performed in triplicate, and the average values are reported.

3. Results and discussion

3.1. Characterisation of the CaP1-NA-modified zeolites

The conversion of FA into zeolitic materials through the batch hydrothermal synthesis process involves three stages: i) the dissolution of Al and Si from FA, ii) the deposition of aluminosilicate gel on the FA surface, and iii) the crystallisation of zeolite from aluminosilicate gel (Murayama et al., 2002). The three Al- and Si-containing phases of the FA are i) amorphous aluminosilicate glass, ii) quartz, and iii) mullite. Aluminosilicate glass is the largest component and is the most unstable in the hydrothermal environment, and therefore, it exhibits the highest rate of dissolution (C. Poole, 2000; Querol et al., 2001) makes the largest contribution to the produced zeolites.

The XRD patterns of the Na zeolite (NaP1-NA) and the synthesised Ca zeolite (CaP1-NA) are shown in Figure 5.1a. NaP1 ($Na_6(Al_6Si_{10}O_{32})\cdot 12H_2O$),

mullite ($Al_2Si_2O_{13}$), and a trace of quartz (SiO_2) were the main phases identified in NaP1-NA. The XRD patterns of CaP1-NA indicated the presence of mullite, quartz, calcite ($CaCO_3$), and garronite ($NaCa_{2.5}(Si_{10}Al_6)O_{32}\cdot 14H_2O$) as the predominant phases. The SEM observation (Figure 5.1b) showed that NaP1-NA and CaP1-NA coat the FA. As shown in Figure 5.1b, the coating of NaP1-NA is not complete, as reported by Cama et al. (Cama et al., 2005).

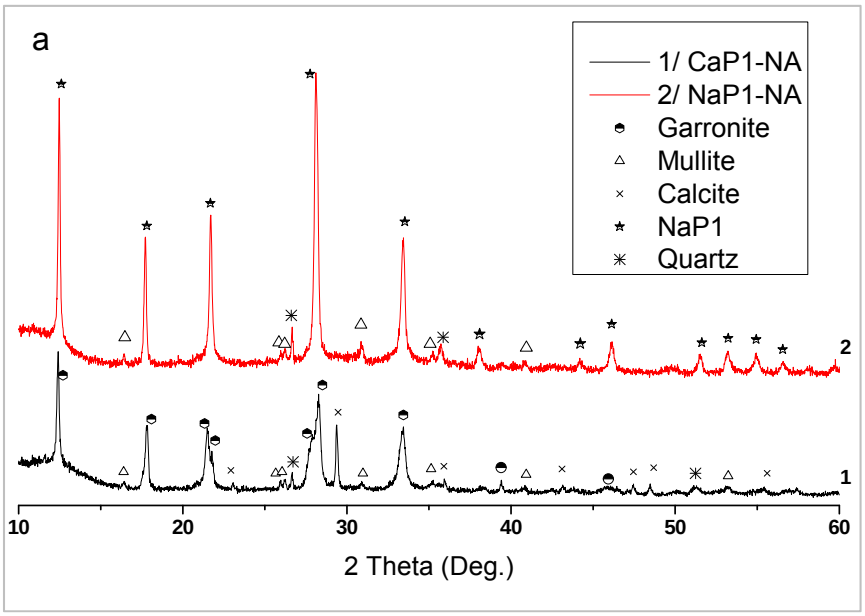

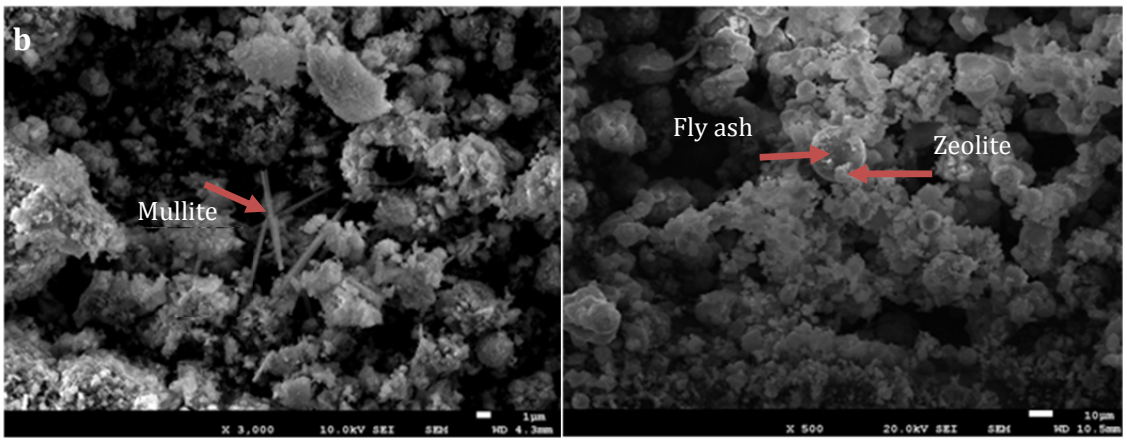

Figure 5.1. (a) XRD patterns of NaP1-NA and its Ca-modified zeolite CaP1-NA and (b) SEM images of NaP1-NA and CaP1-NA.

The chemical compositions of both zeolitic materials are listed in Table 5.2 and indicate that NaP1-NA and CaP1-NA contained mainly Al_2O_3 and SiO_2,

which accounted for a total of 74%. The synthesis of CaP1-NA considerably increased the Ca^{2+} content (from 1.4 to 7.4% (82.5 mg/g)). Accordingly, the Na content decreased significantly (from 7.6 to less than 1%) because of treatment with $CaCl_2$ and the partial exchange of Na and Ca ions in the zeolite structure.

Table 5.2. Average chemical compositions of the zeolitic adsorbents NaP1-NA and CaP1-NA obtained via FSEM-EDX and the specific surface area (S_{BET}).

	C	O	Na	Mg	Al	Si	K	Ca	P	Fe	S_{BET} ($m^2\ g^{-1}$)
NaP1-NA (%)	11.6	50.6	7.6	0.5	8.1	15.1	1.9	1.4	0.4	2.9	6.3
CaP1-NA (%)	12.5	51.3	1.0	0.6	8.1	14.6	1.7	7.4	0.4	2.6	13.6

The acid-base characterisation revealed pH_{PZC} values of 6.1±0.2 for CaP1-NA and 5.4±0.2 for NaP1-NA (Figure 5.2), which are in agreement with values reported for natural zeolites (clinoptilolite) (5.2±0.2) (Guaya et al., 2015). The increased pH_{PZC} of CaP1-NA suggests a decrease in the acidity of the metal-hydroxide groups (≅MOH) of the zeolite structure after modification with Ca salts resulting from complexation with Ca(II) ions. The determined pH_{PZC} value is in agreement with values reported for α-$Al(OH)_3$(s) (pH_{PZC}=5.0) and $Fe(OH)_3$ (pH_{PZC}=5–7). Indeed, some studies (Reed et al., 2000; Chen et al., 2006; Zhang et al., 2007) have reported that Fe- and Al-based surface groups on zeolites become positively charged and that their anion-sorption capacity (e.g., $H_2PO_4^-$/HPO_4^{2-}) via ligand exchange increase because of chemical interactions and electrostatic forces. The latter give rise to Columbic attraction or repulsion between binding sites and sorbing ions (Onyango et al., 2007).

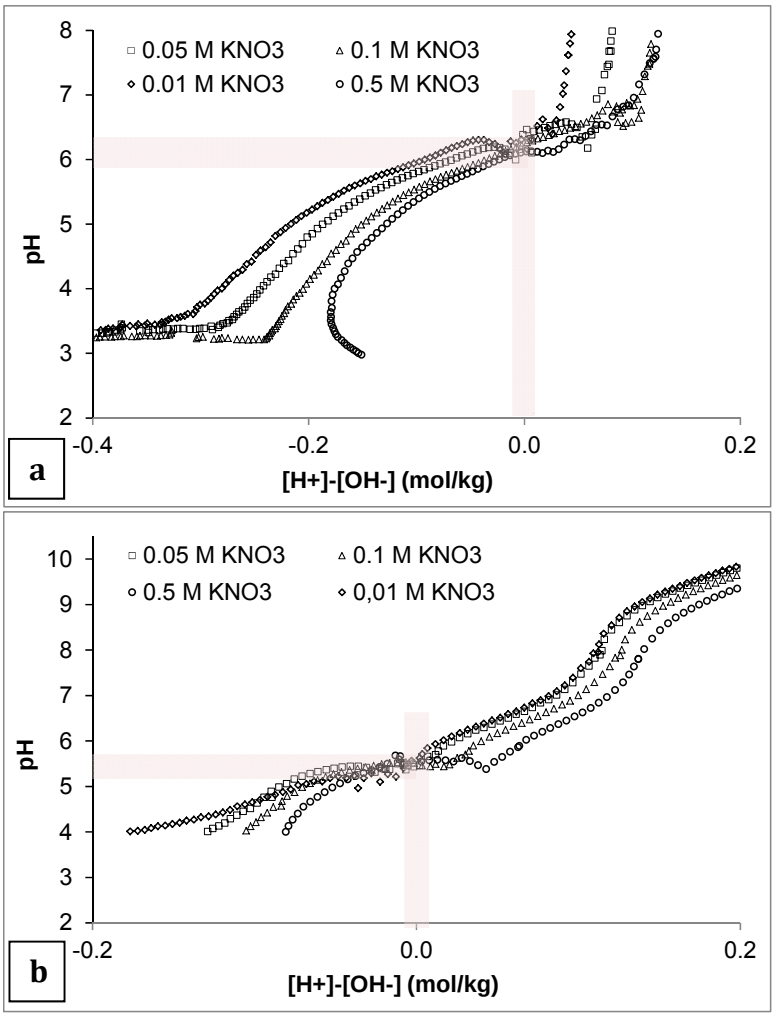

Figure 5.2. Potentiometric titration curves obtained at 0.01-, 0.05-, 0.1-, and 0.5-M KNO_3 for a) CaP1-NA and b) NaP1-NA.

3.2. P(V)-sorption capacities of CaP1-NA and NaP1-NA: Dependence on pH and P(V) concentration

The effects of the initial P(V) concentration on phosphate sorption and the equilibrium pH for both zeolites are shown in Figure 5.3a. The P(V)-sorption capacity increased as the initial P(V) concentration increased. Additionally, the equilibrium pH exceeds the initial pH (8), reaching values as high as 9.5 for CaP1-NA and 9 for NaP1-NA, at lower initial P(V) concentrations (up to 20 mmol/L) and then decreases back to the initial value for NaP1-NA and 7.5 for CaP1-NA.

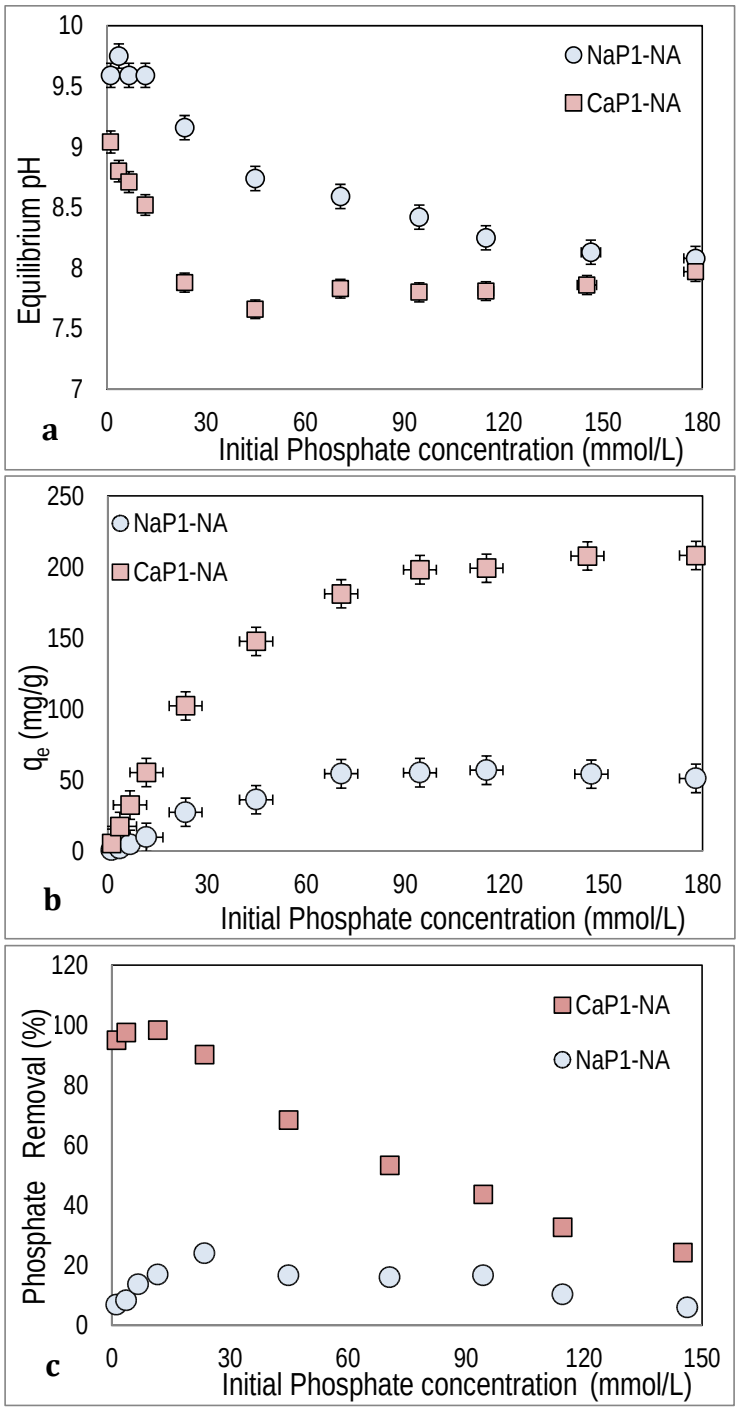

Figure 5.3. (a) Evolution of the equilibrium pH as a function of the initial phosphate concentration (initial pH 8) for CaP1-NA and NaP1-NA and (b-c) the uptake concentration and the percentage of removal as a function of the equilibrium-adsorbed concentration.

Moreover, the shape of the phosphate-sorption isotherm indicates that CaP1-NA has a higher affinity for phosphate than NaP1-NA, as shown by the

higher slope of the isotherm. This high affinity results in the nearly quantitative removal of phosphate by CaP1-NA (98%) at low residual phosphate concentrations in solution. In contrast, for NaP1-NA, the removal ratios achieved were below 25%. As the initial phosphate concentration was increased, the sorption capacities of the zeolites increased, reaching maxima of 207 mg/g and 50 mg/g for CaP1-NA and NaP1-NA, respectively (Figure 5.3b-c).

According to the removal patterns exhibited by NaP1-NA and CaP1-NA zeolitic materials, the sorption of P(V) ions, mainly $H_2PO_4^-$ and HPO_4^{2-}, that occurs in the expected pH range (7 to 9) may follow two postulated mechanisms:

a) Surface complexation with ≅AlOH and ≅FeOH functional groups originally present as Al and Fe oxides or in the zeolitic structure via two main reactions:

a1) Labile complexes with $\cong MOH_2^+$ surface groups

$$\cong MOH_2^+ + H_2PO_4^-/HPO_4^{2-} \leftrightarrow \cong MOH_2^+ H_2PO_4^-/HPO_4^{2-} \quad (3)$$

a2) Inner-sphere complexes with ≅MOH surface groups

$$\cong MOH + H_2PO_4^-/HPO_4^{2-} \leftrightarrow \cong MH_2PO_4^-/HPO_4^{2-} + OH^- \quad (4)$$

where M represents Al or Fe.

b) Formation of Ca phosphate minerals with Ca(II) ions present on the zeolite through two main reactions:

b1) Ca phosphate minerals with Ca(II) present on the zeolitic material as CaO(s) and $CaCO_3$(s):

$$H_2PO_4^-/HPO_4^{2-} + CaO(s) = \text{Ca phosphates } (CaHPO_4 \text{ or } Ca_5(OH)(PO_4)_3(s)) \quad (5)$$

Both mineral phases can be formed in the expected pH range, as shown in Figure 5.4.

b2) Formation of Ca phosphate minerals with Ca(II) ions occupying the ion-exchange groups of the zeolitic structure

$$(\cong ZO^-)_2Ca^{2+} + H_2PO_4^- + 2Na^+ \leftrightarrow 2\cong(ZO^-Na^+) + CaHPO_4(s) + H^+ \quad (6)$$

$$5(\cong ZO^-)_2Ca^{2+} + 3H_2PO_4^- + 10Na^+ \leftrightarrow 10\cong(ZO^-Na^+) + Ca_5(OH)(PO_4)_3\,(s) + 7H^+ \quad (7)$$

where $\cong ZO^-$ represents the anionic groups of the zeolite structure.

The P(V) sorption that occurs via the formation of surface complexes (Eqs. 3–4) is consistent with the observed results at low phosphate concentrations (Figure 5.3b), which involved the removal of $H_2PO_4^-$ (Eq. 3) and the formation of inner-sphere complexes (Eq. 4).

For high initial P(V) concentrations (50–200 mmol/L), the most favoured reaction is the formation of Ca phosphates (e.g., brushite or Hap) (Eqs. 6–7) with the release of H^+ ions and the resulting decrease in the pH to 7.5 for CaP1-NA. For NaP1-NA, the lower Ca(II) content results in a lower sorption capacity, and thus, the recovery of P(V) ions should be conceived of as a combination of Eqs. 3–6.

XRD analysis of the samples after the sorption experiments revealed the presence of brushite in most of the analysed CaP1-NA samples, while for NaPa1-NA, the presence of Ca phosphate minerals was not observed. This could be attributable to the contents of these minerals on the samples being below the limit of detection or the formation of the minerals within the small channels of the zeolite as undetectable nanocrystals.

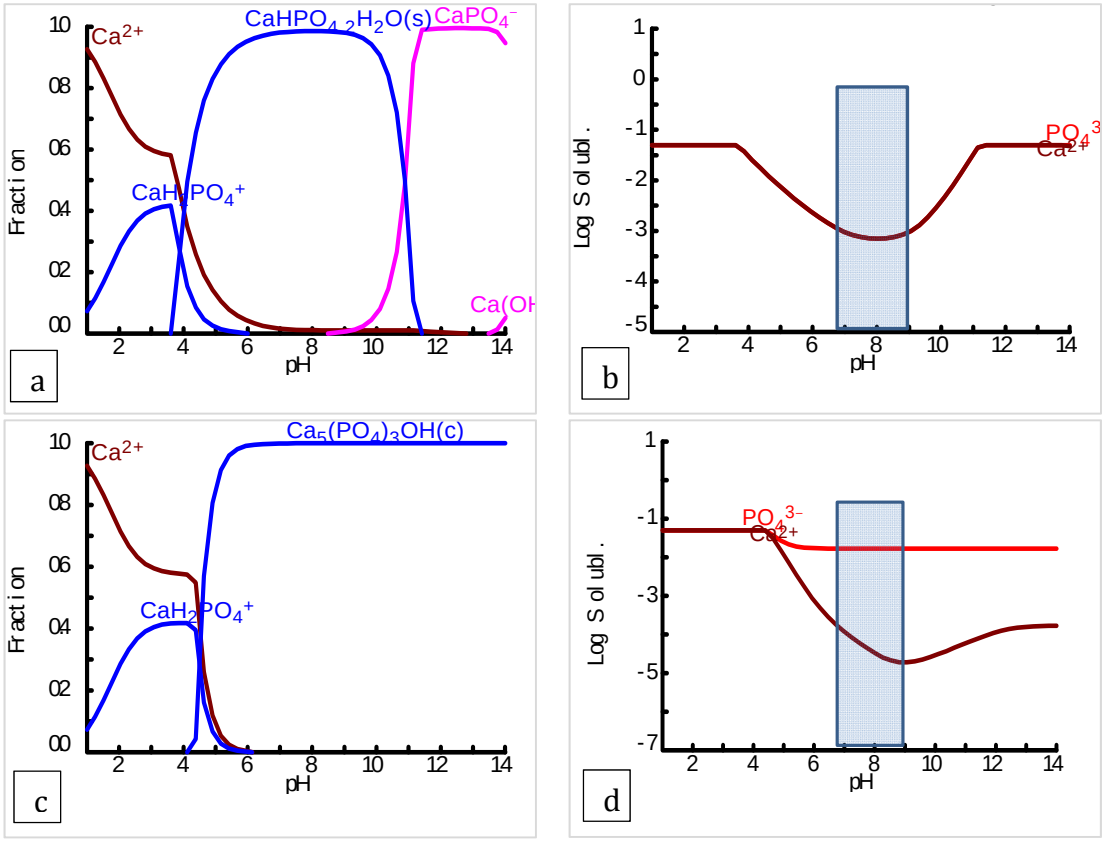

Figure 5.4. Species distribution diagrams and solubilities as a function of pH for the Ca and phosphate system using the HYDRA-Medusa database (Puigdomènech, 2001) for both phases: (a-b) $CaHPO_4.2H_2O$ (brushite) and (c-d) $Ca_5(PO_4)_3OH$ (Hap). The box indicates the pH range evaluated (maximum and minimum values).

The formation of Ca phosphates (brushite and Hap) is thermodynamically favoured in the expected pH range, as shown in Figure 5.4. Hap is more stable than brushite, which is considered its precursor phase. However, as the reaction proceeds on the microporous zeolite structure, brushite is formed and then stabilised, thereby stopping the conversion to Hap.

The phosphate-sorption isotherms of CaP1-NA and NaP1-NA at different pH values (7, 8, and 9) are shown in Figure 5.5. The P(V)-loading capacity of CaP1-NA is higher than that of NaP1-NA; e.g., 203±11 mg/g compared with

57±5 mg/g at pH 8. The larger sorption capacity of CaP1-NA is associated with its Ca content and high availability for reaction, mainly at the ion-exchange sites, while the lower sorption capacity of NaP1-NA is related to unreacted Ca in the form of CaO. It should be mentioned that the initial S_{BET} increased during zeolite modification from 6.3 to 13.6 m^2/g. Thus, the higher Ca content and larger surface area enhance the phosphate sorption, as previously reported (Ji et al., 2014). The surface charge properties of the active sites (Fe and Al sites) of both zeolites were 8% Al and 2.5% Fe (Table 5.2). The larger amount of Al in NaP1-NA plays an important role in phosphate removal at neutral pH, and the magnitude of the Columbic attractive force decreases as the active sites become neutral.

The sorption isotherm data were fitted using Langmuir (Eq. 7) and Freundlich isotherm models (Eq. 8):

$$\frac{C_e}{q_e} = \frac{1}{K_l q_m} + \frac{C_e}{q_m} \quad (7)$$

$$\log q_e = \log K_f + \frac{1}{n} \log C_e \quad (8)$$

where C_e (mg/L) and q_e (mg/g) are the equilibrium total P(V) concentrations in the aqueous and solid phases, respectively; q_m (mg/g) is the maximum sorption capacity; K_L (L/mg) is the Langmuir sorption equilibrium constant; n is a constant indicating the Freundlich isotherm curvature; and K_f ((mg/g)/(mg/L)^n) is the Freundlich equilibrium constant. The sorption parameters and regression coefficients (R^2) obtained from the linear regression of Eqs. 7 and 8 are listed in Table 5.3.

The experimental and predicted sorption isotherm data by the Langmuir model at different pH values for the CaP1-NA and NaP1-NA zeolites are shown in Figure 5.5.

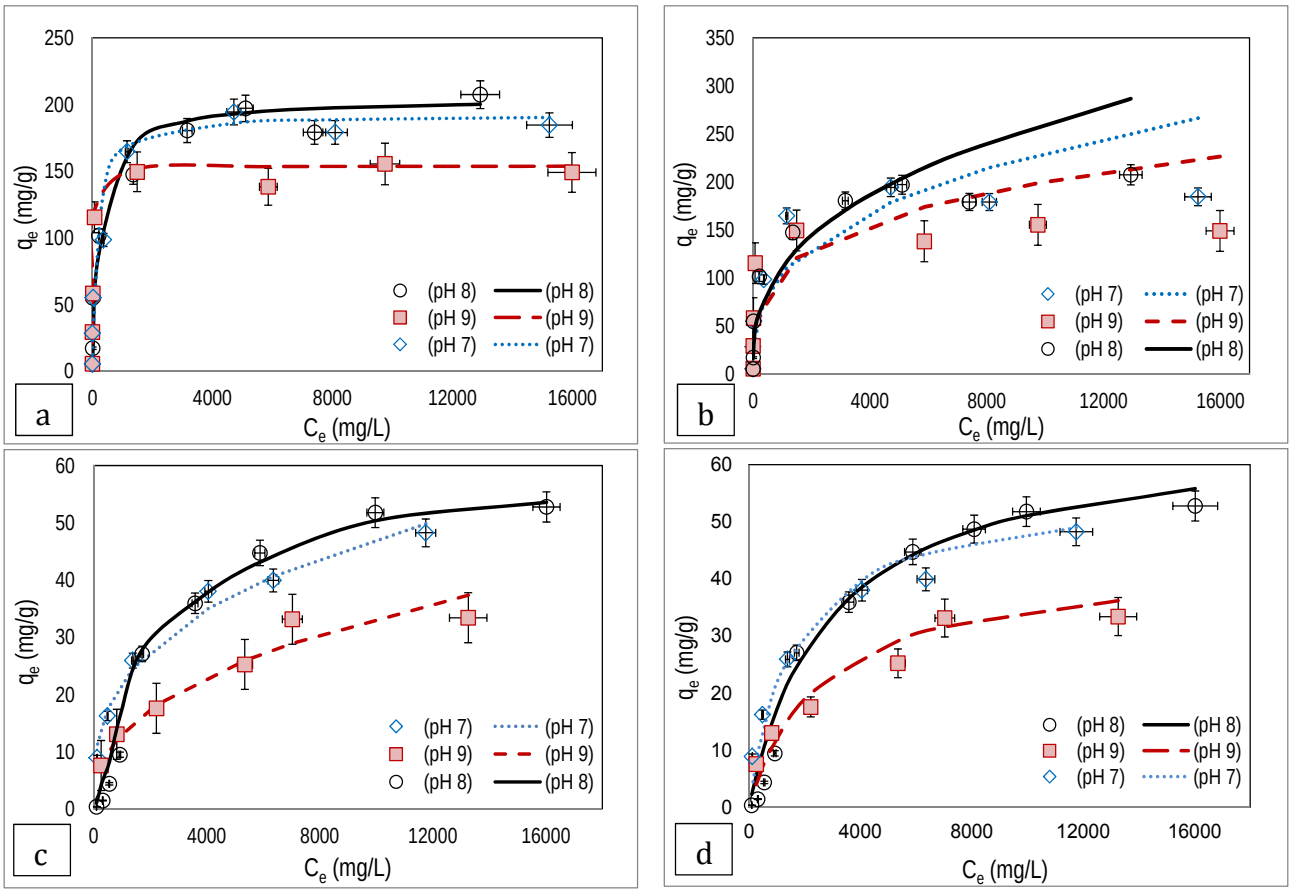

Figure 5.5. Phosphate-sorption isotherms at different pHs and uptakes predicted by the Langmuir (left) and Freundlich (right) isotherms for (a,b) CaP1-NA and (c,d) NaP1-NA modified zeolitic material (dots: experimental data; line: predicted values).

The P(V)-removal data for CaP1-NA were well described by the Langmuir isotherm, while for NaP1-NA, the Freundlich isotherm was more suitable. This behaviour was explained by Pengthamkeerati et al. (2008), who reported that the phosphate-adsorption processes of zeolite derived from FA using different treatment methods can be described using different isotherm models. The Langmuir isotherm is more suitable for the adsorption pattern of phosphate on the alkaline-treated and Ca-rich zeolite CaP1-NA.

In contrast, the Freundlich isotherm better describes physical adsorption, and

as a result, this model is suitable for the phosphate-adsorption pattern of NaP1-NA.

Table 5.3. Langmuir and Freundlich isotherm parameters for CaP1-NA and NaP1-NA at different pH values.

Adsorbent Models		CaP1-NA			NaP1-NA		
		pH 7	pH 8	pH 9	pH 7	pH 8	pH 9
Langmuir equation	q_m K_L R^2	192 0,004 0,96	203.6 0.004 0.99	153 0.006 0.96	55.9 0.0006 0.82	57.3 0.00035 0.90	43.3 0.0004 0.91
Freundlich equation	K_f n R^2	1.45 1.36 0.94	8.8 2.7 0.88	17.6 2.9 0.93	2.23 3.01 0.88	4.21 3.80 0.98	0.81 2.48 0.98

The XRD patterns of phosphate-loaded CaP1-NA samples with initial P(V) concentrations ranging from 8 to 15 g/L at pH values of 7, 8, and 9 are shown in Figure 5.6. These patterns revealed the formation of Ca phosphate in the form of brushite ($CaPO_3(OH).2H_2O(s)$) as the major phase at pH 7 and 8 and as a minor phase at pH 9. Similar P(V)-removal and brushite-formation results were reported by Pengthamkeerati et al. (2008) with Ca-zeolites and by other researchers (Lu et al., 2009; Xu et al., 2010) with FA.

The formation of brushite instead of Hap is associated with the prevalence of kinetic control. In fact, the reactive crystallisation of brushite has been described to occur (Ferreira et al., 2003; Oliveira et al., 2007) through five successive stages:

(i) spontaneous Hap precipitation, (ii) complete dissolution of Ca and Hap growth, (iii) initial appearance of brushite nuclei, (iv) coexistence of Hap and

brushite, and (v) transformation of Hap into brushite and subsequent brushite growth.

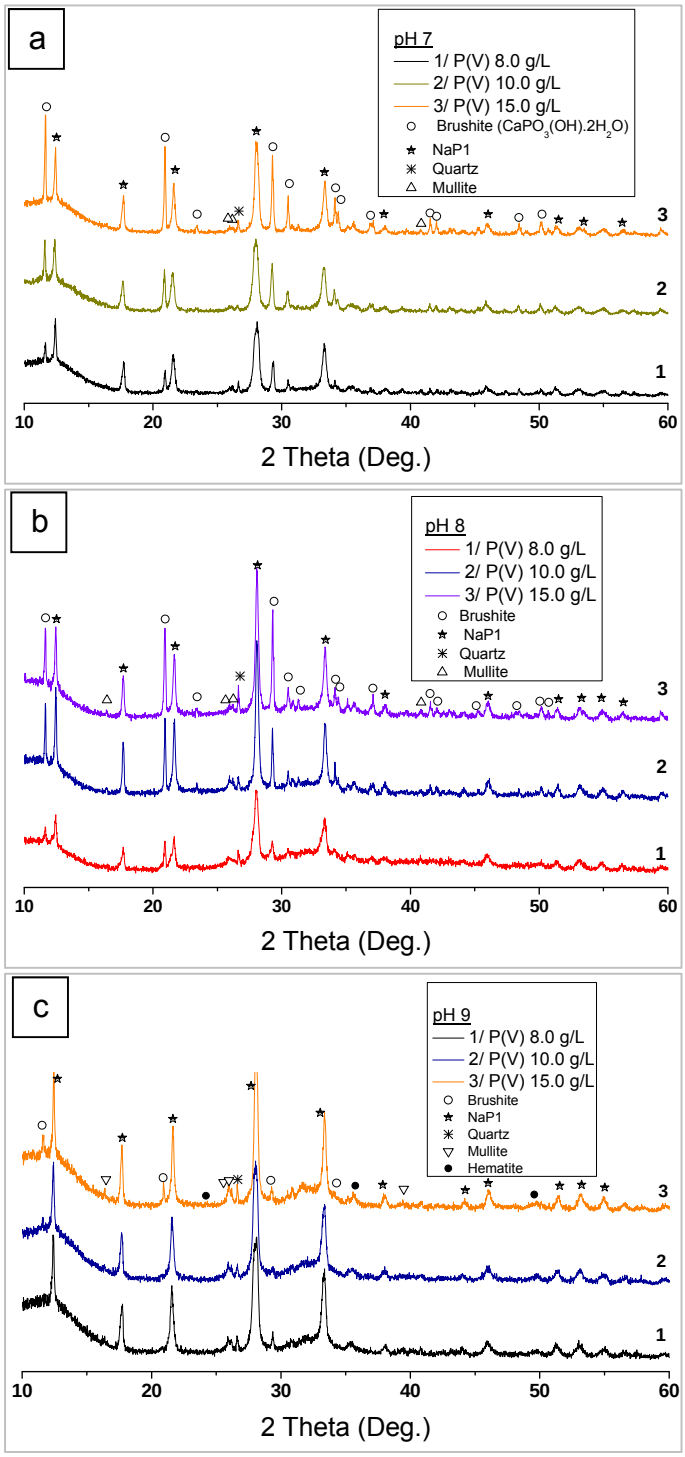

Figure 5.6. XRD patterns after phosphate sorption by modified CaP1-NA zeolitic material and brushite formation at different pH values.

The transformation of Hap into brushite would not be expected because Hap is the most thermodynamically stable species. Nevertheless, under the experimental conditions, Hap appears to be in a low-crystallinity state and in metastable equilibrium with brushite, whose faster crystal growth drives the transformation.

Both zeolites exhibit maximum sorption capacities at pH 8, which slightly decrease as the pH increases to 9 or decreases to 7. This pH-dependent sorption behaviour is in agreement with the brushite formation observed in most of the samples analysed by XRD (Figure 5.6). The logarithmic solubility dependence of brushite and the P(V)-loading capacity as a function of pH are plotted in Figure 5.7. The minimum solubility corresponding the highest brushite stability occurs at pH 8 (maximum loading capacity) and decreases slightly as the pH is decreased to pH 7 or increased to 9.

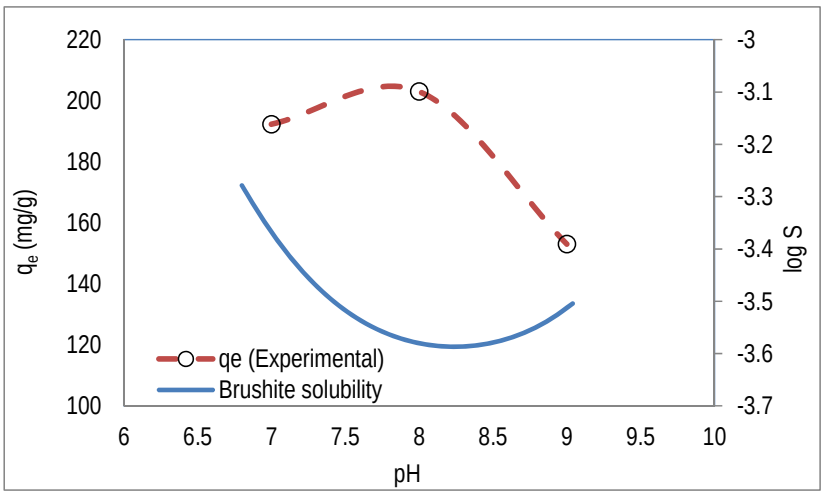

Figure 5.7. The experimental P(V)-sorption capacities at different pH values and the estimated curves of brushite solubility for the CaP1-NA isotherm.

Similar behaviour was observed for NaP1-NA: the maximum sorption capacities were observed at pH 8 and 7 and were slightly reduced when the pH increased to 9, which could be in agreement with the potential

involvement of the CaO(s) present on the zeolite in brushite formation and the acid-base properties of the ≅AlOH and ≅FeOH surface groups, which exhibit pH_{pcz} of approximately 6 for hydrated Al oxides (Simsek et al., 2013) and 7 for hydrated Fe oxides. As a result, at basic pH values exceeding the pH_{pcz}, the formation of labile complexes will be negligible. Additionally, in alkaline conditions, the formation of inner-sphere complexes is not favoured, and thus, the removal ratio decreases.

The phosphate-sorption capacities of zeolites and FA as reactive materials for phosphate removal are compared in Table 5.4, which shows that the phosphate-sorption capacities of CaP1-NA exceed previously reported values.

Table 5.4. Comparison of the phosphate-sorption capacities of various zeolite- and FA-based materials.

Material	q_m (mg/g)	pH	Reference
Zeolite NaP1-NA	57.33	8	This study
Calcium modified Zeolite NaP1-NA (CaP1-NA)	203.6	8	This study
Zeolite/Lanthanum hydroxide (La-ZFA)	71.94	>9.24	(Jie Xie et al., 2014)
Zeolite/hydrate iron oxide (ZFA/Fe_2O_3)	18.2	6.6	(J Xie et al., 2014)
Zeolite synthesized from fly ash (alkaline fusion)	132, 157	7	(Zhang et al., 2011)
NaOH treated fly ash (TFA-NaOH)	57.14	8-12	(Pengthamkeerati et al., 2008)
Calcium modified Zeolite NaP1/hydroxyapatite	24.1	9	(Watanabe et al., 2014)
Fly ashes from three coal-burning power plants	90, 108	11, 12	(Lu et al., 2009)
Synthesis zeolite –Ca	30.46	6.78	(Wu et al., 2006)
Natural zeolite (Clinoptilolite)	13.8	n.a	(Chmielewská et al., 2013)

n.a = not available

3.3. P speciation of the phosphate in loaded CaP1-NA/NaP1-NA

The speciation results of CaP1-NA and NaP1-NA zeolitic materials are shown in Figure 5.8. The easily exchangeable speciation (KCl-P) associated with exchange reactions as defined by Eq. 3 accounts for up to 20% for NaP1-NA and less than 10% for CaP1-NA. The dissolved species obtained using NaOH solutions (NaOH-P) reveal that the P bound to the hydrated metal oxides (the inner-sphere and labile complexes described by Eqs. 3–4) makes only a small contribution for NaP1-NA (less than 5%) and no contribution for CaP1-NA. In NaOH solutions, the $\cong MOH^{2+}$ and $\cong MOH$ groups are deprotonated, and the excess OH ions disrupt the $\cong MH_2PO_4^-/HPO_4^{2-}$ complexes. The HCl-P speciation (Meis et al., 2012; Wang et al., 2012) associated with Ca phosphate mineral phases (brushite and Hap) accounts for up to 80% for NaP1-NA and more than 90% for CaP1-NA. The species produced by the residual speciation contributed less than 1% for both zeolites.

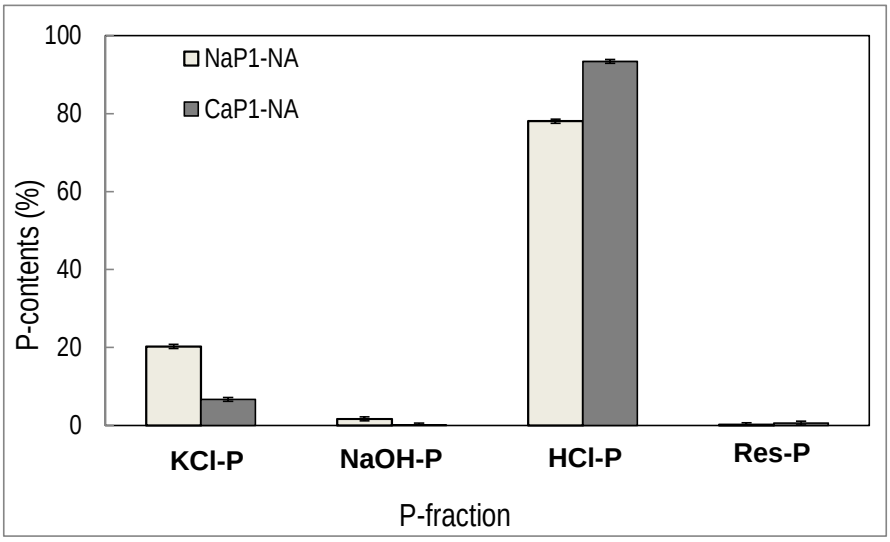

Figure 5.8. Phosphate speciation of NaP1-NA and CaP1-NA with an initial equilibrium concentration of phosphate (q_e=12±1 mg/g).

3.4. Effect of competing ions on phosphate sorption

Coexisting ions, such as chloride, sulfate, nitrate, and carbonate, that are generally present in treated wastewater do not interfere with phosphate uptake through competitive sorption, as shown in Figure 5.9. Differences between the samples containing individual species, mixtures of species, and no coexisting ions are not statistically significant. Given that the main phosphate-removal mechanism is based on the formation of insoluble Ca-P minerals and weak complexes with MOH surface groups, none of the evaluated anions could form insoluble forms with Ca anions, and their complexation with Fe and Al oxides was also less favoured than that with P(V) anions.

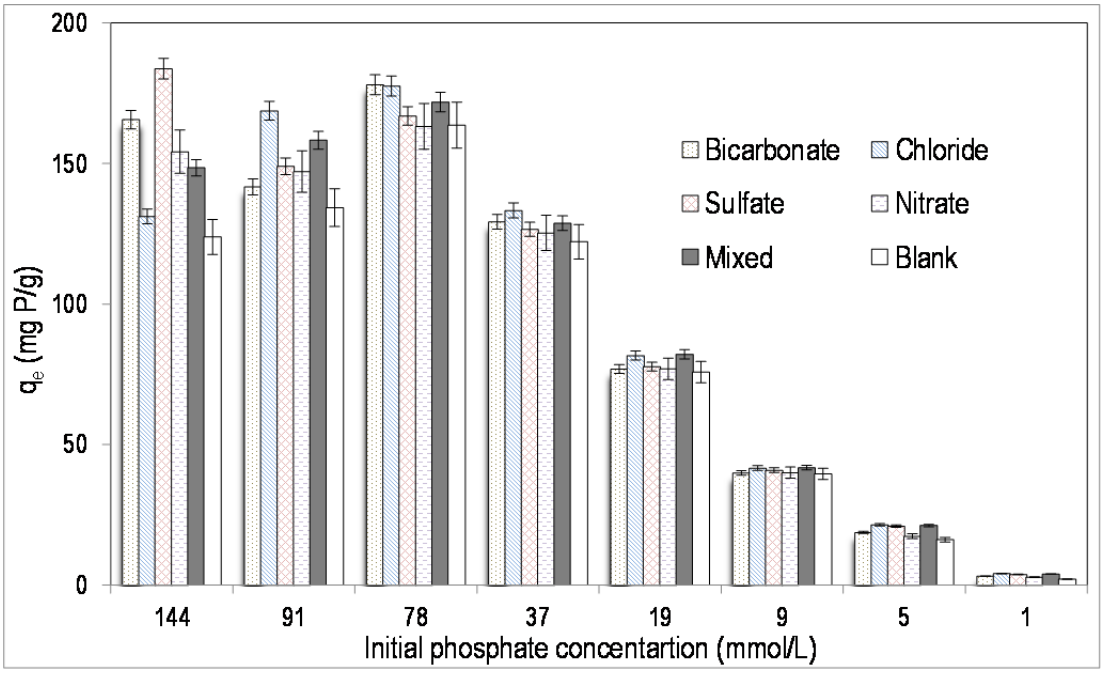

Figure 5.9. Effect of coexisting anions on phosphate recovery at different initial phosphate concentrations with individual and mixtures of anions (Cl^- =300 mg/L, SO_4^{2-}=250 mg/L, NO_3^-=50 mg/L, and HCO_3^-=300 mg/L).

According to Zhang et al. (2009), this can be attributed to the specific

sorption of phosphate on the adsorbent because the phosphate ions adsorbed on the strongly specific sites were rarely exchangeable, even in solutions containing excessive amounts of coexisting ions. This suggests that CaP1-NA has high sorption selectivity for phosphate anions and great potential for use in treated wastewater expected to contain high concentrations of theses anions.

3.5. Desorption of phosphate from loaded zeolite samples

The phosphate desorption achieved using 0.1 mol/L $NaHCO_3/Na_2CO_3$ solutions increased as the amount of phosphate on the zeolitic material decreased (Figure 5.10a-b). Partial desorption (30 to 70%) was reported for CaP1-NA, whereas values of 10 to 70% were observed for NaP1-NA in a single-extraction trial. These results are in agreement with the speciation results obtained in using excess bicarbonate ions.

Indeed, during labile speciation (P-KCl), phosphate anions will be displaced by bicarbonate ions, and partial brushite dissolution will be achieved, as indicated in Figure 5.7, which shows that increasing the pH increases the solubility of brushite by up to an order of magnitude. It can be concluded that P(V) sorption on CaP1-NA is relatively irreversible and that the bonding between the actives sites and the adsorbed phosphate is quite strong.

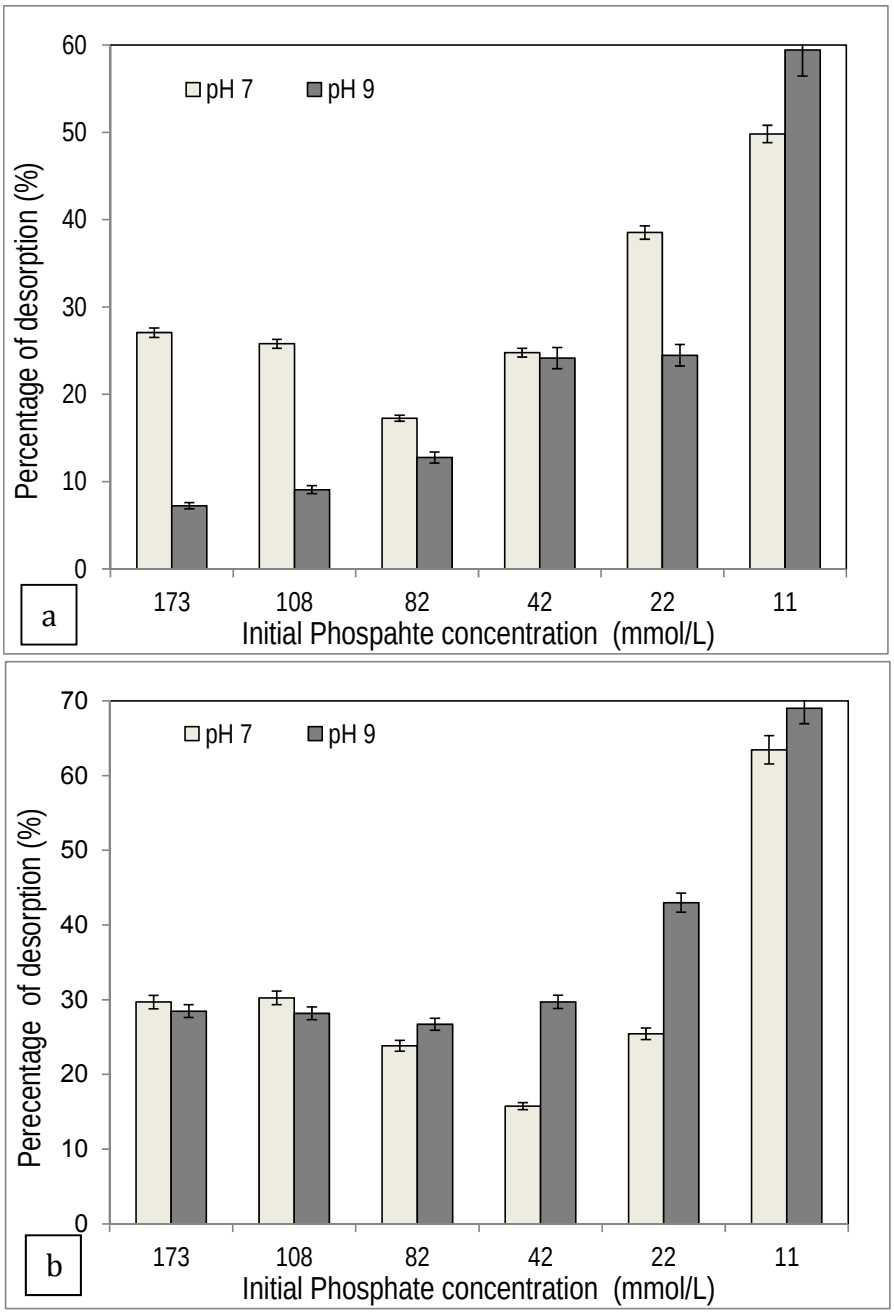

Figure 5.10. Phosphate desorption using a mixture of $NaHCO_3$ (0.1 M) and Na_2CO_3 (0.1 M) from loaded (a) CaP1-NA and (b) NaP1-NA.

4. Conclusions

NaP1-NA zeolitic material synthesised from Narcea FA and its Ca-modified form (CaP1-NA) are capable of high phosphate sorption in neutral to slightly basic conditions. The maximum phosphate-sorption capacities determined at pH 8 were 65±7 and 203±11 mgP-PO4/g zeolite for NaP1-NA and CaP1-NA,

respectively. The sorption capacity in the expected pH range of wastewater effluents (e.g., from 7 to 9) was slightly dependent on the pH and was maximised at pH 8 for CaP1-NA and pH 9 for NaP1-NA.

Phosphate removal by NaP1-NA occurred via a surface complexation mechanism involving the AlOH and FeOH surface groups of the unreacted Fe and Al oxides originally present on the FA or the potential formation of Ca phosphate phases using the original CaO present on the FA. In contrast, for CaP1-NA, the main removal mechanism included the formation of a Ca phosphate, brushite, as confirmed by XRD analyses. Thus, the higher solubility of brushite compared with that of Hap makes this zeolitic material promising as a novel slow-release inorganic zeolite/CaP1-NA/brushite fertiliser.

5. References

Ann, Y., Reddy, K.R., Delfino, J.J., 2000. Influence of chemical amendments on phosphorus immobilization in soils from a constructed wetland. Ecological Engineering. 14, 157–167.

Ansari, M., Aroujalian, A., Raisi, A., Dabir, B., Fathizadeh, M., 2014. Preparation and characterization of nano-NaX zeolite by microwave assisted hydrothermal method. Adv. Powder Technol. 25, 722–727.

Blissett, R.S., Rowson, N. A., 2012. A review of the multi-component utilisation of coal fly ash. Fuel. 97, 1–23.

Boyer, T.H., Persaud, A., Banerjee, P., Palomino, P., 2011. Comparison of low-cost and engineered materials for phosphorus removal from organic-rich surface water. Water Res. 45, 4803–4814.

Poole, C., Prijatama, H., and Rice, N.M., 2000. Synthesis of zeolite adsorbents by hydrothermal treatement of PFA wastes: A comparative study. Miner. Eng. 13, 831–842.

Cama, J., Ayora, C., Querol, X., Ganor, J., 2005. Dissolution kinetics of synthetic zeolite NaP1 and its implication to zeolite treatment of contaminated waters. Environ. Sci. Technol. 39, 4871–7.

Chen, J., Kong, H., Wu, D., Hu, Z., Wang, Z., Wang, Y., 2006. Removal of phosphate from aqueous solution by zeolite synthesized from fly ash. J. Colloid Interface Sci. 300, 491–497.

Chmielewská, E., Hodossyová, R., Bujdoš, M., 2013. Kinetic and thermodynamic studies for phosphate removal using natural adsorption materials. Polish J. Environ. Stud. 22, 1307–1316.

Desmidt, E., Ghyselbrecht, K., Zhang, Y., Pinoy, L., Van der Bruggen, B., Verstraete, W., Meesschaert, B., 2013. Global phosphorus scarcity and full-scale P-recovery techniques-a review. Crit. Rev. Environ. Sci. Technol. 336–384.

Dorozhkin, S. V., 2012. Self-Setting Calcium Orthophosphate Formulations: Cements, Concretes, Pastes and Putties. Int. J. Mater. Chem. 1, 1–48.

Ferreira, A., Oliveira, C., Rocha, F., 2003. The different phases in the precipitation of dicalcium phosphate dihydrate. J. Cryst. Growth 252, 599–611.

Golden, D.C., Ming, D.W., 1999. Division s-9-soil mineralogy. 664, 657–664.

Guaya, D., Valderrama, C., Farran, A., Armijos, C., Cortina, J.L., 2015. Simultaneous phosphate and ammonium removal from aqueous solution by a hydrated aluminum oxide modified natural zeolite. Chem. Eng. J. 271, 204–213.

Hedley, M.J., Stewart, J.W. B., Chauhan, B. S.,1982. Changes in Inorganic and Organic Soil Phosphorus Fractions Induced by Cultivation Practices and by Laboratory Incubations. Soil.Sci.AM.J 46, 970–976.

Hollman, G.G., Steenbruggen, G., Janssen-Jurkovičová, M., 1999. A two-step process for the synthesis of zeolites from coal fly ash. Fuel. 78, 1225–1230.

Jacobs, P.A., Flanigen, E.M., Jansen, J.C., van Bekkum, H., 2001. Introduction to Zeolite Science and Practice, 2nd ed, Studies in Surface Science and Catalysis. Elsevier Science.

Ji, X., Zhang, M., Wang, Y., Song, Y., Ke, Y., Wang, Y., 2014. Immobilization of ammonium and phosphate in aqueous solution by zeolites synthesized from fly ashes with different compositions. J. Ind. Eng. Chem. 22, 1–7.

Kitson, R.E; Mellon, M.G., 1944. Colorimetric determination of phosphorus as molybdovanadophosphoric acid. Ind. Eng. Chem.16, 379.

Liu, R., Lal, R., 2014. Synthetic apatite nanoparticles as a phosphorus fertilizer for soybean (Glycine max). Sci. Rep. 4, 1–6.

Liu, X., Ding, C., 2002. Morphology of apatite formed on surface of

wollastonite coating soaked in simulate body fluid. Mater. Lett. 57, 652–655.

Liu, Y., Naidu, R., Ming, H., 2013. Surface electrochemical properties of red mud (bauxite residue): zeta potential and surface charge density. J Colloid Interface Sci. 394, 451–457.

Lu, S.G., Bai, S.Q., Zhu, L., Shan, H.D., 2009. Removal mechanism of phosphate from aqueous solution by fly ash. J. Hazard. Mater. 161, 95–101.

Martinez, R.E., Pokrovsky, O.S., Schott, J., Oelkers, E.H., 2008. Surface charge and zeta-potential of metabolically active and dead cyanobacteria. J. Colloid Interface Sci. 323, 317–325.

Masters, A.F., Maschmeyer, T., 2011. Zeolites - From curiosity to cornerstone. Microporous Mesoporous Mater. 142, 423–438.

Meis, S., Spears, B.M., Maberly, S.C., O'Malley, M.B., Perkins, R.G., 2012. Sediment amendment with Phoslock® in Clatto Reservoir (Dundee, UK): Investigating changes in sediment elemental composition and phosphorus fractionation. J. Environ. Manage. 93, 185–193.

Moharami, S., Jalali, M., 2014. Phosphorus leaching from a sandy soil in the presence of modified and un-modified adsorbents. Environ. Monit. Assess. 186, 6565–6576.

Moreno, N., Querol, X., Ayora, C., Alastuey, A., Fernández-Pereira, C., Janssen-Jurkovicová, M., 2001. Potential Environmental Applications of Pure Zeolitic Material Synthesized from Fly Ash. J. Environ. Eng. 127, 994–1002.

Moreno, N., Querol, X., Ayora, C., Pereira, C.F., Janssen-Jurkovicová, M., 2001. Utilization of zeolites synthesized from coal fly ash for the purification of acid mine waters. Environ. Sci. Technol. 35, 3526–34.

Murayama, N., Yamamoto, H., Shibata, J., 2002. Zeolite synthesis from coal fly ash by hydrothermal reaction using various alkali sources. J. Chem. Technol. Biotechnol. 77, 280–286.

Oliveira, C., Georgieva, P., Rocha, F., Ferreira, A., Feyo de Azevedo, S., 2007. Dynamical model of brushite precipitation. J. Cryst. Growth 305, 201–210.

Onyango, M.S., Kuchar, D., Kubota, M., Matsuda, H., 2007. Adsorptive removal of phosphate ions from aqueous solution using synthetic zeolite. Ind. Eng. Chem. Res. 46, 894–900.

Parvinzadeh Gashti, M., Stir, M., Bourquin, M., Hulliger, J., 2013. Mineralization of Calcium Phosphate Crystals in Starch Template Inducing a Brushite Kidney Stone Biomimetic Composite. Cryst. Growth Des. 13, 2166–2173.

Pengthamkeerati, P., Satapanajaru, T., Chularuengoaksorn, P., 2008. Chemical modification of coal fly ash for the removal of phosphate from aqueous solution. Fuel. 87, 2469–2476.

Puigdomènech, I., 2001. Chemical Equilibrium Software Hydra and Medusa. Inorg. Chem. Dep.

Querol, X., Moreno, N., Alastuey, A., Juan, R., Ayora, C., Medinaceli, A., Valero, A., Productos, C., 2007. Synthesis of high ion exchange zeolites from coal fly ash. Geol. Acta. 5, 49–57.

Querol, X., Moreno, N., Uman, J.C., Alastuey, A., Hernandez, E., Lopez-Soler, A., Plana, F., 2002. Synthesis of zeolites from coal fly ash : an overview. 50, 413–423.

Querol, X., Umana, J.., Plana, F., Alastuey, A., Lopez-soler, A., Medinaceli, A., Valero, A., Domingo, M.J., Garcia-rojo, E., 2001. Synthesis of zeolites from fly ash at pilot plant scale. Fuel. 80, 857–865.

Reed, B.E., Vaughan, R., Jiang, L., 2000. As (III), As (V), Hg and removal by Fe-Oxide impregnated activated carbon. J. Environ .Eng. 126, 869–873.

Simsek, E.B., Özdemir, E., Beker, U., 2013. Zeolite supported mono- and bimetallic oxides: Promising adsorbents for removal of As(V) in aqueous solutions. Chem. Eng. J. 220, 402–411.

Singer, P. A., Salamanca-Buentello, F., Daar, A.S., 2005. Harnessing nanotechnology to improve global equity. Issues Sci. Technol. 21, 57–64.

Skartsila, K., Spanos, N., 2007. Surface characterization of hydroxyapatite: Potentiometric titrations coupled with solubility measurements. J. Colloid Interface Sci. 308, 405–412.

Wang, C., Qi, Y., Pei, Y., 2012. Laboratory investigation of phosphorus immobilization in lake sediments using water treatment residuals. Chem. Eng. J. 209, 379–385.

Watanabe, Y., Ikoma, T., Yamada, H., Stevens, G.W., Moriyoshi, Y., Tanaka, J., Komatsu, Y., 2010. Formation of hydroxyapatite nanocrystals on the surface of Ca-Al-layered double hydroxide. J. Am. Ceram. Soc. 93, 1195–1200.

Watanabe, Y., Yamada, H., Ikoma, T., Tanaka, J., Stevens, G.W., Komatsu, Y., 2014. Preparation of a zeolite NaP1/hydroxyapatite nanocomposite and study of its behavior as inorganic fertilizer. J. Chem. Technol. Biotechnol. 89, 963–968.

Wu, D., Zhang, B., Li, C., Zhang, Z., Kong, H., 2006. Simultaneous removal of ammonium and phosphate by zeolite synthesized from fly ash as

influenced by salt treatment. J. Colloid Interface Sci. 304, 300–306.

Xie, J., Wang, Z., Fang, D., Li, C., Wu, D., 2014. Green synthesis of a novel hybrid sorbent of zeolite/lanthanum hydroxide and its application in the removal and recovery of phosphate from water. J. Colloid Interface Sci. 423, 13–19.

Xie, J., Wang, Z., Wu, D., Kong, H., 2014. Synthesis and properties of zeolite/hydrated iron oxide composite from coal fly ash as efficient adsorbent to simultaneously retain cationic and anionic pollutants from water. Fuel. 116, 71–76.

Xie, J., Wang, Z., Wu, D., Zhang, Z., Kong, H., 2013. Synthesis of Zeolite/Aluminum Oxide Hydrate from Coal Fly Ash: A New Type of Adsorbent for Simultaneous Removal of Cationic and Anionic Pollutants. Ind. Eng. Chem. Res. 52, 14890–14897.

Xu, K., Deng, T., Liu, J., Peng, W., 2010. Study on the phosphate removal from aqueous solution using modified fly ash. Fuel. 89, 3668–3674.

Yang, M., Lin, J., Zhan, Y., Zhang, H., 2014. Adsorption of phosphate from water on lake sediments amended with zirconium-modified zeolites in batch mode. Ecol. Eng. 71, 223–233.

Yao, Z.T., Ji, X.S., Sarker, P.K., Tang, J.H., Ge, L.Q., Xia, M.S., Xi, Y.Q., 2015. A comprehensive review on the applications of coal fly ash. Earth-Science Rev. 141, 105–121.

Zebardast, H.R., Pawlik, M., Rogak, S., Asselin, E., 2014. Potentiometric titration of hematite and magnetite at elevated temperatures using a ZrO2-based pH probe. Colloids Surfaces A Physicochem. Eng. Asp. 444, 144–152.

Zhang, B.-H., Wu, D.-Y., Wang, C., He, S.-B., Zhang, Z.-J., Kong, H.-N., 2007. Simultaneous removal of ammonium and phosphate by zeolite synthesized from coal fly ash as influenced by acid treatment. J. Environ. Sci. (China) 19, 540–545.

Zhang, G., Liu, H., Liu, R., Qu, J., 2009. Removal of phosphate from water by a Fe-Mn binary oxide adsorbent. J. Colloid Interface Sci. 335, 168–74.

Zhang, M., Zhang, H., Xu, D., Han, L., Zhang, J., Zhang, L., Wu, W., Tian, B., 2011. Removal of Phosphate from Aqueous Solution Using Zeolite Synthesized from Fly Ash by Alkaline Fusion Followed by Hydrothermal Treatment. Sep. Sci. Technol. 46, 2260–2274.

Zhou, J.Z., Feng, L., Zhao, J., Liu, J., Liu, Q., Zhang, J., Qian, G., 2012. Efficient and controllable phosphate removal on hydrocalumite by multi-step treatment based on pH-dependent precipitation. Chem. Eng. J. 185-186, 219–225.

Zhou, L., Chen, Y.L., Zhang, X.H., Tian, F.M., Zu, Z.N., 2014. Zeolites developed from mixed alkali modified coal fly ash for adsorption of volatile organic compounds. Mater. Lett. 119, 140–142.

Chapter 6

Integration of Powdered Calcium Activated Zeolites in a hybrid sorption-membrane ultrafiltration process (PAZ-UF) for phosphate recovery

This chapter is based on the work presented in a publication submitted to the Journal of the Taiwan Institute of Chemical Engineers

M. Hermassi, C. Valderrama, O. Gibert, N. Moreno, O. Font, X. Querol, N.H. Batis and J.L. Cortina. Integration of powdered Ca-activated zeolites in a hybrid sorption-membrane ultrafiltration process (PAZ-UF) for phosphate recovery. 2016 (Impact factor: 3.000)

The performance of CaP1 as a Ca-activated powdered activated zeolite (PAZ) in recovering phosphate P(V) from aqueous solutions was evaluated using a hybrid sorption-membrane ultrafiltration (UF) system with a hollow fibre module. The objective of this study was to explore the influence of process parameters such as initial P(V) concentration, pH and PAZ dose on P(V) recovery from a tertiary treatment effluent. The hydrodynamic parameters of the UF operation were also evaluated as a function of the PAZ dose. The P(V) sorption capacity of PAZ decreased by increasing the PAZ dose in the system from 12±2 to 7.5±2% for a doses of 2 and 2.5 g_{PAZ}/L respectively with 25 mg P-PO_4/L solutions at pH 8. Comparing both doses performance, longer filtration cycle times and a permeability reduction were measured for the low dose (2 g_{PAZ}/L) due to the higher time required for the formation of the PAZ cake layers onto the membrane surface.

The P(V) recovery profiles as a function of the initial P(V) concentrations, at pH 8 and 2.5 g_{PAZ}/L, showed that the P(V) sorption capacity of PAZ increased by increasing the P(V) concentration, in fact, the sorbent was not saturated and recoveries were 6±2% (for 10 mg P-PO_4/L), 11±2% (for 25 mg P-PO_4/L), and 20±3% (for 100 mg P-PO_4/L). The increase of the pH of the feed solution from 8 to 9 for the initial P(V) concentration 10 mg P-PO_4/L increased the P(V) recovery percentage up to 70±4% due to combined kinetic mechanisms. Analysing loaded samples according to a fractionation protocol and XRD analysis confirmed that the phosphate-sorption process involves the formation of Ca phosphates (mainly brushite and Hap).

1. Introduction

The recovery and reuse of phosphates from industrial and domestic wastes has been identified as important topic to slow the continuous reduction of global phosphate rock reserves. Because economically exploitable phosphate rock is limited to only a few countries, food security in countries with limited or no domestic phosphate rock reserves is potentially vulnerable. This situation has forced the European Union to include phosphate rock as a critical element (Schröder et al., 2010; European Commission, 2014), creating a series of programmes and initiatives to reduce consumption and use alternative resources.

Phosphorus P is typically found in domestic and industrial streams in anionic forms at typically low levels (10-150 mgP/L) compared with the total carbon content (Ashekuzzaman and Jiang, 2014).

Physicochemical treatment and biological nutrient removal are the two most commonly used techniques for removal P(V) from municipal and industrial wastewater. The coagulation–sedimentation method, which removes P(V) as slightly soluble phosphorous salts by adding a coagulant (such as $FeCl_2$, $FeSO_4$ or Al_2 $(SO_4)_3$), is a common physicochemical treatment method, and its usage depends on the economy and efficiency of the process. However, the cost and sludge treatment make this method an unattractive option for wastewater recovery pathway (de-Bashan and Bashan, 2004; Zelmanov and Semiat, 2014). In recent years, a new approach has been evaluated that relies on the use of inorganic species-based adsorbents (e.g., minerals, clays, FA, and zeolites) suitable for direct use as a fertiliser or soil conditioner. Indeed, such P-loaded adsorbents, which can contain 5 to 10% P(w/w), may be suitable as secondary P sources for the production of high-

purity fertilisers by fertiliser companies (Bartzokas, 2001; Schoumans et al., 2015; Lalley et al., 2016). The most relevant sorbent properties for phosphate recovery from solution are as follows: a) high phosphate-sorption capacity and selectivity, b) fast kinetics from solution, c) low sorption capacity for dissolved organic matter, and d) high stability and resistance to reactor agitation, or column operation involving granular materials. Additionally, a set of properties are required for the materials to under subsequent valorisation: e) high soil and plant availability, f) slow release ratios, and g) limited release of potentially harmful components sorbed from the treated waters or originally present on the sorbent.

Recently, Na^{+}-zeolite (NaP1-NA) synthesised from coal fly ash (CFA) and its Ca-modified form (CaP1) were evaluated for the recovery of phosphate from aqueous solution. The sorption of phosphate ions (mainly $H_2PO_4^{-}$/HPO_4^{2-}) in the conditions expected for most industrial and domestic effluents (pH values of 6–9) was postulated to proceed via a combined mechanisms including surface complexation with the ≅MOH groups from the zeolitic structure and precipitation of Ca-phosphate with Ca(II) ions present on the zeolite. At low P(V) concentrations (< 50 mg P-PO_4/L) the dominant mechanism involves surface complexation reactions, whereas at relatively high P(V) concentrations (> 100 mg P-PO_4/L), the formation of Ca-phosphate, mainly brushite ($CaHPO_4$(s)), is favoured.

Application of pressure-driven membrane processes as microfiltration (MF) and ultrafiltration (UF) has expanded in recent years as an alternative technology for developing hybrid systems of sorption/filtration (Dong et al., 2014; Wang et al., 2016). UF has proved to be an effective physical barrier to

particles and colloids larger than the UF membrane pores, which are retained by size-exclusion mechanisms. Furthermore, UF provides extra advantages over conventional treatments such as small footprint, low energy consumption, limited chemical dosing, capability of coping with wide fluctuations in feed quality and delivering permeate of relatively constant quality, and reduced scale-up risks (Lee et al., 2008). Water recovery for MF/UF systems is typically 85 to 97% and is a function of the backwash (BW) strength and the method of BW disposal (Ferrer et al. 2015).

Scarce studies have been reported on the integration of sorption on powder sorbents (e.g. powder zeolites) and membrane filtration (e.g. MF, or UF). Yildiz (2004) investigated the effects of pH and Ca(II) concentration on the removal of phosphate by FA in a crossflow MF and demonstrated that membrane MF was more efficient than classical batch separation. More recently, an adsorption-UF process for phosphate recovery using a hydrated ferric oxide (HFO)-based agglomerated sorbent was studied by Zelmanov and Semiat, (2014). A residual P(V) concentration lower than 0.1 mgP/L was reported in a dead-end configuration. Hybrid membrane (UF)-sorption systems can be operated in several configurations, (e.g. dead-end flow or cross-flow modes..) (Hui et al., 2014; Vincent Vela et al., 2009), however, it is necessary to assess the performance of the system by determining the capacity to recover P(V) and the maxim amount of P(V) recovered under the more realistic conditions or those commonly used in WWTP, for instance by pumping continuously the feeding solution to stirring reactor. In view of this knowledge gap it is necessary to evaluate the feasibility in terms of operation parameters of these hybrid systems. The goal of this study was to investigate P(V) adsorption using powdered Ca-activated zeolite (CaP1) and a

membrane separation step using a hollow fibre UF crossflow configuration. The influence of process parameters, such as the initial P(V) concentration, pH and PAZ dose on P(V) recovery from a tertiary treatment effluent were evaluated. Furthermore, the specific cake resistances were calculated and its effects on the permeate flux was also discussed.

2. Materials and methods

2.1. Materials

Powdered Ca-activated PAZ (CaP1-NA)

Na^+-zeolite (NaP1-NA) synthesised from Narcea CFA with 3-mol/L NaOH solution at 125°C for 8 h was used as a precursor in a hydrothermal method, as described elsewhere (Querol et al., 2007). Ca (CaP1-NA) PAZ was prepared by a cation-exchange process. First, 250 g of NaP1-NA was immersed in 1000 mL of a 0.5-mol/L $CaCl_2$ solution for 1 h at room temperature, and the mixture was then filtered with a 0.2-μm membrane filter and rinsed with distilled water to remove the $CaCl_2$ solution. The cation-exchange and washing cycle was repeated five times. Samples obtained were dried for 72 h at 50–60°C as described elsewhere (chapter 5).

P(V)-containing model feed solution composition

Aqueous P(V) solutions were prepared by dissolving known amounts of Na_2HPO_4 in water containing common competing ions present in tertiary wastewater treatment effluents. The background ion concentrations were fixed by using the average annual composition of the tertiary stream from a wastewater treatment (WWT) facility (El Prat, Barcelona, Spain) as a

reference. The anion solution composition was as follows: chloride (320 mg/L), bicarbonate (280 mg/L), sulfate (240 mg/L) and nitrate (30 mg/L) (prepared from the corresponding Na salts). The cation solution composition was as follows: Na (300 mg/L), Ca (80 mg/L), Mg (20 mg/L) and K (34 mg/L) (prepared from the corresponding chloride salts). As tap water was used to prepare the test solutions a 5±2 mg TOC/L was measured.

2.2. Experimental methodology

Membrane UF-powder activated zeolite (UF-PAZ) hybrid system

The UF-PAZ consisted of a clear acrylic cylinder reactor with a volume of 60 L combined with a crossflow UF module consisting of 100 hollow fibres with a molecular weight cut-off of>100000 Da. The membrane fibres consisted of a hydrophilic polyethersulfone blend of polyvinylpyrrolidone and polyethersulfone and had an inner diameter of 0.8 mm and a length of 1.0 m, corresponding to a surface area of 0.251 m^2. The module was mounted in a frame also equipped with a positive displacement peristaltic pump (Masterflex® 77411-00 model, I/P® 26), pressure stabiliser, pressure sensor, valves, tubing, and the mixing reactor. The experimental set-up is illustrated in Figure 6.1.

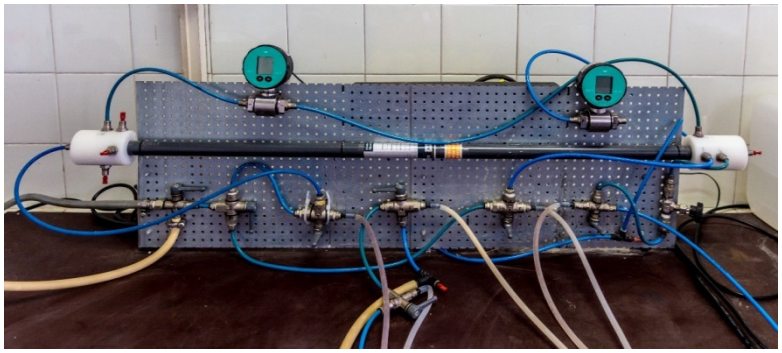

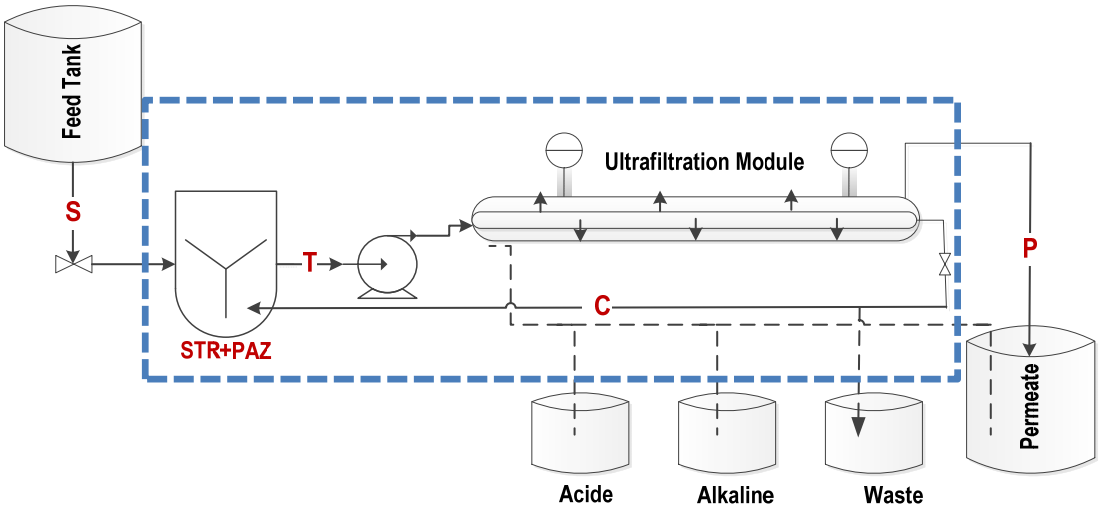

Figure 6.1. Schematic of the hybrid membrane UF-sorption system including an ultrafiltration hollow fibre module, the feed P(V) stream (S); stirred tank reactor (STR); the stream leaving the tank (T); the concentrate (C) and the permeate (P) streams from the membrane module with a flow-rate of Q(m^3/s).The dashed line represents the control surface used for P(V) mass balance .

P(V)-removal experiments were conducted as follows: 40 L of influent phosphate solutions (10, 25, and 100 mgP-PO_4/L) and specified amounts of PAZ (80 and 100 g) were added to the (STR). The reactor was agitated by a mechanical stirrer (IKA RW 20), and the stirring speed was fixed. The mixture was agitated in the tank for 30 min at 400 rpm for P(V) sorption process to take place and was then fed to the UF system. The water was pumped through the membrane fibres at a constant flow rate of 1.2 L/min. A phosphate containing solution was pumped continuously from the feed tank to the reactor to compensate the volume of solution leaving the system through the permeate stream. Pressure transducer sensors were located at the inlet and outlet of the membrane module. The resulting PAZ slurry was

fed to the STR. A filtration cycle interval of 0.3±0.05 to 0.85±0.05 bar of transmembrane pressure (TMP) was used and the membrane backwashed was performed by using permeated water, when the TMP reached 0.85±0.05 bar and thus restore the initial permeability of the membrane. The backwashing procedure also involved a crossflow flush of the membrane surface in both directions to scour the PAZ layer from inside the hollow fibres and an outside-in flow to remove PAZ and other particles accumulated on the inside surface of the membrane. The experiments were performed under constant pH monitored by an in-line pH potentiometer (Crison pH 28). When the pH was 0.1 units above or below the set point, strong acid (1-mol/L HCl) or strong base (1-mol/L NaOH) was added using a peristaltic pump (Master Flex console drive). Chemical cleaning was carried out using an oxidant solution (0.01-mol/L NaClO), an acidic solution (0.01-mol/L HCl), and a basic solution (0.01-mol/L NaOH) to prevent biological growth and mineral scaling on the surface of the membrane at the end of each experiment.

2.3. Speciation of P(V) sorbed onto PAZ

The speciation of phosphate on the loaded PAZ was performed according to a modified four-step sequential extraction methodology (Moharami and Jalali, 2014). The sorbed phosphate was sequentially extracted using 1-g samples and 50 mL of the extraction solutions summarised in Table 6.1. The samples were mechanically shaken at 21±1°C. After equilibrium was achieved (24 h), the samples were centrifuged, and the phosphate content of the liquid phase was analysed. At the end of each sorption-filtration and subsequent extraction tests the suspensions were centrifuged and the PAZ samples were dried at 50-60°C.

Table 6.1. Chemical extraction scheme for phosphate speciation of loaded PAZ samples.

Extraction solutions	Speciation name	Phosphate Speciation	Step
40-mL 2 M KCl for 2h	KCl-P	Soluble and exchangeable	1
40-mL 0.1 M NaOH for 17h	NaOH-P	Fe- and Al-bound	2
40-mL 0.5 M HCl for 24h	HCl-P	Ca-bound	3

2.4. Analytical methods

The P(V) concentration was determined using the vanadomolybdophosphoric acid colourimetric method (4500-P C) in a Shimadzu UVmini-1240 UV-vis spectrophotometer. Ions were determined using a Thermo Scientific Ionic Chromatograph (Dionex ICS-1100 and ICS-1000). After completing the sorption-filtration experiments, loaded PAZ samples were examined by FSEM-EDX, and mineral phases were identified by XRD and characterised by FTIR.

The suspended solid concentration (C_{SS}) (kg/m^3) in the feed tank solution was determined as described elsewhere (Spellman, 2009).

2.5. Evaluation of the sorption-filtration system performance: P(V) mass balance analysis

The sorbed amount of P(V) was calculated from the mass balance on the hybrid system schematically described in Figure 6.1. At time zero, the STR is filled with a 40 L of a P(V) solution with the same concentration as the feed stream (C_0). The P(V) mass balance in the system is properly described.

The mass of P(V) sorbed onto the PAZ—$m(PO_4)_{PAZ}$ ($mgP\text{-}PO_4\text{-}PAZ/L$)—can be calculated using Eq. 1:

$$m(PO_4)_{PAZ} = m(PO_4)_0 + m(PO_4)_S - m(PO_4)_P - m(PO_4)_T \quad (1)$$

m $(PO_4)_0$(mg) is the initial mass of P(V) introduced to the STR of 40 L at time zero calculated by Eq. 2

$$m(PO_4)_0 = V * C_0 \quad (2)$$

where: $m(PO_4)_S$ (mg) is the mass of P(V) fed to the reactor for a given filtration interval ($\Delta t = t_j - t_i$) calculated by Eq. 3

$$m(PO_4)_s = Q_S(t) * \Delta t * \frac{C_{S(i)} + C_{S(j)}}{2} \quad (3)$$

$m(PO_4)_P$ (mg) is the mass of P(V) leaving the system through the permeate stream (P) for a given filtration interval according to Eq. 4:

$$m(PO_4)_p = Q_P(t) * \Delta t * \frac{C_{p(i)} + C_{P(j)}}{2} \quad .(4)$$

$m(PO_4)_T$ (mg) is the mass of P(V) at the STR for a given filtration interval according to Eq. 5:

$$m(PO_4)_T = V_T * \frac{C_{T(i)} + C_{T(j)}}{2} \quad .(5)$$

where C_i and C_j (mgP-PO_4/L) are the P(V) concentrations in a given stream of reactor volume at times i and j respectively.

The performance of the hybrid membrane UF-sorption system was evaluated by estimating the bfollowing:

i) P(V) sorption on $PAZ_{(t)}$, Q_{PO4t} (mgP-PO4/g PAZ) according to Eq. 6:

$$Q_{PO4(t)} = \frac{mg(PO_4)}{g(PAZ)} = \frac{m(PO_4)_{PAZ}}{V_t * g_{zeolite}} \quad (6)$$

ii) P(V) removal efficiency ($R_P - PO_4$ (%)) according to Eq. 7:

$$R_P - PO_4(\%) = \left(1 - \frac{C_p(t)}{C_s(t)}\right) \times 100 \quad .(7)$$

where $C_{s(t)}$ and $C_{p(t)}$ are P(V) concentrations in the feed and permeate streams, respectively, at a given time t.

2.6. Membrane filtration performance

The performance of the UF unit was characterised by two parameters: permeation flux and cake resistance. The permeation flux (J ($L.m^{-2}.h^{-1}$)) can be calculated using Eq 8:

$$J = \frac{V_m}{A\Delta t} = \frac{(TMP)}{R_t \mu} \quad (8)$$

where V_m (L) is the volume of permeate, A (m^2) is the membrane module area and Δt (h) is the permeation time. ΔP is the TMP (bar), μ is the solution viscosity (Pa·s) (at to 20ºC) and R_t is the total resistance of the membrane (m^{-1}). Intrinsic water permeability (Lm^2h^{-1}/bar) is determined according to Eq.9:

$$(\mathrm{Lp} = \frac{\mathrm{J}}{(\mathrm{TMP})}) \quad (9)$$

According to Darcy's law, decreasing J with constant ΔP during membrane filtration (or, equivalently, increasing ΔP with constant J) indicates membrane fouling. The total resistance (R_t) can be described by the resistance-in-series model (Lee et al., 2008; Remize et al., 2010; Peldszus et al., 2011). The specific cake resistance (α) represents the hydrodynamic resistance to the flow caused by the PAZ layer generated as the filtration cycles continue and is the only factor determining the permeate flux when the rest of the system parameters (i.e., membrane type, membrane surface area, and crossflow velocity) are fixed. The dependence of α on system properties, such as the feed solution, membrane pore size, applied ΔP, and crossflow velocity, is described by Eq. 10 (Keskinler, 1997; Yildiz, 2004).

$$\frac{t}{V} = \frac{\mu R_t}{(TMP)} + \frac{\mu \alpha C_{SS} V}{2(TMP)} \quad (10)$$

where V (L/m^2) is the permeate volume per unit filtration area and μ the

viscosity of permeate (Pa s). Thus, varying the t/V function versus V should yield a straight line with a slope ($\frac{\mu\alpha C_{SS}}{2(TMP)}$).

Thus, α value can be estimated from the slope and considering that other terms in Eq. 10 are known for given set of experimental conditions. This (α) method determination was well described elsewhere.by Teoh et al., (2006).

2.7. Prediction of P(V) precipitation processes

P(V) precipitation and the corresponding saturation index (SI) were studied using the HYDRA-MEDUSA (Puidomènech, 2001) and Visual Minteq codes (Gray-Munro and Strong, 2013). The equilibrium solubility data for Ca and Mg-P(V)s from the HYDRA and PHREEQ C databases were critically reviewed.

3. Results and discussion

3.1. Membrane hydraulic performance

The evolution of the TMP as the sorption-filtration experiments progressed is shown in Figure 6.2. The TMP values increased with time from initial values of approximately 0.3 and 0.38 bar for 2 and 2.5 g_{PAZ}/L, respectively, to a threshold value of 0.8 bar when the filtration cycle was considered finished and a cleaning protocol applied (BW clean-up). Comparing the two PAZ doses, longer filtration cycles (up to 135 min) were measured for the low dose than for 2.5 g_{PAZ}/L (70 min).It seems that more dose promote a fast particles accumulation on the membrane surface instead of being accumulated on membrane pores causing a fast cake formation. After the cleaning procedure (BW) the initial membrane permeability was recovered (180–190 $Lm^{-2}h^{-1}bar^{-1}$).

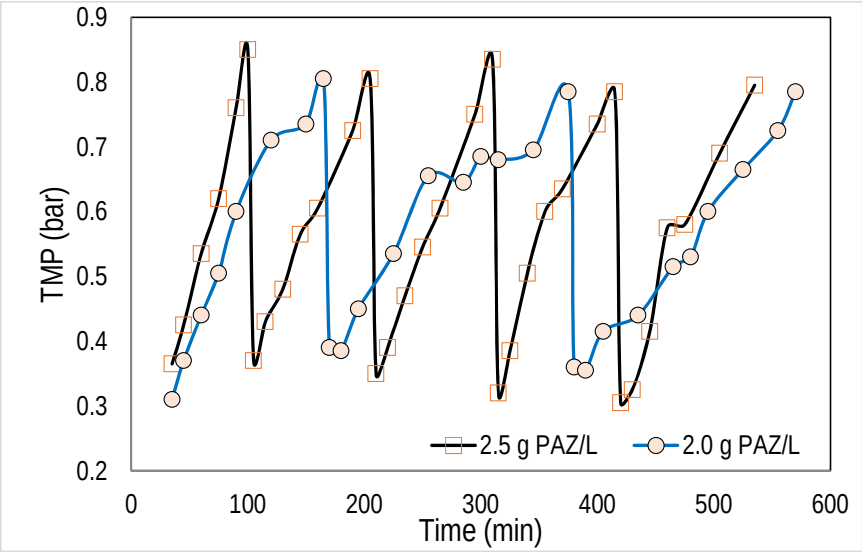

Figure 6.2. Variation of transmembrane membrane pressure (TMP) with time/filtration volume (m^3/m^2) for 2.0 and 2.5 g_{PAZ}/L.

The reduction in the permeability can be explained by the formation of a PAZ cake on the membrane surface (Campinas and Rosa, 2010). The higher recoveries in terms of water permeability between cycles, confirmed the high reversibility of the membrane PAZ-cake. For both doses similar recoveries on water permeability were measured, indicating that the increase of dose provided an increase of the PAZ-cake, as the filtration cycles were reduced, however BW procedure efficiently recovered water filtration membrane properties.

The higher recoveries in terms of water permeability between cycles, which led to a total loss of permeate flux (near 3–7%) from the beginning of cycle 1 to the end of cycle 3 (2 g/L) or 5 (2.5 g/L), support the high reversibility of the membrane fouling.

These results are consistent with those of Laîné et al. (1991), who applied a dead-end powdered activated carbon-UF system (PAC-UF) for the removal

of dissolved organic matter in drinking water potabilisation, and also with those of Yildiz (2004) using Ca rich fly ash in a cross flow microfiltration.

3.2. Effect of PAZ dosage on P(V) recovery: Evaluation of the membrane resistance

The effect of the PAZ dose on membrane fouling during filtration cycles was studied by evaluating the membrane resistance. The variation in t/V versus V is follows a linear relationship as described by Eq. 10. The linear regression analysis for both doses has a regression coefficient of 0.9 (Figure 6.3a) and the specific cake resistance (α) was determined from the slopes of the t/V-V plots.

The α values increased with filtration time to as high as $1x10^{11}$, (Figure 6.3b) with slightly similar profiles for both PAZ doses and the various filtration cycles. Zeolite particles with sizes exceeding those of the membrane pores (20 nm) tended to accumulate on the membrane surface instead of being accumulated on membrane pores and then causing cake formation. The specific cake resistance values for 2.5 g_{PAZ}/L were slightly lower than those for 2.0 g_{PAZ}/L.

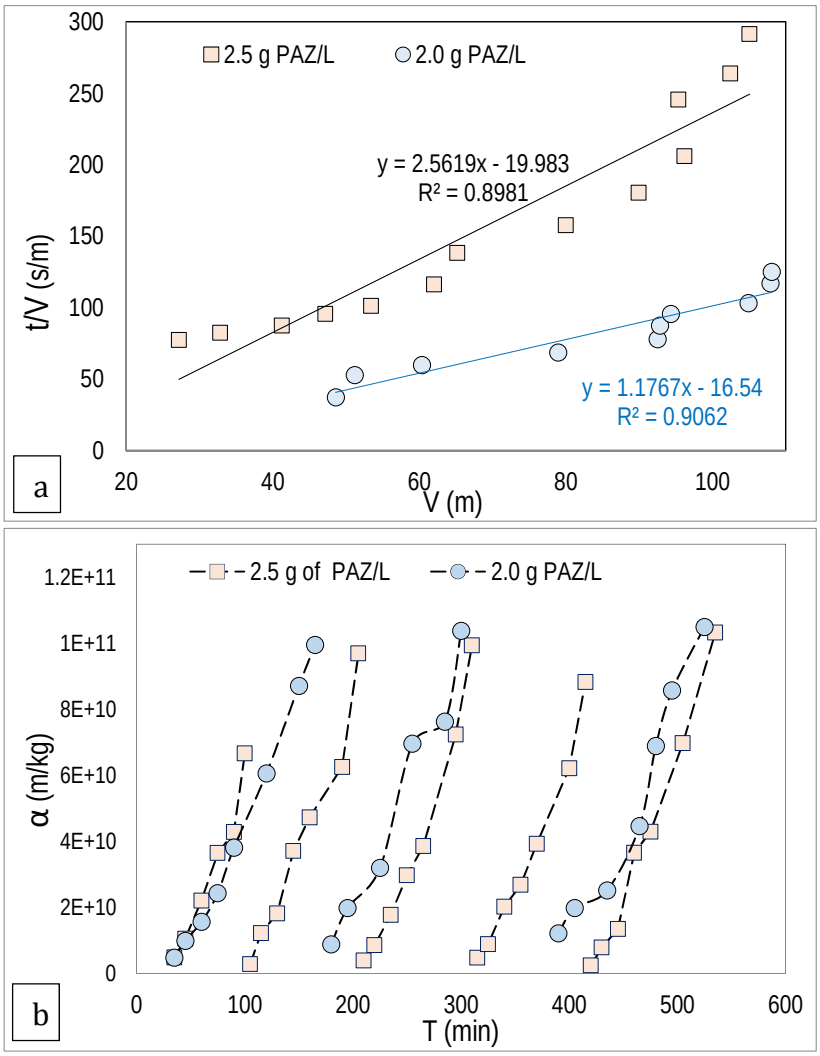

Figure 6.3. a) Variation of t/V with V at various PAZ dosage , b) The effect of PAZ dose on the specific cake resistance (α) during filtration cycle (2 g_{PAZ} /L; 2.5g_{PAZ}/L and P(V) = 25 mg/L).

3.3. Performance of the hybrid membrane UF-sorption system (PAZ/UF)

3.3.1. Effect of initial P(V) concentration

The P(V) removal efficiency profiles (Rp-P(V) (%)) for a 2.5 g_{PAZ}/L at three different initial P(V) concentrations (10, 25 and 100 mg P-PO_4/L) and an initial pH of 8 are shown in Figure 6.4a. The P(V)-removal efficiency

remained fairly constant during filtration cycle for the three evaluated concentrations, returning values of 6±2%, 11±2% and 20±3% for 10, 25 and 100 mg P-PO_4/L respectively.

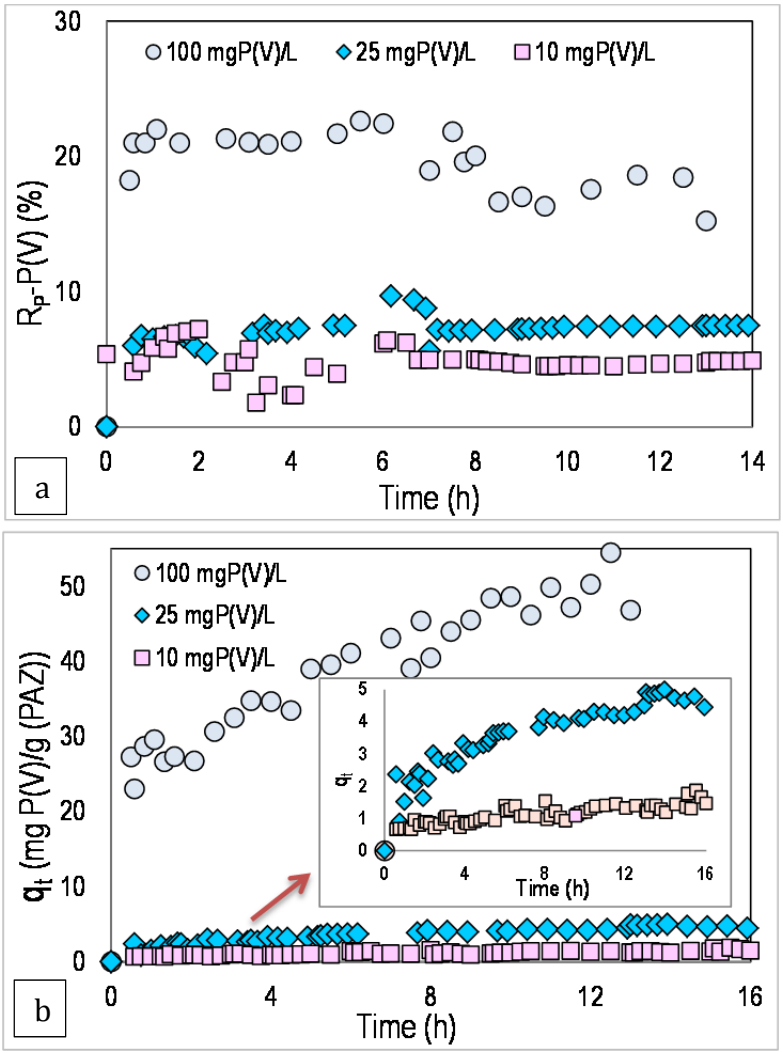

Figure 6.4 a) Effect of the initial P(V) concentration (10, 25 and 100 mgP/L) on the P(V) recovery percentage and b) (q_t) (sorption capacity) profile during filtration cycle with 2.5 g_{PAZ}/L.

The P(V)-loading values (q_t) during filtration cycle (Figure 6.4b), increased over time, and at the end of the experiment, the Ca zeolite was not saturated at any of the tested P(V) concentrations. The sorption of P(V) ions (mainly

$H_2PO_4^-/HPO_4^{2-}$) was postulated to proceed via a combined mechanisms (Eqs. 11-14):

a) Surface complexation with the ≅MOH groups from the zeolitic structure (where M represents Al or Fe):

$$\cong MOH_2^+ + HPO_4^{2-} \leftrightarrow \cong MOH_2^+HPO_4^{2-} \quad (11)$$

$$\cong MOH + HPO_4^{2-} \leftrightarrow \cong MHPO_4^- + OH^- \quad (12)$$

b) Formation of Ca-phosphate with Ca(II) ions occupying the ion exchange groups ($\cong ZO^-$) of the zeolitic structure

$$(\cong ZO^-)_2Ca^{2+} + HPO_4^{-2} + 2N^+ \leftrightarrow 2\cong(ZO^-N^+) + CaHPO_4(s) \quad \text{where N: Na, K} \quad (13)$$

$$(\cong ZO^-)_2Ca^{2+} + HPO_4^{-2} + M^{2+} \leftrightarrow (\cong ZO^-)_2M^{2+} + CaHPO_4(s) \quad \text{where M: Mg} \quad (14)$$

The concentration ratios of P(V) in the STR effluent and the feed stream ($C_{(PO4)T}/C_{(PO4)S}$) were below 1 during filtration cycle (Figure 6.5a). Additionally, the Ca and Na concentration decreased with ($C(Ca)_T/C(Ca)_S$) and ($C(Na)_T/C(Na)_S$) to values below 1 (Figure 6.5b), while the Mg(II) concentration ratios were generally slightly lower than 1 (Figure 6.5c-d). As indicated by equations 13 and 14, the negative groups of the zeolite structure must be neutralised after the consumption of Ca(II) during brushite formation. XRD analysis of the loaded zeolite samples after sorption-filtration tests at initial P(V) concentrations (10, 25 and 100 mgP/L) revealed the presence of the Ca phosphate-containing mineral brushite (Figure 6.6). At low P(V) concentrations (10 mg $P\text{-}PO_4/L$) the dominant mechanism is the initial formation of surface complexation reactions, whereas at high P(V) concentrations (100 mg $P\text{-}PO_4/L$) the formation of brushite (CaHPO4(s)), is favoured. As described by Eq. 13, for a given dose of zeolite, the increase of the initial P(V) concentration favours the formation of brushite and

accordingly the decrease of P(V) concentration in solution. Then reduction of Ca(II) in solution is associated to the formation of brushite, while the reduction of Na(I) and Mg(II) is associated to the ion-exchange reactions with Ca(II) described by Eq. 13 and Eq. 14.

These results are in agreement with previously reported findings (Yildiz, 2004) for a FA-MF/UF hybrid system in which increasing the FA dose from 0.1 to 1 g FA /L considerably increased the P(V) recovery because of the increase in the Ca(II) concentration associated with the FA (26% CaO weight).

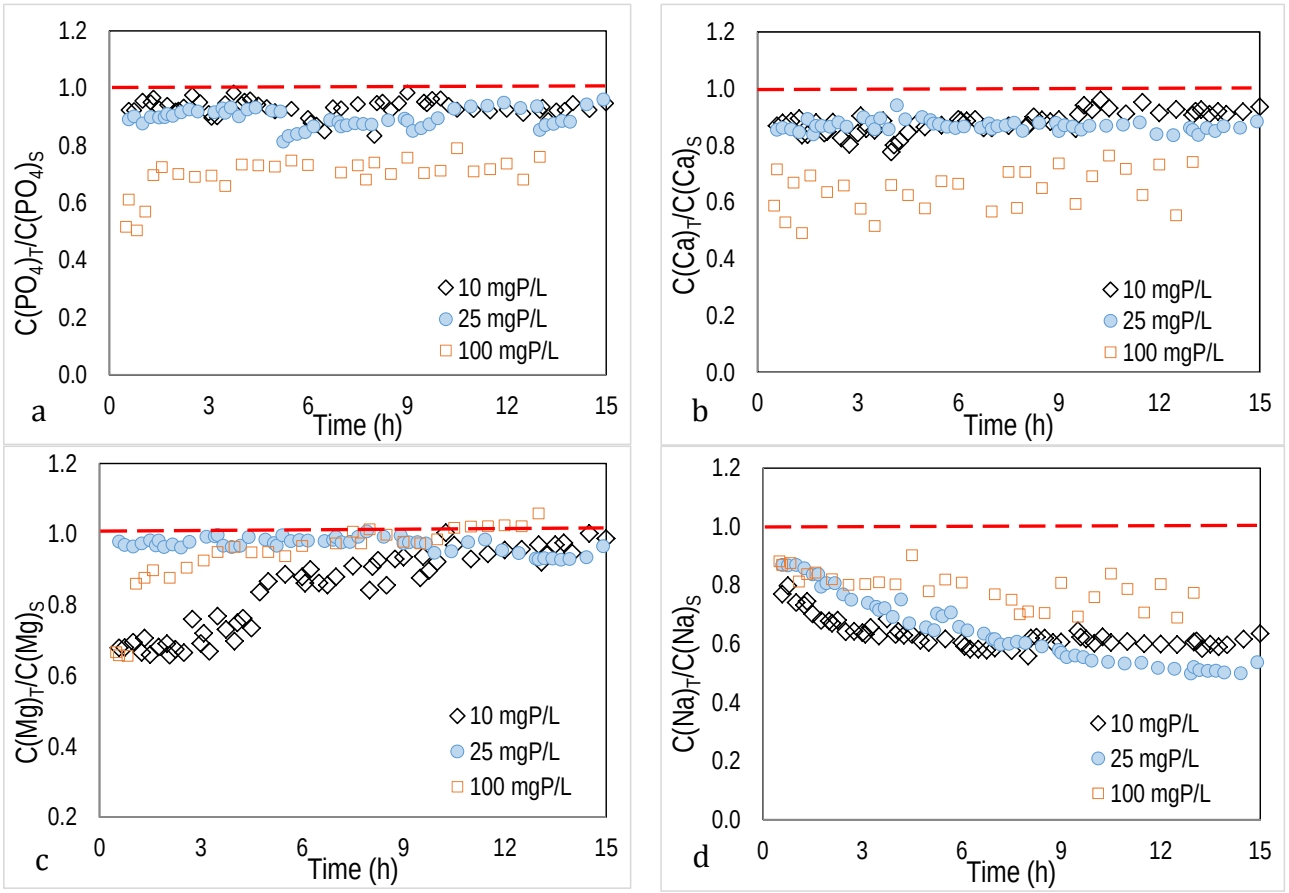

Figure 6.5. Variation in the C_T/C_S ratios of a) P(V), b) Ca(II), c) Mg(II) and d) Na(I) during filtration cycle at various initial P(V) concentrations (10, 25 and 100 mgP/L) with a PAZ dose of 2.5 g_{PAZ}/L.

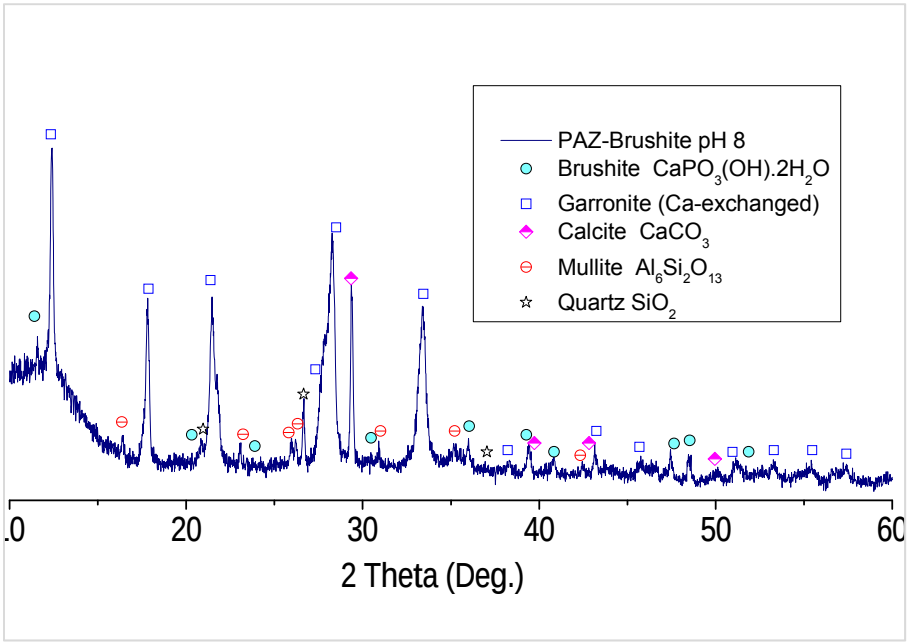

Figure 6.6. XRD example of PAZ samples after P(V) sorption's at pH 8, for an initial P(V) concentration100 mgP-PO_4/L.

3.3.2. Effect of PAZ dose on P(V) removal

The phosphate-removal efficiency (R_p-P(V)(t)) profiles variations at different PAZ doses for a 25 mgP/L solution at an initial pH of 8, (Figure 6.7), an exhibit constant values of 12±2 and 7.5±2% for the two different PAZ doses 2 and 2.5 g_{PAZ}/L respectively during filtration cycle. This is accompanied by a continuous increase of the PAZ sorption capacity (q(t)) up to maximum values of 6.1±0.5 and 5.7±0.3mgP-PO_4/g (after 10 h of filtration cycles for 2 g_{PAZ}/L and 36 h for 2.5 g_{PAZ}/L). The variation in the concentration ratios in the tank and the feed stream (P(V), Ca and Mg) are shown in Figure 6.8.

The concentration ratios profiles (C_T/C_S) for P(V), Ca(II) and Na(I) remained below 1 during filtration cycles (Figure 6.8a,b-d) while the Mg(II) concentration ratios were generally slightly lower than 1 (Figure 6.8c) for 2.5 g_{PAZ}/L, in contrast for 2.0 g_{PAZ}/L the ratio increases from its initial values of

below 1 to slightly higher than 1. The values lower than 1 indicate the exchange of Na(I) and Mg(II) with Ca(II) ions that promotes the precipitation of Ca-phosphate as described by equations 13-14. XRD analysis of the samples at the end of the filtration cycles revealed the presence of the Ca-phosphate mineral phase brushite on the loaded zeolite samples (Figure 6.6).

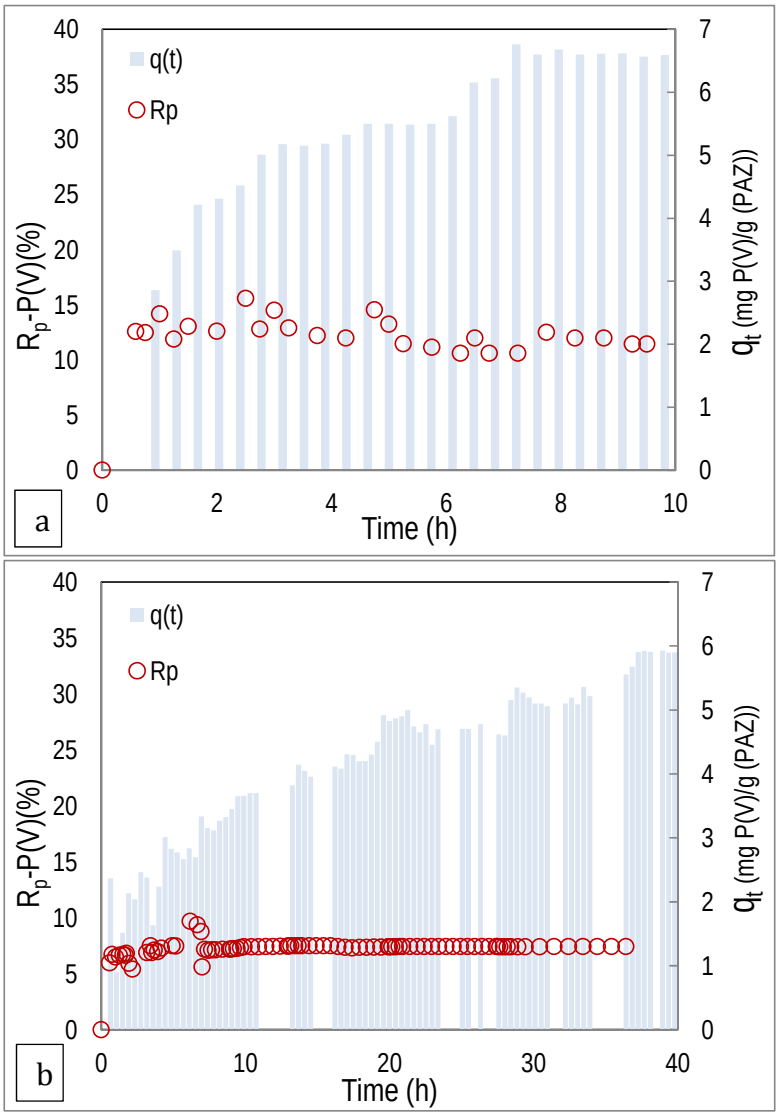

Figure 6.7. Effect of PAZ dose on the P(V) recovery percentage (R_p) and on the P(V) sorption capacity (q(t) according to the mass balance (P(V) = 25 mg/L, a) 2 g_{PAZ} /L and b) 2.5g_{PAZ}/L).

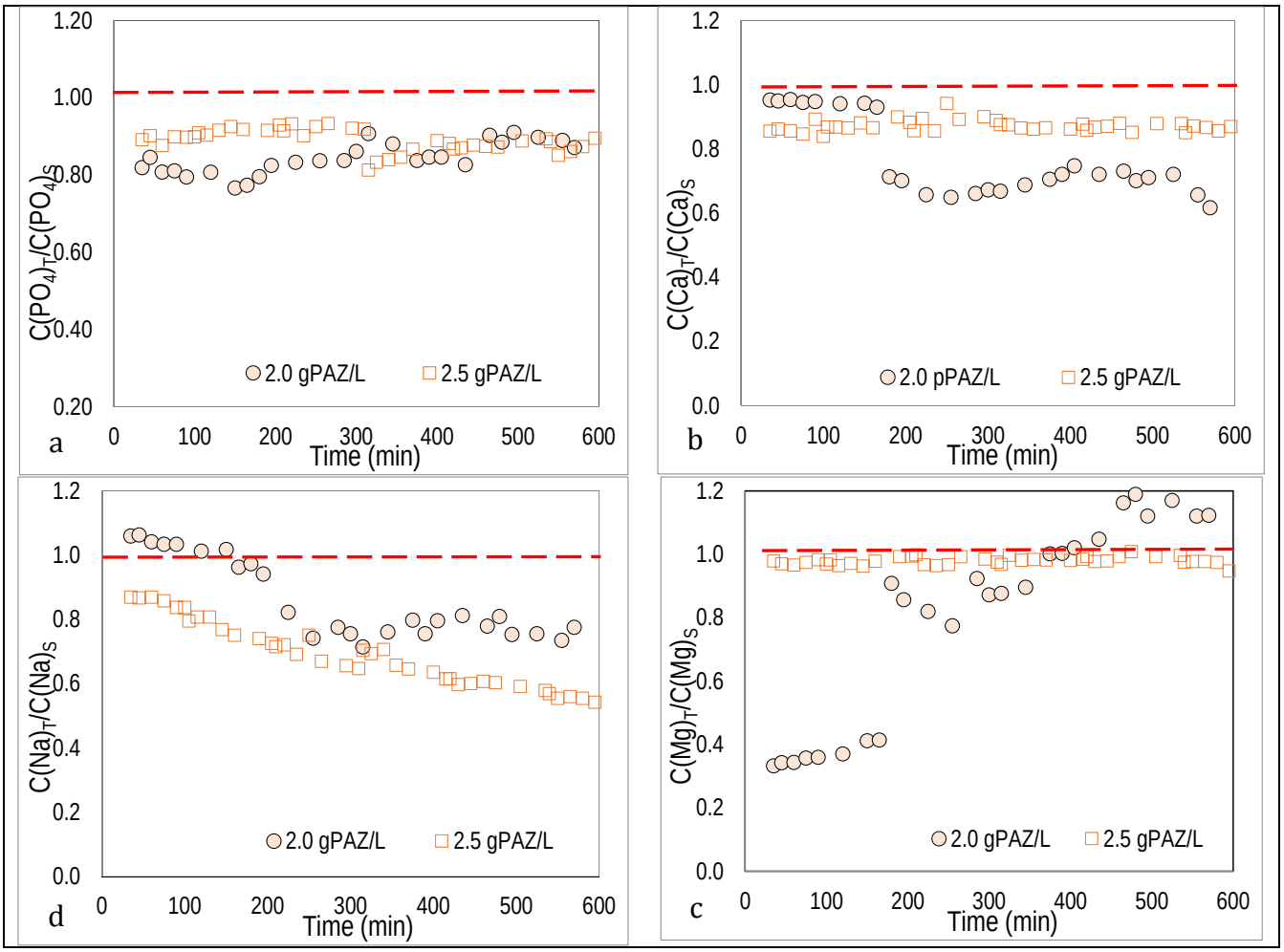

Figure 6.8. a–d) Variation in the C_T/C_S ratios of P(V), Ca(II), Mg(II), and Na(I) during filtration cycle at an initial P(V) concentration of 10 mg/L and PAZ doses of 2 and 2.5 g_{PAZ}/L.

3.3.3. Improvement of P(V) removal by control pH

The influence of pH on P(V) removal by PAZ at an initial P(V) concentration of 10 mg P-PO_4/L with a PAZ dose of 2.5 g_{PAZ}/L was evaluated in two contexts: i) at an initial pH of 8.0±0.2 controlled by the bicarbonate content of the aqueous solution, and ii) at a fixed pH of 9.0±0.2 achieved using a pH-control set-up. The influence of pH on the P(V) sorption capacity (qt) and efficiency (R_p-P(V) (%)) for a solution of 10 mgP-PO_4/L is shown in Figure

6.9a.

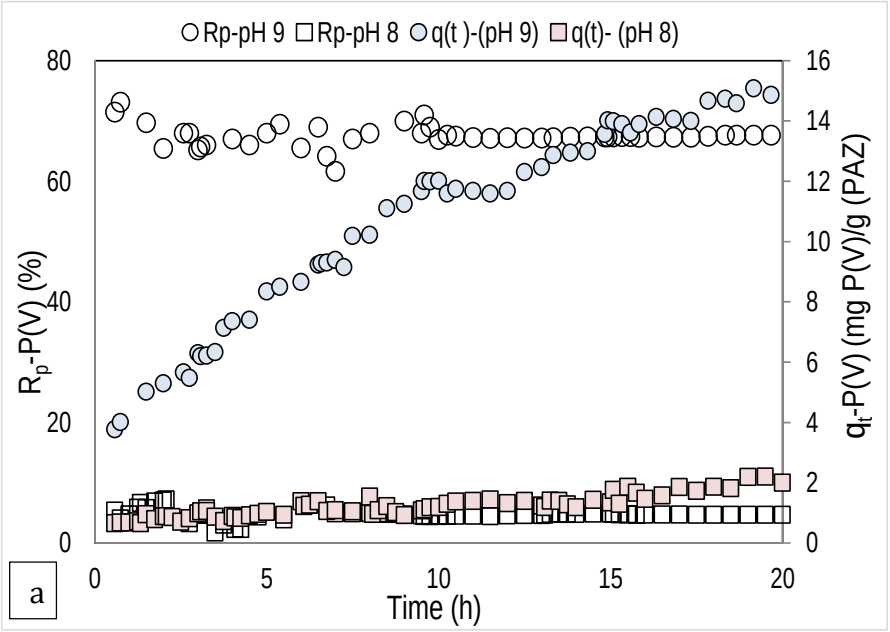

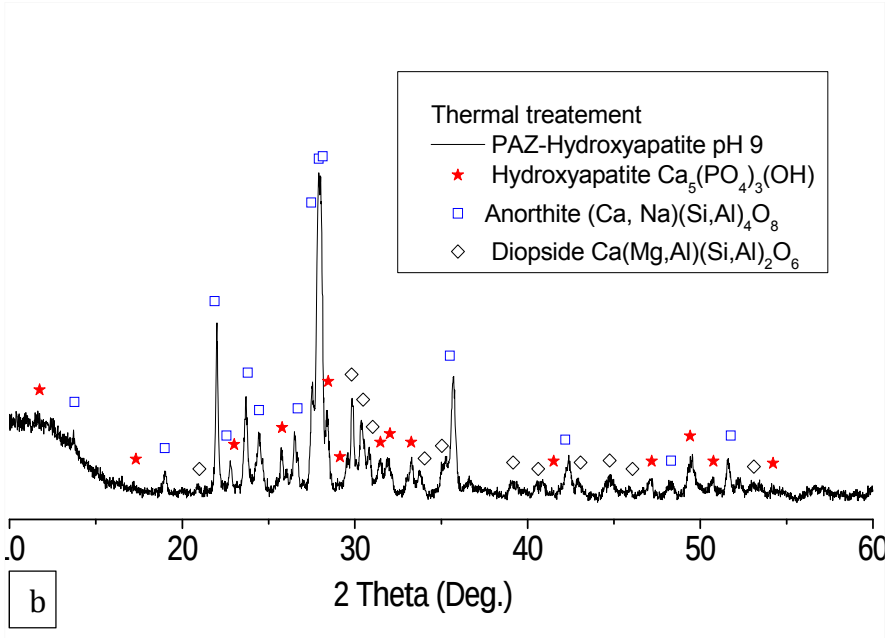

Figure 6.9. a) Sorption capacity (q_t) profile and P(V) recovery (R_p) percentage as a function of filtration time with different initial pH values (8 and 9) by PAZ (2.5 g_{PAZ}/L) at an initial P(V) concentration of 10 mg P-PO_4/L and b) XRD of loaded PAZ samples after phosphate sorption at pH 9. A thermal treatment at 1050 °C was necessary due to the low crystallinity of the sample.

The P(V) sorption capacity reached a 1.6±0.3 mgP(V)/g_{PAZ} (corresponding to 6±2% removal efficiency) and 14±0.5 (corresponding to 70±3% removal

efficiency) at pH 8 and pH 9, respectively after 20 h of filtration. During this time period the removal efficiency remained constant for both pH values.

The concentration ratio (C_T/C_S) profiles for P(V), Ca(II) and Mg(II) as a function of filtration time are shown in Figure 6.10.

The concentration ratio profiles of Ca(II) and P(V) were around 0.5 at pH 9 indicating that a net consumption of Ca(II) is required to accomplish the P(V) removal ratios measured inside the zeolite structure and in the solution. A similar trends were also observed in the Mg(II) profiles suggesting that the consumption of Ca(II) to remove P(V) is accompanied by the substitution of the Mg(II) ions on the zeolite by Ca(II), as described by Eq. 14, and, a subsequent reduction in the concentration of the reactors stream.

XRD analysis of PAZ samples collected at the end of the sorption-filtration experiment revealed the presence of brushite at pH 8 (Figure 6.6). However, no Ca-phosphate mineral phase was detected at pH 9.

FSEM-EDX analysis Figure 6.11 identified the presence of amorphous particles containing P, Ca and O on the loaded PAZ samples evaluated at pH 9. Based on the analysis of the saturation index Figure 6.12, the most reasonable hypothesis is the formation of amorphous Ca-phosphate minerals (hydroxyapatite (Hap) or brushite (Dicalcium phosphate Dihydrate)) that cannot be detected by XRD.

The loaded PAZ sample evaluated at pH 9 was treated at 1050°C to increase its crystallinity, and the presence of (Hap ($Ca_5OH(PO_4)_3(s)$) was detected as is shown in Figure 6.9b.

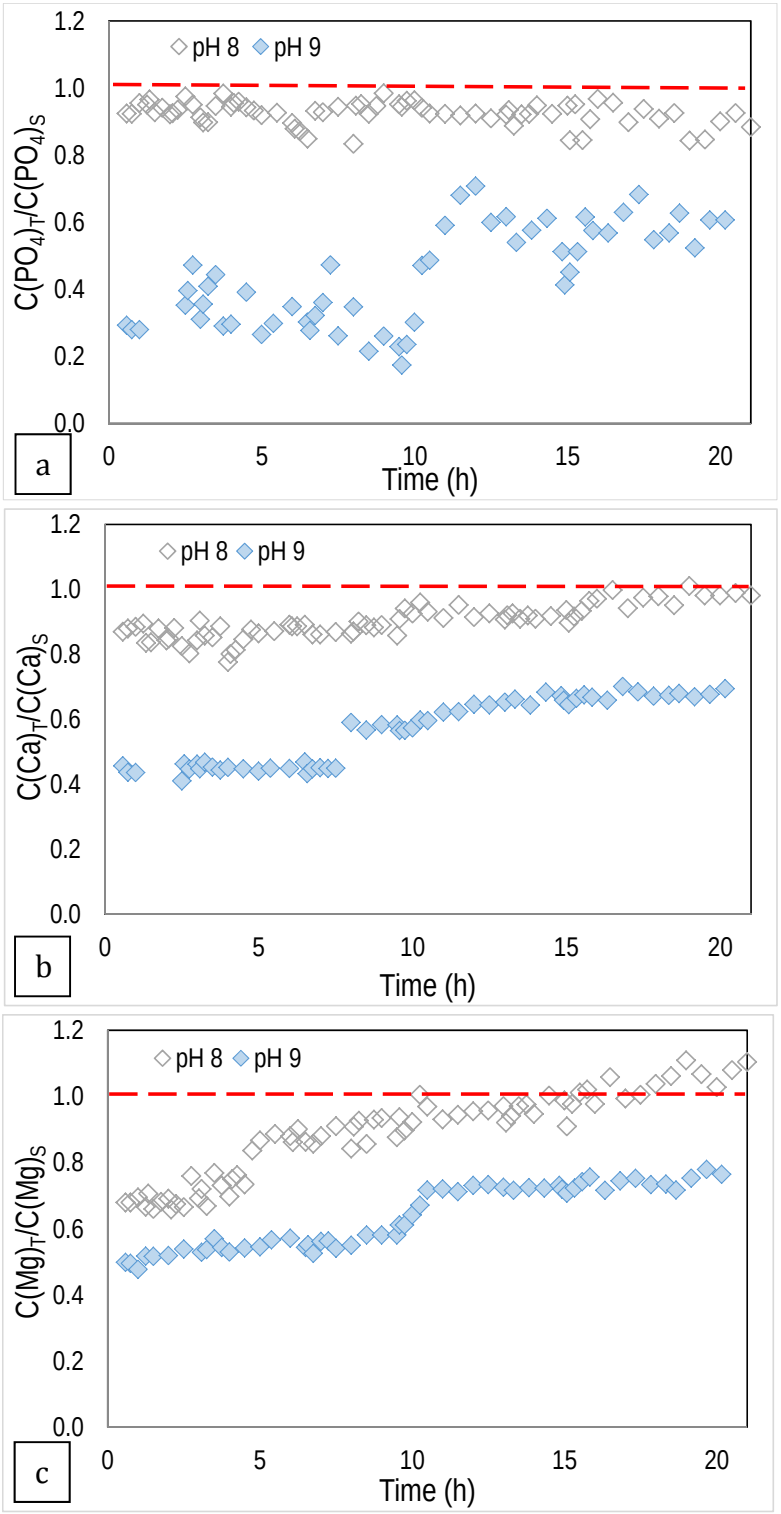

Figure 6.10. Variation in the C_T/C_S ratios of P(V), Ca(II), Mg(II) and Na(I) during filtration cycle at an initial P(V) concentrations of 10 mg/L and a PAZ dose of 2.5 g_{PAZ}/L at pH 8 and 9.

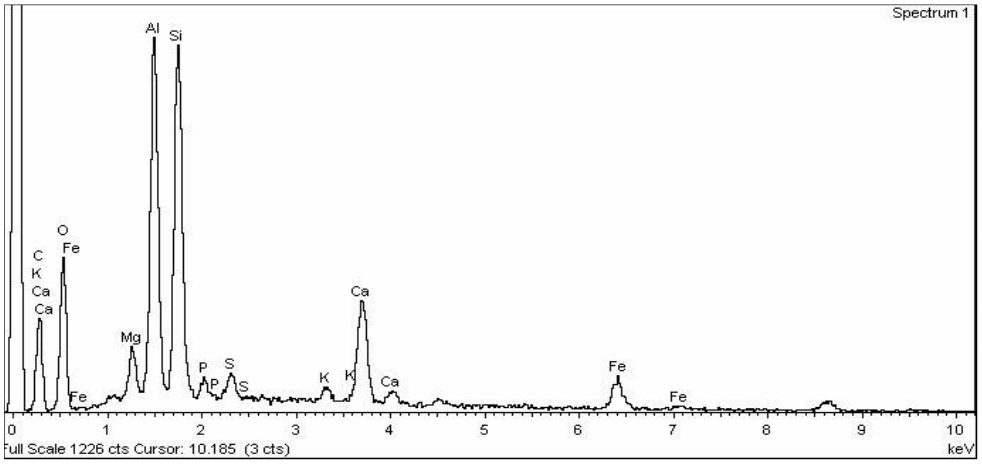

Figure 6.11. FE-SEM of Ca–phosphate with respect to Hap at pH 9 as a function of the precipitation time in the STR

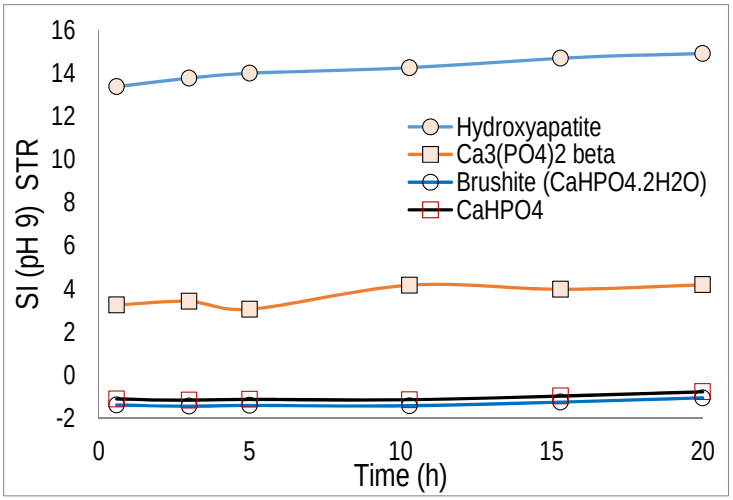

Figure 6.12. SI of Ca –P(V) with respect to Hap at pH 9 as a function of the precipitation time in the STR

The formation of Hap was confirmed by FTIR analysis of the PAZ samples evaluated at pH 8 and 9 (Figure 6.13). With the antisymmetric (v_3) and symmetric (v_1) P-O stretching vibrations of PO_4 at 1050, 1100 and 962 cm^{-1}, and O-P-O bending (V_4) vibrations of PO_4 at 565 and 603 cm^{-1} were observed. The vibration bands at 1050 and 1225 cm^{-1} can be considered as brushite's signature peaks (pH 8). Hap is characterised by an intense and

symmetric (V_1) vibrational peak at 960 cm^{-1} (pH 9), which is assigned to the v_1 vibration of PO_4^{3-}, and a vibrational mode at 630 cm^{-1} that corresponds to OH (Xie et al., 2001; Štulajterová and Medvecký, 2008).

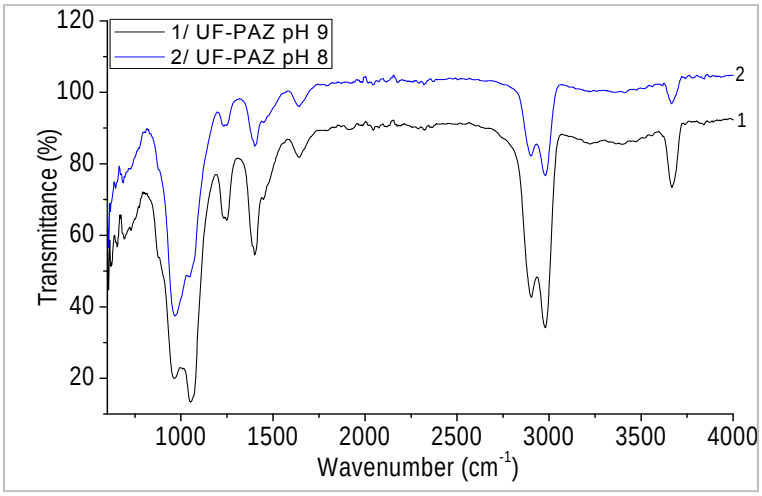

Figure 6.13. FTIR spectra of the powdered UF-PAZ after P(V) recovery at pH 8, 9 and 25°C.

3.4. Evaluation of the P(V) speciation of loaded zeolite samples

PAZ samples were collected after sorption-filtration experiments to identify the processes involved by studying P(V) speciation and characterising the samples. Table 6.2 presents the P (V)-leaching ratios of the loaded PAZ samples using a P-fractionation procedure. Table 6.2 also lists the P(V)-sorption capacities determined for the different experiments according to the mass balance.

For all the experiments at pH 8±0.3, brushite was identified on the loaded samples, whereas only Hap was identified in the sample tested at pH 9 after treatment at 1050°C (Figure 8b). The P speciation confirmed that in all cases, the HCl-P fraction associated with the presence of Ca-phosphate mineral forms, represents between 85-95% of the total of P(V) content in the PAZ.

Additionally, the labile forms (KCl-P) associated with the formation of labile complexes with the Al and Fe metal oxides contributed 5–10%.

Values determined from the speciation analysis ($q_{t(speciation)}$) were similar to those calculated according to the phosphate mass balance [$q_{t(end)}$, (q_t-P(V) (mgP(V)/g(PAZ))], differing by less than 15%.

Table 6.2. Comparison of the total P(V) sorption capacities (qt_{end}) and total P(V) contents determined using a sequential speciation protocol ($qt_{speciation}$).

Experimental Conditions					q-P-Speciation (mg/g)				XRD
Exp	pH	P(V)(mg/L)	g_{PAZ}/L	q_{tend}	KCl-P	NaOH-P	HCl-P	$q_{t(speciation)}$	
1	8±0.3	25	2	6.6	0.39	0.05	5.1	5.6±0.4	Brushite
2	8±0.3	25	2.5	5.9	0.47	0.08	6.2	6.7±0.3	Brushite
3	8±0.3	100	2.5	47.2	0.28	0.31	41.0	41.5±0.8	Brushite
4	8±0.3	10	2.5	1.8	0.20	0.07	2.1	2.4±0.2	Brushite
5	9±0.2	10	2.5	14.6	0.25	0.02	15.0	15.3±0.6	N.D[1], Hap[2]

[1]N.D.: No Ca-phosphate phases detected; [2]Hap detected after being treated at 1050ºC

4. Conclusions

In the light of the results obtained in this work, the following conclusions can be drawn:

The recovery of the P(V) using the PAZ-UF hybrid sorption-filtration process was not subjected to irreversible fouling. A fast membrane fouling and a less filtration time was observed for higher dose 2.5 g_{PAZ}/L compared with 2 g_{PAZ}/L where the irreversible fouling was never completely, mainly determined by the cake layer on the surface of the membrane. Resulting a specific cake resistance values for 2.5 g_{PAZ}/L slightly lower than those for 2.0 g_{PAZ}/L. According to the PAZ doses experiments not significantly differences

on the membrane performance were observed.

The P(V) removal capacity remained constant during filtration cycles and removal efficiency increased as the initial P(V) concentration increases. The P(V) removal capacity is substantially improved by increasing the pH to 9, because the combined sorption mechanisms.

The mechanism of P(V) removal by the hybrid membrane UF-sorption system involves the formation of Ca-phosphate precipitate. XRD confirmed the precipitation of P(V) by Ca as brushite at pH 8 and Hap at pH 9 after treatment of the sample to 1050ºC. Also, the P-speciation confirms that for all cases the fraction HCl-P (associated with the presence of Ca-phosphate mineral forms.

Thus in brief, the hybrid sorption-UF configuration allow to evaluate the potential application of a sorption-filtration system as pre-treatment step of water reuse schemes in conventional WWTPs incorporating pressure driven membrane technologies.

5. References

Ann, Y., Reddy, K.R., Delfino, J.J., 2000. Influence of chemical amendments on phosphorus immobilization in soils from a constructed wetland. Ecological Engineering. 14, 157–167.

Ashekuzzaman, S.M., Jiang, J.-Q., 2014. Study on the sorption–desorption–regeneration performance of Ca-, Mg- and CaMg-based layered double hydroxides for removing phosphate from water. Chem. Eng. J. 246, 97–105.

Bartzokas, A., 2001. Technological Change and Corporate. Strategies in the Fertiliser Industry. Discussion Paper Series. The United Nations University, Institute for New Technologies, UNU/INTECH.2001-7

Campinas, M., Rosa, M.J., 2010. Assessing PAC contribution to the NOM fouling control in PAC/UF systems. Water Res. 44, 1636–1644.

de-Bashan, L.E., Bashan, Y., 2004. Recent advances in removing phosphorus from wastewater and its future use as fertilizer (1997-2003). Water Res. 38, 4222–46.

Dong, H., Gao, B., Yue, Q., Sun, S., Wang, Y., Li, Q., 2014. Floc properties and membrane fouling of different monomer and polymer Fe coagulants in coagulation–ultrafiltration process: The role of Fe (III) species. Chem. Eng. J. 258, 442–449.

European Commission, 2014. Report on critical raw materials for the EU, Report of the Ad hoc Working Group on defining critical raw materials 41.

Ferrer, O., Lefèvre, B., Prats, G., Bernat, X., Gibert, O., Paraira, M., 2015. Reversibility of fouling on ultrafiltration membrane by backwashing and chemical cleaning: differences in organic fractions behaviour. Desalin. Water Treat. 1–15.

Gray-Munro, J.E., Strong, M., 2013. A study on the interfacial chemistry of magnesium hydroxide surfaces in aqueous phosphate solutions: influence of Ca^{2+}, Cl^- and protein. J. Colloid Interface Sci. 393, 421–428.

Hedley, M.J., Stewart, J.W.B., Chauhan, B.S., 1982. Changes in Inorganic and Organic Soil Phosphorus Fractions Induced by Cultivation Practices and by Laboratory Incubations. Soil.Sci.AM.J 46, 970–976.

Hui, B., Zhang, Y., Ye, L., 2014. Preparation of PVA hydrogel beads and adsorption mechanism for advanced phosphate removal. Chem. Eng. J. 235, 207–214.

Keskinler, B., Danis, U., Çakici, A., Akay, G., 1997. Chromate Removal from Water Using Surfactant-Enhanced Crossflow Filtration. Sep. Sci. Technol. 32, 1899–1920.

Laine, J.M., Jacangelo, J.G., Patania, N.L., Montogomery, J.M., Booe, W., Mallevialle, Eaux-Du- mez, J. L.D., 1991. Evaluation of ultrafiltration membrane fouling and parameters for its control Proceedings of the AWWA. Membrane. Technol. Water Ind. Orlando, FL.

Lalley, J., Han, C., Li, X., Dionysiou, D.D., Nadagouda, M.N., 2016. Phosphate adsorption using modified iron oxide-based sorbents in lake water: Kinetics, equilibrium, and column tests. Chem. Eng. J. 284, 1386–1396.

Lee, E.K., Chen, V., Fane, A. G., 2008. Natural organic matter (NOM) fouling in low pressure membrane filtration - effect of membranes and operation modes. Desalination 218, 257–270.

Moharami, S., Jalali, M., 2014. Phosphorus leaching from a sandy soil in the presence of modified and un-modified adsorbents. Environ. Monit.

Assess. 186, 6565–76.

Peldszus, S., Hallé, C., Peiris, R.H., Hamouda, M., Jin, X., Legge, R.L., Budman, H., Moresoli, C., Huck, P.M., 2011. Reversible and irreversible low-pressure membrane foulants in drinking water treatment: Identification by principal component analysis of fluorescence EEM and mitigation by biofiltration pretreatment. Water Res. 45, 5161–5170.

Puidomènech, I.S.S., 2001. Chemical Equilibrium Software Hydra and Medusa. Stock. Sweden.

Querol, X., Moreno, N., Alastuey, A., Juan, R., Ayora, C., Medinaceli, A., Valero, A., Productos, C., 2007. Synthesis of high ion exchange zeolites from coal fly ash. Geol. Acta 5, 49–57.

Remize, P.J., Guigui, C., Cabassud, C., 2010. Evaluation of backwash efficiency, definition of remaining fouling and characterisation of its contribution in irreversible fouling: Case of drinking water production by air-assisted ultra-filtration. J. Memb. Sci. 355, 104–111.

Schoumans, O.F., Bouraoui, F., Kabbe, C., Oenema, O., van Dijk, K.C., 2015. Phosphorus management in Europe in a changing world. Ambio 44, 180–192.

Schröder, J.J., Cordell, D., Smit, A. L., Rosemarin, A., 2010. Sustainable use of phosphorus. Plant Research International, part of Wageningen UR Business Unit Agrosystems. Rep. 357, EU Tender ENV.B.1/ETU/2009/002

Spellman, F., 2009. Handbook of Water and Wastewater Treatment Plant Operations.

Štulajterová, R., Medvecký, Ľ., 2008. Effect of calcium ions on transformation brushite to hydroxyapatite in aqueous solutions. Colloids Surfaces A Physicochem. Eng. Asp. 316, 104–109.

Teoh, S.K., Tan, R.B.H., Tien, C., 2006. A new procedure for determining specific filter cake resistance from filtration data. Chem. Eng. Sci. 61, 4957–4965.

Vincent Vela, M.C., Álvarez Blanco, S., Lora García, J., Bergantiños Rodríguez, E., 2009. Analysis of membrane pore blocking models adapted to crossflow ultrafiltration in the ultrafiltration of PEG. Chem. Eng. J. 149, 232–241.

Wang, H., Qu, F., Ding, A., Liang, H., Jia, R., Li, K., Bai, L., Chang, H., 2016. Combined effects of PAC adsorption and in situ chlorination on membrane fouling in a pilot-scale coagulation and ultrafiltration process. Chem. Eng. J. 283, 1374–1383.

Xie, J., Riley, C., Chittur, K., 2001. Effect of albumin on brushite transformation to hydroxyapatite. J. Biomed. Mater. Res. 57, 357–365.

Yildiz, E., 2004. Phosphate removal from water by fly ash using crossflow microfiltration. Sep. Purif. Technol. 35, 241–252.

Zelmanov, G., Semiat, R., 2014. Phosphate removal from aqueous solution by an adsorption ultrafiltration system. Sep. Purif. Technol. 132, 487–495.

Conclusions and future work

In this chapter the specific aims of this study are reviewed to present an overview of the major findings. Recommendations for further work are also given.

1. Summary of results

Various studies in the last decade have demonstrated that P recovery at low levels (e.g., 2–10 mg/L) from urban wastewaters is not economically feasible using conventional removal processes (coagulation, chemical precipitation, adsorption, and ion exchange). However, newly introduced processes using P-selective sorbents (e.g., metal oxide sorbents or metal oxide-impregnated ion-exchange resins) can provide concentrated phosphate effluents (e.g., 0.1 to 2 g $P\text{-}PO_4^{3-}$/L) typically at alkaline pH values (9 to 12) because the regeneration step requires the addition of 2 to 5% NaOH.

The main goal of this thesis was to recover and valorise low- and high-concentration phosphate effluents as P carriers to assess their technological feasibility and the final powder characteristics after being subjected to various experiments conditions. The conclusions of this investigation are summarised in the following sections:

1.1. **Phosphate valorisation using a batch reactor**

a) The precipitation of phosphate using batch reactors for the valorisation of alkaline phosphate concentrates from WWTP using $CaCl_2$ brines indicated the following:

i) Precipitation under alkaline conditions (pH 8, 10, and 11.5) proceeds via three well-defined steps at pH 10 and 11.5 and two steps at pH 8. In the first stage, the induction period, early nucleation occurred, and a small amount of phosphate was removed. At pH 10, the precipitation of an amorphous Ca phosphate (ACP) phase occurred at the initial reaction time, and this material then crystallised into Hap. In the second stage, Hap underwent homogenous nucleation. During the nucleation stage, the total concentration of Ca(II) remained constant, and the P(V) removal increased at pH 10 and 11.5. In the final stage, further homogeneous nucleation precipitation of bulk Hap was observed until final P(V)-removal efficiencies of 81% and 95% were reached at pH 10 and 11.5, respectively. Analysing the samples confirmed the presence of Hap. At pH 8, when the Hap phase was directly observed, the reaction started immediately; the two observed stages were the precipitation of Hap, followed by a homogeneous Hap-nucleation stage with a phosphate removal ratio of up to 80%.

ii) Precipitation of concentrated phosphate effluents (from 0.25 to 1.0 g/L) at constant pH (11.5) achieved quantitative phosphate removal (>99%) as Hap with a Ca/P ratio of approximately 1.67. The rate of Hap precipitation followed a first-order rate law with respect to Ca^{2+}, PO_4^{3-}, and surface area.

iii) The main effect of increasing the initial P(V) concentration was the formation of Hap precipitate powders with higher degrees of crystallinity and

crystal diameters and lower mean particle sizes. Increasing the stirring speed and the Ca(II)-dosing rate increased the phosphate-precipitation rate, thereby increasing the mean size and degree of crystallinity of the prepared particles. At lower stirring speeds (between 50 and 250 rpm), no significant effect on the phosphate-precipitation rate was observed.

b) The precipitation of phosphate from alkaline concentrates in the presence of inhibiting agents typically found in industrial desalinated brines used as Ca sources (Mg/Ca molar ratios (2.2 and 3.3)) confirmed the following:

i) For both brines, inhibited Hap precipitation and formation of the amorphous mineral phases of Ca, Mg, and Ca/Mg phosphates were observed at pH >9.5. Mg(II) severely inhibited phosphate precipitation, allowing the formation of amorphous Ca phosphate from meta-stable clusters through the incorporation of Mg(II) into the Ca phosphate. Mg(II) also substantially decreased the precipitate crystallinity and the precipitation rate, allowing the formation of ACP. Thermal treatment of the amorphous solids to increase their crystallinity confirmed the presence of Hap and chlorapatite (Ca phosphate), stanfieldite (Ca/Mg phosphate), and farringtonite (Mg phosphate). The surface adsorption of Mg(II) played a critical role in regulating the transformation rate of ACP to Hap. Mg(II) altered the stability of the mineral phases, and more soluble solids were precipitated (e.g., $Mg_3(PO_4)_2.22H_2O$) at pH 11.5.

ii) For experiments at pH 8, the formation of stable clusters increased the reaction barrier, thereby inhibiting nucleation.

iii) Industrial desalinated brines containing mixtures of Ca and Mg could constitute a suitable source for phosphate recovery in the form of mixed Ca/Mg phosphates that could be used by the chemical industry to produce

fertilisers because of their significant advantages in terms of process, costs, and wasted materials.

1.2. Phosphate removal/recovery by low-cost materials (FA and zeolites)

Phosphate removal/recovery solutions have been developed to use low-cost inorganic materials with high pollutant-removal efficiencies in terms of equilibrium and kinetics.

a) Two types of FA from two coal power stations with different CaO(s) contents (Los Barrios (FA-LB (2.8% w)) and Teruel (FA-TE (4.8% w))) were evaluated for the recovery of phosphate from aqueous solution. Phosphate removal using these materials was found to be highly efficient, as indicated by the rapid removal rates and high P loadings at pH 8.

Sorption proceeds via a diffusion-controlled process of phosphate ions inside FA particles coupled with CaO(s) dissolution and brushite ($CaHPO_4$(s)) formation on the FA particles; this process avoids the formation of relatively insoluble Ca phosphates, such as Hap, with limited fertilising properties.

b) The Na^+-zeolite (NaP1-NA) synthesised from CFA and its Ca-modified form (CaP1-NA) were evaluated for the recovery of phosphate from aqueous solution. The sorption capacities of both zeolites in the pH range expected for wastewater effluents (7 to 9) was slightly dependent on the pH, exhibiting maxima pH 8. Phosphate removal by NaP1-NA occurred via a surface complexation mechanism involving the AlOH and FeOH surface groups of the unreacted Fe and Al oxides originally present on the FA or the potential formation of Ca phosphate phases with the original CaO present on the FA.

In contrast, for CaP1-NA, the main removal mechanism consisted of the formation of a Ca phosphate, brushite, as confirmed by XRD. Thus, the higher solubility of brushite compared with that of Hap indicates that this zeolitic material has great potential for use in a novel slow-release inorganic zeolite CaP1-NA/brushite fertiliser.

Based on the aforementioned results, CaP1-NA was evaluated as a powdered activated zeolite, and the adsorption of phosphate onto (PAZ) adsorbents under more realistic conditions in a sorption reactor followed by a UF system. Comparing PAZ doses of 2 gPAZ/L and 2.5 gPAZ/L revealed that the membrane fouling was mainly reversible and determined by the cake layer on the surface of the membrane.

The phosphate-removal capacity is significantly affected by the pH, initial concentration, and phosphate level in the permeate stream.

The desorption tests confirmed that the higher solubility of brushite compared with that of Hap indicates that this zeolitic material has great potential for use in a novel slow-release inorganic zeolite PAZ/brushite fertiliser.

Finally, although batch reactors and the mineral materials FA and zeolite have not been applied in full-scale production units, they may contribute to the development of a cost-effective platform for the production of by-products, such as Hap, using industrial or domestic brine and a Ca source or as fertilisers consisting of supported FA or zeolitic materials.

2. Future work

A variety of questions can be asked based on the results of this thesis and pursued in the future. Here, we list the most interesting ones.

- This thesis provides a good basis for the validation steps using real industrial brines to obtain more information about the characteristics of the recovered Hap particles and testing the effects of various operating conditions on the particle sizes and size distributions obtained using different reactors.
- It would also be interesting to evaluate the influence of Mg(II) and sulfate on phosphate-recovery mechanism in high-salinity brines (NF and RO).
- The simultaneous recovery of ammonium and phosphate from wastewater in batch reactors or with new zeolite forms involving K (KP1) or Mg (MgP1) could be investigated.
- Work could be done to achieve higher purities after the precipitation and crystallisation processes to improve the valorisation of the produced fertiliser.
- The proposed treatment systems could be evaluated and the needs for further purification determined.